THE UNIVERSITY of ADELAIDE

Palaeoenvironments of the Tonian to Cryogenian transition in the Adelaide Superbasin

Georgina Virgo

This thesis is submitted in fulfilment of the requirements for the degree of Doctor of Philosophy

School of Physics, Chemistry and Earth Sciences

Faculty of Sciences, Engineering and Technology

The University of Adelaide

July 2023

Table of Contents

Abstract

The Neoproterozoic (~1000 to 539 Ma) was one of the most dynamic eras in Earth history and was punctuated by significant tectonic, biological, atmospheric, and climatic events. This includes: the Neoproterozoic Oxygenation Event, the breakup of Rodinia and amalgamation of Gondwana, and extreme climatic shifts associated with an extreme icehouse (referred to as "Snowball Earth"). The transition from the Tonian (ca. 1000–720 Ma) to the Cryogenian (ca. 720–635 Ma) was marked by the onset of the Sturtian glaciation, which was the first, and arguably most intense, glaciation during this period. These global changes facilitated the development of distinct lithologies with geochemical signatures that correspond to a suite of depositional conditions, from warm shallow carbonate-rich seas to cold, ice-covered continents.

The Neoproterozoic sedimentary rocks of the Adelaide Superbasin, in South Australia, record the variability and distribution of these environments through this unique time in Earth's past. Despite the geological significance of this basin, it remains understudied. Historical research has established broad characterisations of Neoproterozoic successions across the basin. However, these regional studies lack resolution and contribution from modern analytical methods. More contemporary research of these Neoproterozoic rocks in South Australia commonly investigates particular formations or locations, which provides the detailed insights of stratigraphic horizons but lacks the temporal and/or spatial continuity provided from the aforementioned studies. Additionally, there has been considerable advances in research from other Neoproterozoic basins globally, including those in North America, Africa, Asia, and Europe. This further highlights the need for new, comprehensive research in South Australia to better constrain the temporal and spatial variability across the basin, and how this correlates with other coeval basins.

This thesis presents sequence stratigraphic and geochemical analyses of the Tonian to Cryogenian across the northern Flinders Ranges in order to address this subject. Facies analyses reveal deposition in a carbonate platform setting for the pre-glacial succession, represented by carbonate and clastic lithologies. Deposition is controlled by basin geometry and proximity to uplifted source areas, where the topographic variability was largely fault-controlled and possibly constrained by salt diapirism. Carbonate samples in the pre-glacial succession record a shift from semi-restricted, dysoxic waters to a more restricted setting. This transition coincides with several negative carbon isotope excursions, demonstrating the fluctuating bioproducitvity that was governed by relative water depth and sediment supply. A glaciomarine setting was interpreted for the syn-glacial succession, characterised by two glacial advance-retreat phases and significant variations in thickness across the basin. This was likely the result of contemporaneous faulting and glacial erosion that occurred with climatically driven regression. At the end of the Sturtian glaciation, the basin experienced subsidence and widespread transgression into a more distal setting. The post-glacial succession records a geochemical pivot to more open, oxic to suboxic conditions that was stimulated from increased nutrient input associated with the widespread melting of continental glaciers. Consequently, this multifaceted approach provides a comprehensive framework for what controlled the distribution of depositional environments during this critical and unique time in Earth's past.

Declaration

I certify that this work contains no material which has been accepted for the award of any other degree or diploma in my name, in any university or other tertiary institution and, to the best of my knowledge and belief, contains no material previously published or written by another person, except where due reference has been made in the text. In addition, I certify that no part of this work will, in the future, be used in a submission in my name, for any other degree or diploma in any university or other tertiary institution without the prior approval of the University of Adelaide and where applicable, any partner institution responsible for the joint-award of this degree.

I acknowledge that copyright of published works contained within this thesis resides with the copyright holder(s) of those works.

I also give permission for the digital version of my thesis to be made available on the web, via the University's digital research repository, the Library Search and also through web search engines, unless permission has been granted by the University to restrict access for a period of time.

I acknowledge the support I have received for my research through the provision of an Australian Government Research Training Program Scholarship.

Signed: …… Date: ……07/07/2023……

Acknowledgements

I'd like to start by thanking my incredible supervisory panel: Kathryn Amos, Alan Collins and Juraj Farkaš. You have all provided me with invaluable knowledge, unwavering support and absolute respect throughout my PhD. I feel particularly lucky to have completed this project under your guidance as without all of you, I would not be nearly as confident a scientist or person. Thanks also for the many experiences travelling to far and wide places, I will never forget those adventures.

The Mawson geo crew (Alex, Monica, Zara, Ellyse, Angus, Brad, Mitchell, Nanks)… where do I begin? I couldn't have asked for a better bunch of comrades to have gone on this journey with. You are all amazingly smart, kind, fun and loyal people, and I know that we will keep in touch for the years to come. In particular, I'd like to give a shout out to a few of you that made a significant impact on me…

Morgan (queen Morgs) you are the glue that holds this place together. Never have I met a more generous person that will drop everything to help someone: whether that be assisting with anything work related, providing wise advice during a stressful moment, or even taking a poor PhD friend out for fancy dinner. I'm so glad I get to continue working with you and I look forward to the many boujee experiences to come.

Darwin, my P.I.C. I have exceptionally fond memories of us working side by side in the office…. which as we know equates to dancing/singing along to bangers and laughing at tiktoks. You are an absolute genius and saved me throughout multiple points of my PhD (especially when it came to geochemistry!). I am eternally grateful for your support with work and as a dear friend.

Renee, you are one of a kind! I feel so lucky to have met you and am thankful that you took me under your wing in the early years of my PhD. You were invaluable in helping me navigate through that part of my life and shaped them into some of my fondest years. Thank you for providing me with many unforgettable memories that I will hold with me for a lifetime.

Jarred, firstly I'd like to say sorry for being hangry in the field. But also thank you for knowing to provide me with either chips, lollies or a sledgehammer when I was having one of these moments. I couldn't have asked for a better field buddy to have gone on those frontier adventures with – you are immeasurably kind, patient and loyal.

I would also like to give a huge shoutout to my family. You have always been my biggest support and I know I wouldn't be here without everything you've done for me. Thank you for allowing me to pursue my rock doc dream.

Finally, to Tom. My absolute rock (no pun intended) from the moment I met you. No words can describe how much you mean to me and how much you did for me throughout my PhD. You mean everything to me. I love you

Chapter 1: Introduction and Geological Background

1.1 Thesis aims and rationale

The Adelaide Rift Complex in South Australia is an integral part of the Adelaide Superbasin (Lloyd et al., 2020) and hosts a thick and complete record of rocks deposited during middle to late Neoproterozoic time (Preiss, 2000; Hoffman & Schrag, 2002; Keeman et al., 2020; Lloyd et al., 2020). The Neoproterozoic is subdivided into three periods: Tonian (ca. 1000–720 Ma; the South Australia record begins at ca. 850 Ma), Cryogenian (ca. 720–635 Ma) and Ediacaran (ca. 635–539 Ma). These mark chapters in Earth's past as it evolved tectonically (Li et al., 2008; Merdith et al., 2017; 2019; 2021), biologically (Butterfield, 2011; Lenton et al., 2014; Brocks et al., 2017), chemically (Shields-Zhou & Och, 2011) and climatically (Kirschvink, 1992; Hoffman et al., 1998; 2017). The sedimentary rocks deposited in this South Australian basin preserve these major environmental shifts through distinct variations in lithology and geochemistry (Hoffman & Schrag, 2002; Fairchild & Kennedy, 2007; Halverson et al., 2010; Hoffman et al., 2017).

Historical literature established the foundation for the sedimentologic and tectonic evolution of the basin (Howchin, 1929; Segnit, 1939; Mawson & Sprigg, 1950; Preiss & Forbes, 1981; Preiss, 1987; Preiss et al., 1993), as well as providing early geochemical datasets through Neoproterozoic stratigraphy in South Australia (Sumartojo & Gostin, 1976; von der Borch & Lock, 1979; Belperio, 1990; Uppill, 1990). Since then, there have been a number of studies that have addressed various aspects of the palaeoenvironmental record, with fewer broad studies that characterise the basin (Barovich & Foden, 2000; Preiss, 2000; Walter et al., 2000; Halverson et al., 2005; Swanson-Hysell et al., 2010; Cox et al., 2016; Counts, 2017; Wallace et al., 2017), and appreciably more targeted at specific stratigraphic horizons or locations (Young & Gostin, 1988; 1991; Preiss & Cowley, 1999; Hill & Walter, 2000; McKirdy et al., 2001; Frank & Fielding, 2003; Giddings & Wallace, 2009; 2009a; Giddings et al., 2009; Preiss et al., 2009; Fromhold & Wallace, 2011; 2012; Grey et al., 2011; Hood et al., 2011; 2016; 2018; Le Heron et al., 2011; 2011a; 2014; Preiss et al., 2011; Hood & Wallace, 2012; 2014; 2015; Busfield & Le Heron, 2014; Lechte & Wallace, 2015; 2016; Wallace et al., 2015; 2019; Cox et al., 2018; O'Connell et al., 2020; 2022). Although each approach provides beneficial understanding of Neoproterozoic environments, they also have drawbacks. The broad studies lack high-resolution data, which is necessary for identifying small-scale variability in sedimentation and water column chemistry, while the targeted studies lack the temporal and spatial continuity that is required for correlating regional sequence stratigraphic packages.

Further, there have been a number of studies in other notable locations with exposed Neoproterozoic strata, including Namibia (Frimmel et al., 1996; Halverson et al., 2005; 2007; Hoffman & Halverson, 2008; Busfield & Le Heron, 2013; Le Heron et al., 2013; Miller, 2013; Hood et al., 2015; Lechte & Wallace, 2016; Hoffman et al., 2017a; 2021; Lamothe et al., 2019), northern Ethiopia (Alene et al., 2006; Avigad et al., 2007; Miller et al., 2009; 2011; Swanson-Hysell et al., 2015; Park et al., 2020), Scotland (Spencer & Spencer, 1972; Glover & Winchester, 1989; Smith et al., 1999; Sawaki et al., 2010; Anderson et al., 2013; Stephenson

et al., 2013; Fairchild et al., 2017; Ali et al., 2018), Svalbard (Halverson et al., 2004; 2007; 2011; 2017; 2022; Maloof et al., 2006; Hoffman et al., 2012; 2017a; Kunzmann et al., 2015; Cox et al., 2016; Fairchild et al., 2016; 2016a; Millikin et al., 2022), western USA (Crittenden et al., 1983; Link et al., 1994; Lund et al., 2003; Fanning & Link, 2004; Link & Christie-Blick, 2011; Keeley et al., 2012; Balgord et al., 2013; Busfield & Le Heron, 2016; Le Heron & Busfield, 2016; Le Heron et al., 2020; Nelson et al., 2020; 2021), northern Canada (Chartrand & Brown, 1985; Eisbacher, 1985; Asmerom et al., 1991; Park & Jefferson, 1991; Narbonne et al., 1994; Narbonne & Aitken, 1995; Batten et al., 2004; Halverson et al., 2006; 2007; Jones et al., 2010; Macdonald et al., 2010; Long & Turner, 2013; Rooney et al., 2014; Cox et al., 2016; Milton et al., 2017); Siberia (Bartley et al., 2001; Kuznetsov et al., 2006; Cox et al., 2016), Mongolia (Brasier et al., 1996; Bold et al., 2016), south China (Wang & Li, 2001; Li et al., 2003; Zhang et al., 2008; Zhang et al., 2011; Lan et al., 2015; Busigny et al., 2018), and Greenland (Cox et al., 2016). These studies have investigated the litho- and/or chemo-stratigraphic variation across the basins and analysed the relationship between these variations and shifting climate and tectonic regimes. Comparison between these sites provides an opportunity to distinguish between local fluctuations in basins and paleoenvironmental changes that are occurring on a global scale.

This thesis aims to advance the understanding of Neoproterozoic palaeoenvironments, specifically those in the late Tonian and early Cryogenian, which were deposited at the onset of the Sturtian glaciation. The significance of establishing a facies- and chemo-stratigraphic architecture for this basin extends to others that are being developed globally, as it allows us to unravel what signatures are local to South Australia, and which are representative of global environmental changes.

1.2.1 Research questions

The key objectives for this research can be divided into three big picture questions that aim to answer gaps in knowledge for lithostratigraphic- and chemostratigraphic-correlations at regional and global scales:

(1) *How does the lithostratigraphic framework in the northern Flinders Ranges fit with existing models for the Snowball Earth climate state?*
(2) *Was the northern part of the Adelaide Superbasin restricted from the global ocean during the Tonian and if so, how did this influence the chemostratigraphy and viability for global correlation?*
(3) *Do the environmental conditions and geochemical variations recorded for palaeo-water in the northern Flinders Ranges support the evolution of complex multicellular life?*

1.2 Geological Background

1.2.1 Basin evolution

The Adelaide Superbasin (Figure 1.1) is a large sedimentary system that developed during the Neoproterozoic to middle Cambrian (Myers et al., 1996; Walter & Veevers, 1997; Preiss, 2000; Li & Powell, 2001; Direen & Crawford, 2003; Cawood, 2005; Cawood & Korsch, 2008; Boger, 2011; Lloyd et al., 2020). The breakup of supercontinent Rodinia at approximately 1000 Ma initiated rifting, particularly along the margin between Laurentia and Australia-East Antarctica that would eventually become the Palaeo-Pacific (Merdith et al., 2019). This developed a ~750 km north–south trending basin, the Adelaide Rift Complex (Figure 1.1), along the south-eastern margin of Proterozoic Australia, which eventually formed an aulacogen in the north and filled with a thick succession of Neoproterozoic sediment (Lloyd et al., 2022).

Sedimentation began during the Tonian (ca. 830 Ma), during a phase of subsidence of the stable craton (Preiss, 1987; 1988; 2000; Powell et al., 1994; Powell, 1998; Counts, 2017). Sediment was transported into the basin from the surrounding rift shoulders and was focused along a NW–SE rift valley that became the Willouran Trough (Figure 1.1; Preiss, 2000; Lloyd et al., 2020). The transition into the Cryogenian was marked by a shift to a period of tectonic quiescence (Powell et al., 1994; Cawood, 2005), and was accompanied by widespread erosion across the basin that was driven by the Sturtian glaciation. The final period of the Neoproterozoic, the Ediacaran, is represented by second phase of rifting and magmatism, which reactivated the rift shoulders and supplied material to the basin (Meffre et al., 2004; Lloyd et al., 2020). Deposition was eventually terminated in the middle Cambrian at the onset of the Delamerian Orogeny (ca. 514 Ma; Foden et al., 2006; 2020). This phase of uplift, along with subsequent orogenesis in the Cenozoic, exposed these Neoproterozoic rocks in the modern-day Flinders Ranges and Mount Lofty Ranges (Figure 1.1). The northern Flinders Ranges provides thick and complete exposures of Neoproterozoic stratigraphy due to the often barren landscape and mountainous topography.

1.2.2 Stratigraphic constraints

The Neoproterozoic succession in the Adelaide Rift Complex can be divided into two supergroups, the Warrina and Hysen, which were subdivided based on relative changes in tectonic setting, from a phase of tectonic subsidence to thermal sag (Preiss, 1987). Within these supergroups are four lithostratigrphically distinguished groups: Callanna, Burra, Umberatana, and Wilpena (Figure 1.1; Thomson et al., 1964; Preiss et al., 1998; Preiss & Cowley, 1999; Preiss, 2000; Preiss et al., 2011; Lloyd et al., 2020). The Tonian to Cryogenian period boundary aligns with the boundary between the Warrina and Hysen supergroups, and the Burra and Umberatana group boundary (Mawson & Sprigg, 1950; Thomson et al., 1964; Powell et al., 1994; Lloyd et al., 2020). These show a transition from interbedded clastic and volcanic successions (Callanna) to clastic and carbonate lithologies (Burra), through diamictites and fine-grained clastics with dropstones to persistent interbedded fine-grained clastics and carbonates (Preiss, 1987; 2000). These can be further classified into a set of formations, which are consistently found throughout the northern Flinders Ranges. The Skillogalee Dolomite and Myrtle Springs Formation represent deposition in the upper Burra Group (Preiss & Cowley,

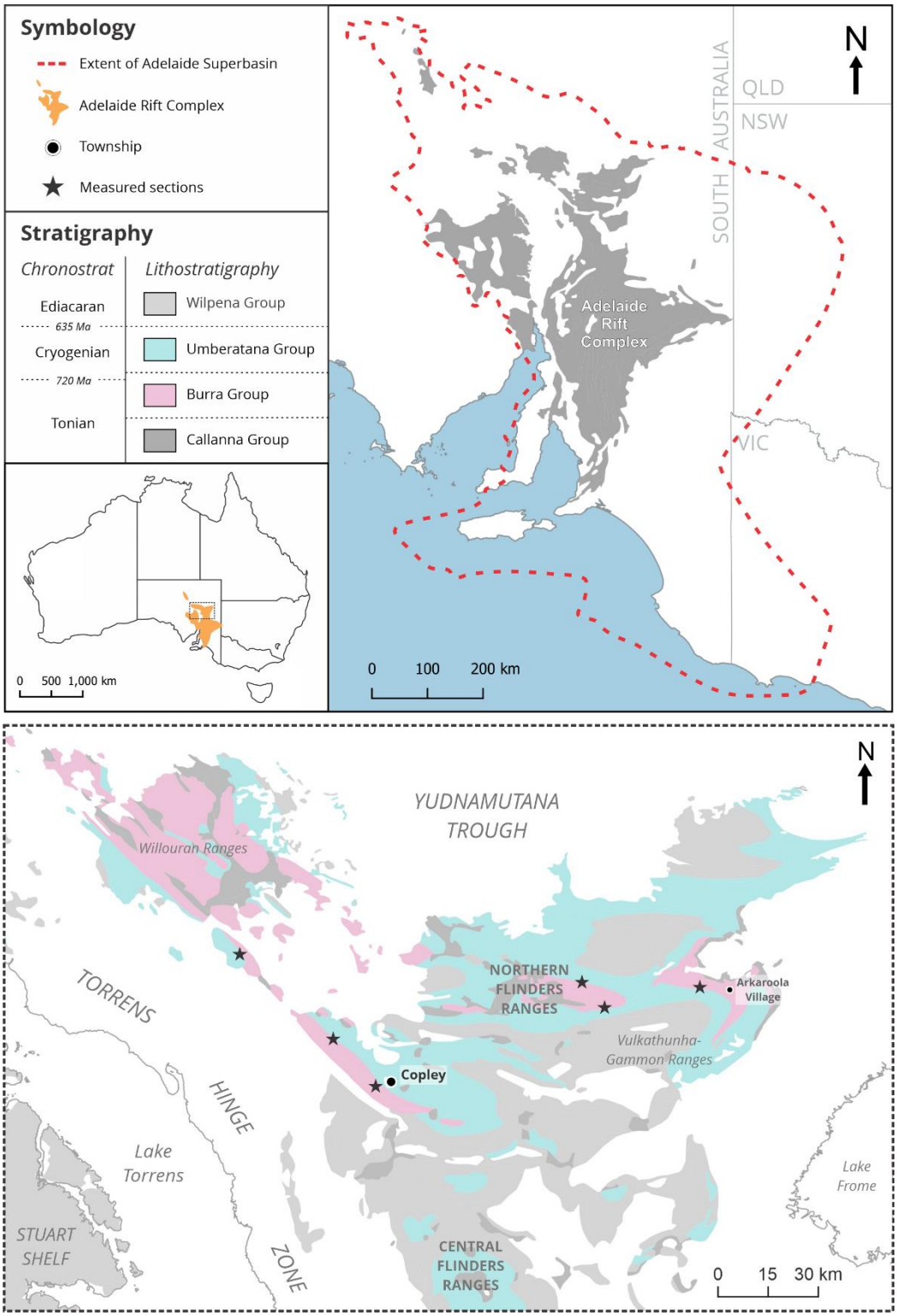

Figure 1.1: Top map shows the extent of the Adelaide Superbasin and highlights the position of the Adelaide Rift Complex within the superbasin. Insert shows position of Adelaide Rift Complex within Australia. The bottom geological map presents the Neoproterozoic lithostratigraphic groups in the northern Flinders Ranges, as well as the locations of the measured sections in this study. Modified from Lloyd et al. (2020)

1999), while the Sturt Formation (previously classified by several "Tillite" derivatives; Lloyd et al., 2022a), Wilyerpa Formation and Tapley Hill Formation characterise the Umberatana Group succession (Preiss et al., 1998).

Chronostratigraphically, the Tonian to Cryogenian transition is constrained by U–Pb dating of tuff and volcanic units, and detrital zircons recording coherent age populations. The base of the Callanna Group is constrained by a maximum depositional age of 893 ± 9 Ma (Paralana Quartzite, Lloyd et al., 2022), which compliments the 802 ± 10 Ma age from a volcanic layer in the middle of the Callanna Group (Rook Tuff, Fanning et al., 1986). There are also two age constraints from the base of the overlying Burra Group, 788 ± 6 Ma (Boucaut Volcanics, Armistead et al., 2020) and 794 ± 4 Ma (Kooringa Member, Preiss et al., 2009). The Umberatana Group has a precise age of 663.03 ± 0.76 Ma provided from a thin tuff layer deposited at the end of the Sturtian glaciation (zircon U–Pb CA-ID-TIMS; Cox et al., 2018) and a new in-situ laser Rb–Sr age from shales that subdivide diamictite packages within the Sturt Formation provides an additional age of 684 ± 37 Ma (Lloyd et al., 2022a).

1.3 Thesis Outline

This thesis is divided into a series of chapters, starting with an introductory chapter that provides detail on the thesis aims and rationale, as well as a geological background that delves into the basin evolution and stratigraphic constraints. The next two chapters (Chapters 1 and 2) address the key sedimentological, geochemical and sequence stratigraphic changes from a Tonian to Cryogenian succession that acts as a case study for this project. Chapter 2 has been published as a peer-reviewed journal article. The following two chapters (Chapters 3 and 4) use the same techniques but applied to several sections across the basin to construct regional correlations that are then compared globally to other notable Tonian–Cryogenian sites. Chapter 3 is currently accepted in a peer-reviewed journal. The final chapter acts to summarise and discuss the findings in this study, as well as propose prospective research possibilities for the region.

1.3.1 Chapter 2

This chapter has been published in Precambrian Research as:
Virgo, G. M., Collins, A. S., Amos, K. J., Farkaš, J., Blades, M. L., & Subarkah, D. (2021). Descending into the "snowball": High resolution sedimentological and geochemical analysis across the Tonian to Cryogenian boundary in South Australia. *Precambrian Research*, 367, 106449. doi: https://doi.org/10.1016/j.precamres.2021.106449

Chapter 2 presents high-resolution sedimentological and geochemical data to characterise palaeoenvironments through a Tonian–Cryogenian succession in the northern Flinders Ranges. The Tonian succession is marked by river delta rippled and cross-stratified sandstones in the Copley Quartzite, through intraclastic magnesite and stromatolitic inner platform carbonates in the Skillogalee Dolomite, to subtidal fine-grained siltstones and microbial buildups in the Myrtle Springs Formation. Rare earth element (REE) data from carbonate samples support deposition in a nearshore, dysoxic setting that was fed by anoxic deep-water and shallow oxic water in the lead up to the Cryogenian. The syn-glacial succession is characterised by

diamictites interbedded with finer grained clastic units that reflect glacial grounding-line advance and retreat in a glaciomarine setting. These are overlain by a deglacial succession (Wilyerpa Formation) that is represented by proglacial turbidites and mudstones with dropstones. The Tapley Hill Formation marks widespread transgression following the Sturtian glaciation and is marked by deposition of subtidal shales and carbonates. Elemental geochemistry from carbonate samples reveal a shift to a more open, oxic to suboxic water column after one of the most intense icehouses in Earth's history.

1.3.2 Chapter 3

This chapter is, as yet, unpublished, but written in a manuscript style.

Chapter 3 provides multiproxy geochemistry to better constrain the depositional setting before, during and after the Sturtian glaciation through the same succession as presented in Chapter 2. Carbonate samples from the Skillogalee Dolomite reveal overall positive $\delta^{13}C$ values and two clusters of $^{87}Sr/^{86}Sr$ and $\delta^{88/86}Sr$ values. A maximum regressive surface (MRS) that represents a low in base level is marked by anomalously light $\delta^{13}C$ and the most radiogenic Sr values. This was likely the result of increased continental input, which has more evolved Sr and can shutdown the carbonate factory, driving the $\delta^{13}C$ to lighter values. The base of the Myrtle Springs Formation is characterised by a transgression to an anoxic deep-water setting and marked by a maximum flooding surface (MFS). This coincides with a negative excursion in $\delta^{13}C$ that likely reflects decreased bioproductivity. Up-section, there appears to be an increasing trend in $\delta^{13}C$ and $^{87}Sr/^{86}Sr$ that is supported by light $\delta^{88/86}Sr$ values. These coincide with a shallowing trend to a relatively oxic-rich, shallow-water supratidal environment that was more bioproductive and had increased continental input due to the more proximal setting. Overall, the partially restricted, carbonate platform setting of the northern Flinders Ranges in the Tonian is isotopically similar to the modern Coorong lagoon and presents a reasonable analogue for these ancient rocks.

1.3.3 Chapter 4

This chapter is accepted in Sedimentologika as:
Virgo, G. M., Collins, A. S., Blades, M. L., Amos, K. J. (2023). Tectonic, eustatic and climate controls on facies architecture during the transition to the Neoproterozoic icehouse in the Adelaide Superbasin, Australia. *Sedimentologika*

Chapter 4 establishes a sequence stratigraphic framework and facies architecture for the Tonian to Cryogenian in a 150 km east–west transect across the northern Flinders Ranges. Sequence stratigraphy is characterised by seven major sequences and several minor sequences that coincide with changes in tectonic regimes, climate, eustacy and sediment input into the basin. Lithofacies in the pre-glacial succession reveal varying proportions of carbonate and clastic deposition in an overall carbonate platform setting. Deposition was largely controlled by basin geometry and proximity to sediment sources. Transition into the syn-glacial succession is marked by diamictite and interbedded sand lithofacies that correspond to advance-retreat cycles in a glaciomarine setting that relate to climatically driven changes in eustacy. The deposition of very fine-grained clastic and carbonate material in the post-glacial succession represents

widespread transgression to a more distal subaqueous setting associated with melting of continental ice sheets. The lithostratigraphy and sequence stratigraphy was analysed for other sites in North America, Africa, Asia, and Europe. These reveal pre-glacial successions that were largely influenced by local rifting associated with the breakup of Rodinia, which overprinted litho- and chemo-stratigraphic signals. Deposition of glaciomarine syn-glacial successions are also documented at these locations, however, the timing and cyclicity remains contentious. Subsidence and climatically controlled sea level rise appears to be the main driver for transgression globally following the Sturtian glaciation.

1.3.4 Chapter 5

This chapter is, as yet, unpublished, but written in a manuscript style.

Chapter 5 determines chemostratigraphic correlations across the northern Flinders Ranges during the Tonian, and how they fit into the global record. The relationship between productivity, redox and relative water level and sediment input were analysed using the $\delta^{13}C$ record, rare earth element tracers (Ce/Ce* and Eu/Eu*) and sequence stratigraphy, respectively. These reveal four depositional conditions that exist during deposition of Tonian stratigraphy in the northern Flinders Ranges: (1) a bioproductive, dysoxic inner platform setting that developed during slow transgression; (2) a bioproductive, suboxic outer platform setting that formed during a highstand systems tract; (3) a biologically stunted inner platform setting, associated with continental progradation during a highstand systems tract; (4) and a biologically inactive, anoxic deep subtidal setting that formed during a transgressive systems tract. When compared to the global $\delta^{13}C$ record, it appears that only one negative $\delta^{13}C$ excursion at ca. 735 Ma can be correlated globally across several coeval basins. Overall, the geochemical signature in this study is unique and likely indicates local fluctuations in tectonics, sediment input and climate rather than global shifts during the Tonian.

1.3.5 Chapter 6

Chapter 6 provides a summary and discussion on the findings from this thesis and overall, how the palaeoenvironments changed through the Tonian and Cryogenian across the basin in the northern Flinders Ranges. This chapter also highlights the research gaps in the current state of literature and establishes a set of recommendations for future work in this region that could build on the research presented in this thesis.

Chapter 2: Descending into the "snowball": High resolution sedimentological and geochemical analysis across the Tonian to Cryogenian boundary in South Australia

Published article in peer-reviewed journal *Precambrian Research*:

Virgo, G. M., Collins, A. S., Amos, K. J., Farkaš, J., Blades, M. L., & Subarkah, D. (2021). Descending into the "snowball": High resolution sedimentological and geochemical analysis across the Tonian to Cryogenian boundary in South Australia. *Precambrian Research*, 367, 106449.
https://doi.org/10.1016/j.precamres.2021.106449

Statement of Authorship

Title of Paper	Descending into the "snowball": High resolution sedimentological and geochemical analysis across the Tonian to Cryogenian boundary in South Australia
Publication Status	☑ Published ☐ Accepted for Publication ☐ Submitted for Publication ☐ Unpublished and Unsubmitted work written in manuscript style
Publication Details	Virgo, G. M., Collins, A. S., Amos, K. J., Farkaš, J., Blades, M. L., & Subarkah, D. (2021). Descending into the "snowball": High resolution sedimentological and geochemical analysis across the Tonian to Cryogenian boundary in South Australia. Precambrian Research, 367, 106449. https://doi.org/10.1016/j.precamres.2021.106449

Principal Author

Name of Principal Author (Candidate)	Georgina Virgo		
Contribution to the Paper	All manuscript text and figure drafting; data collection, processing and analysis; methodology; interpretations; and literature review and field investigation		
Overall percentage (%)	80%		
Certification:	This paper reports on original research I conducted during the period of my Higher Degree by Research candidature and is not subject to any obligations or contractual agreements with a third party that would constrain its inclusion in this thesis. I am the primary author of this paper.		
Signature		Date	07/07/2023

Co-Author Contributions

By signing the Statement of Authorship, each author certifies that:

i. the candidate's stated contribution to the publication is accurate (as detailed above);

ii. permission is granted for the candidate in include the publication in the thesis; and

iii. the sum of all co-author contributions is equal to 100% less the candidate's stated contribution.

Name of Co-Author	Alan Collins		
Contribution to the Paper	Reviews and commentary		
Signature		Date	07/07/2023

Name of Co-Author	Kathryn Amos		
Contribution to the Paper	Reviews and commentary		
Signature		Date	07/07/2023

Please cut and paste additional co-author panels here as required.

Name of Co-Author	Juraj Farkas		
Contribution to the Paper	Reviews and commentary; assistance with methodology and analysis		
Signature		Date	07/07/2023

Name of Co-Author	Morgan Blades		
Contribution to the Paper	Reviews and commentary; assistance with methodology		
Signature		Date	07/07/2023

Name of Co-Author	Darwinaji Subarkah		
Contribution to the Paper	Reviews and commentary; assistance with methodology and formal analysis		
Signature		Date	07/07/2023

2.1 Abstract

The Tonian–Cryogenian transition (ca. 720 Ma) represents a period of significant environmental change in Earth history, involving variations in oceanic and atmospheric oxygenation, significant changes in the biosphere, tectonic reorganisation, and the onset of the global 'Sturtian' glaciation. South Australia has some of the thickest, continuous and best exposed sections of this unique interval globally. Here we present detailed palaeoenvironmental interpretations for a complete, ca. 3 km thick, pre- to post-glacial succession near Copley in the northern Flinders Ranges, South Australia. Elemental concentration data, complemented by screening for diagenesis, demonstrates the preservation of marine or primary REE signatures for studied carbonate samples and supports the proposed sedimentological and palaeoenvironmental interpretations. Multiple Tonian regressive-transgressive cycles are defined, which are recorded by deltaic rippled and cross-stratified sandstones (Copley Quartzite), through inner platform intraclastic magnesite and stromatolitic carbonates (Skillogalee Dolomite), to subtidal laminated siltstone and platform carbonates (Myrtle Springs Formation). The REE patterns from carbonate samples in the Skillogalee Dolomite and Myrtle Springs Formation indicate low Y/Ho, slight light rare earth element (LREE) depletion, weak negative Ce/Ce* and high Eu/Eu*. This suggests a nearshore, dysoxic setting fed by anoxic deep waters and more oxic shallow waters. In combination, the sedimentological and geochemical data build a picture of a partially restricted, shallow marine to lagoonal setting for the northern Flinders Ranges directly before the climate pivot to the Sturtian glaciation. These pre-glacial formations are unconformably overlain by Cryogenian subglacial to grounded ice-margin pebbly diamictites with immature, massive sand interbeds (Bolla Bollana Tillite). We suggest these facies reflect glacial grounding-line advance and retreat in a glaciomarine setting. These grade into turbiditic laminated sandstone and mudstone with dropstones (Wilyerpa Formation), which were likely deposited at the onset of deglaciation in a subaqueous proglacial environment. The post-glacial succession (Tapley Hill Formation) consists of subtidal laminated shales and carbonates, which are represented by increased Y/Ho, moderate LREE depletion, slight negative Ce/Ce* and low Eu/Eu*. This significant geochemical shift to a more open, oxic to suboxic subtidal setting coincides with widespread transgression and relative sea level rise after one of the most severe glaciations ever recorded.

2.2 Introduction

The Neoproterozoic Era (ca.1000 to 541 Ma) represents a period of Earth history in which significant physiochemical change occurred (Halverson et al., 2009), including: the Neoproterozoic Oxygenation Event (Shields-Zhou & Och, 2011), the evolution from bacterial oceans to eukaryotic dominated ecosystems (Butterfield, 2011; Lenton et al., 2014; Brocks et al., 2017), the breakup of supercontinent Rodinia and formation of Gondwana (Li et al., 2008; Merdith et al., 2017; 2019; 2021); and extreme climatic shifts to an icehouse referred to as "Snowball Earth" (Kirschvink, 1992; Hoffman et al., 1998; 2017). The transition from the oldest Neoproterozoic period (the Tonian ca. 1000–720 Ma) to the Cryogenian (ca. 720–635 Ma) is marked by the onset of the Sturtian glaciation (Halverson, 2006; Hoffman et al., 2017). Sedimentary rocks from this transition record major environmental shifts through distinct

variations in lithology and geochemistry (Hoffman & Schrag, 2002; Fairchild & Kennedy, 2007; Halverson et al., 2010; Hoffman et al., 2017).

There are a number of notable Tonian–Cryogenian sections globally, including those in South Australia (Preiss et al., 2011), Namibia (Hoffman et al., 2017a; Lamothe et al., 2019), Ethiopia (Park et al., 2020), Scotland (Fairchild et al., 2017), Svalbard (Halverson et al., 2017), Canada (Long & Turner, 2013; Thomson et al., 2015), China (Zhang et al., 2008), and the USA (Macdonald et al., 2013). South Australia provided the names of the 'Sturtian' and 'Marinoan' Cryogenian glaciations (Howchin 1920; Mawson & Sprigg, 1950; Cooper, 2010) and has some of the best exposed, continuous and thickest sections compared to its global counterparts (Preiss, 2000; Hoffman & Schrag, 2002; Keeman et al., 2020; Lloyd et al., 2020). For example, there are up to 5 km thickness of continuous Sturtian glaciogenic sedimentary rocks over hundreds of kilometres along strike in the Flinders Ranges (Preiss et al., 2011; Le Heron et al., 2011a), and late Tonian strata up to 8 km thick in the Mid-North region of South Australia (Preiss, 1987). This is four times the thickness of the late Tonian succession in Svalbard (Halverson et al., 2017) and approximately three times thicker than the equivalent strata in Death Valley, USA (Shuster et al., 2018). Although this highlights the geological significance of the South Australian sections, they remain understudied, with few modern geochronological, sedimentological and geochemical data available (see Lloyd et al., 2020, and references therein). For example, over the past 50 years, there have been a very limited number of studies focused on late Tonian sedimentology and geochemistry in South Australia (e.g. von der Borch & Lock, 1979; von der Borch, 1980; Belperio, 1990; Uppill, 1990; Preiss & Cowley, 1999; Hill & Walter, 2000; Frank & Fielding, 2003; Preiss et al., 2009). There has been appreciably more research conducted on early Cryogenian strata (e.g. Sumartojo & Gostin, 1976; Link & Gostin, 1981; Young & Gostin, 1988; 1991; Giddings & Wallace, 2009; Grey et al., 2011; Le Heron et al., 2011; 2011a; 2014; Preiss et al., 2011; Lechte & Wallace, 2015; 2016; Cox et al., 2018) and mid Cryogenian strata (e.g. McKirdy et al., 2001; Giddings & Wallace, 2009a; Giddings et al., 2009; Fromhold & Wallace, 2011; 2012; Hood et al., 2011; 2016; 2018; Hood & Wallace, 2012; 2014; 2015; Wallace et al., 2015; O'Connell et al., 2020), yet research gaps still exist regarding the transition into the Sturtian glaciation. Although the existing studies present detailed findings, they often focus on specific formations. This highlights the distinct lack of complete, contemporary Tonian–Cryogenian research that is crucial for understanding the sequence stratigraphic changes in depositional setting before, during and after the Sturtian glaciation. Conversely, there have been a number of papers that present an overview of the sedimentology and geochemistry of Neoproterozoic strata in South Australia (e.g. Preiss & Forbes, 1981; Preiss, 1987; Preiss et al., 1993; Barovich & Foden, 2000; Preiss, 2000; Walter et al., 2000; Halverson et al., 2005; Swanson-Hysell et al., 2010; Cox et al., 2016; Counts, 2017; Wallace et al., 2017; Ward et al., 2019), but these lack the stratigraphic resolution from the former, local studies. In addition, the degree of incision at the base of the Sturtian glacial deposits, and therefore, the extent of conformability between the Tonian and Cryogenian successions, is unknown (Lloyd et al., 2020). Recent sedimentological and geochemical analyses of Tonian–Cryogenian sections at other significant Neoproterozoic sites (Fairchild et al., 2017; Halverson et al., 2017; Hoffman et al., 2017a; Lamothe et al., 2019; Park et al., 2020) further warrants the necessity for a new, comprehensive study in South Australia.

Glacial deposits, later determined as Cryogenian, were initially recognised and mapped in South Australia at Sturt Gorge (Howchin, 1901) and Marino Rocks (Mawson & Sprigg, 1950), leading to the current designations of Sturtian and Marinoan for the glacial epochs (Hoffman et al., 2017). Since this discovery, Sturtian glacial deposits have been recorded on every continent except Antarctica and are marked by distinct glaciogenic packages that define the base of the Cryogenian (Hoffman et al., 2017). Globally, pre-glacial and post-glacial successions comprise a mix of clastic and carbonate sediments that have largely been interpreted as marine deposits (Narbonne & Aitken, 1995; Zhang et al., 2008; Preiss et al., 2011; Babinski et al., 2012; Fairchild et al., 2017; Halverson et al., 2017; Hoffman et al., 2017a), while the syn-glacial strata have been interpreted as glaciomarine (Link & Gostin, 1981; Young & Gostin, 1988; 1991; Eyles et al., 2007; Preiss et al., 2011; Le Heron et al., 2014). Clear identification of a conformable and well-preserved transition between the Tonian and Cryogenian has so far eluded researchers. However, precise U–Pb tuff ages from Canada have dated the start of the Sturtian glaciation there to between 717 $\pm$ 0.1 Ma and 716.9 $\pm$ 0.4 Ma (Macdonald et al., 2010; Macdonald & Wordsworth, 2017). High precision U–Pb zircon ages from South China (715.9 $\pm$ 2.8 Ma; Lan et al., 2014) and Ethiopia (719.68 $\pm$ 0.46 Ma, 719.58 $\pm$ 0.56 Ma; MacLennan et al., 2018; Park et al., 2020) are consistent with the hypothesis of this being an effectively globally synchronous phenomenon (e.g. Rooney et al., 2014; 2015; Halverson et al., 2017; Hoffman et al., 2017; MacLennan et al., 2018; Park et al., 2020). Carbon- and strontium-isotope values from carbonate units have been interpreted also to reflect seawater signatures that can be correlated globally (e.g. Halverson, 2006; Halverson et al., 2010; Shields et al., 2018; Park et al., 2020).

From a sedimentological perspective, the Tonian–Cryogenian sections of South Australia are comparable with sections at other significant global sites; represented by mixed clastic and carbonate packages in the Tonian, through a thick basal Cryogenian diamictite succession, to interbedded shales and carbonates in the mid Cryogenian (Preiss, 1987; Preiss et al., 2011). However, palaeoenvironmental interpretations for particular formations within South Australia distinguish the depositional setting from other sections globally. One of the most rigorously studied Tonian formations in South Australia, the Skillogalee Dolomite, is made up of distinctive carbonates, notably magnesite beds (Belperio, 1990; Frank & Fielding, 2003), which have a contentious depositional origin. The Skillogalee Dolomite occurs within the central and northern Flinders Ranges and has been variously interpreted as representing overall "non-marine" or "marine" environments, including playa lake to lacustrine (Murrell, 1977; Veevers & Cotterill 1978; Uppill 1980; von der Borch 1980; Rutland et al 1981), marginal marine to lagoonal (von der Borch & Lock, 1979; Preiss & Forbes 1981; Belperio, 1990; Frank & Fielding, 2003; Hearon et al., 2015), and shallow to deep marine (Backé et al., 2010). A non-marine origin for these sediments would signify preservation of restricted and potentially altered brackish or fresh-water column properties, which would hinder global chemostratigraphic correlation with other sections (Oehlert & Swart, 2014; Bold et al., 2020). This emphasises the requirement for robust understanding of Tonian–Cryogenian depositional settings in South Australia, and implications for palaeo-seawater reconstructions and chemostratigraphic applications.

This study presents detailed sedimentological analysis, elemental geochemistry and palaeoenvironmental interpretations for a thick and complete Tonian–Cryogenian succession in the northern Flinders Ranges of South Australia. Detailed descriptions of grain size, sedimentary structures, bedding thickness and palaeocurrent direction were measured in the field, and subsequent interpretations of the lithostratigraphy, sequence stratigraphy and palaeoenvironmental setting were conducted. Samples were collected from carbonate lithofacies throughout the succession and investigation of their geochemical properties, including indicators of diagenesis, detrital input and redox conditions further constrained the depositional setting. This multifaceted approach provides substantially higher resolution interpretations of the palaeoenvironments present in this classic location and inform improved global reconstructions for this critically important period in Earth's history.

2.3 Geological Setting

The Adelaide Rift Complex, part of the Adelaide Superbasin (Lloyd et al., 2020), is a 600 km north-south trending basin that is exposed in the Flinders Ranges and Mount Lofty Ranges of South Australia (Figure 1). Here, the Neoproterozoic is lithostratigraphically divided into the Callanna, Burra, Umberatana, and Wilpena groups (Thomson et al., 1964; Preiss et al., 1998; Preiss & Cowley, 1999; Preiss, 2000; Preiss et al., 2011; Lloyd et al., 2020) (Figure 1). The Tonian to Cryogenian transition aligns with the boundary between the Burra and Umberatana groups (Mawson & Sprigg, 1950; Thomson et al., 1964).

The older Tonian siliciclastic sediments were initially derived from the surrounding emerging rift shoulders during rifting of this then-central part of Rodinia (Preiss 2000; Lloyd et al., 2020). Sediment transport was focussed into the rift valley marked by the NW–SE trending Willouran Trough (Lloyd et al., 2020). The Sturtian glaciation marks a short-lived reversion to erosion and sediment sourced from rift shoulders, followed by further sedimentation along the Willouran Trough (Lloyd et al., 2020). The pre-glacial succession examined in this paper is divided into three formations: the Copley Quartzite, the Skillogalee Dolomite and the Myrtle Springs Formation (Preiss & Cowley, 1999) (Figure 1). In its type area near Mount Aroona, the Copley Quartzite is lithologically uniform, represented by interpreted proximal deltaic medium to coarse-grained feldspathic quartzite with minor siltstone interbeds (Preiss, 1987). The Skillogalee Dolomite has previously been divided into an upper and lower sequence (Uppill, 1980). The lower unit is interpreted to have been deposited in a marginal to shallow marine low-relief ramp setting, represented by clastic dominated interbedded siltstone, quartzitic sandstone and dolomite (Preiss, 1987; Counts, 2017). The upper unit is represented by subaerial to shallow marine magnesite conglomerate, black chert, stromatolites, dolomite and minor terrigenous material interpreted as tidal flat deposits (Preiss, 1987; Belperio, 1990; Frank & Fielding, 2003; Counts, 2017). The Myrtle Springs Formation primarily consists of interbedded laminated siltstone, fine-grained sandstone, quartzite and dolomite (Coats, 1973), with stromatolitic dolomite in the north-western Flinders Ranges (Murrell, 1977). These have been interpreted as subtidal to marginal marine deposits, respectively (Preiss, 1987). The Bolla Bollana Tillite represents the syn-glacial unit and was deposited during the Sturtian glaciation (Coats, 1973; Young & Gostin, 1988), while the overlying Wilyerpa Formation defines the

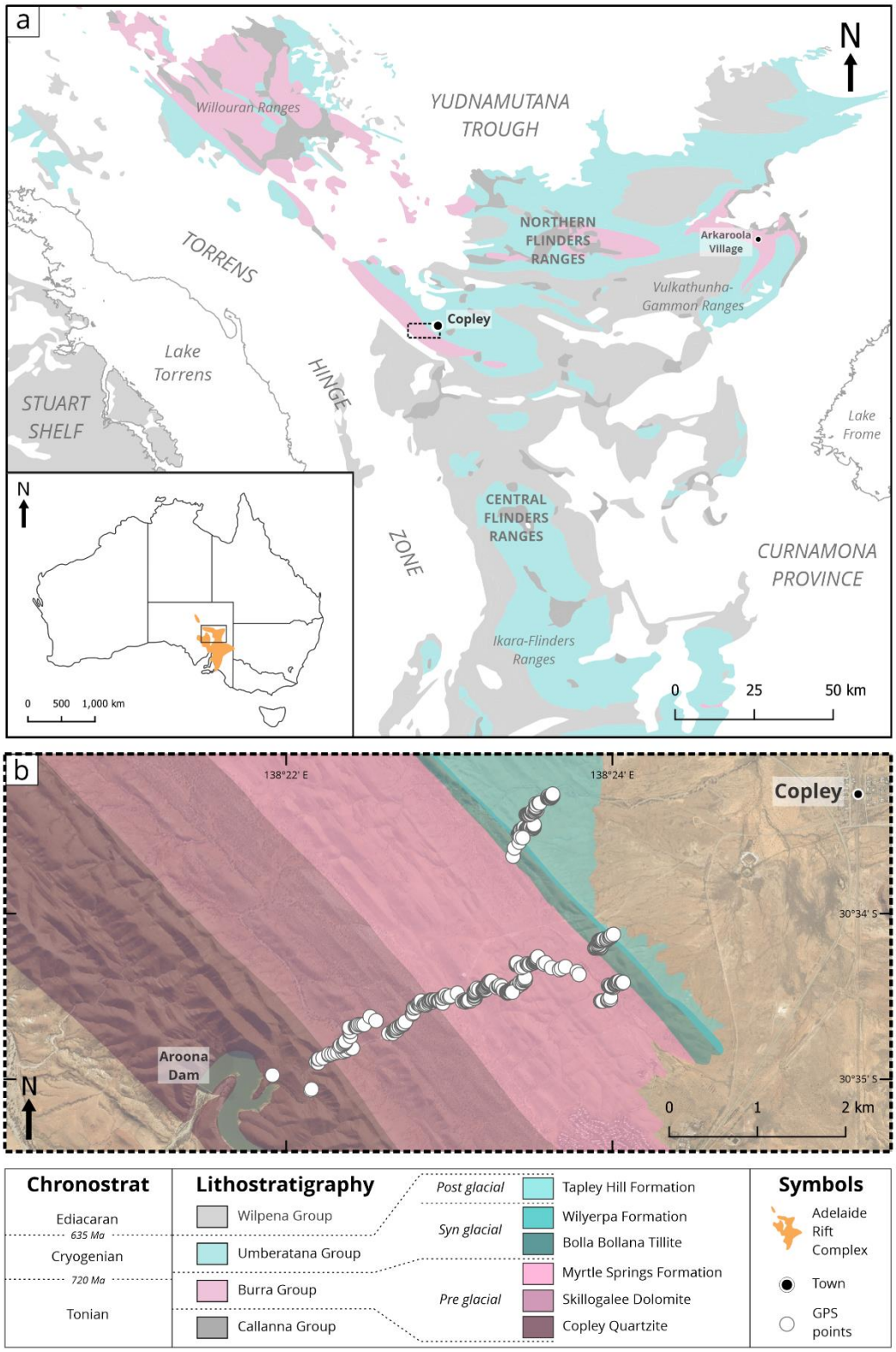

Figure 1: (a) Geological map of Tonian and Cryogenian lithostratigraphic groups in the Adelaide Rift Complex, northern Flinders Ranges, South Australia. Insert shows position of Adelaide Rift Complex within Australia. (b) Fieldwork location southwest of Copley township and northeast of Aroona Dam. Global chronostratigraphic nomenclature. Local lithostratigraphic nomenclature. GPS points recorded along log highlighted in white circles.

deglacial strata (Preiss et al., 2011; Cox et al., 2018). The former is composed of massive and stratified diamictite with conglomerate, quartzite and siltstone interbeds (Preiss, 1987; Le Heron et al., 2014), while the latter comprises graded diamictite, sand and silt with dropstones (Link & Gostin, 1981; Young & Gostin, 1988; 1991; Preiss et al., 2011; Counts, 2017). These syn-glacial units have previously been interpreted to have been deposited from ice sheet advance and retreat in a glaciomarine setting (Link & Gostin, 1981; Preiss, 1987; Young & Gostin, 1991; Preiss et al., 2011; Le Heron et al., 2014). The post-glacial succession examined here is represented by the Tapley Hill Formation (Preiss et al., 1998) (Figure 1). Laminated shale and fine-grained limestone and dolomite are the dominant lithologies, interpreted to have been deposited in a basinal setting in a stratified ocean (Preiss, 1987; Giddings & Wallace, 2009; Counts, 2017).

Maximum age constraints on the timing of deposition of the studied section are provided by a U–Pb zircon age of 802 ± 10 Ma from the Rook Tuff that lies within the Callana Group of the Willouran Ranges (Fanning et al., 1986), stratigraphically below the Burra Group (Preiss et al., 2009; Lloyd et al., 2020). Elsewhere in the Flinders Ranges, volcanic rocks at the base of the Burra Group are dated at 788 ± 6 Ma (Boucaut Volcanics, Armistead et al., 2020) and 794 ± 4 Ma (Kooringa Member, Preiss et al., 2009). This is stratigraphically equivalent to the base of the Skillogalee Dolomite (Lloyd et al., 2020). A precise tuff age of 663.03 ± 0.11 Ma (zircon U–Pb CA-ID-TIMS) was identified from the Wilyerpa Formation at the same location as this study (Cox et al., 2018), constraining the timing of deglaciation.

2.4 Methods

2.4.1 Fieldwork

The field area for this study was located 2 km southwest of Copley township in the northern Flinders Ranges (Figure 1). The section was measured at metre-resolution using a tape measure and handheld GPS. Detailed descriptions of grain size, sedimentary structures, bedding thicknesses and palaeocurrent direction were recorded. Carbonate samples were collected from dolomite and magnesite beds for geochemical analyses.

2.4.2 Facies Analysis

The sedimentary log produced in the field was then digitised using EasyCore software. Palaeocurrent directions were digitised and analysed using the software Stereonet. Using a lithostratigraphic approach, lithofacies were classified based on grain size and sedimentary structures, which enabled interpretation of depositional processes. Lithofacies were then grouped into facies associations, determined by the stacking pattern of facies. Each facies association represents multiple depositional processes in a genetically related interval, facilitating interpretation of depositional environment.

2.4.3 Sequence Stratigraphy

The stratigraphic distribution and grain size trends of lithofacies allowed packages of sediment to be subdivided into intervals, known as systems tracts (Vakarelov & Ainsworth, 2013). These intervals are largely controlled by variations in accommodation space and sediment input, and are bounded by time equivalent surfaces called sequence boundaries (e.g. Vakarelov &

Ainsworth, 2013; Feldman et al., 2014; Kunzmann et al., 2019; 2020). The interpreted systems tracts within the measured section were used to infer temporal changes in base level through the Tonian to Cryogenian at this site.

2.4.4 Carbonate leaching for elemental analysis

The leaching procedure for the elemental analysis was modified from Halverson et al. (2010) and Liu et al. (2014) to selectively leach carbonate phases, thus avoiding or minimising possible clastic contamination. Carbonate samples were drilled along laminae to target the carbonate matrix, making sure to avoid veins, weathered surfaces and clasts. The resultant rock powder was first reacted with a 1M ammonium acetate ($NH_4CH_3CO_2$) solution to remove exchangeable cations associated with clays and/or detrital phases. To separate the carbonate-bearing fraction from the acetate supernatant, the solution was then sonicated for 20 minutes and centrifuged for 10 minutes at 4000 rpm. The remaining powders were then leached twice with 0.2M acetic acid (CH_3COOH) to extract the carbonate-associated elements, then sonicated and centrifuged using the parameters from the previous step. The supernatant was set aside for inductively coupled plasma (ICP) analysis.

2.4.5 Major and trace element analysis

The supernatant was digested with 2% nitric acid (HNO_3) and split into aliquots of ~1:1000 and ~1:10000 dilutions for major and trace elemental analysis, respectively. Calibration solutions were prepared using standards from multi-element stock standard solutions and diluting with 2% nitric acid ranging from 0 ppb to 1000 ppb. Samples were measured along with dolomite standard JDo-1, and possible effect of contamination was monitored using JDo-1 standard and blanks. Elemental analysis was performed in Adelaide Microscopy at the University of Adelaide using an Agilent 8900x triple quad (QQQ) -ICP-MS instrument, with typical accuracy and precision on elemental concentration data within 5% (2 SD). Geochemical data can be found in Supplementary Data 1.

2.5 Sedimentary Log

A summary graphic sedimentary log of the entire measured section is presented in Figure 2. It has a total stratigraphic thickness of 3,150 m at an average dip of ~53° towards NNE. The section is composed of three pre-glacial formations, two syn-glacial formation and one post-glacial formation (Figure 1).

The pre-glacial formations in the Copley section are ~2,600 m thick and are represented by both siliciclastic and carbonate lithofacies of the Copley Quartzite, Skillogalee Dolomite and Myrtle Springs Formation. The Bolla Bollana Tillite and Wilyerpa Formation characterise syn-glacial deposition, are ~150 m thick, and represents the base of the Cryogenian in Copley. The top of the succession is represented by the post-glacial Tapley Hill Formation, which is >400 m thick and is represented by siliciclastic and carbonate lithofacies.

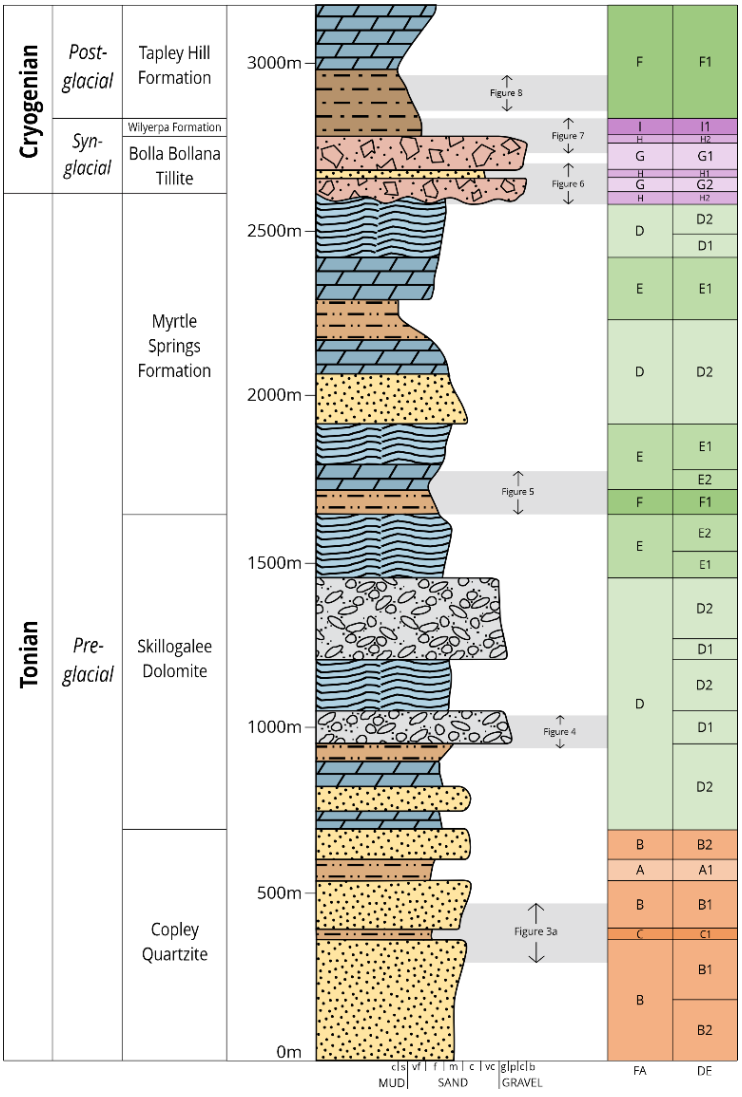

Legend for all sections

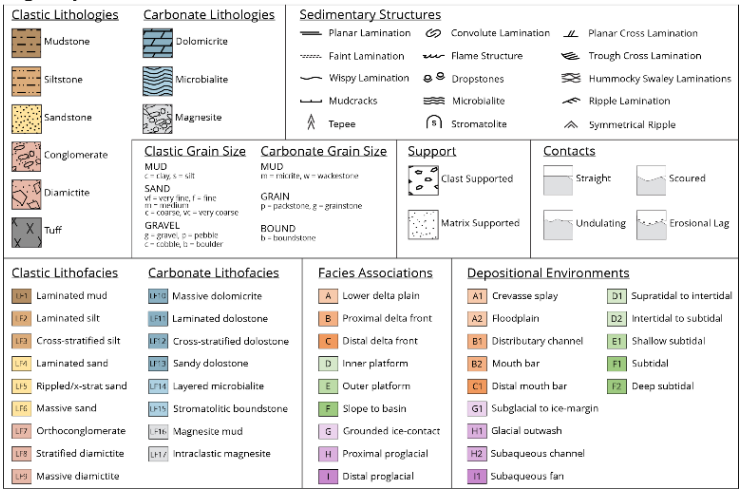

Figure 2: Generalised sedimentary log through complete Tonian-Cryogenian section in northern Flinders Ranges, South Australia. FA=Facies Association, DE = Depositional Environment. Position of detailed logged section from each formation highlighted in grey. Legend for symbology in all sedimentary logs.

2.6 Facies Analysis

Detailed excerpts from each formation are presented in Figures 3 – 7, presenting key lithofacies and sedimentary structures observed. Seventeen lithofacies were classified (Table 1), nine clastic and eight carbonate. The pre-glacial succession encompasses twelve lithofacies, both clastic and carbonate; the syn-glacial succession comprises seven clastic lithofacies; and the post-glacial is characterised by one clastic and two carbonate lithofacies.

Nine facies associations have been interpreted (Table 2); three deltaic, three carbonate platform and three glaciomarine facies associations. Depositional processes within facies associations were used to identify eighteen specific depositional environments throughout the section (Table 2); nine pre-glacial depositional environments, four syn-glacial, and one post-glacial.

2.6.1 Copley Quartzite

2.6.1.1 Observations

The Copley Quartzite (~700 m thick) is composed of laminated, rippled and cross-stratified sandstone, with minor laminated siltstone and mudstone. The base of the formation is characterised by 1 m to 14 m thick coarsening-up beds, comprises laminated sandstone (LF4) at the base to cross-stratified and rippled sandstone (LF5) towards the top. Laminated sandstone is represented by planar and wavy laminations, and large (up to 2 m) tabular and small (<10 cm) ripple cross-stratification comprise cross-stratified lithofacies. There are also rare wavy flaser beds developed in this lithofacies. Bed tops predominantly develop asymmetrical ripples with minor symmetrical bedforms, as well as subaqueous and desiccation cracks. Palaeocurrent data from the unidirectional current ripples show a strong SE-directed flow with minor NW, NE and SW orientated flow directions (Figure 3b). The shrinkage cracks superimposed on some of these rippled bedding surfaces are characterised by branching, sinuous and curlicue geometries.

Up-section are two siltstone dominated successions with interbedded sandstones, separated by normally graded beds of laminated, rippled and cross-stratified sandstone. The first 12 m siltstone package is composed of fining-up and coarsening-up beds of thinly laminated siltstone (LF2). The other 13 m package also comprises siltstone, coarsening-up ripple cross-stratified sandstone and fining-up laminated sandstone. The laminated siltstone intervals have developed load structures, expressed as detached pseudonodules that deform the surrounding laminae.

The top of the Copley Quartzite is characterised by laminated siltstone with interbedded mudstone (LF1) and sandstone, where deposition of coarser sediment increases up-section. Beds are between 2 m and 10 m thick and dominantly inverse graded.

2.6.1.2 Interpretations

The predominant SE palaeoflow for the majority of the unidirectional bedforms in the base of the formation are perpendicular to the NE–SW trending palaeocoastline in this region (Preiss, 1987; Powell, 1994). The basinward (offshore) orientation of these structures, as well as the lack of recognisable tidally induced structures, including herringbone crossbedding, tidal

Table 1: Lithofacies and their subsequent characteristics and depositional processes and occurrence throughout the measured section. LF = lithofacies. *CQ* = Copley Quartzite, *SD* = Skillogalee Dolomite, *MSF* = Myrtle Springs Formation, *BBT* = Bolla Bollana Tillite, *WF* = Wilyerpa Formation, *THF* = Tapley Hill Formation

Lithofacies	**Descriptions**	**Depositional Processes**	**Occurrence**
LF1 Laminated mudstone	Fresh medium grey to dark brown/blue; weathered red, pink, purple, blue green and white; planar and wavy laminated (mm to cm scale; rare inverse grading, mud to very fine silty mud (*CQ*); rare crude laminations and kaolinite (*MSF*); dropstones (gravel to cobble clasts), soft sediment deformation (convolute stratification, simple load cast and flame structures), subcritical (15° climb) climbing ripples (~20 cm stoss, 5 cm foresets) (*WF*)	Planar laminations - settled out of suspension, lower flow regime, slow sedimentation rate (Boggs, 2014; Yawar & Schieber, 2017); ice-rafted debris - transported in floating ice and deposited as rainout (e.g. Link & Gostin, 1981; Young & Gostin, 1988; 1991; Powell, 2002; Eyles et al., 2007; Preiss et al., 2011; Boggs, 2014; Le Heron et al., 2013; 2014; 2021; Le Heron & Busfield, 2016); soft sediment deformation - liquefaction induced from rapid sedimentation (Postma, 1983; Stromberg & Bluck, 1998; Moretti et al., 2001); convolute laminations - bottom current reworking (Shanmugam, 1997); simple load casts and flame structures - formed in response to differential sediment densities or lateral loading during liquefaction (Owen, 2003); subcritical climbing ripples - deceleration of turbulent current activity and net deposition (high sediment supply and rapid sedimentation rate), stoss-side erosion and bedform migration (Ashley et al., 1982; Young & Gostin, 1988; Cheel, 1990; Baas et al., 2000; Jobe et al., 2012; Boggs, 2014; Le Heron & Busfield, 2016; Maciaszek et al., 2019)	Copley Quartzite, Myrtle Springs Formation, Wilyerpa Formation, Tapley Hill Formation
LF2 Laminated siltstone	Fresh light grey/blue/purple to dark brown; weathered white, yellow, orange, pink, red; planar and wavy laminated (mm to cm scale); occasionally crude planar laminated (mm scale) and massive; occasional normal and inverse grading, silt to very fine sandy silt; soft sediment deformation (convolute stratification, load and fold and drag structures) (*CQ, SD*); stacked and linear, detached pseudonodules, fine sand, inclined, ~10 cm - 15 cm length, ~2 cm – 8 cm thickness (*CQ*); horizontally aligned pseudonodules, fine sand, smooth and hemispherical, 10 cm and 20 cm lengths, 2 cm and 10 cm thicknesses (*CQ*); occasionally dolomitic; folded and crumpled laminations (*SD*); rare gravel lags in base of bed (*MSF*)	Planar laminations – *same as LF1*; soft sediment deformation – *same as LF1*; pseudonodules - response to differential densities (density loading) or lateral load variations (uneven loading) (Owen, 2003; Oliveira et al., 2009; 2011; Li et al., 2016; Tinterri et al., 2016), inclination from vertical gravitational instability and lateral shear stress (Dasgupta, 1998; Moretti et al., 2001); gravel lag - winnowing unidirectional flows, high sediment supply and rapid deposition (Boggs, 2014)	All formations
LF3 Cross stratified siltstone	Light grey/purple to green; very fine silt; small (2cm and 5 cm foresets) concave-down (hummock) and concave-up (swale) cross laminations (*MSF*); cross	Hummocky and swaley cross stratification - suspended load, decreasing flow regime (storm activity), waning combined unidirectional and oscillatory flow (Nottvedt & Kreisa, 1987; Arnott & Southard, 1990; Cheel, 1991; Duke et	Myrtle Springs Formation,

	sets marked by curved erosional surfaces; ripple cross laminations (cm scale foresets) (*BBT*)	al., 1991; Cheel & Leckie, 1993; Dumas & Arnott, 2006; Reading, 2009; Basilici et al., 2012; Boggs, 2014); ripple cross lamination – bedload and suspended load; lower flow regime, unidirectional flow, downcurrent migration of small sinuous and catenary ripples (Ashley, 1990; Reading, 2009; Boggs, 2014; Momta et al., 2015; Jorissen et al., 2018)	Bolla Bollana Tillite
LF4 Laminated sandstone	Fresh light grey/yellow/brown; weathered white, orange, purple to dark brown/red/black; feldspathic and quartzitic; normal and inverse grading, very fine to very coarse sand; planar and wavy laminated (mm to cm scale); occasionally massive; asymmetrical rippled on bedding surfaces (mm to cm scale wavelengths), straight, sinuous and catenary ripple crests with minor erosion of some sinuous crests (*CQ*); rare shrinkage cracks, branching triple junction cracks superimposed on eroded sinuous ripple surfaces, sinuous and curlicue cracks deposited in troughs of sinuous and catenary ripple sets (*CQ*)	Planar laminations - traction transport as bedload, upper flow regime, unidirectional laminar flow (Cheel, 1990; Bridge, 2009; Boggs, 2014; Jorissen et al., 2018); wavy laminations - bedload and suspended load, lower flow regime, unidirectional flow (Colquhoun, 1995; Bridge, 2009; Boggs, 2014; Momta et al., 2015; Jorissen et al., 2018); straight to catenary ripple crests - increasing flow velocities and/or decreasing water depth (Boggs, 2014); orthogonal branching cracks - desiccation during exposure (Plummer & Gostin, 1981; Boggs, 2014); sinuous and curlicue cracks - subaqueous shrinkage of cohesive sediment in ripple troughs, filled with overlying sand (Plummer & Gostin, 1981; Pfluger, 1999; Gehling, 2000; McMahon et al., 2016)	All pre-glacial formations
LF5 Rippled and cross stratified sandstone	Fresh light grey/yellow/brown, weathered white, orange, purple to dark brown/red; feldspathic and quartzitic; normal and inverse grading, very fine to coarse sand (*CQ*, *MSF*); symmetrical rippled (mm to cm scale wavelengths), straight crests with minor bifurcations and terminations (*CQ*); interference rippled (cm scale wavelengths), symmetrical and asymmetrical (*SD*); wavy connected mud flasers (mm thickness), concavely and convexly bowed, fill sand ripple troughs and overlie sand ripple crests (*CQ*); tabular cross stratified (0.02m – 2m foresets) (*CQ*); small ripple cross stratification (*CQ*), occasional mud drapes on foresets (10 cm foresets) (*MSF*); concave-down (hummock) and concave-up (swale) cross laminations (10 cm foresets), cross sets marked by curved erosional surfaces (*SD*)	Symmetrical ripples - traction transport as bedload, lower flow regime, oscillatory flow (Reading, 2009; Boggs, 2014; Counts et al., 2016), straight to bifurcating and terminating crests, decreasing flow velocities (Nelson & Voulgaris, 2014); interference ripples - lower flow regime, bidirectional and unidirectional flow (Colquhoun, 1995; Bridge, 2009; Boggs, 2014; Momta et al., 2015; Jorissen et al., 2018), two sets of current directions intersecting at high angles (Gough, 2020); heterolithic laminations - bedload and suspended load, alternating high and low energy flows, rippled sand, energetic unidirectional or bidirectional flow, mud drapes, settle out of suspension during slackwater (Reineck & Wunderlich, 1968; Bhattacharya, 1997; Daidu, 2013; Boggs, 2014); tabular cross beds - traction transport as bedload, lower flow regime, unidirectional flow, downcurrent migration of straight crested dunes (Ashley, 1990; Bridge, 2009; Boggs, 2014; Momta et al., 2015); ripple cross-stratification – *same as LF3*; mud drapes - settle out of suspension during slackwater (Reineck & Wunderlich, 1968; Bhattacharya, 1997; Daidu, 2013; Boggs, 2014); hummocky and swaley – *same as LF3*	All pre-glacial formations
LF6 Massive sandstone	Light grey/yellow/brown/blue to dark red; immature, lithics, angular to sub-rounded, fine sand to gravel; massive; occasional thin planar laminations; rare normal grading, very fine to coarse sand (*BBT*); rare	Hyperconcentrated debris flows, rapid deposition; normal grading – high density turbidity current (Lowe, 1982; Kneller, 1995; Shanmugam, 2000; Winsemann et al., 2009; Talling et al., 2012; Le Heron & Busfield, 2016); scoured base - erosion from high velocity flow, filled by coarse material	Bolla Bollana Tillite,

	scoured base (*BBT*); rare thin, heavy mineral ripple cross-laminations (*WF*)	during waning stage of flow (Fielding, 2006; Bridge, 2009; Boggs, 2014); cross-laminations – *same as LF2* OR low density turbidity current (Shanmugam, 1997; Talling et al., 2012)	Wilyerpa Formation
LF7 Ortho-conglomerate	Fresh light grey/brown/grey/green/blue, weathered dark grey/blue/black; clast supported (up to 70% clasts); very coarse sand to cobble clasts (sub-angular to well-rounded); massive; occasionally pierces top surface (*WF*)	Subaqueous hyperconcentrated debris flows, rapid deposition, non-cohesive, laminar flows (Lowe, 1982; Kneller, 1995; Shanmugam, 2000; Winsemann et al., 2009; Talling et al., 2012; Le Heron & Busfield, 2016)	Bolla Bollana Tillite, Wilyerpa Formation
LF8 Stratified diamictite	Light blue/purple/green/brown/red; thin (cm scale) laminations; clast-poor (<15% clasts), gravel clasts and casts, silt to fine sand matrix (*BBT*); clast-supported (50-60% clasts), carbonate pebbles and sand pebbles/cobbles, casts, silt to very fine sand matrix (*WF*)	Subaqueous sediment gravity flow (Young & Gostin, 1988; Anderson, 1989; Eyles et al., 2007; Le Heron et al., 2013; 2014); stratification - sorting through clast settling (Anderson, 1989) OR current reworking (Boggs, 2014)	Bolla Bollana Tillite, Wilyerpa Formation
LF9 Massive diamictite	Light green/yellow; matrix to clast supported (<5% - 60% clasts), pebble to boulder carbonate and quartz clasts, conglomerate fragments and casts, mud to fine sand matrix; rare inverse grading, clast-poor gravel to clast-rich boulder (BBT)	Deposition directly from the ice as melt-out (Link & Gostin, 1981; Young & Gostin, 1988; Preiss et al., 2011) OR cohesive debris flows, moderate to high strength (Talling et al., 2012); rapid deposition (Young & Gostin, 1988; Anderson, 1989; Eyles et al., 2007; Le Heron et al., 2013; 2014), kinetic sieving during flows (Legros, 2002; Talling et al., 2012; Le Heron et al., 2014)	Bolla Bollana Tillite, Wilyerpa Formation
LF10 Massive dolostone	Fresh blue/grey, weathered yellow/pink/red; micritic texture; rare elephant skin weathering style	Authigenic precipitation from the water column, due to chemical, salinity or temperature fluctuations (Tucker, 1982; Tucker & Wright, 2009; Flugel, 2013) OR syn-sedimentary dolotimisation (mimetic replacement), carbonates retain primary textures and water column geochemical signatures (Hood et al., 2011; 2018; Hood & Wallace, 2012; 2014; Shuster et al., 2018)	Tapley Hill Formation
LF11 Laminated dolostone	Fresh light yellow/brown/pink/blue/grey, weathered yellow/pink; occasional fine crystalline texture; elephant skin weathering style; thinly (mm to cm scale) planar laminated with fine (mud to silt) clastic material; occasionally wavy laminated and massive; small (cm scale) tepee structures, chert and breccia fills space under tepee crests (SD)	Carbonate material – *same as LF10* OR secondary diagenetic recrystallisation (non-mimetic replacement), poorly preserves original carbonate textures (Tucker & Wright, 2009; Flugel, 2013); clastic material - transported as suspended load, low energy tidal currents (Tucker & Wright, 2009; Chiarella et al., 2017; O'Connell et al., 2020); tepee structures - fracturing/crustal cracking, periods of desiccation (Asserto & Kendall, 1977; Kendall & Warren, 1987; Belperio, 1990; Frank & Fielding, 2003; Tucker & Wright, 2009; O'Connell et al., 2020)	Skillogalee Dolomite, Myrtle Springs Formation, Tapley Hill Formation
LF12 Cross stratified dolostone	Yellow/brown; fine crystalline texture; elephant skin weathering style; ripple cross-laminations (5 cm foresets), obliquely stacked in opposing directions	Carbonate material – *same as LF10 and LF11*; ripple cross-laminations – *same as LF3*; bimodal palaeoflow - deposition from tidal processes (Ashley,	Myrtle Springs Formation

		1990; Colquhoun, 1995; Chakrabarti, 2005; Reading, 2009; Daidu, 2013; Boggs, 2014; Thomson et al., 2014; Momta et al., 2015)	
LF13 Sandy dolostone	Fresh dark blue/grey/purple, weathered light grey/brown; crystalline texture; normal and inverse grading, fine to very coarsely crystalline (*MSF*); thinly (mm scale) wavy laminated, interlaminated fine sand; minor crudely laminated to massive (*SD*)	Carbonate material – *same as LF11*; clastic material - transported as suspended load, moderate to high energy wave action (Wanless et al., 1988; Tucker & Wright, 2009)	Skillogalee Dolomite, Myrtle Springs Formation
LF14 Layered microbialite boundstone	Light blue/grey to yellow; thin (mm to cm scale) stratiform and undulating dolomite laminations, interlaminated mud; small (cm scale) tepee structures, chert and breccia fills space under tepee crests; occasional large (up to 10 cm) tepee structures in stratiform microbialites (*SD*); occasional soft sediment deformation, small (1 cm) load and flame structures (*SD*); rare inverse grading, very finely to medium crystalline (*MSF*)	Microbial material - precipitated in-situ (authigenic) (Tucker, 1982; Tucker & Wright, 2009; Flugel, 2013); clastic sediment - trapped and bound by microbial material (Wright, 1984; Tucker & Wright, 2009; O'Connell et al., 2020); stratiform microbialite; suspended load, low flow regime, gentle current action (Tucker & Wright, 2009; Chiarella et al., 2017; O'Connell et al., 2020); small tepee structures – *same as LF11*; large tepee structures - crystallisation expansion in carbonate-supersaturated subaqueous conditions (Shinn, 1969; Kendall & Warren, 1987; O'Connell et al., 2020); soft sediment deformation – *same as LF1*	Skillogalee Dolomite; Myrtle Springs Formation
LF15 Stromatolitic boundstone	Light blue/grey to yellow; thin (cm scale) domical and columnar dolomite laminations, interlaminated (silt to fine sand) clastic material; inverse grading, very fine to medium crystalline (*SD*); small (30 cm wide, 15 cm high) columnar biostrome buildup (*SD*); small (cm scale) nested domical bioherm (*SD*); large openly spaced (3 cm wide, 5 cm high) domical and (15 cm wide, 40 cm high) columnar buildup, brecciated material and chert replacement (*MSF*)	Microbial material – *same as LF14*; clastic sediment – *same as LF14*; stromatolitic buildup - suspended load, higher energy wave activity (Hoffman, 1974; 1976; Wanless et al., 1988; Tucker & Wright, 2009; Jahnert & Collins, 2012; Kunzmann et al., 2019); columnar buildups – *Baicalia burra* (Preiss, 1973; Belperio, 1990)	Skillogalee Dolomite, Myrtle Springs Formation
LF16 Magnesite mudstone	Light grey/cream to white; micritic; massive to laminated (cm scale); rare small (cm scale) tepee structures (*SD*)	Magnesite material - precipitated in-situ, evaporative magnesium-rich water column (Mur & Urpinell, 1987; Warren, 1990; Melezhik et al., 2001); small tepee – *same as LF11*	Skillogalee Dolomite
LF17 Intraclastic magnesite	Light grey/cream to white; massive to crudely laminated (cm scale); occasionally conglomerate (clast-rich), sub-angular to rounded clasts, mud to sand sized matrix; normal grading, gravel to very coarse-grained; rare undulating top surfaces; rare soft sediment deformation (convolute)	Magnesite material - *same as LF16*; conglomerate - reworked sedimentary magnesite by storm activity (Uppill, 1980; Belperio, 1990; Preiss, 2000; Frank & Fielding, 2003; Counts, 2017); soft sediment deformation – *same as LF1*	Skillogalee Dolomite

Table 2: Facies associations and their constituent lithofacies and depositional environments. LF = lithofacies.

Facies Association	Constituent lithofacies	Depositional Environment
River Delta		
A – Lower delta plain	Major: LF2, LF4 Minor: LF1, LF5	A1 – Splay A2 - Floodplain
B – Proximal delta front	Major: LF4, LF5	B1 – Distributary channel B2 – Mouth bar
C – Distal delta front	Major: LF2, LF4 Minor: LF5	C1 – Distal mouth bar
Carbonate Platform		
D - Inner platform	Major: LF2, LF4, LF11, LF14 Minor: LF5, LF12, LF13, LF15, LF16, LF17	D1 – Supratidal to intertidal D2 – Intertidal to lagoonal
E – Outer platform	Major: LF11, LF15 Minor: LF1, LF2, LF4, LF13, LF14	E1 – Lagoon E2 – Reef margin
F – Slope to basin	Major: LF1, LF11 Minor: LF2, LF3, LF10	F1 – Subtidal
Glaciomarine		
G – Grounded ice-contact	Major: LF8, LF9	G1 –Subglacial to ice-margin
H – Proximal proglacial	Major: LF2, LF3, LF6 Minor: LF7, LF8, LF9	H1 – Subaqueous glacial outwash H2 – Proximal subaqueous channel
I – Distal proglacial	Major: LF1, LF2 Minor: LF6, LF7, LF8, LF9	I1 – Distal subaqueous fan

bundles, reactivation surfaces and mud-drapes on ripple cross-stratified foresets, favours fluvial driven processes rather than tidal influence (Ashley, 1990; Colquhoun, 1995; Daidu, 2013; Momta et al., 2015). However, rare heterolithic wavy and flaser bedding was likely developed from alternating high and low energy tidal currents (Reineck & Wunderlich, 1968; Bhattacharya, 1997; Olariu & Bhattacharya, 2006; Daidu, 2013; Boggs, 2014). Minor symmetrical ripple structures deposited under oscillatory flow conditions may indicate the infrequent presence of waves (Olariu & Bhattacharya, 2006; Reading, 2009; Boggs, 2014; Counts et al., 2016). Due to the orthogonal geometry and association with flat-topped ripples, branching shrinkage cracks on bedding surfaces were likely formed from desiccation during exposure (Plummer & Gostin, 1981; Boggs, 2014). Conversely, sinuous and curlicue cracks in ripple troughs were probably the result of subaqueous shrinkage of cohesive sediment (Plummer & Gostin, 1981; Pflüger, 1999; Gehling, 2000; McMahon et al., 2017). We suggest that this indicates a deltaic environment (Boyd et al., 1992; Yang et al., 2005; Daidu, 2013), such as a proximal delta front (B), which is consistent with regional interpretations for the Copley Quartzite (Preiss, 1987). Although beach and tidal flat environments are common coastal systems, there is insufficient wave and tidal influence to invoke these (Boyd et al., 1992; Yang et al., 2005; Daidu, 2013; Counts et al., 2016). Distributary channels (B1) and mouth bars (B2) are common architectural elements within the delta front setting and are intimately linked within deltaic parasequences (Plink-Björklund & Steel, 2005; Olariu & Bhattacharya, 2006; Gani & Bhattacharya, 2007; Olariu et al., 2010; Schomacker et al., 2010; Ahmed et al., 2014; Jorissen et al., 2018). Within this facies association, successions solely composed of unidirectional structures are interpreted to have been deposited in distributary channels (e.g.

Plink-Björklund & Steel, 2005; Gani & Bhattacharya, 2007; Olariu et al., 2010; Ahmed et al., 2014; Momta et al., 2015; Counts et al., 2016; Jorissen et al., 2018), where desiccation cracks on top beds probably developed during channel abandonment (Nichols, 1987; Nichols & Fisher, 2007). Packages of unidirectional and bidirectional structures that deposited from mixed fluvial, tidal and wave processes could represent mouth bars (e.g. Allen, 1983; Plink-Björklund & Steel, 2005; Gani & Bhattacharya, 2007; Olariu et al., 2010; Schomacker et al., 2010; Momta et al., 2015; Counts et al., 2016; Jorissen et al., 2018).

In the middle portion of the formation, thinly laminated siltstone intervals were probably deposited out of suspension in an interpreted low energy setting with slow sedimentation rate (Boggs, 2014; Yawar & Schieber, 2017). Soft sediment deformation structures in some siltstone beds are interpreted to have formed in response to liquefaction from differential densities (density loading) or lateral load variations (uneven loading) (Owen, 2003; Oliveira et al., 2009; 2011; Li et al., 2016; Tinterri et al., 2016). These soft sediment deformation structures are consistent with rapid deposition from turbidity flows in a slope environment (Stromberg & Bluck, 1998; Moretti et al., 2001; Oliveira et al., 2011), in particular a distal delta front (C) (e.g. Postma, 1983; Olariu & Bhattacharya, 2006; Gani & Bhattacharya, 2007; Olariu et al., 2010; Ahmed et al., 2014; Li et al., 2016; Tinterri et al., 2016; Jorissen et al., 2018). Within this setting, deposition as a mouth bar (C1) is interpreted as it would account for the high sedimentation rate, soft sediment deformation, unidirectional structures and mix of fine and coarse-grained clastic material (e.g. Plink-Björklund & Steel, 2005; Gani & Bhattacharya, 2007; Schomacker et al., 2010; Ahmed et al., 2014; Jorissen et al., 2018).

The same processes likely deposited the laminated sandstone, siltstone and mudstone in the top of the Copley Quartzite as the comparable lithofacies previously outlined in the proximal and distal delta front environments, respectively. The dominance of traction structures and lack of wave or tidally induced structures supports fluvial deposition without marine influence, which is consistent with a more continental, fluvio-deltaic setting (Boggs, 2014; Counts et al., 2016; Jorissen et al., 2018). Channels and floodplains are common architectural elements of these fluvial dominated systems (Bridge, 2009). Preferential deposition of fine-grained material and absence of channelisation, including channel scours and lateral accretion surfaces (Counts et al., 2016), supports deposition as floodplain sediments (Bridge, 2009; Fielding, 2010; Boggs, 2014; Burns et al., 2017; Gulliford et al., 2017). These deposits are congruent with a lower delta plain (A), where mudstone and siltstone packages could reflect low energy floodplain deposits (A2) and sandstone and siltstone successions could have been deposited as a splay (A1) under high energy conditions (e.g. Roberts, 1997; Bridge, 2009; Fielding, 2010; Boggs, 2014; Gulliford et al., 2014; 2017; Burns et al., 2017). This interpretation is corroborated by minor SW-oriented palaeocurrent data in sand beds, which develop geometries tangential to SE oriented river discharge (e.g. Burns et al., 2017).

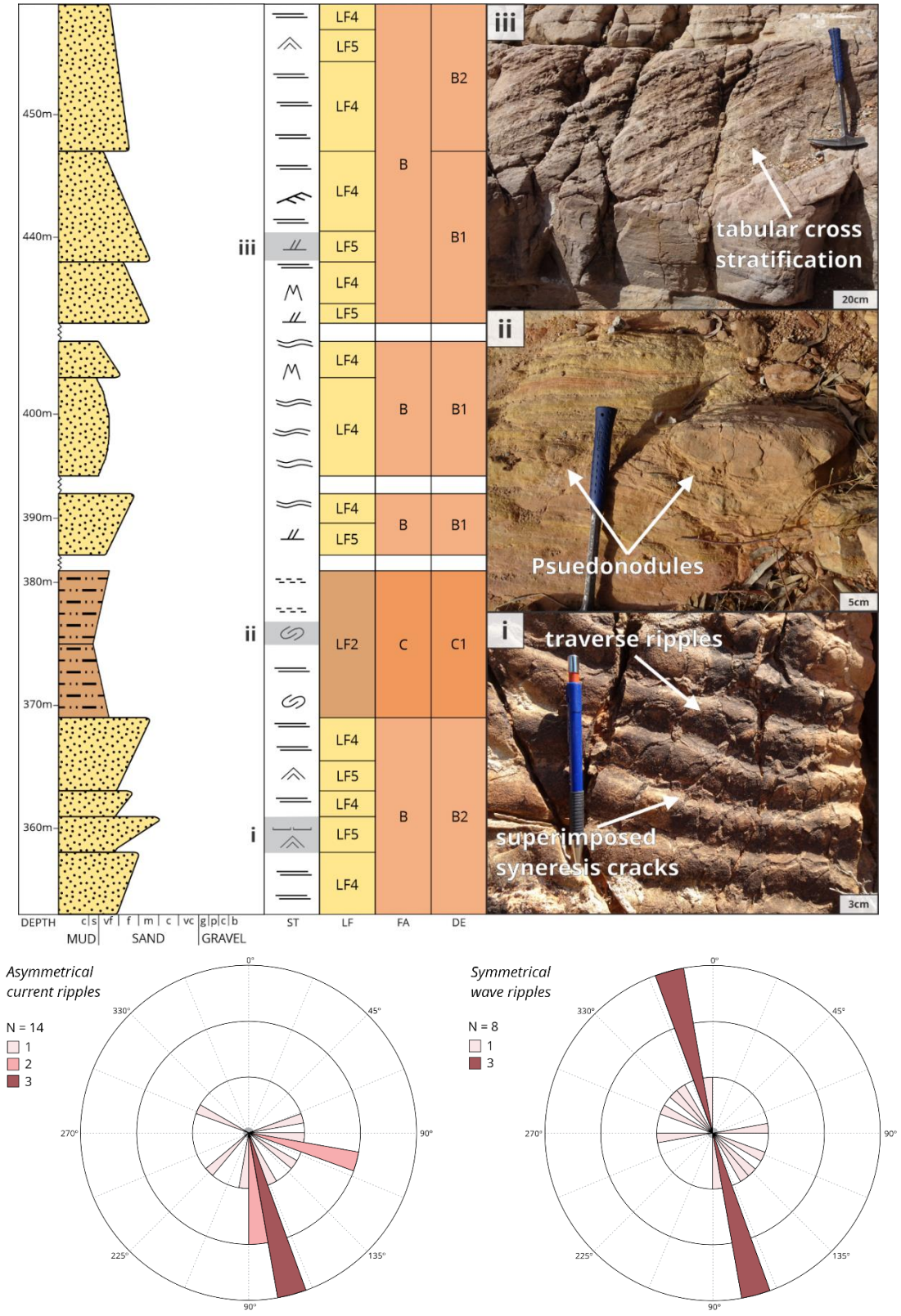

Figure 3: (a) Lithostratigraphic logged section through Copley Quartzite in northern Flinders Ranges, South Australia. FA = Facies Association, DE = Depositional Environment, LF = Lithofacies, ST = Structure. (i) unidirectional traverse current ripple superimposed with syneresis cracks. (ii) fine sandstone psuedonodules in siltstone. (iii) large scale tabular cross-stratified sandstone. (b) Rose diagrams for palaeocurrent data measured from rippled bedding surfaces in Copley Quartzite.

2.6.2 Skillogalee Dolomite

2.6.2.1 Observations

Interbedded siliciclastics and carbonates, the latter including both dolomite and magnesite mineralogies, characterises the Skillogalee Dolomite (~930 m thick). Siliciclastic and carbonate lithologies comprise 37% (siltstone 24%, sandstone 13%) and 63% (dolostone 23%, microbialite 28% and magnesite 12%) of the total thickness of the formation, respectively (Figure 4). A 14 m break in exposed outcrop separates the Copley Quartzite with the overlying Skillogalee Dolomite. The lower portion of the formation comprises fining and coarsening-up (2 m to 8 m thick) clastic beds, interbedded with dolostone. Siltstone (LF2) lithofacies are planar laminated and massive, while laminated sandstone (LF4) is planar and wavy, appearing faint in highly quartzitic beds. Dolostone (LF11) units are often massive and ferruginous. This clastic dominated package is overlain by 4 m to 12 m sandy dolostone (LF13) beds with thinner (< 5 m) wavy laminated, dolomitised siltstone beds. Clastic dominated deposition returns, represented by 2 m to 14 m thick wavy laminated sandstone and siltstone beds. Minor interference rippled sandstone (LF5) beds, represented by symmetrical and asymmetrical ripples, record strong NNW-SSE and minor ESE palaeoflow directions, respectively.

These successions grade into a variable carbonate dominated package with thinly (~2 m thick) interbedded and interlaminated dolostone, microbialiate, magnesite and minor siltstone and sandstone. Minor siltstone units convolute, expressed as folded and crumpled laminations. Dolostone beds are massive or wavy laminated, with small (cm scale) tepee structures, where breccia and chert fills the space under the tepee crests. Layered microbialite (LF14) and stromatolitic boundstone (LF15) constitute the microbialite lithofacies. The former is represented by stratiform to undulating dolomitic laminations, with small-scale tepee structures and load and flame soft sediment deformation structures. Stromatolitic boundstones have developed nested domical bioherms with chert bases. Magnesite mudstone (LF16) and intraclastic magnesite (LF17) constitute the remaining carbonate lithofacies. The fine-grained beds are micritic with rare small tepee structures, while the conglomerates are normally graded, massive to crudely laminated, with gravel to very coarse-grained sub-angular to rounded clasts, mudstone to sandstone sized matrix and undulating top surfaces.

Towards the top of the formation are 2 m to 10 m thick beds of layered microbialite, stromatolitic buildups and minor sandstone. Large (up to 10 cm) tepee structures are developed in stratiform layered microbialite, while stromatolitic boundstones are characterised by columnar biostrome buildups. Occasional coarsening-up microbialite beds are associated with more crystalline textured stromatolites.

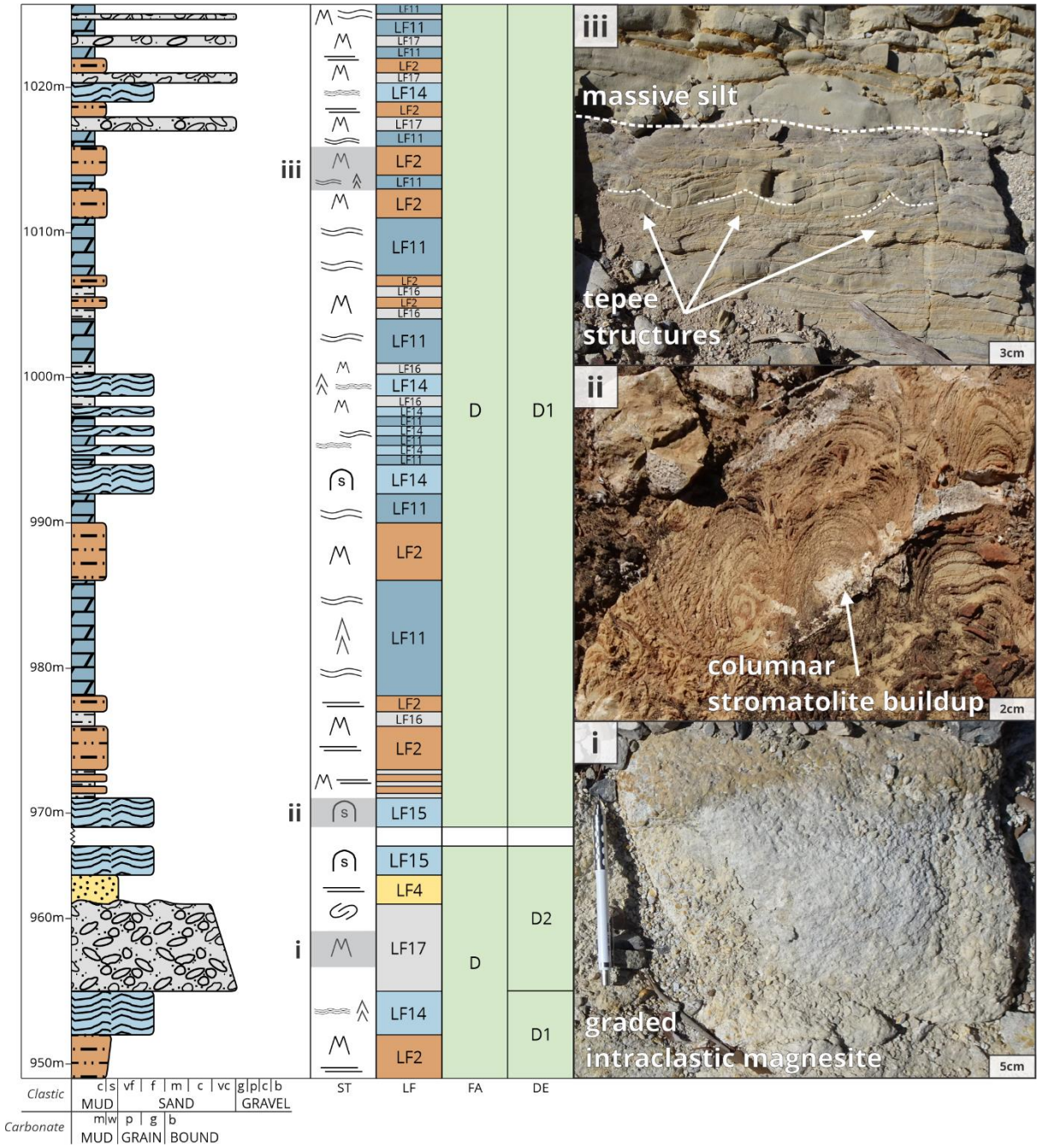

Figure 4: Lithostratigraphic logged section through Skillogalee Dolomite in northern Flinders Ranges, South Australia. FA = Facies Association, DE = Depositional Environment, LF = Lithofacies, ST = Structure. (i) graded intraclastic magnesite. (ii) columnar stromatolitic buildup. (iii) wavy laminated dolostone with tepee structures and massive siltstone.

2.6.2.2 Interpretations

The wavy and planar laminated siltstone and sandstone lithofacies in the base of the Skillogalee Dolomite, as well as interlaminated coarse clastic material in sandy dolostone beds, indicate deposition from low and upper flow regimes, and were transported as bed load and in suspension (Ashley, 1990; Cheel, 1990; Colquhoun, 1995; Reading, 2009; Boggs, 2014). Further, the symmetrical and asymmetrical interference rippled sandstone was likely deposited from lower flow regime bidirectional and unidirectional currents (Colquhoun, 1995; Reading,

2009; Boggs, 2014), where the two sets of currents intersected at high angles (Gough, 2020). The strong NNW–SSE mode for symmetrical ripples is oriented perpendicular to the palaeocoastline and is consistent with palaeocurrent data measured from wave ripples near this location (e.g. Frank & Fielding, 2003). Meanwhile, the minor ESE palaeoflow measured from intersecting asymmetrical ripples are oriented in an approximately offshore direction, indicating primary sediment dispersal towards the east (Frank & Fielding, 2003; Lloyd et al., 2020), and likely resulting from fluvial drainage systems or tidal currents (Ashley, 1990; Colquhoun, 1995; Frank & Fielding, 2003). This is consistent with a dynamic shallow-water environment with large clastic input and mixed wave, tidal and fluvial processes.

The suite of carbonate lithologies (e.g. dolostone, microbialite and magnesite) in the overlying succession presents several genetic modes of origin. Dolostone lithofacies could represent secondary diagenetic recrystallisation (Flügel, 2004; Tucker & Wright, 2009) or syn-sedimentary dolomitisation (Hood et al., 2011; 2018; Hood & Wallace, 2012; 2014; Shuster et al., 2018), while microbialite lithofacies likely precipitated authigenically (Wright, 1984; Tucker & Wright, 2009; O'Connell et al., 2020). Interlaminated clastic material in stratified dolostone and layered microbialite intervals were probably transported as suspended load by low energy tidal currents (Tucker & Wright, 2009; Chiarella et al., 2017; O'Connell et al., 2020). Magnesite mudstone lithofacies could have precipitated in-situ in an evaporative water column (Mur & Urpinell, 1987; Warren, 1990; Melezhik et al., 2001), while conglomeratic, graded magnesite beds may represent sedimentary reworking (Uppill, 1980; Belperio, 1990; Preiss, 2000; Frank & Fielding, 2003; Counts, 2017). Small tepee structures in dolostone, layered microbialite and magnesite beds were interpreted to have formed from fracturing/crustal cracking, reflecting periods of desiccation (Asserto & Kendall, 1977; Kendall & Warren, 1987; Belperio, 1990; Frank & Fielding, 2003; Tucker & Wright, 2009; O'Connell et al., 2020). Desiccation cracks have been extensively recorded within this succession at other locations around the northern Flinders Ranges (e.g. von der Borch & Lock, 1979; Uppill 1980; Rutland et al 1981; Preiss, 1987; Belperio, 1990; Frank & Fielding, 2003; Hearon et al., 2015), and are likely present at this location but were not recognised due to outcrop exposure. Rare simple load casts and flame structures are likely the result of liquefaction induced from rapid deposition of overlying material (Owen, 2003). The mixed deposition of clastic and carbonate lithofacies, with evidence for current reworking and the latter demonstrating periodic exposure, is consistent with a shallow-water to subaerial setting (Belperio, 1990; Preiss, 2000; Frank and Fielding, 2003; Thomson et al., 2014; Kunzmann et al., 2019; Thorie et al., 2020). We suggest that these sediments developed in an inner platform (D), a predominantly low energy setting dominated by tidal processes that were responsible for development of layered carbonate lithofacies, agitated by minor high energy wave and/or fluvial fluxes that deposited intraclastic magnesite and coarse clastic material (e.g. von der Borch & Lock, 1979; Uppill, 1980; Belperio, 1990; Frank & Fielding, 2003). Packages comprising authigenic magnesite and those with evidence for desiccation are interpreted to have been deposited in the supratidal to intertidal zone (D1), while all other units are characteristic of deposition in the intertidal to lagoonal zone (D2) (e.g. Belperio, 1990; Frank & Fielding, 2003; Thomson et al., 2014; Kunzmann et al., 2019).

In the upper portion of the Skillogalee Dolomite, large tepee structures in layered microbialites without the presence of brecciation or chert most likely developed from crystallisation expansion in carbonate-supersaturated subaqueous conditions (Shinn, 1969; Kendall & Warren, 1987; O'Connell et al., 2020). These layered microbialites reflect a low energy, quiescent and productive setting (Shinn, 1969; Kendall & Warren, 1987; Belperio, 1990; Jahnert & Collins, 2012; Kunzmann et al., 2019; O'Connell et al., 2020; Thorie et al., 2020). Conversely, inversely graded stromatolitic buildup lithofacies, previously interpreted as *Baicalia burra* (Preiss, 1973; Belperio, 1990), could reflect deposition from higher energy wave activity (Hoffman, 1976; Wanless et al., 1988; Tucker & Wright, 2009; Jahnert & Collins, 2012; Kunzmann et al., 2019). This facies association is interpreted as an outer platform (E), where layered microbialites with large tepee structures deposit in a low energy, subtidal lagoon (E1) (e.g. Belperio, 1990; Jahnert & Collins, 2012; Kunzmann et al., 2019; Thorie et al., 2020), and stromatolitic buildups depositing in a higher energy reef margin environment (E2) (e.g. Hoffman, 1974, 1976; Giddings et al., 2009a; Hood & Wallace, 2012; 2015; Wallace et al., 2015; O'Connell et al., 2020; Kunzmann et al., 2019; Thorie et al., 2020).

2.6.3 Myrtle Springs Formation

2.6.3.1 Observations

Like the Skillogalee Dolomite, the Myrtle Springs Formation (~970 m thick) is represented by both siliciclastic and carbonate lithofacies (Figure 5). However, the Myrtle Springs Formation has more siliciclastic deposition (42% clastic, 58% carbonate). A 33 m gap in exposed outcrop separates the stromatolitic boundstone in the top of the Skillogalee Formation to the base of the Myrtle Springs Formation, which is represented by 2 m to 12 m thick beds of laminated siltstone (LF2) with minor cross-stratified siltstone (LF3). Thin (mm scale) planar laminations dominate siltstone lithofacies, and cross-stratified siltstone lithofacies are characterised by small (2 cm – 5 cm) foresets of concave-down (hummock) and concave-up (swale) cross laminations.

Up-section is a ~200 m thick succession of laminated siltstone, laminated dolostone (LF11), layered microbialite (LF14) and stromatolitic boundstone (LF15). Laminated dolostone lithofacies are planar to wavy laminated (mm to cm scale), appearing blue in fresh outcrop and weathering yellow and pink. Thin (cm thick) stratiform and undulating laminae dominate microbialite lithofacies, with minor domical bioherms at the base of this package. These carbonate lithofacies become more prevalent towards the top of the succession, where dolostone and microbialites become closely interbedded at metre scale.

These carbonates grade into a succession dominated by coarse clastic and carbonate material. Laminated sandstone (LF4) beds are 2 m to 30 m thick, occasionally graded (normally), and composed of planar and wavy laminae, while minor ripple cross-stratified sandstones (LF5) are represented by 10 cm foresets with mud drapes. A ~20 m thick normal and inverse graded sandy dolostone (LF13) bed in the base of the package are planar laminated with a crystalline texture. Laminated siltstone lithofacies are deposited throughout the succession, becoming less dolomitic up-section.

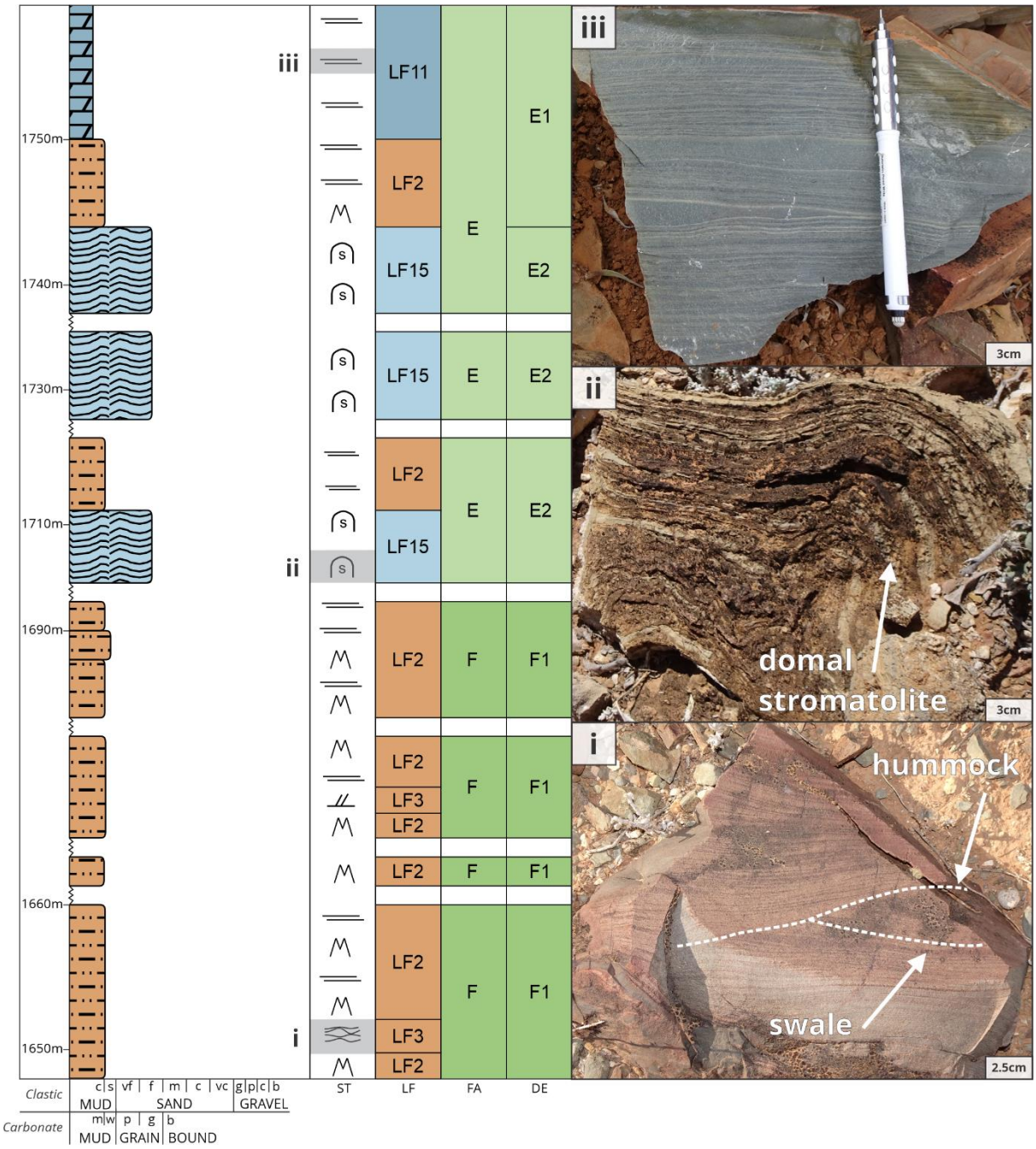

Figure 5: Lithostratigraphic logged section through Myrtle Springs Formation in northern Flinders Ranges, South Australia. FA = Facies Association, DE = Depositional Environment, LF = Lithofacies, ST = Structure. (i) hummocky and swaley cross-stratified siltstone. (ii) domal stromatolitic boundstone. (iii) thinly, planar laminated siltstone.

These clastic units culminate in deposition of laminated mudstone (LF1), followed by the return of laminated dolostone and layered microbialite lithofacies. The 20 m thick mudstone bed is kaolinitic with thin (mm scale) crude laminations, while laminated dolostone beds are highly altered with planar and wavy laminations. Microbialite beds are 2 m and 4 m thick, characterised by openly spaced, linked domical and stratiform laminae.

The top of the Myrtle Springs Formation is represented by laminated siltstone, laminated dolostone, cross-stratified dolostone (LF12), layered microbialites, and stromatolitic boundstone. Siltstone lithofacies towards the top of the succession have occasional gravel lags in the base of thin (~2 m thick) beds. Small ripple cross laminations with 5 cm foresets obliquely stacked in opposing directions distinguishes the 2 m thick cross-stratified dolostone lithofacies. Thin (<4 m thick) microbialite beds are characterised by stratiform laminae with rare small (cm scale) tepee structures and brecciated material under the crests. The top of the package is dominated by stromatolitic boundstone, which are characterised by small (cm scale) domical and large (metre scale) unlinked columnar bioherms, with minor chert replacement.

2.6.3.2 Interpretations

The laminated siltstone in the base of the Myrtle Springs Formation could have formed below storm wave base by the same processes that deposited comparable lithofacies in the middle and top of the Copley Quartzite (Boggs, 2014; Yawar & Schieber, 2017). The small hummocky swaley cross-stratified siltstone was likely deposited as suspended load from waning unidirectional and oscillatory flows following high-energy storm activity close to wave base (Nøttvedt & Kreisa, 1987; Arnott & Southard, 1990; Cheel, 1991; Duke et al., 1991; Cheel & Leckie, 1993; Dumas & Arnott, 2006; Reading, 2009; Basilici et al., 2012; Boggs, 2014). The prevalence of low energy planar laminated fine-grained lithofacies with minor higher energy cross-stratified siltstone is consistent with a slope to basinal (F), subtidal setting (F1), oceanward of the reef margin (e.g. Thomson et al., 2014; Wilmsen et al., 2018; Kunzmann et al., 2019).

Overlying these basinal siltstones are beds with domical bioherms that likely represent a similar outer platform reef margin (E2) setting, but slightly lower energy deposition, as the stromatolitic buildups in the top of the Skillogalee Dolomite (e.g. Giddings et al., 2009a; Hood & Wallace, 2012; 2015; Wallace et al., 2015; O'Connell et al., 2020; Kunzmann et al., 2019; Thorie et al., 2020). The gradation to thinly interbedded dolostone and layered microbialite lithofacies could reflect transition to a lagoonal setting (E1), characterised by deposition under tranquil conditions with limited tide or wave influence (e.g. Belperio, 1990; Jahnert & Collins, 2012; Kunzmann et al., 2019; Thorie et al., 2020).

Up section, the prevalence of coarse material and clastic lithologies indicates a transition to a higher energy and more marginal setting, respectively. Mud drapes in cross-stratified sandstone are typical features of tidal deposition, settling out of suspension during slackwater (Reineck & Wunderlich, 1968; Bhattacharya, 1997; Daidu, 2013; Boggs, 2014). The coarse clastic material in well-laminated sandy dolostone beds were likely transported from wind action or moderate to high energy storms (Wanless et al., 1988; Tucker & Wright, 2009). Further, the coarsely crystalline texture of these dolostone lithofacies is indicative of diagenetic processes (Sibley & Gregg, 1987; Wright, 1992; Tucker & Wright, 2009). Interbedded fine-grained material, including laminated siltstone and dolostone lithofacies, could indicate intermittent deposition from lower flow regime processes (Tucker & Wright, 2009; Boggs, 2014; Yawar & Schieber, 2017). This mix of coarse- and fine-grained siliciclastic and carbonate lithofacies, as well as tidally induced structures (mud drapes on foresets), is indicative of an inner platform

environment with fluctuating high- and low-energy currents and tidal influence (Chakrabarti, 2005; Daidu, 2013; Boggs, 2014; Thomson et al., 2014; Solak et al., 2016; Kunzmann et al., 2019; Thorie et al., 2020). As there is no evidence for periods of exposure, this is likely representative of the intertidal to lagoonal zone (D2).

Overlying mudstone beds, and fine interlaminated clastic material in dolostone and layered microbialite intervals likely represent deposition from low energy processes similar to those outlined previously (e.g. Tucker & Wright, 2009; Boggs, 2014; Chiarella et al., 2017; Yawar & Schieber, 2017; O'Connell et al., 2020). This could be representative of a quiescent, shallow-water environment that favours deposition of fine siliciclastics and carbonates, such as an outer platform lagoonal setting (E1) (e.g. Belperio, 1990; Jahnert & Collins, 2012; Kunzmann et al., 2019; Thorie et al., 2020).

At the top of the formation, gravel lags present in the base of some siltstone units could suggest winnowing high-energy pulses, rapid deposition and/or high sediment supply (Boggs, 2014), likely from continentally-derived flash flood events (North & Davidson, 2012). Bimodal (herringbone) palaeoflow of cross-stratified dolostone lithofacies is indicative of deposition from tidal processes (Ashley, 1990; Colquhoun, 1995; Chakrabarti, 2005; Reading, 2009; Daidu, 2013; Boggs, 2014; Thomson et al., 2014; Momta et al., 2015). Microbialite units transition from stratiform to domical and large columnar bioherms, reflecting deposition under increasing energy (Hoffman, 1976; Tucker & Wright, 2009; Jahnert & Collins, 2012). The brecciated material under the crests of tepee structures in stratiform microbialite lithofacies and chert replacement within domical bioherms provides evidence for periods of exposure (Asserto & Kendall, 1977; Kendall & Warren, 1987; Tucker & Wright, 2009; O'Connell et al., 2020). This succession at the top of the Myrtle Springs Formation is likely representative of a carbonate inner platform environment, where cross-stratified dolostone and stromatolitic bioherms could represent a higher energy, marginal, intertidal to lagoonal zone (D2) (e.g. Thomson et al., 2014; Kunzmann et al., 2019); and beds with gravel lags and tepee structures are characteristic of an exposed, supratidal to intertidal setting (D1) (e.g. Frank & Fielding, 2003; O'Connell et al., 2020).

2.6.4 Bolla Bollana Tillite

2.6.4.1 Observations

The syn-glacial Bolla Bollana Tillite is approximately 110 m thick (Figure 6), and dominated by diamictites lithofacies with minor gravelstones, sandstone, and siltstone. An unconformity separates the Myrtle Springs Formation from the Bolla Bollana Tillite and marks the Tonian to Cryogenian transition. The basal massive sandstone (LF6) unit is 12 m thick, normally graded, texturally immature (angular to sub-rounded and fine sand to gravel) and has a scoured base.

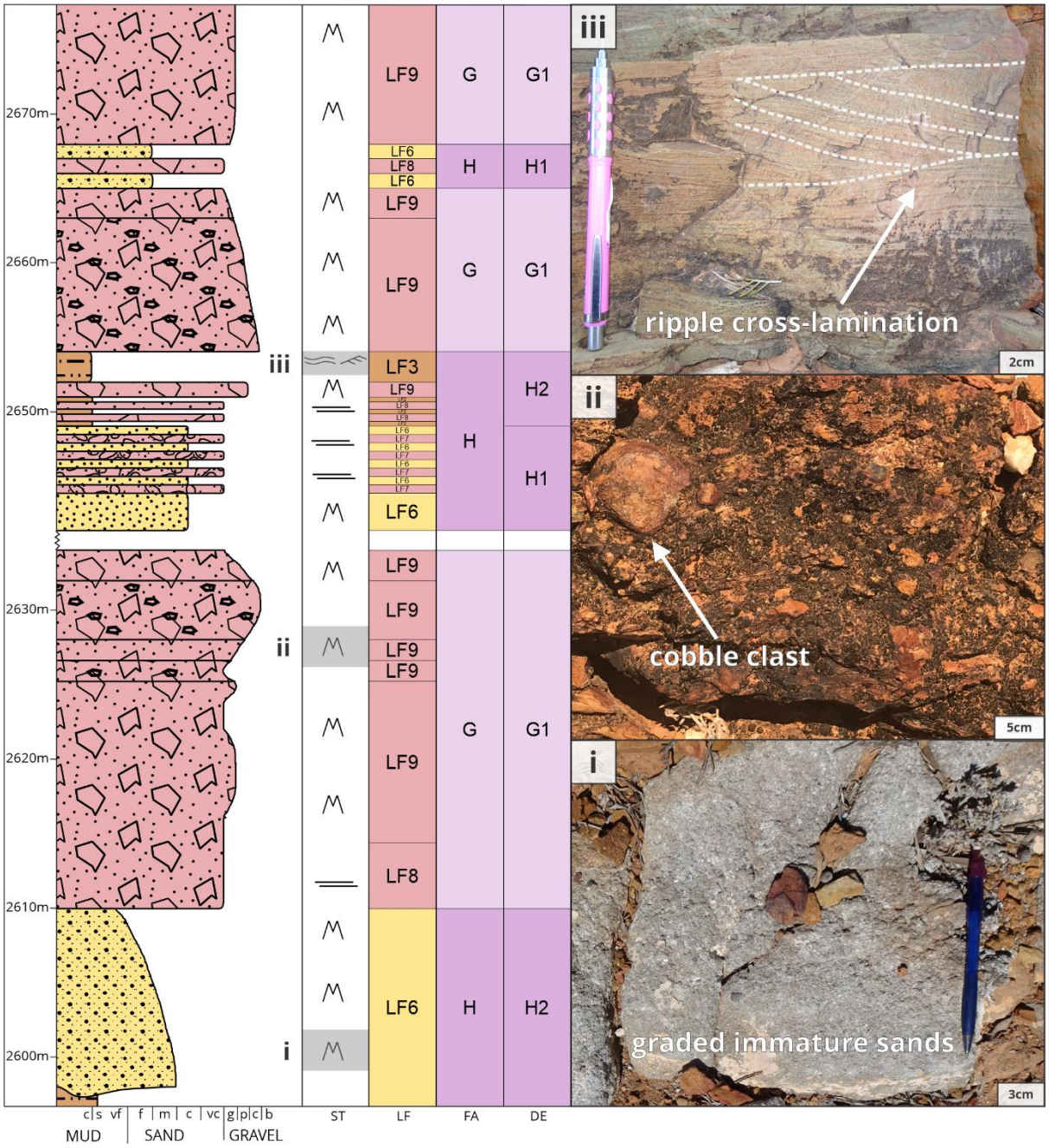

Figure 6: Lithostratigraphic logged section through Bolla Bollana Tillite in northern Flinders Ranges, South Australia. FA = Facies Association, DE = Depositional Environment, LF = Lithofacies, ST = Structure. (i) graded immature sandstone. (ii) massive diamictite with pebble clasts. (iii) small scale ripple cross laminated foresets.

A 25 m thick diamictite bed overlies this, transitioning from clast-poor stratified diamictites in the base to clast-rich massive diamictite towards the top. The stratified diamictite (LF8) contains <5% clasts, with a silt matrix and centimetre scale laminations. The massive diamictite (LF9) is highly variable, containing <5% to 60% gravel to boulder size clasts within mudstone to fine sandstone matrices. The clasts are sub- to well-rounded, comprising sandstone, carbonate, quartz and conglomerate fragments.

Up-section, the massive, immature sandstones return, and are interbedded (1 m scale) with gravel ortholoconglomerates (LF7) in a 7 m interval. These clast-supported gravelstones form thin (cm scale) lenses, comprising sub-angular to well-rounded clasts. This is overlain by a 5 m succession of interbedded diamictite and siltstone lithofacies. Siltstone lithofacies display thin planar laminations (LF2), and wavy and ripple cross-stratifications (LF3) with centimetre foresets.

Deposition of massive diamictite beds returns, represented by a thinner (11 m), normally graded package, and thicker (40 m), homogeneous package. These successions are both clast rich and clast poor (<10% to 40% clasts), composed of sub- to well-rounded sandstone; and quartzite, sandstone and carbonate gravel to boulder sized clasts, in a siltstone to very fine sandstone matrix.

2.6.4.2 Interpretations

The normally graded sandstone beds with scoured bases at the bottom of the Bolla Bollana Tillite may reflect flows controlled by high-density turbidity currents (Lowe, 1982; Kneller, 1995; Shanmugam, 2000; Winsemann et al., 2009; Talling et al., 2012; Le Heron & Busfield, 2016). Scours likely developed during erosion from high velocity flows that were then filled by coarse material as current energy waned (Fielding, 2006; Boggs, 2014). These immature sandstone beds are consistent with a subaqueous environment dominated by turbidite deposition, such as proximal channels (H2) in a proglacial fan setting (H) (e.g. Lowe, 1982; Reading & Richards, 1994; Powell & Domack, 2002; Winsemann et al., 2009; Boggs, 2014; Le Heron et al., 2013; 2014; Busfield & Le Heron, 2013; 2016).

Overlying diamictite beds possibly reflect deposition directly from the ice as melt-out (Link & Gostin, 1981; Young & Gostin, 1988; Preiss et al., 2011), or rapid deposition as subaqueous sediment gravity flows (Young & Gostin, 1988; Anderson, 1989; Eyles et al., 2007; Le Heron et al., 2013; 2014). The inverse grading from gravel clast-poor to boulder clast-rich in this unit can be attributed to kinetic sieving during flows (Legros, 2002; Talling et al., 2012; Le Heron et al., 2014). As there is no evidence for shear deformation or attenuation in stratified diamictites (Busfield & Le Heron, 2013; Le Heron et al., 2013), sorting through clast settling (Anderson, 1989) or current reworking (Boggs, 2014) are preferred depositional processes. From previous literature, these diamictite successions were likely deposited from meltwater at the ice-contact zone (G) (e.g. Link & Gostin, 1981; Young & Gostin, 1988; 1991; Preiss et al., 2011; Le Heron et al., 2014). Due to the deposition of both thick, massive diamictites, and well-sorted and/or current reworked stratified diamictites, this succession was likely deposited in a subglacial to grounded ice-margin environment (G1) (Young & Gostin, 1988; Anderson, 1989; Powell & Domack, 2002; Eyles et al., 2007; Boggs, 2014; Busfield & Le Heron, 2013; 2016; Le Heron et al., 2013; 2014; Fleming et al., 2016).

The lack of internal structure within gravel orthoconglomerate and massive sandstone units could represent rapid deposition from hyperconcentrated debris flows (Lowe, 1982; Kneller, 1995; Shanmugam, 2000; Winsemann et al., 2009; Talling et al., 2012; Le Heron & Busfield, 2016), while cross-stratified siltstone beds were likely deposited from unidirectional, turbiditic

flows (Bouma, 1964; Middleton & Hampton, 1973; Lowe, 1982; Shanmugam, 1997; 2000; Talling et al., 2012; Le Heron et al., 2014; Busfield & Le Heron, 2016; Le Heron & Busfield, 2016). Similar to the massive sandstone unit in the base of the formation, a proximal proglacial fan (H) would be dominated by debris and turbidity flows responsible for depositing interbedded fine to gravel siliciclastic lithofacies (e.g. Powell & Domack, 2002; Winsemann et al., 2009; Boggs, 2014; Le Heron et al., 2013; 2014; Busfield & Le Heron, 2013; 2016). Within this environment, interbedded immature sandstones and poorly sorted gravelstones were likely deposited as glacial outwash (H1) (e.g. Young & Gostin, 1988; 1991; Powell & Domack, 2002; Le Heron et al., 2014; Le Heron & Busfield, 2016), while fine-grained beds with unidirectional structures could reflect turbidite deposition in proximal channels (H2) (e.g. Lowe, 1982; Reading & Richards, 1994; Le Heron et al., 2014).

Processes similar to those outlined above for the first diamictite unit (e.g. Link & Gostin, 1981; Young & Gostin, 1988; Anderson, 1989; Eyles et al., 2007; Preiss et al., 2011; Le Heron et al., 2013; 2014) likely deposited the second massive diamictite succession. However, due to the vertical thickness of this diamictite succession, it can be further classified to reflect moderate to high strength, cohesive debris flows (Talling et al., 2012). Like the other diamictite lithofacies, this too could represent deposition at the ice-contact zone (G) (e.g. Link & Gostin, 1981; Young & Gostin, 1988; 1991; Preiss et al., 2011; Le Heron et al., 2014). Differentiating the depositional setting of these thick, massive diamictite units can be ambiguous (Anderson, 1989; Eyles et al., 2007), therefore, a more generalised subglacial to grounded ice-margin setting (G1) has been interpreted (Anderson, 1989; Powell & Domack, 2002; Boggs, 2014; Fleming et al., 2016).

2.6.5 Wilyerpa Formation

2.6.5.1 Observations

The Wilyerpa Formation (~40 m thick) is represented by a range of very fine to very coarse siliciclastics (Figure 7). The Bolla Bollana Tillite conformably grades into the Wilyerpa Formation, which is marked by a 6 m thick coarsening-up succession of massive sandstone (LF5), stratified (LF8) and massive (LF9) diamictite. Rare sand boulder lonestones are recorded in finer-grained sandstone lithofacies, and a very thin (~3 cm thick) tuffaceous horizon has also been identified (Fanning & Link, 2006, 2008; Cox et al., 2018). The diamictite beds in this formation are dissimilar to their underlying Bolla Bollana counterparts, where stratified units are clast-rich (50% to 60% clasts) with very fine sandstone matrices and massive units are clast-poor (<5% clasts) with a siltstone sized matrix.

This is overlain by a 35 m unit of interlaminated mudstone (LF1) and siltstone (LF2) with dropstones, sandstone and diamictite lithofacies. Mudstone beds are characterised by planar laminations, climbing ripples and soft sediment deformation structures. These include simple load casts, flame structures and convolute stratification. Dropstones are deposited throughout mud lithofacies, with larger lonestones deforming underlying laminae and smaller clasts commonly depositing together. They are composed of angular to sub-rounded pebble to boulder sized (up to 50 cm) carbonate, quartz and conglomerate fragments. Thin, heavy mineral

trough cross-laminations are developed in immature sandstones. Diamictites contain <5% to 65% clasts in a siltstone to very fine sandstone matrix, which is commonly laminated. Minor orthoconglomerates beds are up to 70% clasts, characterised by sub-angular to sub-rounded, very coarse sand to cobbles.

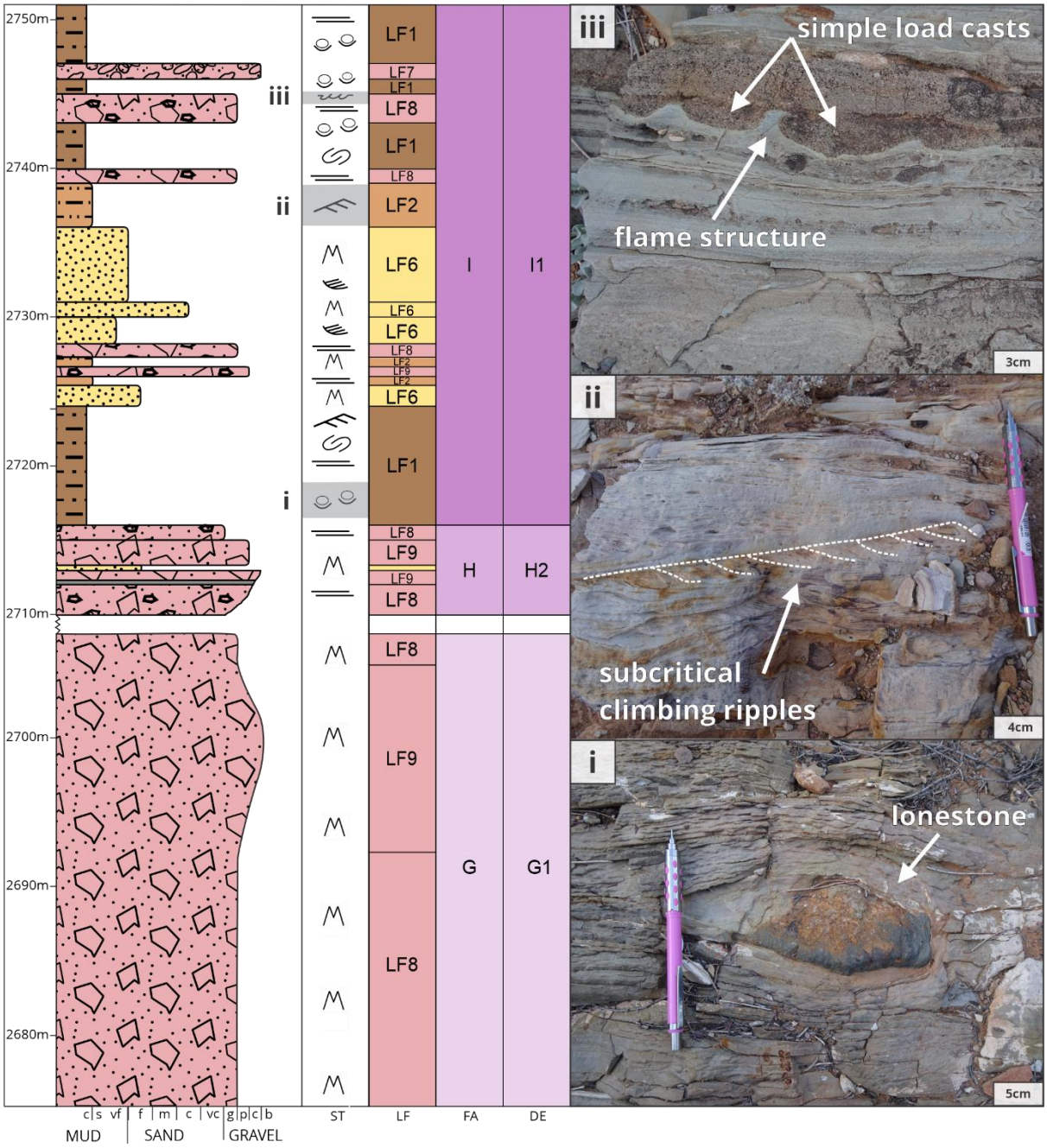

Figure 7: Lithostratigraphic logged section through Wilyerpa Formation in northern Flinders Ranges, South Australia. FA = Facies Association, DE = Depositional Environment, LF = Lithofacies, ST = Structure. (i) thinly, planar laminated siltstone with pebble lonestone deforming beds. (ii) subcritically climbing ripples in siltstone. (iii) flame structures in underlying siltstone and simple load casts in overlying sandstone.

2.6.5.2 Interpretations

Rare boulder-sized dropstones in sandstone beds in the base of the Wilypera Formation are strong evidence for glacial influence, and were likely deposited as ice rafted debris, transported in floating ice and deposited as rainout (e.g. Link & Gostin, 1981; Young & Gostin, 1988; 1991; Powell & Domack, 2002; Eyles et al., 2007; Preiss et al., 2011; Le Heron et al., 2013; 2014; 2021; Boggs, 2014; Le Heron & Busfield, 2016). Further, the prevalence of stratification in diamictite beds could indicate current reworking from unidirectional currents (Boggs, 2014). The presence of dropstones in fine-grained beds, internal structure within diamictites, close interbedded relationship and inverse grading is characteristic of deposition in an ice-proximal subaqueous setting, such as a proglacial fan (H) (e.g. Powell & Domack, 2002; Winsemann et al., 2009; Busfield & Le Heron, 2013; 2016; Le Heron et al., 2013; 2014; Boggs, 2014). This unit was likely deposited as a subaqueous channel (H2) due to the evidence for unidirectional current reworking (Lowe, 1982; Reading & Richards, 1994; Le Heron et al., 2014).

Fine siliciclastic lithofacies likely reflect deposition from low density, turbidity currents (Talling et al., 2012; Tinterri et al., 2016), where bottom current reworking developed planar and convolute laminations (Dzuynski & Smith, 1963; Shanmugam, 1997). Simple load casts and flame structures likely formed in a similar manner to those outlined in the Skillogalee Dolomite (Owen, 2003). Unidirectional climbing ripple cross-laminations within siltstone beds provide evidence for turbulent current activity, high sediment supply and rapid sedimentation rate (Ashley et al., 1982; Young & Gostin, 1988; Cheel, 1990; Baas et al., 2000; Jobe et al., 2012; Boggs, 2014; Le Heron & Busfield, 2016). Massive and cross-stratified sandstone units could reflect transition from high to low-density turbidity currents or sandy debris flow and low-density turbidity flow, respectively (Shanmugam, 1997; Talling et al., 2012). The fining-up nature of these successions, and transition from massive and cross-stratified sandstone, through ripple and convoluted siltstone to laminated mudstone, is reflective of stacked turbidite sequences (Bouma, 1964; Middleton & Hampton, 1973; Lowe, 1982; Shanmugam, 1997; 2000; Talling et al., 2012; Le Heron et al., 2014; Busfield & Le Heron, 2016; Le Heron & Busfield, 2016). Unstable slopes (turbidity currents) and rapid deposition of material (soft sediment deformation) are common in subaqueous fan environments, and the presence of dropstones throughout could indicate deposition in the distal proglacial zone (I) (e.g. Eyles et al., 1983; Powell & Domack, 2002; Boggs, 2014; Le Heron et al., 2014; Busfield & Le Heron, 2016). Within this environment, the lack of channelised features (scour and fill structures) and predominance of fine-grained material is consistent with deposition in the inter-channel zone of a distal subaqueous fan (I1) (Le Heron et al., 2014).

2.6.6 Tapley Hill Formation

2.6.6.1 Observations

Fine-grained siliciclastic (57% of formation thickness) and carbonate (43% of formation thickness) lithofacies characterise the Tapley Hill Formation (~400 m thick; Figure 8). A small gap in outcrop separates the underlying Wilyerpa Formation from the Tapley Hill Formation, but the transition appears to be conformable. The base of the Tapley Hill is dominated by

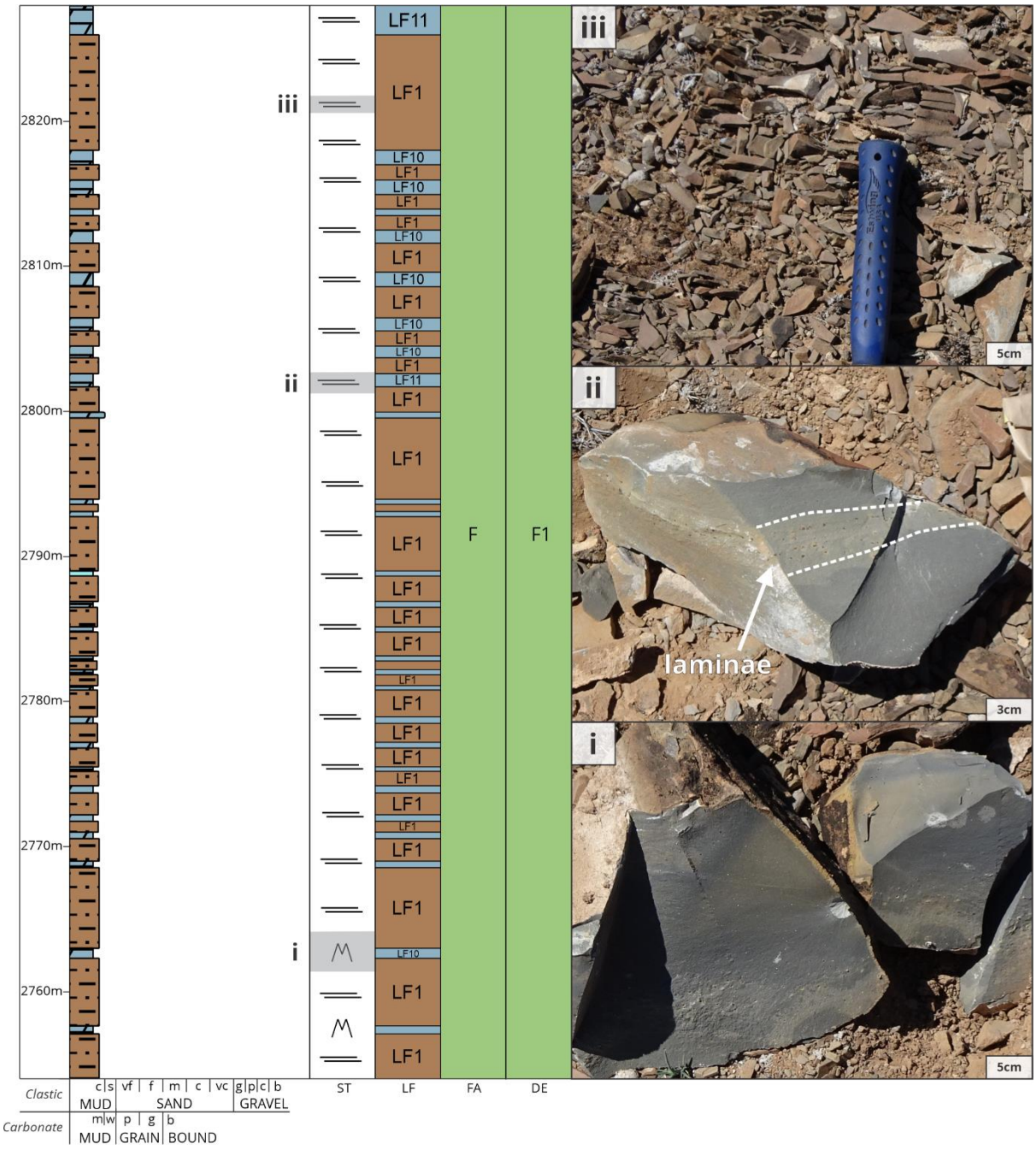

Figure 8: Lithostratigraphic logged section through Tapley Hill Formation in northern Flinders Ranges, South Australia. FA = Facies Association, DE = Depositional Environment, LF = Lithofacies, ST = Structure. (i) massive dolostone. (ii) thinly, planar laminated dolostone. (iii) thinly, planar laminated mudstone.

laminated shale (<1 m to 20 m packages), with minor thin (~1 m) laminated dolostone interbeds. Laminated mudstone (LF1) is thinly (mm scale) planar stratified, with minor weathering to green, yellow, red and purple colours. This lithofacies shows a close interbedded relationship with massive (LF10) and laminated dolostone (LF11) and appear blue and yellow

in fresh and weathered outcrops, respectively. Lithofacies abundances reverse up-section, where laminated dolostone increases in proportion (Preiss, 1987), resulting in thick (up to 52 m) packages of well- and weakly-laminated dolostones with varying degrees of weathering.

2.6.6.2 Interpretations

The laminated mudstone intervals were likely the product of gravitational settling in a low energy environment (Pazos, 2002; Boggs, 2014; Yawar & Schieber, 2017), while carbonate lithofacies appear to be authigenic due to their micritic texture and homogeneity, precipitating directly from the water column (Tucker, 1982; Flügel, 2004; Tucker & Wright, 2009). Based on previous literature for these post-glacial carbonates in the northern Flinders Ranges, the increasing carbonate content up-section could represent submarine hardground or firmground (Wallace et al., 2019). Although the thin carbonate beds in the base of the formation have been previously interpreted as a cap carbonate (Cox et al., 2018), they are less distinct than the cap dolostone deposited at other localities in the northern Flinders Ranges (e.g. Arkaroola, Giddings and Wallace, 2009; Giddings et al., 2009). The prevalence of fine-grained lithologies and lack of evidence for reworking could reflect deposition in a subtidal setting (F1), under low energy conditions (Giddings and Wallace, 2009; Giddings et al., 2009; Thomson et al., 2014; Kunzmann et al., 2019; Wallace et al., 2019).

2.7 Sequence Stratigraphy

The Copley section presents four third order (major) regressive-transgressive (R-T) cycles and one incomplete cycle (Figure 9). Three of these R-T cycles are within the pre-glacial successions, and one is represented by the syn-glacial and post-glacial formations. There are seven complete fourth order (minor) R-T cycles, five are in the pre-glacial succession and two within the syn-glacial formation. There are also several incomplete, minor R-T cycles, which represent transgressive and regressive parasequences.

2.7.1 Pre-glacial

The Copley Quartzite comprises stacked coarsening-up cycles likely reflecting overall regression during deposition (Figure 9). The base of the formation is marked by several minor regressive systems tracts (RST), from mouth bar to distributary channels in a proximal delta front (B) environment. Each of these parasequences are capped by sequence boundaries (SB) and are represented by deposition of laminated and cross-stratified sandstone, through to rippled sandstone with desiccation cracks. Overlying these successions is a minor transgressive systems tract (TST) to a more distal delta front setting (C). This is characterised by fining-up sandstone and siltstone with soft sediment deformation. A final minor regression at the top of the Copley Quartzite to lower delta plain (A) coarsening-up siltstone and sandstone is represented by a major maximum regressive surface (MRS) (Figure 9). This MRS also coincides with a low in base level. A TST transitions from the top of the Copley Quartzite to the base of the Skillogalee Dolomite and is characterised by proximal delta front (B) sandstones to inner platform (D) sandstone, siltstone and dolostone. The top of this sequence is likely marked by a maximum flooding surface (MFS) and is composed of the most fine-grained lithofacies. The following inferred regressive systems tract (RST) transitions from subtidal to supratidal setting in a mixed clastic and carbonate inner platform (D) and is capped by a MRS.

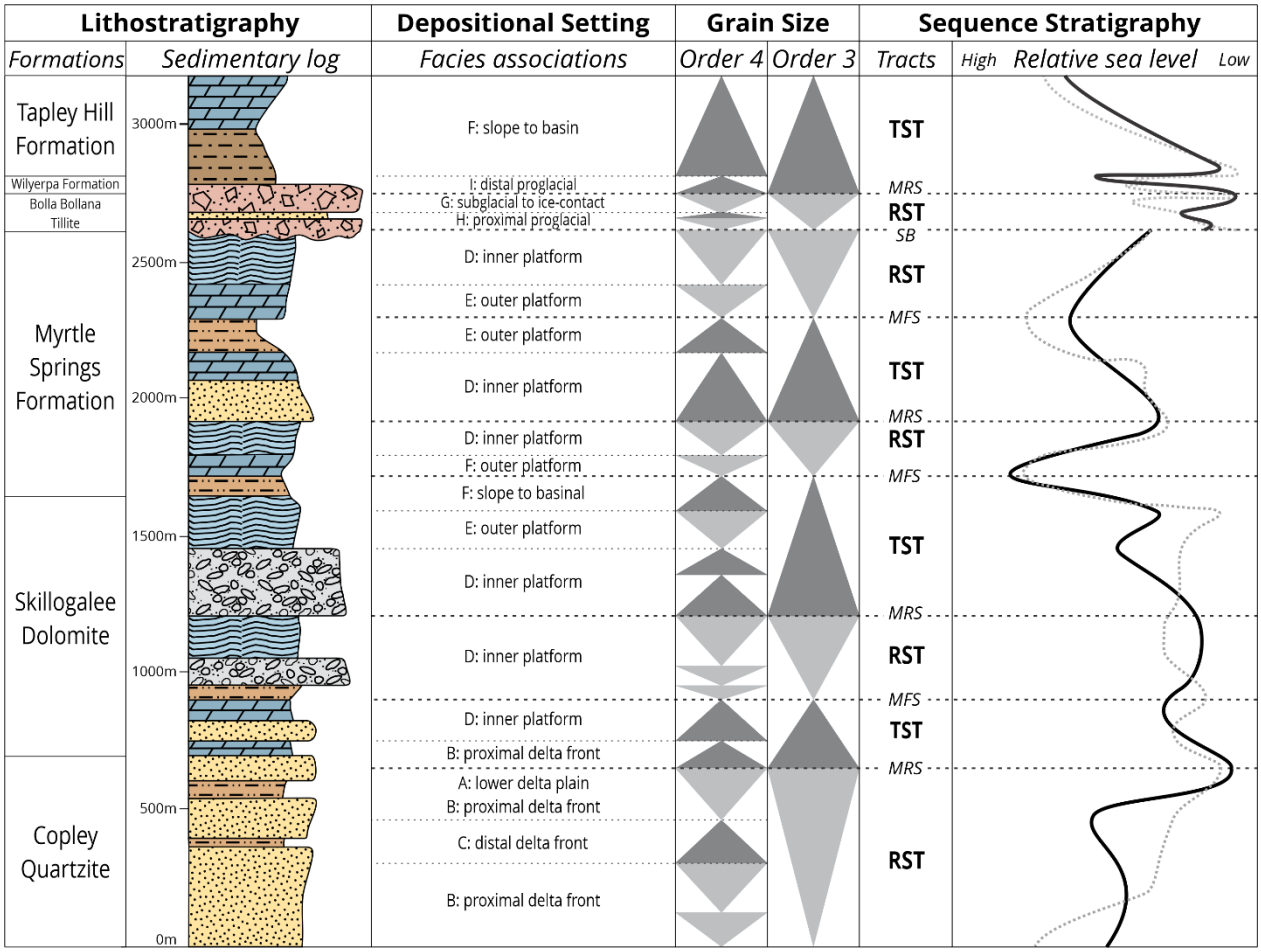

Figure 9: Sequence stratigraphy and relative sea level through Tonian to Cryogenian section near Copley, northern Flinders Ranges, South Australia. RST = Regressive Systems Tract, TST = Transgressive Systems Tract, MRS = Maximum Regressive Surface, MFS = Maximum Flooding Surface, SB = Sequence Boundary. Solid relative sea level curve is from this study, dotted relative sea level curve is from Preiss (2000).

Deposits with evidence for exposure (tepee structures and chert replacement) mark the sequence boundaries of the three minor regressive parasequences. The top of the Skillogalee Formation is composed of inner platform (D) interbedded siltstone and magnesite that grade through outer platform (E) layered microbialites and stromatolitic buildup deposits to basinal (F) laminated and cross-stratified siltstone in the overlying Myrtle Springs Formation. This major transgression is composed of four parasequences, where convoluted siltstone and coarsely crystalline carbonates mark the sequence boundaries (Figure 9). The third parasequence coincides with minor regression during deposition of the reef margin stromatolitic buildup. The deep-water siltstone likely represents the top of the major TST and culminates in a MFS and marked high in base level. The following inferred RST is composed of outer platform stromatolitic bioherms (E), through interbedded dolostone and layered microbialites to inner platform (D) sandstone and carbonates. The MRS interpreted at the top of the regressive sequence is marked by the deposition of coarsest clastic material. A series of minor, fining-up parasequences characterise the following inferred transgression, where inner platform (D) coarse sandstone and dolostone grade into outer platform (E) laminated mudstone.

The major TST is likely capped by a MFS, representing the second high in base level during the deposition of the Myrtle Springs Formation (Figure 9). The top of the formation is distinguished by coarsening-up cycles that are interpreted as regression from outer platform (E) mudstone, laminated dolostone and stratiform microbialites to inner platform (D) stromatolitic bioherms, cross-stratified dolostone, layered microbialties and gravel lagged siltstones. The parasequence SB is distinguished by tepee structures developed during periods of desiccation.

2.7.2 Syn-glacial

An inferred sequence boundary (SB) separates the Bolla Bollana Tillite from the underlying Myrtle Springs Formation (Figure 9). The base of the formation is represented by minor regression, possible grounding-line advance, from proximal proglacial (H) to ice-contact (G) settings. This is represented by a shift from immature sandstone to massive diamictite. A minor transgression back into proximal proglacial (H) sandstones and siltstones is overlain by further ice-contact zone (G) diamictites that are interpreted to represent the top of the major RST. This sequence culminates in a MRS that likely represents a relative low in base level and high grounding-line advance. An inferred transgressive parasequence composed of proximal proglacial (H) sandstones and diamictites through stacked distal proglacial (I) turbidites with dropstones marks the Wilyerpa Formation and the start of major deglaciation.

2.7.3 Post-glacial

The inferred TST in the Wilyerpa Formation conformably transitions into the overlying Tapley Hill Formation (Figure 9). Subtidal (F) shales and dolostones in the base of the Tapley Hill likely reflect widespread transgression and relative base level rise after the glaciation. The increased deposition of interpreted carbonate hardgrounds up-section possibly indicates increased transgression to distal parts of the basin.

2.8 Geochemical Analysis

A total of 42 carbonate samples were measured throughout the Tonian–Cryogenian section at Copley. These include the pre-glacial Skillogalee Dolomite and Myrtle Springs Formation, as well as the post-glacial Tapley Hill Formation. The samples were leached to extract associated carbonate phases, including dolomite, magnesite and calcite, which were then analysed for their major and trace elemental chemistry, screened for diagenetic and contaminant indicators, and analysed for rare earth element (REE) concentrations, where the latter (i.e., Ce anomalies) were also used as redox proxies.

2.8.1 Carbonate classification

The carbonate rock samples were first classified into magnesite, dolostone and limestone using Mg/Ca molar ratios (Jurinak & Bauer, 1956; Chilingar, 1957; Folk & Land, 1975). The Skillogalee Dolomite carbonate samples mostly comprise dolostone with mean ($\pm$ 1 SD) Mg/Ca values of 0.92 $\pm$ 0.07, and minor magnesite samples (Mg/Ca ~2 to ~110) collected from the lower part of the formation. All carbonate samples from the Myrtle Springs Formation produce molar Mg/Ca ratios consistent with being dominated by dolomite (0.83 $\pm$ 0.18), where higher values represent purer dolostone and lower values reflect calcareous dolostone. Tapley

Hill Formation carbonate samples are represented by the overall lowest Mg/Ca ratios, with calcareous dolostone in the basal portion of the formation (0.74 ± 0.06), through slightly dolomitic limestone (0.03 ± 0.003) to highly dolomitic limestone (0.15 ± 0.04) towards the top of the section.

2.8.2 Assessment of diagenetic alteration for carbonates

Mn/Sr ratios have been used widely over the last few decades to screen carbonate samples for post-depositional alteration from meteoric fluids (Brand & Veizer, 1980; Banner & Hanson, 1990; Kaufman & Knoll, 1995; Bartley et al., 2001; Peral et al., 2007; Frimmel, 2010, Hua et al., 2013). During recrystallisation and chemical equilibration of marine carbonates with meteoric waters, Mn is preferentially incorporated into altered marine carbonates while Sr is leached out, causing gradual increase in Mn/Sr ratios of diagenetic carbonates (Veizer, 1983; Vahrenkamp & Swart, 1990; Mazzullo, 1992; Kaufman & Knoll, 1995; Jacobsen & Kaufman, 1999; Bartley et al., 2001; Gilleaudeau et al., 2016). An increase in Mn/Sr ratio in diagenetic carbonates can be explained based on fluid:rock interaction modelling (i.e., exchange between diagenetic fluid and marine carbonate), causing systematic and predictable changes in elemental and isotopic compositions (Banner et al., 1988; Banner & Hanson, 1990; Peral et al., 2007; Chang et al., 2020). In contrast to Mn or Sr, meteoric and diagenetic fluids have typically much lower REE concentrations relative to carbonates, therefore, a large water:rock ratio is required to alter REE patterns in marine carbonates (Banner et al., 1988; Banner & Hanson, 1990). As the volume of meteoric fluid that could alter the Mn/Sr ratio is likely to be less than the volume to reset REE patterns, samples with large Mn/Sr values are still likely to retain primary REE signatures (Kaufman & Knoll, 1995). However, this model might be problematic for Precambrian carbonate diagenesis and behaviour of redox sensitive elements such as Mn and Ce, as it assumes that the original fluid is oxic, which may be contrary to presumably more reducing conditions in Precambrian systems (Bau & Dulski, 1996; Planavsky et al., 2010; Huang et al., 2011; Hood & Wallace, 2015; Kunzmann et al., 2015; Sperling et al., 2015; Hood et al., 2018; Shuster et al., 2018). These conditions would allow more Mn to be soluble in seawater, and thus incorporated in primary marine carbonates, compared to the present-day or Phanerozoic marine carbonate systems.

Different carbonate mineralogies can also influence Mn/Sr ratios (Jacobson & Usdowski, 1976; Vahrenkamp & Swart, 1990; Dietzel et al., 2004). For example, dolomite less readily incorporates Sr into the crystal lattice relative to calcite (and/or aragonite), resulting in systematically higher Mn/Sr ratios in dolostones compared to limestones (Vahrenkamp & Swart, 1990; Gilleaudeau et al., 2016). This suggests that geochemical parameters in Precambrian dolostones, might still be 'primary' even at more elevated Mn/Sr values (Bartley et al., 2001; Fölling & Frimmel, 2002; Peral et al., 2007; Gilleaudeau et al., 2016).

Previous literature has suggested a number of possible Mn/Sr ratio 'thresholds' or cut off values to differentiate well-preserved marine carbonates from those altered by meteoric diagenesis (Gilleaudeau et al., 2016). Generally, the former are expected to yield $Mn/Sr < 1.5$ (Bartley et al., 2001; Fölling & Frimmel, 2002; Peral et al., 2007), whilst some studies used a $Mn/Sr < 10$ (Kaufman & Knoll, 1995; Bartley et al., 2001; Peral et al., 2007; Gilleaudeau et al., 2016).

However, as discussed above, the controls over Mn/Sr systematics in Precambrian waters and marine carbonates are currently poorly constrained. For this reason, we have opted to assess diagenetic alteration using Mn/Sr trends instead of thresholds following Gilleaudeau et al. (2016). No statistically significant correlations were found between Mn/Sr trends and geochemical proxies such as REE, which suggests the robust nature of REE concentrations during diagenesis and justifies the inclusion of all samples for discussion of REE results in this study.

2.8.3 Assessment of detrital or clay contamination

Zr/Ca and Al/Ca ratios were used as an 'index' to assess possible contribution by detrital (such as phyllosilicate) phases in leached carbonates (Frimmel, 2009; Tostevin et al., 2016; Wallace et al., 2017; Ward et al., 2019). Zr/Ca and Al/Ca were plotted against Ce/Ce*, Eu/Eu*, Nd_{PAAS}/Yb_{PAAS} and Y/Ho in Figure 10. Anomalously high (outlier) values are considered contaminated and are marked by squares.

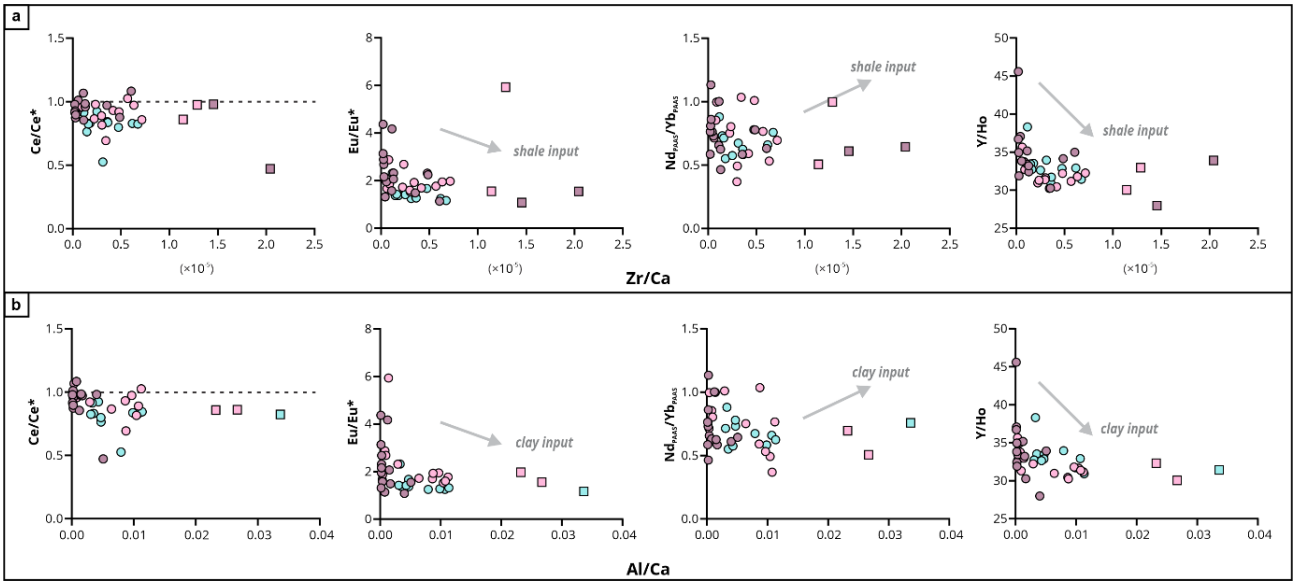

Figure 10: Contamination plots for carbonate samples in the Skillogalee Dolomite (dark pink), Myrtle Springs Formation (light pink) and Tapley Hill Formation (blue). Values are normalised to PAAS (Nance & Taylor, 1976). REE tracers Ce/Ce*, Eu/Eu*, Nd_{PASS}/Yb_{PASS}, Y/Ho were screened against Zr/Ca and Al/Ca, where data was excluded with values above 1×10^{-5} and 0.02, respectively. Samples deemed "contaminated" are shown as squares.

There are two samples within the Skillogalee Dolomite with significantly large Zr/Ca ratios. The sample with the largest Zr/Ca (2×10^{-5}) is a magnesite sample interbedded with siltstone, followed by a silty dolostone sample (1.4×10^{-5}). In addition, there are three samples within the Myrtle Springs Formation that show potential shale contribution. This includes a dolomitic siltstone sample with anomalously large Zr/Ca (1.1×10^{-5}) and Al/Ca (0.027), and two microbial dolostone samples with Zr/Ca of 1.3×10^{-5} and Al/Ca of 0.023, respectively. The Tapley Hill Formation has one highly dolomitic limestone sample that retains the largest Al/Ca ratio (0.034) for the entire dataset. These six samples will be excluded from further discussion of primary setting as they likely represent contamination from detrital phases.

The coefficient of determination (R^2) and statistical significance (p-value) between these trace metals and REE parameters was also used as a measure of non-carbonate contamination. Once filtered for outlier values, there was negligible correlation between Zr/Ca and Al/Ca ratios and REE tracers. This suggests insignificant contamination from detrital and clay phases and preservation of REE trends in the Skillogalee Dolomite, Myrtle Springs Formation and Tapley Hill Formation.

Based on diagenetic and contaminant 'indexes' (Mn/Sr, Zr/Ca and Al/Ca ratio criteria), 36 of the 42 samples preserve 'primary' REE signatures. Fourteen carbonate samples (dolostone and magnesite) are from the Skillogalee Dolomite, 12 dolostone samples from the Myrtle Springs and 10 samples (dolostone and dolomitic limestone) from the Tapley Hill Formation.

2.8.4 REE as palaeo-redox and environmental tracers

Figure 11 presents average REE profiles for each of the formations. Some of these REE elements are of particular interest, such as redox-sensitive Ce and Eu, because they indicate specific environmental and palaeo-redox conditions. Concentrations of REE were normalised to PAAS values (Nance & Taylor, 1976), and LREE depletion was measured from Nothdurft et al. (2004), using *LREE depletion* = Nd_{PAAS}/Yb_{PAAS}. Ce/Ce*, Pr/Pr* and Eu/Eu* were calculated from Bau & Dulski (1996):

(1) $Ce/Ce^* = Ce_{PAAS}/0.5(La_{PAAS}+Pr_{PAAS})$

(2) $Pr/Pr^* = Pr_{PAAS}/0.5(Ce_{PAAS}+Nd_{PAAS})$

(3) $Eu/Eu^* = Eu_{PAAS}/(0.67Sm_{PAAS}+0.33Tb_{PAAS})$

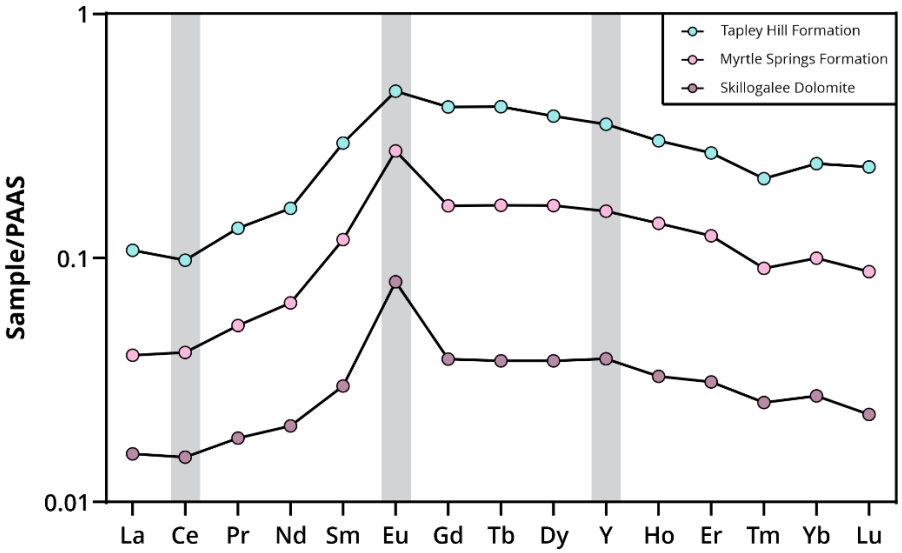

Figure 11: Average REE profiles for carbonate samples in the Skillogalee Dolomite (dark pink), Myrtle Springs Formation (light pink) and Tapley Hill Formation (blue). Values are normalised to PAAS (Nance & Taylor, 1976). Key elements Ce, Eu and Y highlighted in grey. It can be seen that, on average, total REE concentration increases up section from the Skillogalee Dolomite, through the Myrtle Springs Formation to the Tapley Hill Formation.

To assess the redox state of the depositional environment, the Ce anomaly (Ce/Ce*) was calculated for each sample. Increasingly "negative" Ce/Ce* (i.e., values < 1) suggest deposition in equilibrium with oxygenated waters. This is because the oxidised form of cerium (Ce^{4+}) is less soluble than Ce^{3+} and therefore depleted in oxygenated water, and thus precipitated marine carbonate, with respect to the neighbouring and single-valent REEs (German & Elderfield, 1990; Ling et al., 2013; Wallace et al., 2017; Shuster et al., 2018; Liu et al., 2019). Europium is the other REE that has two redox states. Unlike cerium, it has a more reduced state (Eu^{2+}) than the standard REE trivalent condition, which is highly compatible in feldspar. Positive Eu anomalies (Eu/Eu*), values > 1, in carbonates are thought to reflect the involvement of continental waters that have either weathered feldspar-rich rocks (Verdel et al., 2018), or hydrothermal fluids that have leached Eu-rich mineral phases, such as plagioclase from igneous rocks / MORB at depth in submarine settings (Derry & Jacobsen, 1990; Olivarez & Owen, 1991). Further, these positive Eu values are preferentially retained under anoxic conditions (Bau, 1991; Hood & Wallace, 2015). Another constraint on the depositional setting is the Nd_{PAAS}/Yb_{PAAS} ratio, which is used as an 'index' to record the relative depletion of light REEs (LREE) over heavy REEs (HREE) (Frimmel, 2009; Wallace et al., 2017; Ward et al., 2019). In oxic seawater, precipitation of Mn and/or Fe oxyhydroxides increases scavenging of REE (Bau et al., 1997). These oxides preferentially adsorb LREE over HREE, resulting in LREE depletion of the water column (Bertram & Elderfield, 1993; Sholkovitz et al., 1994; Bau et al., 1997; Kamber & Webb, 2001; Bolhar et al., 2004). Transition to a more anoxic water column coincides with dissolution of Mn and Fe, decreasing the scavenging potential of REEs and thus, increasing LREE concentrations in seawater (Sholkovitz et al., 1992; Kamber & Webb, 2001). In addition to this, fresh riverine waters without the presence of significant particulate matter have significantly less fractionated REE patterns, resulting in weak LREE depletion (Lawrence et al., 2006). Therefore, lower Nd_{PAAS}/Yb_{PAAS} ratios can also reflect marine waters and larger ratios are indicative of riverine waters (Nothdurft et al., 2004; Frimmel, 2009; Ward et al., 2019). The fourth REE parameter used here to assist with unravelling the palaeo-depositional environment is the Y/Ho ratio. This ratio, in a similar way to the Nd_{PAAS}/Yb_{PAAS}, discriminates the precipitation of carbonate in various environments (Bau et al., 1997; Kamber & Webb, 2001; Frimmel, 2009). According to Nozaki et al. (1997), Ho is preferentially scavenged from seawater compared to Y (Nothdurft et al., 2004; Bau & Koschinsky, 2009; Frimmel, 2009; Ward et al., 2019). Thus, larger ratios (>40) are representative of a modern, oxic marine setting (Kamber & Webb, 2001; Kamber et al., 2004; Nothdurft et al., 2004; Bau & Koschinsky, 2009; Frimmel, 2009; Bolhar et al., 2015; Ward et al., 2019). Ratios between 30 and 40 correlates with modern restricted and/or nearshore marine environments (Tostevin et al., 2016; Shuster et al., 2018; Ward et al., 2019). Whereas Y/Ho ratios <26 are usually interpreted to represent carbonate precipitation in lacustrine to terrestrial settings if detrital contamination has been ruled out (Bolhar & Van Kranendonk, 2007; Corkeron et al., 2012; Ward et al., 2019).

The geochemical signature of the Skillogalee Dolomite is not consistent with typical oxic and open marine carbonates, and instead demonstrates low Y/Ho (34.90 ± 3.44), negligible negative Ce/Ce* (0.95 ± 0.07), slight LREE depletion (Nd_{PAAS}/Yb_{PAAS} = 0.74 ± 0.17), and high Eu/Eu* (2.47 ± 0.95) (Figure 11). Similar patterns have been noted from ancient and modern settings by Tostevin et al. (2016), where input from non-carbonate material was found

responsible for decreased Y/Ho, weak Ce anomaly, increased LREE and small Eu anomaly (Pourmand et al., 2012). Due to the rigorous contamination screening within this study, input from non-carbonate phases is unlikely to have a strong influence on the interpretation of REE data. In another study, Nothdurft et al. (2004) suggested dolomitisation could result in chondritic Y/Ho, a reduction in the negative Ce anomaly, and decreased LREE depletion. This is possible due to the dolomitic composition of samples within the Skillogalee Dolomite. However, the preservation of fine microbialite laminations and micritic texture suggest that the dolomite is of primary origin, rather than formed from secondary diagenetic fluids. Comparable geochemical trends from Tonian marine dolomites in Death Valley, USA, were also discussed by Shuster et al. (2018), with low uranium concentrations, weak Ce anomalies, middle REE enrichment and positive Eu anomalies. That study suggested extensive oceanic anoxia as the simplest explanation for these REE signatures (Kamber & Webb, 2001; Shuster et al., 2018). Although these REE trends are comparable to those in the Skillogalee samples, samples from Shuster et al. (2018) present less LREE depletion, the most depleted mean values in length-fast dolomite samples (Nd_{PAAS}/Yb_{PAAS} = 0.84 ± 0.34). This could indicate slightly less reducing (dysoxic) local conditions during deposition of the Skillogalee Dolomite, potentially due to interaction between anoxic deep-water and more oxic shallow waters in a semi-restricted setting (Wallace et al., 2017). Further, the presence of evaporitic magnesite and evidence for desiccation in the Skillogalee Dolomite is consistent with more of a marginal-marine environment, with periods of exposure and inundation (Belperio, 1990; Frank & Fielding, 2003).

The Myrtle Springs Formation show only minor geochemical shifts in Y/Ho (31.94 ± 1.45), Ce/Ce* (0.90 $\pm$ 0.08) and Eu/Eu* (2.04 $\pm$ 0.43), and virtually no change in LREE depletion (Nd_{PAAS}/Yb_{PAAS} = 0.74 $\pm$ 0.21) (Figure 11). This could be indicative of a slight shift to a setting with increased riverine input, which would decrease the Y/Ho closer to chondritic values (Bolhar & Kranendonk, 2007; Frimmel, 2009; Corkeron et al., 2012). This is supported by the sedimentological evidence, where coarse-grained clastic lithofacies likely deposited from fluvial processes dominate inner platform successions. The slight depletion in Ce/Ce* could potentially indicate less reducing shallow waters, which corroborates more restriction from anoxic deep waters (Wallace et al., 2017; Shuster et al., 2018).

The largest differences in REE trends for this section is recorded in the Tapley Hill Formation. The Y/Ho mean value slightly increase (33.30 ± 1.87), Ce/Ce* becomes considerably more negative (0.80 $\pm$ 0.10), LREE depletion increases (Nd_{PAAS}/Yb_{PAAS} = 0.68 $\pm$ 0.10) and Eu/Eu* decreases (1.53 $\pm$ 0.31). These shifts, in particular the Ce anomaly, are consistent with deposition in more oxygenated waters (German & Elderfield, 1990). However, the interpretation of Ce/Ce* can be complicated, as anomalous trends can be driven by La abundances (Bau & Dulski, 1996). To test the validity of the recorded Ce anomaly as 'true' negative Ce anomaly, Ce/Ce* can be plotted against Pr/Pr* (Bau & Dulski, 1996; Webb & Kamber, 2000; Bolhar & Kranendonk, 2007; Planavsky et al., 2010; Hood & Wallace, 2015; Cox et al., 2016a; Wallace et al., 2017; Ward et al., 2019). From Figure 12, Tapley Hill samples plot mostly in the positive La anomaly field (Ce/Ce* < 0.95 and Pr/Pr* = 1), with two samples

in negative Ce anomaly field (Ce/Ce* < 0.95 and Pr/Pr* > 1.05), and largest mean Pr/Pr* values (1.02 ± 0.05).

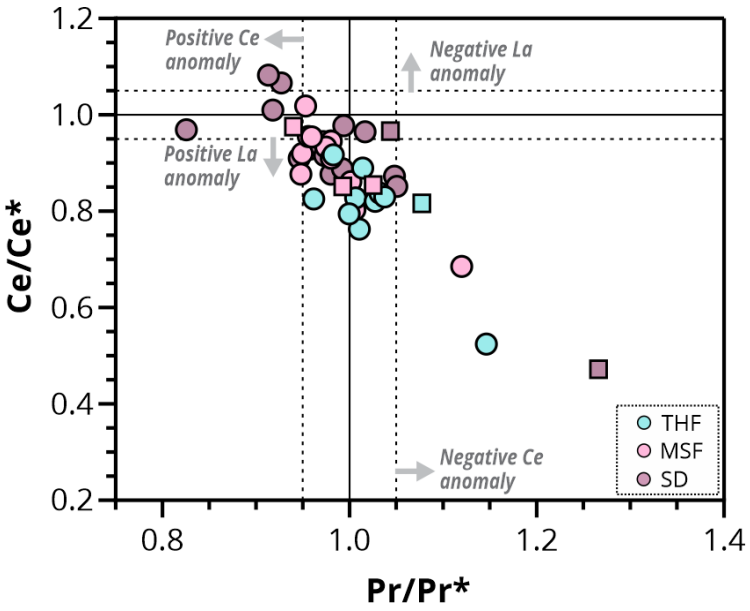

Figure 12: Graph of Ce/Ce* vs Pr/Pr* for carbonate samples. SD = Skillogalee Dolomite (dark pink), MSF = Myrtle Springs Formation (light pink), THF = Tapley Hill Formation (blue). Values are normalised to PAAS (Nance & Taylor, 1976). Samples deemed "contaminated" are shown as squares. Fields are marked by arrows. No anomaly (Ce/Ce* = 1 and Pr/Pr* = 1), true positive Ce anomaly (Ce/Ce* > 1.05 and Pr/Pr* < 0.95), true negative Ce anomaly (Ce/Ce* < 0.95 and Pr/Pr* > 1.05), true positive La anomaly (Ce/Ce* < 0.95 and Pr/Pr* = 1), true negative La anomaly (Ce/Ce* > 1.05 and Pr/Pr* = 1).

This confirms that majority of the Tapley Hill samples record a true positive La anomaly, which could be exaggerating anomalous Ce behaviour (Bau & Dulski, 1996). However, the few samples that did record a true negative Ce anomaly could have resulted from increased Mn scavenging in slightly more oxic water (Bau et al., 1997), which is supported by elevated Mn concentrations. Further, these samples record decreased Eu/Eu* values and increased LREE depletion, which is consistent with deposition under less reducing conditions (Bau, 1991; German et al., 1991; Sholkovitz et al., 1992; Hood & Wallace, 2015). Other studies of early to mid-Cryogenian carbonates have suggested a slightly oxygenated (oxic to suboxic) nearshore setting and widespread anoxic conditions for the deeper parts of the water column (Giddings & Wallace, 2009, 2009a; Hood & Wallace, 2015; Wallace et al., 2017; Verdel et al., 2018; Ward et al., 2019; O'Connell et al., 2020). This is consistent with our data, as the carbonate samples that reflect precipitation in more oxic waters are derived from the very base of the Tapley Hill Formation, which coincides with the earliest part of the post-glacial transgression and deposition in a shallower water environment. Although the sedimentological data do not distinguish a clear cap carbonate succession, these geochemical data present evidence for potential cap carbonate deposition at this locality. Up-section, the largest Eu/Eu* (2.31), Nd_{PAAS}/Yb_{PAAS} (0.88) and Y/Ho (38.31) values are recorded, which could mark a transgression into more anoxic, deep-water (Hood & Wallace, 2015; Wallace et al., 2017; Ward et al., 2019).

2.9 Palaeoenvironmental variations through time

The Copley Quartzite represents a siliciclastic, river dominated deltaic system (Preiss, 1987) (Figure 14a). The base of the Copley Quartzite is distinguished by regressive, shallowing-up sandstone successions, deposited in a proximal delta front setting from a mouth bar (B2) to distributary channel (B1). Minor transgression from proximal to distal delta front mouth bar deposits (C1) transition into lower delta plain floodplain (A2) and crevasse splay (A1) laminated siltstones and sandstones, which represent the final regression of the Copley Quartzite. The top of the formation is marked by a transgression into fining-up proximal mouth bar sands. The deposition of these paralic sediments is suggested to represent a minimum for relative sea level (Preiss, 1987). Palaeocurrent data show strong SE and NW–SE signatures, which is consistent with provenance data that indicate material being dominantly continentally sourced from the NW at this time (Lloyd et al., 2020).

The Skillogalee Dolomite encompasses both siliciclastic marginal-marine and carbonate platform environments that display repetitive depositional cycles (Preiss, 1973; von der Borch & Lock, 1979; Belperio, 1990), likely driven by eustatic fluctuations during deposition (Preiss, 1987). The base of the formation is represented by continued transgression from the Copley Quartzite into an inner platform setting (D), represented by intertidal to lagoonal laminated sandstone, siltstone and dolostone (D2). This represents a transition to a low to moderate energy, productive setting (Preiss, 1973; Preiss, 1987), marking the beginning of carbonate dominated successions and an overall shift to a platform architecture (Figure 14b). A large regression overlies this and is marked by three smaller regressive parasequences. The first minor regression is represented by coarsening-up intertidal to lagoonal sandstone and siltstone (D2), culminating in a sequence boundary marked by exposed microbialites in a supratidal to intertidal setting (D1). The remaining parasequences are characterised by cyclical deposition of intertidal to lagoonal (D2) siltstone, sandstone and reworked magnesite, and supratidal to intertidal (D1) dolostone, layered microbialite and magnesite mudstone. Desiccation features, such as tepee structures, represent periods of exposure at sequence boundaries. This regression is overlain by a second succession of interbedded siltstone, dolostone, layered microbialite and magnesite, deposited in a transgressive inner platform setting (D). These inner platform mixed clastic and carbonates grade into outer platform (E) stromatolitic buildups. The parasequences recorded in this transgression are separated by sequence boundaries of convolute siltstone and coarsely crystalline stromatolitic buildups. The carbonate platform water column was likely dysoxic, caused by the mixing of more oxic shallow waters and anoxic deeper marine waters during marine inundation (e.g. Wallace et al., 2017; Shuster et al., 2018). Although there is little stratigraphic variation in Ce/Ce*, values are slightly more oxic (~0.85) towards MRS when relative sea level is lowest and more reduced (>1) near flooding surfaces (Figure 13). Large Eu/Eu* values (4.29 and 4.41) also coincide with these flooding surfaces (Figure 13) and are supported by a high Y/Ho value (45.59) and negligible light REE depletion (Nd_{PAAS}/Yb_{PAAS} = 1). Therefore, these anomalous Eu/Eu* values are likely driven by the contribution of anoxic deep waters during relative sea level highs. Not only could this lagoon have been fed by marine waters, but also may have had a continental freshwater source, interpreted from the light REE enrichment (Nd_{PAAS}/Yb_{PAAS} = 1.13) at the top of MRS (Figure

13). The transgression within the Skillogalee Dolomite displays a weak inverse relationship between LREE depletion and Y/Ho, where Nd_{PAAS}/Yb_{PAAS} decreases (1.13 to 0.59) and Y/Ho increases (31.9 to 36.71), both towards more open seawater signatures (Figure 13). The top of this transgression continues into the overlying Myrtle Springs Formation.

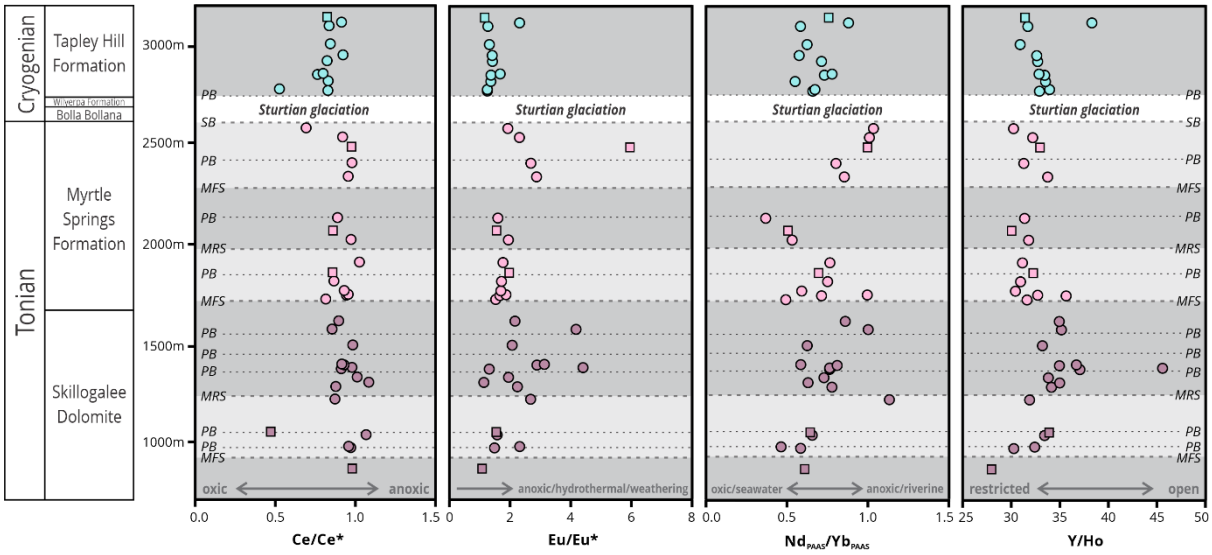

Figure 13: Key REE tracers from carbonate samples in Skillogalee Dolomite (dark pink), Myrtle Springs Formation (light pink), and Tapley Hill Formation (blue). Ce/Ce* = cerium anomaly. Eu/Eu* = europium anomaly. Nd_{PASS}/Yb_{PASS} = LREE depletion. Values are normalised to PASS (Nance & Taylor, 1976). Vertical axis is stratigraphic thickness. Samples deemed "contaminated" are shown as squares. Sequence stratigraphic systems tracts are shaded (RST = light grey, TST = dark grey). Sequence stratigraphic surfaces are dashed lines (MRS = Maximum Regressive Surface, MFS = Maximum Flooding Surface, SB = Sequence Boundary, PB = Parasequence Boundary).

In a similar manner to the Skillogalee Dolomite, the Myrtle Springs Formation represents a carbonate platform setting (Figure 14b). However, the prevalence of fine-grained clastic packages likely reflects relative sea level highs compared with the smaller scale sea level oscillations of the Skillogalee Dolomite (Preiss, 1987). Parasequences at the base of the Myrtle Springs Formation culminates in the deposition of subtidal, basinal laminated and cross-stratified siltstones (F1), probably marking a high in relative sea level. This MFS records significant LREE depletion (0.49) and high Y/Ho (35.66), reflecting more open seawater conditions. This is followed by regression from outer platform to inner platform, characterised by reef margin stromatolitic boundstone (E2), through lagoonal mixed carbonates (E1) to intertidal to lagoonal sandstones and carbonates (D2). This regression coincides with a geochemical shift to more restricted waters with increased riverine input, as evidenced by decreasing Y/Ho (35.66 to 31.16) and LREE depletion (Nd_{PAAS}/Yb_{PAAS} from 0.49 to 0.77) (Figure 13). Restriction would also result in a less reducing water column due to decreased mixing with anoxic seawater, which is supported by a shift to lower Eu/Eu* (average of 1.74) compared to the underlying TST (average of 2.52) (Figure 13). Another set of transgressive parasequences in the intertidal to lagoonal zone (D2) is represented by fining-up sandstones,

siltstones and dolostones, which terminates in deposition of lagoonal, outer platform mudstone (E1). This likely represents the second relative sea level high in the Myrtle Springs Formation (Preiss, 1987) (Figure 13). The top of the formation is characterised by coarsening-up cycles from outer platform (E) dolostones to inner platform (D) silt and stromatolitic bioherms. The sequence boundary of the regressive parasequences is represented by supratidal to intertidal (D1) stratiform microbialites with desiccation structures. Geochemical proxies within these regressive carbonate successions suggest a similar environment of deposition to the RST at the base of the Myrtle Springs Formation. Decreasing Y/Ho values (33.76 to 30.24) and increasing Nd_{PAAS}/Yb_{PAAS} (0.85 to 1.03) coincide with falling relative sea level to a more restricted setting with significant riverine input (Lawrence et al., 2006; Bolhar & Kranendonk, 2007; Frimmel, 2009; Corkeron et al., 2012) (Figure 13). Additionally, decreasing Ce/Ce* (0.93 to 0.69) and Eu/Eu* (2.98 to 1.96) likely reflect reduced input from anoxic deep waters (Wallace et al., 2017; Shuster et al., 2018) (Figure 13).

The Bolla Bollana Tillite unconformably overlies the Myrtle Springs Formation and represents glacial advance-retreat cycles in a glaciomarine environment (Link & Gostin, 1981; Young & Gostin, 1988; 1991; Eyles et al., 2007; Preiss et al., 2011; Le Heron et al., 2014) (Figure 14c). The base of the formation is represented by regression from proximal proglacial channel (H2) immature sandstones, to subglacial to grounded ice-margin (G1) stratified and massive diamictites. This likely reflects a period of glacial grounding-line advance (Young & Gostin, 1988; 1991; Le Heron et al., 2014). Minor transgression through proximal proglacial outwash (H1) interbedded sandstones and orthoconglomerates to proximal channel (H2) cross-stratified sand could indicate a phase of glacial retreat (Young & Gostin, 1988; 1991; Le Heron et al., 2014). This is subsequently overlain by a second diamictite package, which is interpreted as subglacial to grounded ice-margin (G1) and deposited during a second glacial grounding-line advance (Young & Gostin, 1988; 1991; Le Heron et al., 2014).

The start of the deglacial package is represented by transgression from proximal proglacial channel (H1) diamictites and sand to distal proglacial subaqueous fan (I1) deposits in the Wilyerpa Formation (Figure 14c). A thin tuff bed within the proximal proglacial package indicates deposition at 663.03 ± 0.11 Ma (Cox et al., 2018). The distal proglacial sediments are composed of a suite of turbidite successions, represented by mixed orthoconglomerates, sands and silts with an increasing abundance of dropstones up-section, which may be the result of increased floating ice (Link & Gostin, 1981; Young & Gostin, 1988; 1991; Preiss et al., 2011).

The Tapley Hill Formation represents a slope to basinal setting (Figure 14b), coinciding with widespread transgression and sea level rise following the Sturtian glaciation (Preiss, 1987; Young & Gostin, 1988; 1991; Preiss et al., 2011). Subtidal (F1) interbedded shale and dolostone dominate the base of the formation. These sediments represent variations in restriction, redox and water inputs compared with their pre-glacial counterparts. A more open, suboxic proximal setting is reflective of the base of the Tapley Hill Formation, as demonstrated by more negative Ce/Ce* and Eu/Eu*, increased LREE depletion and increased Y/Ho (Figure

13). Continued transgression into carbonate-dominated, anoxic, distal water is reflected by increased Eu/Eu*, Nd_{PAAS}/Yb_{PAAS} and Y/Ho values (Figure 13).

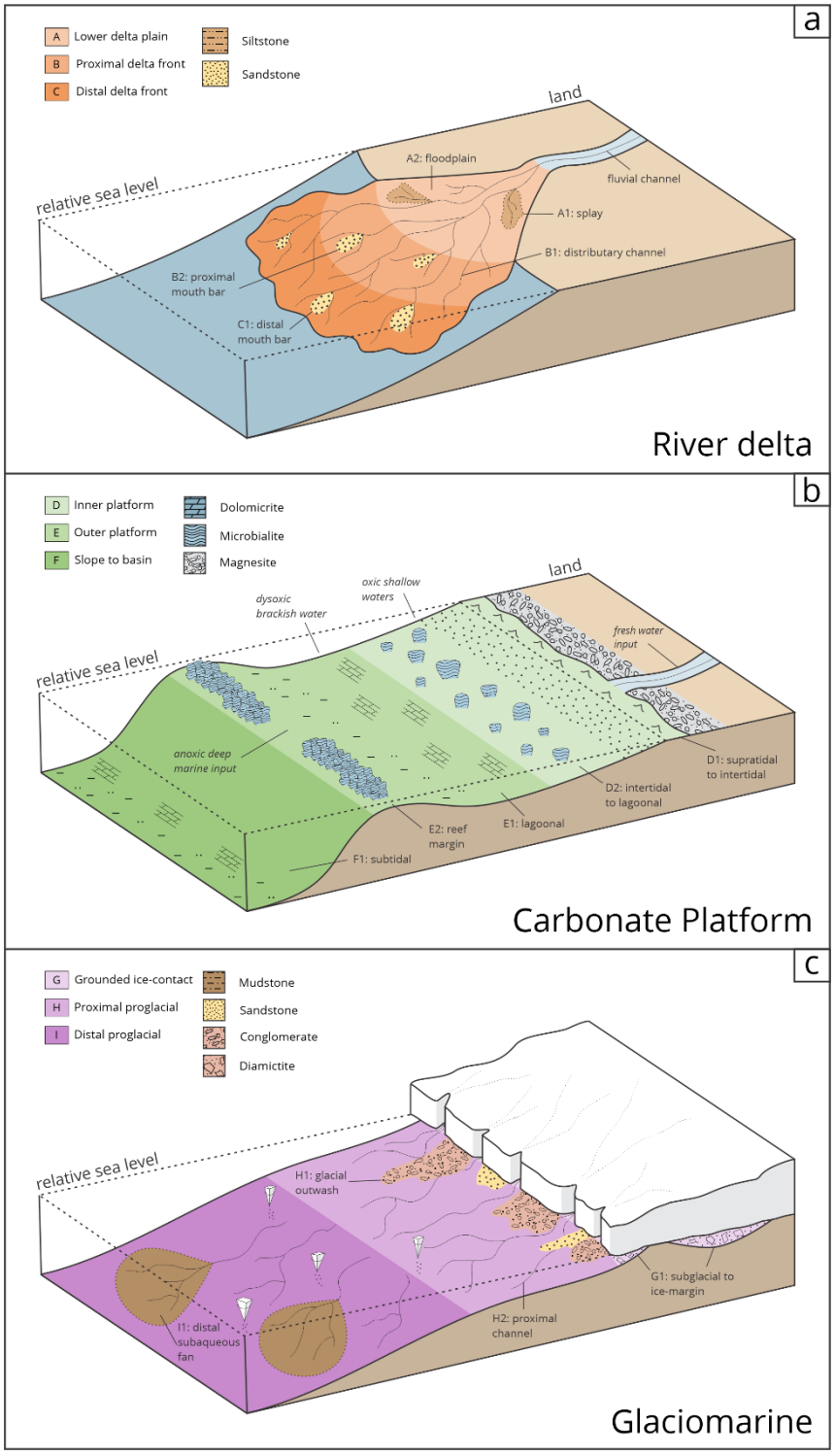

Figure 14: Depositional models for three key settings. (a) River dominated delta environment as interpreted for Copley Quartzite. A/B/C = facies associations. Siltstone/Sandstone = lithologies. (b) Carbonate platform environment as interpreted for Skillogalee Dolomite, Myrtle Springs Formation, Tapley Hill Formation. D/E/F = facies associations. Dolostone/Microbialite/Magnesite = lithologies. (c) Glaciomarine environment as interpreted for Bolla Bollana Tillite. G/H/I = facies associations. Mudstone/Sandstone/Conglomerate/Diamictite = lithologies.

2.10 Conclusions

The Tonian–Cryogenian environmental transition marks a period of significant change to Earth's surface physiological and biogeochemical cycles and seawater composition. South Australia represents some of the thickest, most continuous and best exposed sections recording these global change events. This study presents an over 3 km thick sedimentary log through a Tonian–Cryogenian interval near Copley, northern Flinders Ranges. Seventeen lithofacies, nine facies associations and sixteen depositional environments were classified from this section.

Sedimentological and sequence stratigraphic analyses reveal multiple regressive transgressive cycles through deltaic, carbonate platform and glaciomarine settings. The base of the succession is represented by the Copley Quartzite, which forms rippled and cross-stratified sandstones and siltstones in lower delta plain and delta front environments during relative sea level regression. The overlying Skillogalee Dolomite is characterised by inner platform intraclastic magnesite, dolostone, stromatolitic carbonates and sandstones. The supratidal deposits reflect lows in relative sea level. The top of the pre-glacial package is distinguished by the Myrtle Springs Formation, which is composed of basinal siltstones, outer platform mudstones and dolostone, and inner platform sandstones and layered microbialites. The fine-grained outer platform sediments represent highs in relative sea level. The Bolla Bollana Tillite is the syn-glacial unit and is represented by subglacial to ice-margin diamictites and proximal proglacial immature sandstones and siltstones. This was deposited from glacial advance and retreat in a glaciomarine environment. The Wilyerpa Formation characterises the start of deglaciation and comprises distal proglacial siltstones with dropstones. The Tapley Hill Formation reflects widespread transgression after the Sturtian glaciation and is distinguished by subtidal mudstones and dolostones.

Three hundred and fifty samples were also collected from carbonate lithofacies throughout the section for geochemical analyses. Major and trace elemental data reveal the preservation of REE signatures within the Skillogalee Dolomite, Myrtle Springs Formation and Tapley Hill Formation, assessed via geochemical screening for diagenetic alteration. Carbonates from transgressive intervals in the Skillogalee have low Y/Ho, weak negative Ce/Ce*, slight LREE depletion and high Eu/Eu*. This reflects deposition in a semi-restricted, dysoxic platform setting. It also indicates preferential input from anoxic marine waters with possible minor riverine sources, which is consistent with a marginal marine setting as interpreted from the sedimentology. Carbonate samples from regressive successions in the Myrtle Springs display even lower Y/Ho, more negative Ce/Ce*, weaker LREE depletion and moderate Eu/Eu*. This indicates an overall more restricted environment, with increased riverine input and decreased contribution from marine waters, which supports sedimentological interpretations for a nearshore setting. A geochemical shift into the Cryogenian is marked by more negative Ce/Ce*, decreased Eu/Eu*, more depleted LREE and increased Y/Ho values for samples in the base of the Tapley Hill Formation. This reflects cap carbonate deposition in an open, proximal, suboxic water column. Up-section, samples record slightly increased Eu/Eu*, Nd_{PAAS}/Yb_{PAAS} and Y/Ho

values, which is consistent with deposition in an increasingly anoxic, deeper water environment.

This high-resolution study presents new palaeoenvironmental insights into a key Tonian–Cryogenian succession, which sheds light in our understanding of how the world descended into one of the most severe glaciations ever recorded.

2.11 Supplementary Material

Supplementary material is freely available as PDF and XLSX on Figshare.

Copley log: https://doi.org/10.6084/m9.figshare.23640879.v1

Carbonate leaching for elemental analysis: https://doi.org/10.6084/m9.figshare.23640885.v1

Copley sample list: https://doi.org/10.6084/m9.figshare.23640897.v1

Elemental dataset: https://doi.org/10.6084/m9.figshare.23640903.v1

2.12 Acknowledgments

We acknowledge that this research is conducted on the ancestral lands for the Kuyani Peoples. We acknowledge and respect their deep feelings of attachment and spiritual relationship to Country, and that their cultural and heritage beliefs are still as important to the living people today. We are very grateful to reviewers Dr Maxwell Lechte, Dr Ashleigh Hood and Ms Brennan O'Connell for their insightful, detailed and constructive feedback on the original manuscript. This project was supported by funding from the Geological Survey of South Australia, and an Australian Government Research Training Program (RTP) Scholarship awarded to Virgo. We are very grateful to Jack Ward (The University of Queensland) and Jarred Lloyd (The University of Adelaide) for their field assistance in 2018 and 2019, respectively. We thank David Bruce (The University of Adelaide) for his guidance and technical support with sample leaching and preparation. The authors acknowledge the instruments and scientific and technical assistance of Microscopy Australia at Adelaide Microscopy, The University of Adelaide, a facility that is funded by the University, and State and Federal Governments

2.13 References

Ahmed, S., Bhattacharya, J. P., Garza, D. E. & Li, Y. (2014). Facies architecture and stratigraphic evolution of a river-dominated delta front, Turonian Ferron Sandstone, Utah, USA. Journal of Sedimentary Research, 84(2), 97-121. https://doi.org/10.2110/jsr.2014.6

Allen, J. (1983). Studies in fluviatile sedimentation: bars, bar-complexes and sandstone sheets (low-sinuosity braided streams) in the Brownstones (L. Devonian), Welsh Borders. Sedimentary Geology, 33(4), 237-293. https://doi.org/10.1016/0037-0738(83)90076-3

Anderson, J. B. (1989). Antarctica's glacial setting. Glacial-Marine Sedimentation, 9, 11-57. https://doi.org/10.1002/9781118667675.ch3

Armistead, S. E., Collins, A. S., Buckman, S. & Atkins, R. (2020). Age and geochemistry of the Boucaut Volcanics in the Neoproterozoic Adelaide Rift Complex, South Australia. Australian Journal of Earth Sciences, 1-10. https://doi.org/10.1080/08120099.2021.1840435

Arnott, R. W. & Southard, J. B. (1990). Exploratory flow-duct experiments on combined-flow bed configurations, and some implications for interpreting storm-event stratification. Journal of Sedimentary Research, 60(2), 211-219. https://doi.org/10.1306/212F9156-2B24-11D7-8648000102C1865D

Ashley, G. M. (1990). Classification of large-scale subaqueous bedforms; a new look at an old problem. Journal of Sedimentary Research, 60(1), 160-172. https://doi.org/10.2110/jsr.60.160

Ashley, G. M., Southard, J. B. & BoothRoyd, J. C. (1982). Deposition of climbing-ripple beds: a flume simulation. Sedimentology, 29(1), 67-79. https://doi.org/10.1111/j.1365-3091.1982.tb01709.x

Assereto, R. L. & Kendall, C. G. (1977). Nature, origin and classification of peritidal tepee structures and related breccias. Sedimentology, 24(2), 153-210. https://doi.org/10.1111/j.1365-3091.1977.tb00254.x

Baas, J. H., Van Dam, R. L. & Storms, J. E. A. (2000). Duration of deposition from decelerating high-density turbidity currents. Sedimentary Geology, 136(1-2), 71-88. https://doi.org/10.1016/S0037-0738(00)00088-9

Babinski, M., Pedrosa-Soares, A., Trindade, R. I. F. d., Martins, M., Noce, C. M. & Liu, D. (2012). Neoproterozoic glacial deposits from the Araçuaí orogen, Brazil: Age, provenance and correlations with the São Francisco craton and West Congo belt. Gondwana Research, 21(2-3), 451-465. https://doi.org/10.1016/j.gr.2011.04.008

Backé, G., Baines, G., Giles, D., Preiss, W. & Alesci, A. (2010). Basin geometry and salt diapirs in the Flinders Ranges, South Australia: insights gained from geologically-constrained modelling of potential field data. Marine and Petroleum Geology, 27(3), 650-665. https://doi.org/10.1016/j.marpetgeo.2009.09.001

Banner, J. L. & Hanson, G. N. (1990). Calculation of simultaneous isotopic and trace element variations during water-rock interaction with applications to carbonate diagenesis. Geochimica et Cosmochimica Acta, 54(11), 3123-3137. https://doi.org/10.1016/0016-7037(90)90128-8

Banner, J. L., Hanson, G. N. & Meyers, W. J. (1988). Water-rock interaction history of regionally extensive dolomites of the Burlington-Keokuk Formation (Mississippian): isotopic evidence. Sedimentology and Geochemistry of Dolostones. https://doi.org/10.2110/pec.88.43.0097

Barovich, K. & Foden, J. (2000). A Neoproterozoic flood basalt province in southern-central Australia: geochemical and Nd isotope evidence from basin fill. Precambrian Research, 100(1-3), 213-234. https://doi.org/10.1016/S0301-9268(99)00075-3

Bartley, J. K., Semikhatov, M. A., Kaufman, A. J., Knoll, A. H., Pope, M. C. & Jacobsen, S. B. (2001). Global events across the Mesoproterozoic–Neoproterozoic boundary: C and Sr isotopic evidence from Siberia. Precambrian Research, 111(1-4), 165-202. https://doi.org/10.1016/S0301-9268(01)00160-7

Basilici, G., de Luca, P. H. V. & Poiré, D. G. (2012). Hummocky cross-stratification-like structures and combined-flow ripples in the Punta Negra Formation (Lower-Middle Devonian, Argentine Precordillera): a turbiditic deep-water or storm-dominated prodelta inner-shelf system? Sedimentary Geology, 267, 73-92. https://doi.org/10.1016/j.sedgeo.2012.05.012

Bau, M. (1991). Rare-earth element mobility during hydrothermal and metamorphic fluid-rock interaction and the significance of the oxidation state of europium. Chemical geology, 93(3-4), 219-230. https://doi.org/10.1016/0009-2541(91)90115-8

Bau, M. & Dulski, P. (1996). Distribution of yttrium and rare-earth elements in the Penge and Kuruman iron-formations, Transvaal Supergroup, South Africa. Precambrian Research, 79(1-2), 37-55.

Bau, M. & Koschinsky, A. (2009). Oxidative scavenging of cerium on hydrous Fe oxide: evidence from the distribution of rare earth elements and yttrium between Fe oxides and Mn oxides in hydrogenetic ferromanganese crusts. Geochemical Journal, 43(1), 37-47. https://doi.org/10.1016/0301-9268(95)00087-9

Bau, M., Möller, P. & Dulski, P. (1997). Yttrium and lanthanides in eastern Mediterranean seawater and their fractionation during redox-cycling. Marine Chemistry, 56(1-2), 123-131. https://doi.org/10.1016/S0304-4203(96)00091-6

Belperio, A. (1990). Palaeoenvironmental interpretations of the Late Proterozoic Skillogalee Dolomite in the Willouran Ranges, South Australia. The Evolution of a Late Precambrian–Early Palaeozoic Rift Complex: The Adelaide Geosyncline. Geol. Soc. Aust. Spec. Publ, 16, 85-104.

Bertram, C. J. & Elderfield, H. (1993). The geochemical balance of the rare earth elements and neodymium isotopes in the oceans. Geochimica et Cosmochimica Acta, 57(9), 1957-1986. https://doi.org/10.1016/0016-7037(93)90087-D

Bhattacharya, A. (1997). On the origin of non-tidal flaser bedding in point bar deposits of the river Ajay, Bihar and West Bengal, NE India. Sedimentology, 44(6), 973-975. https://doi.org/10.1111/j.1365-3091.1997.tb02172.x

Boggs Jr, S. (2014). Principles of sedimentology and stratigraphy: Pearson Education.

Bold, U., Ahm, A.-S. C., Schrag, D. P., Higgins, J. A., Jamsran, E. & Macdonald, F. A. (2020). Effect of dolomitization on isotopic records from Neoproterozoic carbonates in southwestern Mongolia. Precambrian Research, 105902. https://doi.org/10.2475/01.2016.01

Bolhar, R., Hofmann, A., Siahi, M., Feng, Y.-x. & Delvigne, C. (2015). A trace element and Pb isotopic investigation into the provenance and deposition of stromatolitic carbonates, ironstones and associated shales of the∼ 3.0 Ga Pongola Supergroup, Kaapvaal Craton. Geochimica et Cosmochimica Acta, 158, 57-78. https://doi.org/10.1016/j.gca.2015.02.026

Bolhar, R., Kamber, B. S., Moorbath, S., Fedo, C. M. & Whitehouse, M. J. (2004). Characterisation of early Archaean chemical sediments by trace element signatures. Earth and Planetary Science Letters, 222(1), 43-60. https://doi.org/10.1016/j.epsl.2004.02.016

Bolhar, R. & Van Kranendonk, M. J. (2007). A non-marine depositional setting for the northern Fortescue Group, Pilbara Craton, inferred from trace element geochemistry of stromatolitic carbonates. Precambrian Research, 155(3-4), 229-250. https://doi.org/10.1016/j.precamres.2007.02.002

Bouma, A. (1964). Turbidites. In Developments in sedimentology (Vol. 3, pp. 247-256). Elsevier. https://doi.org/10.1016/S0070-4571(08)70967-1

Boyd, R., Dalrymple, R. & Zaitlin, B. A. (1992). Classification of clastic coastal depositional environments. Sedimentary Geology, 80(3-4), 139-150. https://doi.org/10.1016/0037-0738(92)90037-R

Brand, U. & Veizer, J. (1980). Chemical diagenesis of a multicomponent carbonate system; 1, Trace elements. Journal of Sedimentary Research, 50(4), 1219-1236. https://doi.org/10.1306/212F7BB7-2B24-11D7-8648000102C1865D

Bridge, J. S. (2009). Rivers and floodplains: forms, processes, and sedimentary record: John Wiley & Sons.

Brocks, J. J., Jarrett, A. J., Sirantoine, E., Hallmann, C., Hoshino, Y. & Liyanage, T. (2017). The rise of algae in Cryogenian oceans and the emergence of animals. Nature, 548(7669), 578-581. https://doi.org/10.1038/nature23457

Burns, C., Mountney, N., Hodgson, D. & Colombera, L. (2017). Anatomy and dimensions of fluvial crevasse-splay deposits: Examples from the Cretaceous Castlegate Sandstone

and Neslen Formation, Utah, USA. Sedimentary Geology, 351, 21-35. https://doi.org/10.1016/j.sedgeo.2017.02.003

Busfield, M. E. & Le Heron, D. P. (2013). Glacitectonic deformation in the Chuos Formation of northern Namibia: implications for Neoproterozoic ice dynamics. Proceedings of the Geologists' Association, 124(5), 778-789. https://doi.org/10.1016/j.pgeola.2012.10.005

Busfield, M. E. & Le Heron, D. P. (2016). A Neoproterozoic ice advance sequence, Sperry Wash, California. Sedimentology, 63(2), 307-330. https://doi.org/10.1016/j.pgeola.2012.10.005

Butterfield, N. J. (2011). Animals and the invention of the Phanerozoic Earth system. Trends in ecology & evolution, 26(2), 81-87. https://doi.org/10.1016/j.tree.2010.11.012

Chakrabarti, A. (2005). Sedimentary structures of tidal flats: A journey from coast to inner estuarine region of eastern India. Journal of earth system science, 114(3), 353-368. https://doi.org/10.1007/BF02702954

Chang, B., Li, C., Liu, D., Foster, I., Tripati, A., Lloyd, M. K., Maradiaga, I., Luo, G., An, Z., She, Z. & Xie, S. (2020). Massive formation of early diagenetic dolomite in the Ediacaran ocean: Constraints on the "dolomite problem". Proceedings of the National Academy of Sciences, 117(25), 14005-14014. https://doi.org/10.1073/pnas.1916673117

Cheel, R. J. (1990). Horizontal lamination and the sequence of bed phases and stratification under upper-flow-regime conditions. Sedimentology, 37(3), 517-529. https://doi.org/10.1111/j.1365-3091.1990.tb00151.x

Cheel, R. J. & Leckie, D. A. (1993). Hummocky cross-stratification. In Sedimentology review 1 (Vol. 1, pp. 103-122): Blackwell Scientific Publications Oxford.

Chiarella, D., Longhitano, S. G. & Tropeano, M. (2017). Types of mixing and heterogeneities in siliciclastic-carbonate sediments. Marine and Petroleum Geology, 88, 617-627. https://doi.org/10.1016/j.marpetgeo.2017.09.010

Chilingar, G. V. (1957). Classification of limestones and dolomites on basis of Ca/Mg ratio. Journal of Sedimentary Research, 27(2), 187-189. https://doi.org/10.1306/74D7069B-2B21-11D7-8648000102C1865D

Coats, R.P. (1973). Copley map sheet. Geological Survey of South Australia. 1:250,000. S.A. Geological Atlas Series, sheet SH54-09.

Colquhoun, G. P. (1995). Siliciclastic sedimentation on a storm-and tide-influenced shelf and shoreline: the Early Devonian Roxburgh Formation, NE Lachlan Fold Belt, southeastern Australia. Sedimentary Geology, 97(1-2), 69-98. https://doi.org/10.1016/0037-0738(94)00142-H

Cooper, B. (2010). 'Snowball Earth': The Early Contribution from South Australia. Earth Sciences History, 29(1), 121-145. https://doi.org/10.17704/eshi.29.1.j8874825610u68w5

Corkeron, M., Webb, G. E., Moulds, J. & Grey, K. (2012). Discriminating stromatolite formation modes using rare earth element geochemistry: Trapping and binding versus in situ precipitation of stromatolites from the Neoproterozoic Bitter Springs Formation, Northern Territory, Australia. Precambrian Research, 212, 194-206. https://doi.org/10.1016/j.precamres.2012.04.019

Counts, J. W., Rarity, F., Ainsworth, R. B., Amos, K. J., Lane, T., Moron, S., Trainor, J., Valenti, C. & Nanson, R. (2016). Sedimentological interpretation of an Ediacaran delta: Bonney Sandstone, South Australia. Australian Journal of Earth Sciences, 63(3), 257-273. https://doi.org/10.1080/08120099.2016.1180322

Counts, J. W. (2017). The Adelaide Rift Complex in the Flinders Ranges: Geologic history, past investigations and relevant analogues. Department of the Premier and Cabinet, South Australia, Adelaide, Report Book, 16, 42.

Cox, G. M., Halverson, G. P., Stevenson, R. K., Vokaty, M., Poirier, A., Kunzmann, M., Li, Z. X., Denyszyn, S. W., Strauss, J. V. and Macdonald, F. A. (2016). Continental flood basalt weathering as a trigger for Neoproterozoic Snowball Earth. Earth and Planetary Science Letters, 446, 89-99. https://doi.org/10.1016/j.epsl.2016.04.016

Cox, G. M., Jarrett, A., Edwards, D., Crockford, P. W., Halverson, G. P., Collins, A. S., Poirier, A. & Li, Z. X. (2016a). Basin redox and primary productivity within the Mesoproterozoic Roper Seaway. Chemical Geology, 440, 101-114. https://doi.org/10.1016/j.chemgeo.2016.06.025

Cox, G. M., Isakson, V., Hoffman, P. F., Gernon, T. M., Schmitz, M. D., Shahin, S., Collins, A. S., Preiss, W., Blades, M. L., Mitchell, R. N. & Nordsvan, A. (2018). South Australian U-Pb zircon (CA-ID-TIMS) age supports globally synchronous Sturtian deglaciation. Precambrian Research 315: 257-263. https://doi.org/10.1016/j.precamres.2018.07.007

Daidu, F., Yuan, W. & Min, L. (2013). Classifications, sedimentary features and facies associations of tidal flats. Journal of Palaeogeography, 2(1), 66-80. https://doi.org/10.3724/SP.J.1261.2013.00018

Derry, L. A. & Jacobsen, S. B. (1990). The chemical evolution of Precambrian seawater: evidence from REEs in banded iron formations. Geochimica et Cosmochimica Acta, 54(11), 2965-2977. https://doi.org/10.1016/0016-7037(90)90114-Z

Dietzel, M., Gussone, N. & Eisenhauer, A. (2004). Co-precipitation of Sr2+ and Ba2+ with aragonite by membrane diffusion of CO2 between 10 and 50 C. Chemical Geology, 203(1-2), 139-151. https://doi.org/10.1016/j.chemgeo.2003.09.008

Duke, W. L., Arnott, R. W. C. & Cheel, R. J. (1991). Shelf sandstones and hummocky cross-stratification: new insights on a stormy debate. Geology, 19(6), 625-628. https://doi.org/10.1130/0091-7613(1991)019<0625:SSAHCS>2.3.CO;2

Dumas, S. & Arnott, R. (2006). Origin of hummocky and swaley cross-stratification—The controlling influence of unidirectional current strength and aggradation rate. Geology, 34(12), 1073-1076. https://doi.org/10.1130/G22930A.1

Dzuynski, S. & Smith, A. J. (1963). Convolute lamination, its origin, preservation, and directional significance. Journal of Sedimentary Research, 33(3), 616-627. https://doi.org/10.1306/74D70ED4-2B21-11D7-8648000102C1865D

Eyles, C., Eyles, N. & Grey, K. (2007). Palaeoclimate implications from deep drilling of Neoproterozoic strata in the Officer Basin and Adelaide Rift Complex of Australia; a marine record of wet-based glaciers. Palaeogeography, Palaeoclimatology, Palaeoecology, 248(3-4), 291-312. https://doi.org/10.1016/j.palaeo.2006.12.008

Eyles, N., Eyles, C. H. & Miall, A. D. (1983). Lithofacies types and vertical profile models; an alternative approach to the description and environmental interpretation of glacial diamict and diamictite sequences. Sedimentology, 30(3), 393-410. https://doi.org/10.1111/j.1365-3091.1983.tb00679.x

Fairchild, I. J. & Kennedy, M. J. (2007). Neoproterozoic glaciation in the Earth System. Journal of the Geological Society, 164(5), 895-921. https://doi.org/10.1144/0016-76492006-191

Fairchild, I. J., Spencer, A. M., Ali, D. O., Anderson, R. P., Anderton, R., Boomer, I., Dove, D., Evans, J. D., Hambrey, M. J., Howe, J. and Sawaki, Y. (2017). Tonian-Cryogenian boundary sections of Argyll, Scotland. Precambrian Research. https://doi.org/10.1016/j.precamres.2017.09.020

Fanning, C., Ludwig, K., Forbes, B. & Preiss, W. (1986). Single and multiple grain U–Pb zircon analyses for the early Adelaidean Rook Tuff, Willouran Ranges, South Australia. Paper presented at the Geological Society of Australia Abstracts.

Feldman, H. R., Fabijanic, J. M., Faulkner, B. L. & Rudolph, K. W. (2014). Lithofacies, parasequence stacking, and depositional architecture of wave-to tide-dominated shorelines in the Frontier Formation, western Wyoming, USA. Journal of Sedimentary Research, 84(8), 694-717. https://doi.org/10.2110/jsr.2014.53

Fielding, C. R. (2006). Upper flow regime sheets, lenses and scour fills: extending the range of architectural elements for fluvial sediment bodies. Sedimentary Geology, 190(1-4), 227-240. https://doi.org/10.1016/j.sedgeo.2006.05.009

Fielding, C. R. (2010). Planform and facies variability in asymmetric deltas: facies analysis and depositional architecture of the Turonian Ferron Sandstone in the western Henry Mountains, south-central Utah, USA. Journal of Sedimentary Research, 80(5), 455-479. https://doi.org/10.2110/jsr.2010.047

Fleming, E. J., Benn, D. I., Stevenson, C. T., Petronis, M. S., Hambrey, M. J. & Fairchild, I. J. (2016). Glacitectonism, subglacial and glacilacustrine processes during a Neoproterozoic panglaciation, north-east Svalbard. Sedimentology, 63(2), 411-442. https://doi.org/10.1111/sed.12251

Flügel, E. (2004). Microfacies of carbonate rocks: analysis, interpretation and application. Springer Science & Business Media.

Folk, R. L. & Land, L. S. (1975). Mg/Ca ratio and salinity: two controls over crystallization of dolomite. AAPG bulletin, 59(1), 60-68. https://doi.org/10.1306/83D91C0E-16C7-11D7-8645000102C1865D

Fölling, P. & Frimmel, H. E. (2002). Chemostratigraphic correlation of carbonate successions in the Gariep and Saldania Belts, Namibia and South Africa. Basin Research, 14(1), 69-88. https://doi.org/10.1046/j.1365-2117.2002.00167.x

Frank, T. D. & Fielding, C. R. (2003). Marine origin for Precambrian, carbonate-hosted magnesite?. Geology, 31(12), 1101-1104. https://doi.org/10.1130/G20101.1

Frimmel, H. E. (2009). Trace element distribution in Neoproterozoic carbonates as palaeoenvironmental indicator. Chemical Geology, 258(3-4), 338-353. https://doi.org/10.1016/j.chemgeo.2008.10.033

Frimmel, H. E. (2010). On the reliability of stable carbon isotopes for Neoproterozoic chemostratigraphic correlation. Precambrian Research, 182(4), 239-253. https://doi.org/10.1016/j.precamres.2010.01.003

Fromhold, T. A. & Wallace, M. W. (2011). Nature and significance of the Neoproterozoic Sturtian–Marinoan Boundary, Northern Adelaide Geosyncline, South Australia. Australian Journal of Earth Sciences, 58(6), 599-613. https://doi.org/10.1080/08120099.2011.579624

Fromhold, T. A. & Wallace, M. W. (2012). Regional recognition of the Neoproterozoic Sturtian–Marinoan boundary, northern and central Adelaide Geosyncline, South Australia. Australian Journal of Earth Sciences, 59(4), 527-546. https://doi.org/10.1080/08120099.2012.673507

Gani, M. R. & Bhattacharya, J. P. (2007). Basic building blocks and process variability of a Cretaceous delta: internal facies architecture reveals a more dynamic interaction of river, wave, and tidal processes than is indicated by external shape. Journal of Sedimentary Research, 77(4), 284-302. https://doi.org/10.2110/jsr.2007.023

Gehling, J. G. (2000). Environmental interpretation and a sequence stratigraphic framework for the terminal Proterozoic Ediacara Member within the Rawnsley Quartzite, South Australia. Precambrian Research, 100(1-3), 65-95. https://doi.org/10.1016/S0301-9268(99)00069-8

German, C. R. & Elderfield, H. (1990). Application of the Ce anomaly as a paleoredox indicator: the ground rules. Paleoceanography, 5(5), 823-833. https://doi.org/10.1029/PA005i005p00823

Giddings, J. A. & Wallace, M. W. (2009). Sedimentology and C-isotope geochemistry of the 'Sturtian' cap carbonate, South Australia. Sedimentary Geology, 216, 1-14. https://doi.org/10.1016/j.sedgeo.2009.01.007

Giddings, J. A. & Wallace, M. W. (2009a). Facies-dependent δ13C variation from a Cryogenian platform margin, South Australia: Evidence for stratified Neoproterozoic oceans?. Palaeogeography, Palaeoclimatology, Palaeoecology, 271(3-4), 196-214. https://doi.org/10.1016/j.palaeo.2008.10.011

Giddings, J. A., Wallace, M. & Woon, E. (2009). Interglacial carbonates of the Cryogenian Umberatana Group, northern Flinders Ranges, South Australia. Australian Journal of Earth Sciences, 56(7), 907-925. https://doi.org/10.1080/08120090903005378

Gilleaudeau, G. J., Frei, R., Kaufman, A. J., Kah, L. C., Azmy, K., Bartley, J. K., Chernyavskiy, P. & Knoll, A. H. (2016). Oxygenation of the mid-Proterozoic atmosphere: clues from chromium isotopes in carbonates. Geochem. Perspect. Lett, 2(0), 178-187. https://doi.org/10.7185/geochemlet.1618

Gough, A. (2020). Sedimentary Structures. In D. Alderton, & N. Lancaster (Eds.), Encyclopaedia of Geology Elsevier.

Grey, K., Hill, A. C. & Calver, C. (2011). Biostratigraphy and stratigraphic subdivision of Cryogenian successions of Australia in a global context. Geological Society, London, Memoirs, 36(1), 113-134. https://doi.org/10.1144/M36.8

Gulliford, A. R., Flint, S. S. & Hodgson, D. M. (2014). Testing applicability of models of distributive fluvial systems or trunk rivers in ephemeral systems: reconstructing 3-D fluvial architecture in the Beaufort Group, South Africa. Journal of Sedimentary Research, 84(12), 1147-1169. https://doi.org/10.2110/jsr.2014.88

Gulliford, A. R., Flint, S. S. & Hodgson, D. M. (2017). Crevasse splay processes and deposits in an ancient distributive fluvial system: The lower Beaufort Group, South Africa. Sedimentary Geology, 358, 1-18. https://doi.org/10.1016/j.sedgeo.2017.06.005

Halverson, G. P. (2006). A Neoproterozoic chronology. In Neoproterozoic geobiology and paleobiology (pp. 231-271): Springer.

Halverson, G. P., Hoffman, P. F., Schrag, D. P., Maloof, A. C. & Rice, A. H. N. (2005). Toward a Neoproterozoic composite carbon-isotope record. Geological Society of America Bulletin, 117(9-10), 1181-1207. https://doi.org/10.1130/B25630.1

Halverson, G. P., Hurtgen, M. T., Porter, S. M. & Collins, A. S. (2009). Neoproterozoic-Cambrian biogeochemical evolution. Developments in Precambrian geology, 16, 351-365. https://doi.org/10.1016/S0166-2635(09)01625-9

Halverson, G. P., Kunzmann, M., Strauss, J. V. & Maloof, A. C. (2017). The Tonian-Cryogenian transition in Northeastern Svalbard. Precambrian Research. https://doi.org/10.1016/j.precamres.2017.12.010

Halverson, G. P., Wade, B. P., Hurtgen, M. T. & Barovich, K. M. (2010). Neoproterozoic chemostratigraphy. Precambrian Research, 182(4), 337-350. https://doi.org/10.1016/j.precamres.2010.04.007

Hearon IV, T. E., Rowan, M. G., Lawton, T. F., Hannah, P. T. & Giles, K. A. (2015). Geology and tectonics of Neoproterozoic salt diapirs and salt sheets in the eastern Willouran Ranges, South Australia. Basin Research, 27(2), 183-207. https://doi.org/10.1111/bre.12067

Hill, A. C. & Walter, M. R. (2000). Mid-Neoproterozoic (~ 830–750 Ma) isotope stratigraphy of Australia and global correlation. Precambrian Research, 100(1-3), 181-211. https://doi.org/10.1016/S0301-9268(99)00074-1

Hoffman, P. (1976). Environmental diversity of Middle Precambrian stromatolites. In Developments in sedimentology (Vol. 20, pp. 599-611). Elsevier. https://doi.org/10.1016/S0070-4571(08)71161-0

Hoffman, P. F., Abbot, D. S., Ashkenazy, Y., Benn, D. I., Brocks, J. J., Cohen, P. A., Cox, G. M., Creveling, J. R., Donnadieu, Y., Erwin, D. H. & Fairchild, I. J. (2017). Snowball Earth climate dynamics and Cryogenian geology-geobiology. Science Advances, 3(11), e1600983. 10.1126/sciadv.1600983

Hoffman, P. F., Kaufman, A. J., Halverson, G. P. & Schrag, D. P. (1998). A Neoproterozoic snowball earth. Science, 281(5381), 1342-1346. 10.1126/science.281.5381.1342

Hoffman, P. F., Lamothe, K. G., LoBianco, S. J., Hodgskiss, M. S., Bellefroid, E. J., Johnson, B. W., Hodgin, E. B. & Halverson, G. P. (2017a). Sedimentary depocenters on snowball Earth: Case studies from the Sturtian Chuos Formation in northern Namibia. Geosphere, 13(3), 811-837. https://doi.org/10.1130/GES01457.1

Hoffman, P. F. & Schrag, D. P. (2002). The snowball Earth hypothesis: testing the limits of global change. Terra Nova, 14(3), 129-155. https://doi.org/10.1046/j.1365-3121.2002.00408.x

Hood, A. v.S., Planavsky, N. J., Wallace, M. W. & Wang, X. (2018). The effects of diagenesis on geochemical paleoredox proxies in sedimentary carbonates. Geochimica et Cosmochimica Acta, 232, 265-287. https://doi.org/10.1016/j.gca.2018.04.022

Hood, A. v.S., Planavsky, N. J., Wallace, M. W., Wang, X., Bellefroid, E. J., Gueguen, B. & Cole, D. B. (2016). Integrated geochemical-petrographic insights from component-selective δ238U of Cryogenian marine carbonates. Geology, 44(11), 935-938. https://doi.org/10.1130/G38533.1

Hood, A. v.S & Wallace, M. W. (2012). Synsedimentary diagenesis in a Cryogenian reef complex: Ubiquitous marine dolomite precipitation. Sedimentary Geology, 255, 56-71. https://doi.org/10.1016/j.sedgeo.2012.02.004

Hood, A. v.S. & Wallace, M. W. (2014). Marine cements reveal the structure of an anoxic, ferruginous Neoproterozoic ocean. Journal of the Geological Society, 171(6), 741-744. https://doi.org/10.1144/jgs2013-099

Hood, A. v.S. & Wallace, M. W. (2015). Extreme ocean anoxia during the Late Cryogenian recorded in reefal carbonates of Southern Australia. Precambrian Research, 261, 96-111.

Hood, A. v.S., Wallace, M. W. & Drysdale, R. N. (2011). Neoproterozoic aragonite-dolomite seas? Widespread marine dolomite precipitation in Cryogenian reef complexes. Geology, 39(9), 871-874. https://doi.org/10.1130/G32119.1

Howchin, W. (1901). Preliminary note on the existence of glacial beds of Cambrian age in South Australia. Transactions of the Royal Society of South Australia, 25(10).

Howchin, W. (1920). Past glacial action in Australia. Official Yearbook Australian Census and Statistics Bureau, 13, 1133-1146.

Hua, G., Yuansheng, D., Lian, Z., Jianghai, Y., Hu, H., Min, L. & Yuan, W. (2013). Trace and rare earth elemental geochemistry of carbonate succession in the Middle Gaoyuzhuang Formation, Pingquan Section: Implications for Early Mesoproterozoic ocean redox conditions. Journal of Palaeogeography, 2(2), 209-221. https://doi.org/10.3724/SP.J.1261.2013.00027

Huang, J., Chu, X., Jiang, G., Feng, L. & Chang, H. (2011). Hydrothermal origin of elevated iron, manganese and redox-sensitive trace elements in the c. 635 Ma Doushantuo cap carbonate. Journal of the Geological Society, 168(3), 805-816. https://doi.org/10.1144/0016-76492010-132

Jacobsen, S. B. & Kaufman, A. J. (1999). The Sr, C and O isotopic evolution of Neoproterozoic seawater. Chemical Geology, 161(1-3), 37-57. https://doi.org/10.1016/S0009-2541(99)00080-7

Jacobson, R. L. & Usdowski, H. E. (1976). Partitioning of strontium between calcite, dolomite and liquids: An experimental study under higher temperature diagenetic conditions, and a model for the prediction of mineral pairs for geothermometry. Contributions to Mineralogy and Petrology, 59(2), 171-185. https://doi.org/10.1007/BF00371306

Jahnert, R. J. & Collins, L. B. (2012). Characteristics, distribution and morphogenesis of subtidal microbial systems in Shark Bay, Australia. Marine Geology, 303, 115-136. https://doi.org/10.1016/j.margeo.2012.02.009

Jobe, Z. R., Lowe, D. R. & Morris, W. R. (2012). Climbing-ripple successions in turbidite systems: depositional environments, sedimentation rates and accumulation times. Sedimentology, 59(3), 867-898. https://doi.org/10.1111/j.1365-3091.2011.01283.x

Jorissen, E. L., de Leeuw, A., van Baak, C. G., Mandic, O., Stoica, M., Abels, H. A. & Krijgsman, W. (2018). Sedimentary architecture and depositional controls of a Pliocene river-dominated delta in the semi-isolated Dacian Basin, Black Sea. Sedimentary Geology, 368, 1-23. https://doi.org/10.1016/j.sedgeo.2018.03.001

Jurinak, J. & Bauer, N. (1956). Thermodynamics of zinc adsorption on calcite, dolomite and magnesite-type minerals. Soil Science Society of America Journal, 20(4), 466-471. https://doi.org/10.2136/sssaj1956.03615995002000040006x

Kamber, B. S., Bolhar, R. & Webb, G. E. (2004). Geochemistry of late Archaean stromatolites from Zimbabwe: evidence for microbial life in restricted epicontinental seas. Precambrian Research, 132(4), 379-399. https://doi.org/10.1016/j.precamres.2004.03.006

Kamber, B. S. & Webb, G. E. (2001). The geochemistry of late Archaean microbial carbonate: implications for ocean chemistry and continental erosion history. Geochimica et Cosmochimica Acta, 65(15), 2509-2525. https://doi.org/10.1016/S0016-7037(01)00613-5

Kaufman, A. J. & Knoll, A. H. (1995). Neoproterozoic variations in the C-isotopic composition of seawater: stratigraphic and biogeochemical implications. Precambrian Research, 73(1-4), 27-49. https://doi.org/10.1016/0301-9268(94)00070-8

Keeman, J., Turner, S., Haines, P. W., Belousova, E., Ireland, T., Brouwer, P., Foden, J. and Wörner, G. (2020). New U-Pb, Hf and O isotope constraints on the provenance of sediments from the Adelaide Rift Complex–documenting the key Neoproterozoic to early Cambrian succession. Gondwana Research. https://doi.org/10.1016/j.gr.2020.02.005

Kendall, C. G. S. C. & Warren, J. (1987). A review of the origin and setting of tepees and their associated fabrics. Sedimentology, 34(6), 1007-1027.

Kirschvink, J. L. (1992). Late Proterozoic low-latitude global glaciation: the snowball Earth. https://resolver.caltech.edu/CaltechAUTHORS:20130117-100718783

Kneller, B. (1995). Beyond the turbidite paradigm: physical models for deposition of turbidites and their implications for reservoir prediction. Geological Society, London, Special Publications, 94(1), 31-49. https://doi.org/10.1144/GSL.SP.1995.094.01.04

Kunzmann, M., Crombez, V., Catuneanu, O., Blaikie, T. N., Barth, G. & Collins, A. S. (2020). Sequence stratigraphy of the ca. 1730 Ma Wollogorang Formation, McArthur Basin, Australia. Marine and Petroleum Geology, 116, 104297. https://doi.org/10.1016/j.marpetgeo.2020.104297

Kunzmann, M., Halverson, G. P., Scott, C., Minarik, W. G. & Wing, B. A. (2015). Geochemistry of Neoproterozoic black shales from Svalbard: Implications for oceanic

redox conditions spanning Cryogenian glaciations. Chemical Geology, 417, 383-393. https://doi.org/10.1016/j.chemgeo.2015.10.022

Kunzmann, M., Schmid, S., Blaikie, T. N. & Halverson, G. P. (2019). Facies analysis, sequence stratigraphy, and carbon isotope chemostratigraphy of a classic Zn-Pb host succession: The Proterozoic middle McArthur Group, McArthur Basin, Australia. Ore Geology Reviews, 106, 150-175. https://doi.org/10.1016/j.oregeorev.2019.01.011

Lamothe, K. G., Hoffman, P. F., Greenman, J. W. & Halverson, G. P. (2019). Stratigraphy and isotope geochemistry of the pre-Sturtian Ugab Subgroup, Otavi/Swakop Group, northwestern Namibia. Precambrian Research, 332, 105387. https://doi.org/10.1016/j.precamres.2019.105387

Lan, Z., Li, X., Zhu, M., Chen, Z. Q., Zhang, Q., Li, Q., Lu, D., Liu, Y. and Tang, G. (2014). A rapid and synchronous initiation of the wide spread Cryogenian glaciations. Precambrian Research, 255, 401-411.Lawrence, M. G., Greig, A., Collerson, K. D. & Kamber, B. S. (2006). Rare earth element and yttrium variability in South East Queensland waterways. Aquatic Geochemistry, 12(1), 39-72. https://doi.org/10.1016/j.precamres.2014.10.015

Lawrence, M. G., Greig, A., Collerson, K. D. & Kamber, B. S. (2006). Rare earth element and yttrium variability in South East Queensland waterways. Aquatic Geochemistry, 12(1), 39-72. https://doi.org/10.1007/s10498-005-4471-8

Le Heron, D. P. & Busfield, M. E. (2016). Pulsed iceberg delivery driven by Sturtian ice sheet dynamics: An example from Death Valley, California. Sedimentology, 63(2), 331-349. https://doi.org/10.1111/sed.12225

Le Heron, D. P., Busfield, M. E. & Collins, A. S. (2014). Bolla Bollana boulder beds: A Neoproterozoic trough mouth fan in South Australia? Sedimentology, 61(4), 978-995. https://doi.org/10.1111/sed.12082

Le Heron, D. P., Busfield, M. E. & Kamona, F. (2013). An interglacial on snowball Earth? Dynamic ice behaviour revealed in the Chuos Formation, Namibia. Sedimentology, 60(2), 411-427. https://doi.org/10.1111/j.1365-3091.2012.01346.x

Le Heron, D. P., Busfield, M. E. & Kettler, C. (2021). Ice-rafted dropstones in “postglacial” Cryogenian cap carbonates. Geology, 49(3), 263-267. https://doi.org/10.1130/G48208.1

Le Heron, D. P., Cox, G., Trundley, A. & Collins, A. (2011). Sea ice− free conditions during the Sturtian glaciation (early Cryogenian), South Australia. Geology, 39(1), 31-34. https://doi.org/10.1130/G31547.1

Le Heron, D. P., Cox, G., Trundley, A. & Collins, A. S. (2011a). Two Cryogenian glacial successions compared: Aspects of the Sturt and Elatina sediment records of South Australia. Precambrian Research, 186(1-4), 147-168. https://doi.org/10.1016/j.precamres.2011.01.014

Lechte, M. & Wallace, M. W. (2016). Sub–ice shelf ironstone deposition during the Neoproterozoic Sturtian glaciation. Geology, 44(11), 891-894. https://doi.org/10.1130/G38495.1

Lechte, M. A. & Wallace, M. W. (2015). Sedimentary and tectonic history of the Holowilena Ironstone, a Neoproterozoic iron formation in South Australia. Sedimentary Geology, 329, 211-224. https://doi.org/10.1016/j.sedgeo.2015.09.014

Legros, F. (2002). Can dispersive pressure cause inverse grading in grain flows? Journal of Sedimentary Research, 72(1), 166-170. https://doi.org/10.1306/041301720166

Lenton, T. M., Boyle, R. A., Poulton, S. W., Shields-Zhou, G. A. & Butterfield, N. J. (2014). Co-evolution of eukaryotes and ocean oxygenation in the Neoproterozoic era. Nature Geoscience, 7(4), 257-265. https://doi.org/10.1038/ngeo2108

Li, Z. X., Bogdanova, S., Collins, A. S., Davidson, A., De Waele, B., Ernst, R. E., Fitzsimons, I. C. W., Fuck, R. A., Gladkochub, D. P., Jacobs, J. & Karlstrom, K. E. (2008). Assembly, configuration, and break-up history of Rodinia: a synthesis. Precambrian Research, 160(1-2), 179-210. https://doi.org/10.1016/j.precamres.2007.04.021

Li, X., Yang, Z., Wang, J., Liu, H., Chen, Q., Wanyan, R., Liao, J. & Li, Z. (2016). Mud-coated intraclasts: a criterion for recognizing sandy mass-transport deposits–deep-lacustrine massive sandstone of the Upper Triassic Yanchang Formation, Ordos Basin, Central China. Journal of Asian Earth Sciences, 129, 98-116. https://doi.org/10.1016/j.jseaes.2016.06.007

Ling, H.-F., Chen, X., Li, D., Wang, D., Shields-Zhou, G. A. & Zhu, M. (2013). Cerium anomaly variations in Ediacaran–earliest Cambrian carbonates from the Yangtze Gorges area, South China: implications for oxygenation of coeval shallow seawater. Precambrian Research, 225, 110-127. https://doi.org/10.1016/j.precamres.2011.10.011

Link, P. K. & Gostin, V. A. (1981). Facies and paleogeography of Sturtian glacial strata (late Precambrian), South Australia. American Journal of Science, 281(4), 353-374. https://doi.org/10.2475/ajs.281.4.353

Liu, C., Wang, Z., Raub, T. D., Macdonald, F. A. & Evans, D. A. (2014). Neoproterozoic cap-dolostone deposition in stratified glacial meltwater plume. Earth and Planetary Science Letters, 404, 22-32.

Liu, X.-M., Hardisty, D. S., Lyons, T. W. & Swart, P. K. (2019). Evaluating the fidelity of the cerium paleoredox tracer during variable carbonate diagenesis on the Great Bahamas Bank. Geochimica et Cosmochimica Acta, 248, 25-42. https://doi.org/10.1016/j.gca.2018.12.028

Lloyd, J. C., Blades, M. L., Counts, J. W., Collins, A.S ., Amos, K. J., Wade, B. P., Hall, J. W., Hore, S., Ball, A. L., Shahin, S. & Drabsch, M. (2020). Neoproterozoic geochronology and provenance of the Adelaide Superbasin. Precambrian Research, 350, 105849. https://doi.org/10.1016/j.precamres.2020.105849

Long, D. & Turner, E. (2013). Formal definition of the Neoproterozoic Mackenzie Mountains Supergroup (Northwest Territories), and formal stratigraphic nomenclature for terrigenous clastic units of the Katherine Group: Geological Survey of Canada.

Lowe, D. R. (1982). Sediment gravity flows; II, Depositional models with special reference to the deposits of high-density turbidity currents. Journal of sedimentary research, 52(1), 279-297. https://doi.org/10.1306/212F7F31-2B24-11D7-8648000102C1865D

Macdonald, F.A., Prave, A.R., Petterson, R., Smith, E.F., Pruss, S.B., Oates, K., Waechter, F., Trotzuk, D. & Fallick, A.E. (2013). The Laurentian record of Neoproterozoic glaciation, tectonism, and eukaryotic evolution in Death Valley, California. Bulletin, 125(7-8), 1203-1223. https://doi.org/10.1130/B30789.1

Macdonald, F. A., Schmitz, M. D., Crowley, J. L., Roots, C. F., Jones, D. S., Maloof, A. C., Strauss, J. V., Cohen, P. A., Johnston, D. T. and Schrag, D. P. (2010). Calibrating the cryogenian. Science, 327(5970), 1241-1243. 10.1126/science.1183325

Macdonald, F. A. & Wordsworth, R. (2017). Initiation of Snowball Earth with volcanic sulfur aerosol emissions. Geophysical Research Letters, 44(4), 1938-1946. https://doi.org/10.1002/2016GL072335

MacLennan, S., Park, Y., Swanson-Hysell, N., Maloof, A., Schoene, B., Gebreslassie, M., Antilla, E., Tesema, T., Alene, M. and Haileab, B. (2018). The arc of the Snowball: U-Pb dates constrain the Islay anomaly and the initiation of the Sturtian glaciation. Geology, 46(6), 539-542. https://doi.org/10.1130/G40171.1

Mawson, D. & Sprigg, R. (1950). Subdivision of the Adelaide system. Australian Journal of Science, 13(3), 69-72.

Mazzullo, S. (1992). Geochemical and neomorphic alteration of dolomite: a review. Carbonates and evaporites, 7(1), 21. https://doi.org/10.1007/BF03175390

McKirdy, D. M., Burgess, J. M., Lemon, N. M., Yu, X., Cooper, A. M., Gostin, V. A., Jenkins, R. J. & Both, R. A. (2001). A chemostratigraphic overview of the late Cryogenian interglacial sequence in the Adelaide Fold-Thrust Belt, South Australia. Precambrian Research, 106(1-2), 149-186. https://doi.org/10.1016/S0301-9268(00)00130-3

McMahon, S., Hood, A. v.S. & McIlroy, D. (2017). The origin and occurrence of subaqueous sedimentary cracks. Geological Society, London, Special Publications, 448(1), 285-309. https://doi.org/10.1144/SP448.15

Melezhik, V. A., Fallick, A. E., Medvedev, P. V. & Makarikhin, V. V. (2001). Palaeoproterozoic magnesite: lithological and isotopic evidence for playa/sabkha environments. Sedimentology, 48(2), 379-397. https://doi.org/10.1046/j.1365-3091.2001.00369.x

Merdith, A. S., Collins, A. S., Williams, S. E., Pisarevsky, S., Foden, J. D., Archibald, D. B., Blades, M. L., Alessio, B. L., Armistead, S., Plavsa, D. and Clark, C. (2017). A full-plate global reconstruction of the Neoproterozoic. Gondwana Research, 50, 84-134. https://doi.org/10.1016/j.gr.2017.04.001

Merdith, A. S., Williams, S. E., Brune, S., Collins, A. S. & Müller, R. D. (2019). Rift and plate boundary evolution across two supercontinent cycles. Global and planetary change, 173, 1-14. https://doi.org/10.1016/j.gloplacha.2018.11.006

Merdith, A.S., Williams, S.E., Collins, A.S., Tetley, M.G., Mulder, J.A., Blades, M.L., Young, A., Armistead, S.E., Cannon, J., Zahirovic, S., Müller, R.D. (2021). A continuous, kinematic full-plate motion model from 1 Ga to present. Earth Science Reviews. https://doi.org/10.1016/j.earscirev.2020.103477

Middleton, G. V. & Hampton, M. A. (1973). Part I. Sediment gravity flows: mechanics of flow and deposition.

Momta, P. S., Omoboh, J. O. & Odigi, M. I. (2015). Sedimentology and depositional environment of D2 sand in part of greater ughelli depobelt, onshore Niger Delta, Nigeria. American Journal of Engineering and Applied Sciences, 8(4), 556.

Moretti, M., Soria, J. M., Alfaro, P. & Walsh, N. (2001). Asymmetrical soft-sediment deformation structures triggered by rapid sedimentation in turbiditic deposits (Late Miocene, Guadix Basin, Southern Spain). Facies, 44(1), 283-294. https://doi.org/10.1007/BF02668179

Mur, J. P. & Urpinell, M. I. (1987). Magnesite formation in recent playa lakes, Los Monegros, Spain. Geological Society, London, Special Publications, 36(1), 119-122. https://doi.org/10.1144/GSL.SP.1987.036.01.10

Murrell, B. (1977). Stratigraphy and tectonics across the Torrens Hinge Zone between Andamooka and Marree, South Australia. University of Adelaide, Department of Geology. https://hdl.handle.net/2440/21084

Nance, W. B. & Taylor, S. R. (1976). Rare earth element patterns and crustal evolution—I. Australian post-Archean sedimentary rocks. Geochimica et Cosmochimica Acta, 40(12), 1539-1551. https://doi.org/10.1016/0016-7037(76)90093-4

Narbonne, G. M. & Aitken, J. D. (1995). Neoproterozoic of the mackenzie mountains, Northwestern Canada. Precambrian Research, 73(1-4), 101-121. https://doi.org/10.1016/0301-9268(94)00073-Z

Nichols, G. J. (1987). Structural controls on fluvial distributary systems-the Luna System, Northern Spain.

Nichols, G. J. & Fisher, J. A. (2007). Processes, facies and architecture of fluvial distributary system deposits. Sedimentary geology, 195(1-2), 75-90. https://doi.org/10.1016/j.sedgeo.2006.07.004

Nothdurft, L. D., Webb, G. E. & Kamber, B. S. (2004). Rare earth element geochemistry of Late Devonian reefal carbonates, Canning Basin, Western Australia: confirmation of a seawater REE proxy in ancient limestones. Geochimica et Cosmochimica Acta, 68(2), 263-283. https://doi.org/10.1016/S0016-7037(03)00422-8

North, C. P. & Davidson, S. K. (2012). Unconfined alluvial flow processes: recognition and interpretation of their deposits, and the significance for palaeogeographic reconstruction. Earth-Science Reviews, 111(1-2), 199-223. https://doi.org/10.1016/j.earscirev.2011.11.008

Nøttvedt, A. & Kreisa, R. D. (1987). Model for the combined-flow origin of hummocky cross-stratification. Geology, 15(4), 357-361. https://doi.org/10.1130/0091-7613(1987)15<357:MFTCOO>2.0.CO;2

Nozaki, Y., Zhang, J. & Amakawa, H. (1997). The fractionation between Y and Ho in the marine environment. Earth and Planetary Science Letters, 148(1-2), 329-340. https://doi.org/10.1016/S0012-821X(97)00034-4

O'Connell, B., Wallace, M. W., Hood, A. v.S, Lechte, M. A. & Planavsky, N. J. (2020). Iron-rich carbonate tidal deposits, Angepena Formation, South Australia: A redox-stratified Cryogenian basin. Precambrian Research, 342, 105668. https://doi.org/10.1016/j.precamres.2020.105668

Oehlert, A. M. & Swart, P. K. (2014). Interpreting carbonate and organic carbon isotope covariance in the sedimentary record. Nature Communications, 5(1), 1-7. https://doi.org/10.1038/ncomms5672

Olariu, C. & Bhattacharya, J. P. (2006). Terminal distributary channels and delta front architecture of river-dominated delta systems. Journal of Sedimentary Research, 76(2), 212-233. https://doi.org/10.2110/jsr.2006.026

Olariu, C., Steel, R. J. & Petter, A. L. (2010). Delta-front hyperpycnal bed geometry and implications for reservoir modeling: Cretaceous Panther Tongue delta, Book Cliffs, Utah. AAPG bulletin, 94(6), 819-845. https://doi.org/10.1306/11020909072

Olivarez, A. M. & Owen, R. M. (1991). The europium anomaly of seawater: implications for fluvial versus hydrothermal REE inputs to the oceans. Chemical Geology, 92(4), 317-328. https://doi.org/10.1016/0009-2541(91)90076-4

Oliveira, C. M., Hodgson, D. M. & Flint, S. S. (2009). Aseismic controls on in situ soft-sediment deformation processes and products in submarine slope deposits of the Karoo Basin, South Africa. Sedimentology, 56(5), 1201-1225. https://doi.org/10.1111/j.1365-3091.2008.01029.x

Oliveira, C. M., Hodgson, D. M. & Flint, S. S. (2011). Distribution of soft-sediment deformation structures in clinoform successions of the Permian Ecca Group, Karoo Basin, South Africa. Sedimentary Geology, 235(3-4), 314-330. https://doi.org/10.1016/j.sedgeo.2010.09.011

Owen, G. (2003). Load structures: gravity-driven sediment mobilization in the shallow subsurface. Geological Society, London, Special Publications, 216(1), 21-34. https://doi.org/10.1144/GSL.SP.2003.216.01.03

Park, Y., Swanson-Hysell, N. L., MacLennan, S. A., Maloof, A. C., Gebreslassie, M., Tremblay, M. M., Schoene, B., Alene, M., Anttila, E. S., Tesema, T. & Haileab, B. (2020). The lead-up to the Sturtian Snowball Earth: Neoproterozoic chemostratigraphy time-calibrated by the Tambien Group of Ethiopia. Bulletin, 132(5-6), 1119-1149. https://doi.org/10.1130/B35178.1

Pazos, P. J. (2002). The Late Carboniferous glacial to postglacial transition: facies and sequence stratigraphy, western Paganzo Basin, Argentina. Gondwana Research, 5(2), 467-487. https://doi.org/10.1016/S1342-937X(05)70736-X

Peral, L. E. G., Poiré, D. G., Strauss, H. & Zimmermann, U. (2007). Chemostratigraphy and diagenetic constraints on Neoproterozoic carbonate successions from the Sierras Bayas Group, Tandilia System, Argentina. Chemical Geology, 237(1-2), 109-128. https://doi.org/10.1016/j.chemgeo.2006.06.022

Pflüeger, F. (1999). Matground structures and redox facies. Palaios, 14(1), 25-39. https://doi.org/10.2307/3515359

Planavsky, N., Bekker, A., Rouxel, O. J., Kamber, B., Hofmann, A., Knudsen, A. & Lyons, T. W. (2010). Rare earth element and yttrium compositions of Archean and Paleoproterozoic Fe formations revisited: new perspectives on the significance and mechanisms of deposition. Geochimica et Cosmochimica Acta, 74(22), 6387-6405. https://doi.org/10.1016/j.gca.2010.07.021

Plink-Björklund, P. & Steel, R. (2005). Deltas on falling-stage and lowstand shelf margins, the Eocene Central Basin of Spitsbergen: importance of sediment supply. https://doi.org/10.2110/pec.05.83.0179

Plummer, P. & Gostin, V. (1981). Shrinkage cracks; desiccation or synaeresis? Journal of Sedimentary Research, 51(4), 1147-1156. https://doi.org/10.1306/212F7E4B-2B24-11D7-8648000102C1865D

Postma, G. (1983). Water escape structures in the context of a depositional model of a mass flow dominated conglomeratic fan-delta (Abrioja Formation, Pliocene, Almeria Basin, SE Spain). Sedimentology, 30(1), 91-103. https://doi.org/10.1111/j.1365-3091.1983.tb00652.x

Pourmand, A., Dauphas, N. & Ireland, T. J. (2012). A novel extraction chromatography and MC-ICP-MS technique for rapid analysis of REE, Sc and Y: Revising CI-chondrite and Post-Archean Australian Shale (PAAS) abundances. Chemical Geology, 291, 38-54. https://doi.org/10.1016/j.chemgeo.2011.08.011

Powell, R. & Domack, G. W. (2002). Modern glaciomarine environments. In Modern and past glacial environments (pp. 361-389): Elsevier. https://doi.org/10.1016/B978-075064226-2/50015-5

Powell, C. M., Preiss, W. V., Gatehouse, C. G., Krapez, B. & Li, Z. X. (1994). South Australian record of a Rodinian epicontinental basin and its mid-Neoproterozoic breakup (~ 700 Ma) to form the Palaeo-Pacific Ocean. Tectonophysics, 237(3-4), 113-140. https://doi.org/10.1016/0040-1951(94)90250-X

Preiss, W. (2000). The Adelaide Geosyncline of South Australia and its significance in Neoproterozoic continental reconstruction. Precambrian Research, 100(1-3), 21-63. https://doi.org/10.1016/S0301-9268(99)00068-6

Preiss, W. & Cowley, W. (1999). Genetic stratigraphy and revised lithostratigraphic classification of the Burra Group in the Adelaide Geosyncline. MESA Journal, 14, 30-40.

Preiss, W., Dyson, I., Reid, P. & Cowley, W. (1998). Revision of lithostratigraphic classification of the Umberatana Group. MESA Journal, 9, 36-42.

Preiss, W. & Forbes, B. (1981). Stratigraphy, correlation and sedimentary history of Adelaidean (Late Proterozoic) basins in Australia. Precambrian Research, 15(3-4), 255-304. https://doi.org/10.1016/0301-9268(81)90054-1

Preiss, W. V. (1973). Palaeoecological interpretations of South Australian Precambrian stromatolites. Journal of the Geological Society of Australia, 19(4), 501-532. https://doi.org/10.1080/00167617308728820

Preiss, W. V. (1987). The Adelaide Geosyncline: Late Proterozoic stratigraphy, sedimentation, palaeontology and tectonics: Department of Mines and Energy.

Preiss, W. V., Drexel, J. F. & Parker, A. J. (1993). The Geology of South Australia: The Precambrian (Vol. 1): Mines and Energy, South Australia, Geological Survey of South Australia.

Preiss, W. V., Drexel, J. F. & Reid, A. J. (2009). Definition and age of the Kooringa Member of the Skillogalee Dolomite: host for Neoproterozoic (c. 790 Ma) porphyry related copper mineralisation at Burra. MESA Journal, 55, 19-33.

Preiss, W. V., Gostin, V. A., McKirdy, D. M., Ashley, P., Williams, G. & Schmidt, P. (2011). Geological Society, London, Memoirs. Geological Society, London, Memoirs, 36(1), 701-712. https://doi.org/10.1144/M36.69

Reading, H. G. (2009). Sedimentary environments: processes, facies and stratigraphy: John Wiley & Sons.

Reading, H. G. & Richards, M. (1994). Turbidite systems in deep-water basin margins classified by grain size and feeder system. AAPG bulletin, 78(5), 792-822. https://doi.org/10.1306/A25FE3BF-171B-11D7-8645000102C1865D

Reineck, H. E. & Wunderlich, F. (1968). Classification and origin of flaser and lenticular bedding. Sedimentology, 11(1-2), 99-104. https://doi.org/10.1111/j.1365-3091.1968.tb00843.x

Roberts, H. H. (1997). Dynamic changes of the Holocene Mississippi River delta plain: the delta cycle. Journal of Coastal Research, 605-627. https://www.jstor.org/stable/4298659

Rooney, A. D., Macdonald, F. A., Strauss, J. V., Dudás, F. Ö., Hallmann, C. & Selby, D. (2014). Re-Os geochronology and coupled Os-Sr isotope constraints on the Sturtian snowball Earth. Proceedings of the National Academy of Sciences, 111(1), 51-56. https://doi.org/10.1073/pnas.1317266110

Rooney, A. D., Strauss, J. V., Brandon, A. D. & Macdonald, F. A. (2015). A Cryogenian chronology: Two long-lasting synchronous Neoproterozoic glaciations. Geology, 43(5), 459-462. https://doi.org/10.1130/G36511.1

Rutland, R., Parker, A., Pitt, G., Preiss, W. & Murrell, B. (1981). The Precambrian of South Australia. In Developments in Precambrian geology (Vol. 2, pp. 309-360): Elsevier. https://doi.org/10.1016/S0166-2635(08)70199-3

Schomacker, E. R., Kjemperud, A. V., Nystuen, J. P. & Jahren, J. S. (2010). Recognition and significance of sharp-based mouth-bar deposits in the Eocene Green River Formation, Uinta Basin, Utah. Sedimentology, 57(4), 1069-1087. https://doi.org/10.1111/j.1365-3091.2009.01136.x

Shanmugam, G. (1997). The Bouma sequence and the turbidite mind set. Earth-Science Reviews, 42(4), 201-229. https://doi.org/10.1016/S0012-8252(97)81858-2

Shanmugam, G. (2000). 50 years of the turbidite paradigm (1950s—1990s): deep-water processes and facies models—a critical perspective. Marine and petroleum Geology, 17(2), 285-342. https://doi.org/10.1016/S0264-8172(99)00011-2

Shields, G. A., Halverson, G. P. & Porter, S. M. (2018). Descent into the Cryogenian. Precambrian Research, 319, 1-5. https://doi.org/10.1016/j.precamres.2018.08.015

Shields-Zhou, G. & Och, L. (2011). The case for a Neoproterozoic oxygenation event: geochemical evidence and biological consequences. GSA Today, 21(3), 4-11. http://dx.doi.org/10.1130/GSATG102A.1

Shinn, E. A. (1969). Submarine lithification of Holocene carbonate sediments in the Persian Gulf. Sedimentology, 12(1-2), 109-144. https://doi.org/10.1111/j.1365-3091.1969.tb00166.x

Sholkovitz, E., Shaw, T. J. & Schneider, D. (1992). The geochemistry of rare earth elements in the seasonally anoxic water column and porewaters of Chesapeake Bay. Geochimica

et Cosmochimica Acta, 56(9), 3389-3402. https://doi.org/10.1016/0016-7037(92)90386-W

Shuster, A. M., Wallace, M. W., van Smeerdijk Hood, A. & Jiang, G. (2018). The Tonian Beck Spring Dolomite: Marine dolomitization in a shallow, anoxic sea. Sedimentary Geology, 368, 83-104. https://doi.org/10.1016/j.sedgeo.2018.03.003

Sibley, D. F. & Gregg, J. M. (1987). Classification of dolomite rock textures. Journal of sedimentary Research, 57(6), 967-975.

Solak, C., Taslı, K. & Koç, H. (2016). Early Cretaceous Shallow-Water Platform Carbonates of the Bolkar Mountains, Central Taurides-South Turkey: Facies Analysis and Depositional Environments. Paper presented at the World Multidisciplinary Earth Sciences Symposium (WMESS 2016) IOP Publishing IOP Conf. Series: Earth and Environmental Science. 10.1088/1755-1315/44/4/042014

Sperling, E. A., Wolock, C. J., Morgan, A. S., Gill, B. C., Kunzmann, M., Halverson, G. P., Macdonald, F. A., Knoll, A. H. & Johnston, D. T. (2015). Statistical analysis of iron geochemical data suggests limited late Proterozoic oxygenation. Nature, 523(7561), 451-454. https://doi.org/10.1038/nature14589

Stromberg, S. G. & Bluck, B. (1998). Turbidite facies, fluid-escape structures and mechanisms of emplacement of the Oligo-Miocene Aljibe Flysch, Gibraltar Arc, Betics, southern Spain. Sedimentary Geology, 115(1-4), 267-288. https://doi.org/10.1016/S0037-0738(97)00096-1

Sumartojo, J. & Gostin, V. (1976). Geochemistry of the late Precambrian Sturt Tillite, Flinders Ranges, South Australia. Precambrian Research, 3(3), 243-252. https://doi.org/10.1016/0301-9268(76)90011-5

Swanson-Hysell, N. L., Rose, C. V., Calmet, C. C., Halverson, G. P., Hurtgen, M. T. & Maloof, A. C. (2010). Cryogenian glaciation and the onset of carbon-isotope decoupling. Science, 328(5978), 608-611. 10.1126/science.1184508

Talling, P. J., Masson, D. G., Sumner, E. J. & Malgesini, G. (2012). Subaqueous sediment density flows: Depositional processes and deposit types. Sedimentology, 59(7), 1937-2003. https://doi.org/10.1111/j.1365-3091.2012.01353.x

Thomson, B., Coats, R., Mirams, R., Forbes, B., Dalgarno, C. & Johnson, J. (1964). Precambrian rock groups in the Adelaide Geosyncline: a new subdivision. Quarterly Journal of the Geological Survey of South Australia, 9, 1-19.

Thomson, D., Rainbird, R. H. & Dix, G. (2014). Architecture of a Neoproterozoic intracratonic carbonate ramp succession: Wynniatt Formation, Amundsen basin, Arctic Canada. Sedimentary Geology, 299, 119-138. https://doi.org/10.1016/j.sedgeo.2013.11.005

Thomson, D., Rainbird, R. H. & Krapez, B. (2015). Sequence and tectonostratigraphy of the Neoproterozoic (Tonian-Cryogenian) Amundsen Basin prior to supercontinent (Rodinia) breakup. Precambrian Research, 263, 246-259. https://doi.org/10.1016/j.precamres.2015.03.001

Thorie, A., Mukhopadhyay, A., Mazumdar, P. & Banerjee, T. (2020). Characteristics of a Tonian reef rimmed shelf before the onset of Cryogenian: Insights from Neoproterozoic Kunihar Formation, Simla Group, Lesser Himalaya. Marine and Petroleum Geology, 104393. https://doi.org/10.1016/j.marpetgeo.2020.104393

Tinterri, R., Magalhaes, P. M., Tagliaferri, A. & Cunha, R. (2016). Convolute laminations and load structures in turbidites as indicators of flow reflections and decelerations against bounding slopes. Examples from the Marnoso-arenacea Formation (northern Italy) and Annot Sandstones (south eastern France). Sedimentary Geology, 344, 382-407. https://doi.org/10.1016/j.sedgeo.2016.01.023

Tostevin, R., Shields, G. A., Tarbuck, G. M., He, T., Clarkson, M. O. & Wood, R. A. (2016). Effective use of cerium anomalies as a redox proxy in carbonate-dominated marine

settings. Chemical Geology, 438, 146-162. https://doi.org/10.1016/j.chemgeo.2016.06.027

Tucker, M. E. (1982). Precambrian dolomites: petrographic and isotopic evidence that they differ from Phanerozoic dolomites. Geology, 10(1), 7-12. https://doi.org/10.1130/0091-7613(1982)10<7:PDPAIE>2.0.CO;2

Tucker, M. E. & Wright, V. P. (2009). Carbonate sedimentology: John Wiley & Sons.

Uppill, R. K. (1980). Sedimentology of the late Precambrian Mundallio Subgroup: a clastic-carbonate (Dolomite, Magnesite) sequence in the Mt. Lofty and Flinders Ranges, South Australia. https://hdl.handle.net/2440/37784

Uppill, R. K. (1990). Sedimentology of a dolomite-magnesite-sandstone sequence in the late Precambrian Mundallio Subgroup, South Australia. The evolution of a late Precambrian–early Paleozoic rift complex: The Adelaide geosyncline: Geological Society of Australia Special Publication, 16, 105-128.

Vahrenkamp, V. C. & Swart, P. K. (1990). New distribution coefficient for the incorporation of strontium into dolomite and its implications for the formation of ancient dolomites. Geology, 18(5), 387-391. https://doi.org/10.1130/0091-7613(1990)018<0387:NDCFTI>2.3.CO;2

Vakarelov, B. K. & Ainsworth, R. B. (2013). A hierarchical approach to architectural classification in marginal-marine systems: Bridging the gap between sedimentology and sequence stratigraphyHierarchical Marginal-Marine Architectural Classification. AAPG bulletin, 97(7), 1121-1161. https://doi.org/10.1306/11011212024

Veevers, J. & Cotterill, D. (1978). Western margin of Australia: evolution of a rifted arch system. Geological Society of America Bulletin, 89(3), 337-355. https://doi.org/10.1130/0016-7606(1978)89<337:WMOAEO>2.0.CO;2

Veizer, J. (1983). Chemical diagenesis of carbonates: theory and application. Stable isotopes in sedimentary geology, 10, 3-100. https://doi.org/10.2110/scn.83.01.0000

Verdel, C., Phelps, B. & Welsh, K. (2018). Rare earth element and 87Sr/86Sr step-leaching geochemistry of central Australian Neoproterozoic carbonate. Precambrian Research, 310, 229-242. https://doi.org/10.1016/j.precamres.2018.02.014

Von der Borch, C. (1980). Evolution of late proterozoic to early paleozoic Adelaide foldbelt, Australia: Comparisons with postpermian rifts and passive margins. Tectonophysics, 70(1-2), 115-134. https://doi.org/10.1016/0040-1951(80)90023-2

Von der Borch, C. & Lock, D. (1979). Geological significance of Coorong dolomites. Sedimentology, 26, 813-824. https://doi.org/10.1111/j.1365-3091.1979.tb00974.x

Wallace, M. W., Hood, A. v.S., Woon, E. M., Giddings, J. A. & Fromhold, T. A. (2015). The Cryogenian Balcanoona reef complexes of the Northern Flinders Ranges: implications for Neoproterozoic ocean chemistry. Palaeogeography, Palaeoclimatology, Palaeoecology, 417, 320-336. https://doi.org/10.1016/j.palaeo.2014.09.028

Wallace, M. W., Shuster, A., Greig, A., Planavsky, N. J. & Reed, C. P. (2017). Oxygenation history of the Neoproterozoic to early Phanerozoic and the rise of land plants. Earth and Planetary Science Letters, 466, 12-19. https://doi.org/10.1016/j.epsl.2017.02.046

Walter, M. R., Veevers, J. J., Calver, C. R., Gorjan, P. & Hill, A. C. (2000). Dating the 840–544 Ma Neoproterozoic interval by isotopes of strontium, carbon, and sulfur in seawater, and some interpretative models. Precambrian Research, 100(1-3), 371-433. https://doi.org/10.1016/S0301-9268(99)00082-0

Wanless, H. R., Tedesco, L. P. & Tyrrell, K. M. (1988). Production of subtidal tubular and surficial tempestites by hurricane Kate, Caicos Platform, British West Indies. Journal of Sedimentary Research, 58(4), 739-750. https://doi.org/10.1306/212F8E31-2B24-11D7-8648000102C1865D

Ward, J. F., Verdel, C., Campbell, M. J., Leonard, N. & Nguyen, A. D. (2019). Rare earth element geochemistry of Australian Neoproterozoic carbonate: Constraints on the Neoproterozoic oxygenation events. Precambrian Research, 335, 105471. https://doi.org/10.1016/j.precamres.2019.105471

Warren, J. K. (1990). Sedimentology and mineralogy of dolomitic Coorong lakes, South Australia. Journal of Sedimentary Research, 60(6), 843-858. https://doi.org/10.1306/212F929B-2B24-11D7-8648000102C1865D

Webb, G. E. & Kamber, B. S. (2000). Rare earth elements in Holocene reefal microbialites: a new shallow seawater proxy. Geochimica et Cosmochimica Acta, 64(9), 1557-1565. https://doi.org/10.1016/S0016-7037(99)00400-7

Wilmsen, M., Berensmeier, M., Fürsich, F. T., Majidifard, M. R. & Schlagintweit, F. (2018). A Late Cretaceous epeiric carbonate platform: the Haftoman Formation of central Iran. Facies, 64(2), 11. https://doi.org/10.1007/s10347-018-0523-6

Winsemann, J., Hornung, J. J., Meinsen, J., Asprion, U., Polom, U., Brandes, C., Bußmann, M. & Weber, C. (2009). Anatomy of a subaqueous ice-contact fan and delta complex, Middle Pleistocene, North-west Germany. Sedimentology, 56(4), 1041-1076. https://doi.org/10.1111/j.1365-3091.2008.01018.x

Wright, V. P. (1992). A revised classification of limestones. Sedimentary geology, 76(3-4), 177-185. https://doi.org/10.1016/0037-0738(92)90082-3

Yang, B. C., Dalrymple, R. W. & Chun, S. S. (2005). Sedimentation on a wave-dominated, open-coast tidal flat, south-western Korea: summer tidal flat–winter shoreface. Sedimentology, 52(2), 235-252. https://doi.org/10.1111/j.1365-3091.2004.00692.x

Yawar, Z. & Schieber, J. (2017). On the origin of silt laminae in laminated shales. Sedimentary Geology, 360, 22-34. https://doi.org/10.1016/j.sedgeo.2017.09.001

Young, G. & Gostin, V. (1988). Stratigraphy and sedimentology of Sturtian glacigenic deposits in the western part of the North Flinders Basin, South Australia. Precambrian Research, 39(3), 151-170. https://doi.org/10.1016/0301-9268(88)90040-X

Young, G. & Gostin, V. (1991). Late Proterozoic (Sturtian) succession of the North Flinders Basin, South Australia: an example of temperate glaciation in an active rift setting. Glacial Marine Sedimentation: Paleoclimatic Significance, 261, 207-222.

Zhang, S., Jiang, G. & Han, Y. (2008). The age of the Nantuo Formation and Nantuo glaciation in South China. Terra Nova, 20(4), 289-294. https://doi.org/10.1111/j.1365-3121.2008.00819.x

Chapter 3: Improving interpretations of Tonian palaeoenvironments with multiproxy isotopic geochemistry: a case study from South Australia

Unsubmitted manuscript prepared for publication:

Georgina M. Virgo, Alan S. Collins, Juraj Farkaš, Morgan L. Blades, Darwinaji Subarkah, Kathryn J. Amos

Statement of Authorship

Title of Paper	Improving interpretations of Tonian palaeoenvironments with multiproxy isotopic geochemistry: a case study from South Australia
Publication Status	☐ Published ☐ Accepted for Publication ☐ Submitted for Publication ☑ Unpublished and Unsubmitted work written in manuscript style
Publication Details	Virgo, G. M., Collins, A. S., Farkaš, J., Blades, M. L., Subarkah, D., & Amos, K. J. (2023). Improving interpretations of Tonian palaeoenvironments with multiproxy isotopic geochemistry: a case study from South Australia

Principal Author

Name of Principal Author (Candidate)	Georgina Virgo		
Contribution to the Paper	All manuscript and figure drafting; data collection, processing and analysis; methodology; interpretations; field investigation		
Overall percentage (%)	80%		
Certification:	This paper reports on original research I conducted during the period of my Higher Degree by Research candidature and is not subject to any obligations or contractual agreements with a third party that would constrain its inclusion in this thesis. I am the primary author of this paper.		
Signature		Date	07/07/2023

Co-Author Contributions

By signing the Statement of Authorship, each author certifies that:

i. the candidate's stated contribution to the publication is accurate (as detailed above);
ii. permission is granted for the candidate in include the publication in the thesis; and
iii. the sum of all co-author contributions is equal to 100% less the candidate's stated contribution.

Name of Co-Author	Alan Collins		
Contribution to the Paper	Reviews and commentary		
Signature		Date	07/07/2023

Name of Co-Author	Juraj Farkas		
Contribution to the Paper	Reviws and commentary; assistance with methodology and formal analysis		
Signature		Date	07/07/2023

Please cut and paste additional co-author panels here as required.

Name of Co-Author	Morgan Blades		
Contribution to the Paper	Reviews and commentary		
Signature		Date	07/07/2023

Name of Co-Author	Darwinaji Subarkah		
Contribution to the Paper	Reviws and commentary; assistance with methodology and formal analysis		
Signature		Date	07/07/2023

Name of Co-Author	Kathryn Amos		
Contribution to the Paper	Reviews and commentary		
Signature		Date	07/07/2023

3.1 Abstract

The Tonian–Cryogenian transition represents a period of significant physiochemical change in Earth history. It involved variations in oceanic and atmospheric oxygenation, significant changes in seawater chemistry, the biosphere, tectonic reorganisation, and the onset of the global 'Sturtian' glaciation. Tonian and Cryogenian marginal marine sedimentary rocks in the Adelaide Superbasin, South Australia (SA), represent some of the most well-exposed, continuous and thickest sections of this interval globally.

We present a coupled sedimentological and multi-proxy isotopic ($\delta^{13}C$, $^{87}Sr/^{86}Sr$, $\delta^{88/86}Sr$) and elemental study through a ~1.9 km thick pre-glacial succession near Copley in the northern Flinders Ranges, SA. Our study reveals a carbonate platform setting during the Tonian, where inner platform intraclastic magnesite and stromatolitic carbonates characterise the Skillogalee Dolomite, and transition to subtidal siltstone and platform carbonates in the Myrtle Springs Formation.

C- and Sr-isotope signatures were analysed to determine primary basin water chemistries and further constrain the depositional setting. In the Skillogalee Dolomite, $\delta^{13}C$ (PDB) is represented by overall positive values (ca. 5‰), two distinctive data clusters for $^{87}Sr/^{86}Sr$ (0.710 and 0.716), and $\delta^{88/86}Sr$ (NBS987) values (0.15‰ and 0.21‰). This corresponds to a regressive systems tract – transgressive systems tract (RST-TST) cycle, where the MRS is represented by the most radiogenic values and heaviest $\delta^{13}C$. This likely resulted from increased riverine input of more evolved and radiogenic Sr and delivery of isotopically light C waters to the inner platform setting. The Ce/Ce* and Eu/Eu* REE data elucidate a dysoxic water column, fed by both anoxic deep waters and more oxic shallow-water that was typical for the Proterozoic stratified ocean. The Myrtle Springs Formation is characterised by two prominent negative isotopic excursions (lower than -3‰), interrupting an increasing $\delta^{13}C$ up-section trend, from -3.0‰ to 3.7‰, paired with increasing $^{87}Sr/^{86}Sr$ (0.709 – 0.711) and light or lower $\delta^{88/86}Sr$ values (0.21). Sequence stratigraphic and REE data present multiple RST-TST cycles and redox states, which record an overall trend from an anoxic, deep-water subtidal setting to a dysoxic, shallow-water supratidal environment. $\delta^{13}C$ values are similar to other near-conformable Tonian–Cryogenian successions worldwide. However, $^{87}Sr/^{86}Sr$ and $\delta^{88/86}Sr$ values differ from Tonian marine carbonates at other global locations (e.g. Mackenzie Mountains, Canada), reiterating the more restricted depositional setting with respect to an open ocean, observed in this study. In combination, the sedimentological and geochemical/isotope data build a picture of a partially restricted, carbonate platform setting for the northern Flinders Ranges periodically flooded by deeper basinal waters, directly before the climate pivot to the Sturtian glaciation. Such restricted settings that facilitate primary magnesite formation seem to have some affinity and isotope similarity to the modern Coorong lagoon depositional system. Consequently, this might present a reasonable analogue for these ancient carbonate rocks.

3.2 Introduction

The Neoproterozoic Era (1000 to 539 Ma) encompasses some of the most critical changes in Earth's history (Halverson et al., 2009), many of which are responsible for shaping the world as we know it today. Consequently, this era has been studied extensively, using a suite of scientific techniques, to unravel what the world was like during this time and how these global shifts may have occurred. Historical literature established a foundation for the key tectonic (Dalziel, 1997; Meert, 2003; Collins & Pisarevsky, 2005), biological (Knoll, 1992; Narbonne, 1998; Butterfield, 2000), geochemical (Berkner & Marshall, 1965; Runnegar, 1991; Marais et al., 1992; Canfield & Teske, 1996), and climatic (Kirschvink, 1992; Hoffman et al., 1998) shifts during this time, while more recent studies have provided a more sophisticated understanding of these phenomena. This includes: tectonic reconstructions that extend into the Precambrian (Li et al., 2008; Merdith et al., 2017; 2019; 2021; Collins et al., 2022); relationship between the rise of algae, shift from bacterial to eukaryotic productivity, and evolution of ocean oxygenation (Shields-Zhou & Och, 2011; Lenton et al., 2014; Lyons et al., 2014; Brocks et al., 2017); and climate dynamics that persisted throughout the "Snowball" event (Micheels & Montenari; Hoffman et al., 2017). With that said, ancient environments are notoriously challenging to piece together due to the limited availability of modern analogues and constraints to properly assess later post-depositional geochemical and isotopic resetting.

The Flinders Ranges of South Australia host an extensive archive of Neoproterozoic marine sedimentary rocks (Preiss, 2000; Hoffman & Schrag, 2002; Keeman et al., 2020; Lloyd et al., 2020). Geochemical research on these ancient rocks has generated multiproxy datasets for several isotopic and elemental systems. Although there have been broad geochemical studies through thick stratigraphic successions (e.g. Barovich & Foden, 2000; Walter et al., 2000; Halverson et al., 2005; Swanson-Hysell et al., 2010; Cox et al., 2016; Wallace et al., 2017; Ward et al., 2019), they often do not analyse all the relevant geochemical proxies, which minimises the resolution of interpreted palaeoenvironments. On the other hand, many studies present highly detailed insights into the depositional environment through a suite of geochemical analyses (e.g. Sumartojo & Gostin, 1976; Belperio, 1990; Hill & Walter, 2000; McKirdy et al., 2001; Frank & Fielding, 2003; Giddings & Wallace, 2009; 2009a; Grey et al., 2011; Hood et al., 2011; 2016; 2018; Hood & Wallace, 2012; 2014; 2015; Lechte & Wallace, 2016; Wallace et al., 2019; O'Connell et al., 2020). However, these are often for one formation, which narrows the temporal scope of the study.

Chapter 2 established high resolution sedimentologic interpretations combined with elemental geochemistry for a stratigraphically thick and conformable Tonian–Cryogenian succession, which provided a foundation for the temporal shifts in depositional setting, relative sea level and redox conditions. Although this work was highly detailed and provided some geochemical constraints on the palaeo-water, it did not ascertain the geochemical conditions responsible for the precipitation of the Mg-rich carbonates (dolomite and magnestite) observed in this section, particularly during the Tonian. To address such limitations, this chapter presents multiproxy isotopic analysis through this same Tonian succession of marine/lagoonal carbonates, to infer variations in palaeo-productivity and relative basin restriction. We used micro-scale (SEM-

EDS) mineral mapping to identify mineralogy and textures, which was coupled with C and O isotope analysis to determine fluctuations in nutrients and organic carbon burial; and finally, $\delta^{88/86}$Sr and ^{87}Sr/^{86}Sr proxies have been used to constrain past changes in carbonate saturation of seawater and various Sr sources into the basin, respectively. These datasets and multi-proxy approach is presented alongside the previous sedimentological, sequence stratigraphic and elemental geochemical analysis from Chapter 2, to provide a robust, high-resolution investigation into the palaeoenvironmental conditions that facilitated the precipitation of Mg-rich carbonates during the Tonian.

3.3 Geological setting

The Neoproterozoic rocks of South Australia were deposited in the Adelaide Superbasin (Figure 1), a large sedimentary system in the south-eastern margin of Proterozoic Australia (Preiss, 2000; Lloyd et al., 2020, and references therein). This basin developed during the rifting of Laurentia from Australia-East Antarctica, associated with the breakup of supercontinent Rodinia (Merdith et al., 2017a). Sedimentation was focused in the Adelaide Rift Complex, a 600 km north-south trending basin that forms the central part of the Adelaide Superbasin (Lloyd et al., 2020; 2022). The Delamerian Orogeny, which peaked at ca. 500 Ma, marks the termination of Neoproterozoic deposition (Foden et al., 2006; 2020), and along with later Phanerozoic orogenesis, resulted in the uplift and exposure of these rocks in the modern-day Flinders Ranges and Mount Lofty Ranges. marks the termination of Neoproterozoic deposition (Foden et al., 2006; 2020), and along with later Phanerozoic orogenesis, resulted in the uplift and exposure of these rocks in the modern-day Flinders Ranges and Mount Lofty Ranges.

Tonian deposition was focused along the western margin of the Adelaide Rift Complex in the Willouran Trough, which was sourcing material from the surrounding rift shoulders (Preiss 2000; Lloyd et al., 2020). These sediments are lithostratigraphically characterised by the Callanna and Burra groups (Figure 1; Thomson et al., 1964; Lloyd et al., 2020), which comprise a mix of sedimentary/volcanic and clastic/carbonate rocks, respectively (Preiss, 1987; 2000). Chronostatigraphically, the base of the Tonian succession is constrained by a maximum depositional age of 893 ± 9 Ma (Paralana Quartzite, Lloyd et al., 2022) and a primary tuff zircon age of 802 ± 10 Ma (Rook Tuff, Fanning et al., 1986) in the Callanna Group. Further, U–Pb zircon constrain the base of the Burra Group to 788 ± 6 Ma (Boucaut Volcanics, Armistead et al., 2021) and 794 ± 4 Ma (Kooringa Member, Preiss et al., 2009).

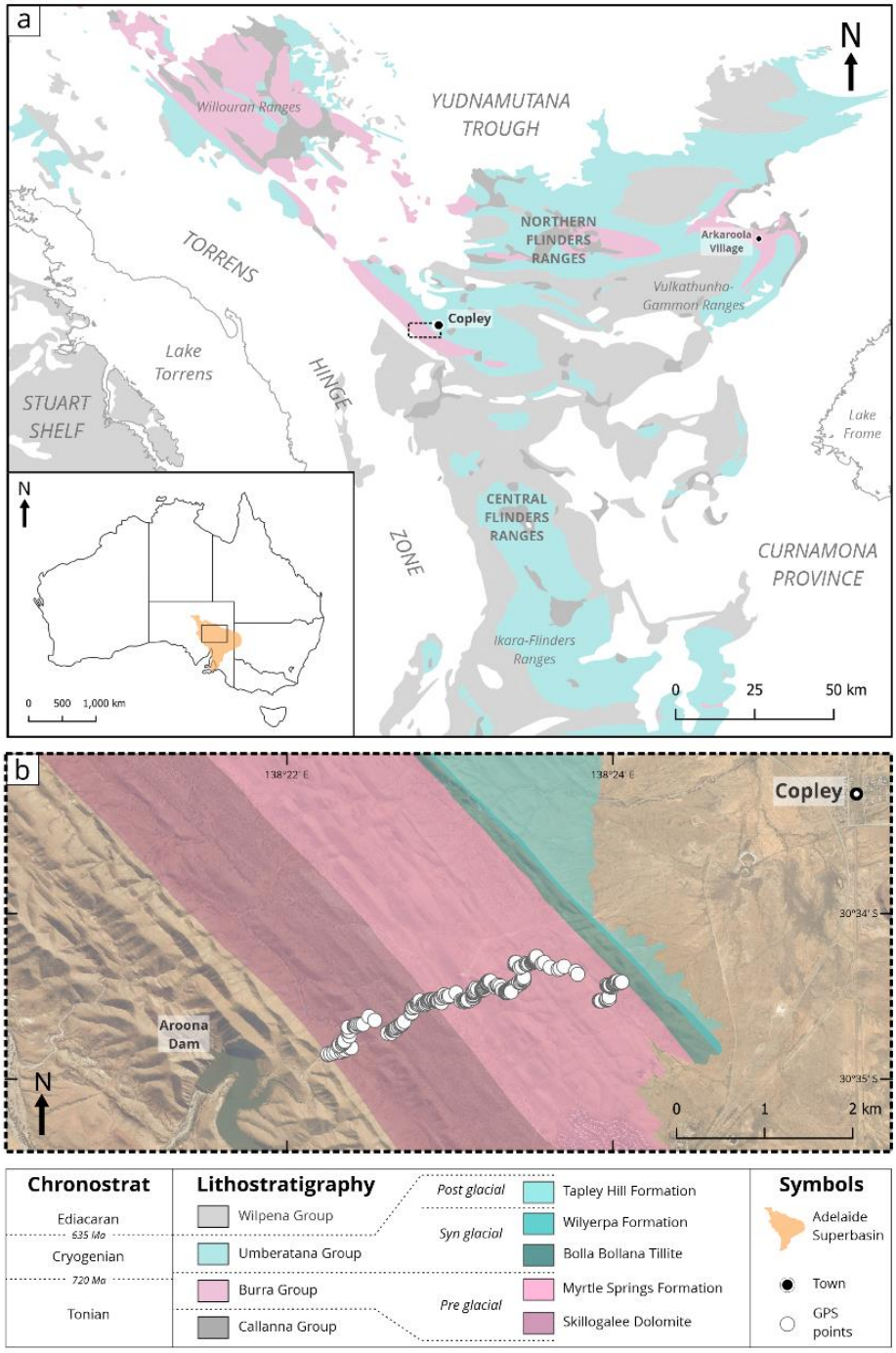

Figure 1: (a) Geological map of the northern Flinders Ranges in the Adelaide Superbasin. Insert shows position of Adelaide Superbasin within Australia. Tonian and Cryogenian lithostratigraphic groups are highlighted in the grey, pink, and blue. (b) Study location through section southwest of Copley township and northeast of Aroona Dam. GPS points recorded along sedimentological log/transect highlighted with white circles.

3.4 Background

3.4.1 Isotopic Systems and their implications on depositional setting

Shifts in carbon isotopes ($\delta^{13}C$) recorded in marine carbonates have long been used as a tool to better understand bioproductivity changes in the ocean. This is reflected in the C isotope composition of the dissolved inorganic carbon (DIC) pool for a water column, and by inference also in precipitated marine carbonates that formed from such DIC sources (Knoll et al., 1986; Schidlowski, 1988). The C isotopic fractionation from biological processes and subsequent burial of organic carbon in the ocean leads to lower concentrations of CO_2 in the surface water and ^{13}C enrichment of the remaining DIC pool, resulting in heavier $\delta^{13}C_{carb}$ values (Kump & Arthur, 1999; Bastow et al., 2002; Frimmel, 2010). Conversely, remineralisation of organic matter in the deep ocean through biological assimilation results in the input of light ^{12}C into seawater and thus, lighter marine $\delta^{13}C_{carb}$ values (Sarmiento et al., 2013). In addition to these biology-driven changes, evaporation can lead to concurrent perturbations in both the $\delta^{13}C$ and $\delta^{18}O$ records (Frimmel, 2010). This is due to CO_2 evasion during evaporation, causing brines to be enriched in ^{13}C and ^{18}O and resulting in positive $\delta^{13}C$ and $\delta^{18}O$ excursions in associated evaporitic carbonates (Frimmel, 2010). Consequently, $\delta^{13}C$ in marine carbonates is a facies dependant isotopic system, as both productivity and evaporation influence the C isotope fractionation and signature of carbonates during their precipitation/deposition.

The ratio of the radiogenic strontium isotope ^{87}Sr to the stable isotope ^{86}Sr (i.e., $^{87}Sr/^{86}Sr$ ratio) has been widely used as a proxy for global variations in the balance between Sr inputs from continental weathering versus submarine hydrothermal or mid ocean ridge (MOR) systems into the ocean through time. This is reflected in $^{87}Sr/^{86}Sr$ of marine carbonates due to the long residence time and global mixing of Sr in the ocean (Chen et al., 2022). Briefly, higher values of $^{87}Sr/^{86}Sr$ in marine carbonates represent enhanced input from more evolved or radiogenic Sr sources from older continental crust, whereas less radiogenic $^{87}Sr/^{86}Sr$ values suggest the input of juvenile, mantle-derived Sr from the oceanic crust (Halverson et al., 2009; Halverson et al., 2010; Kuznetsov et al., 2018; Shields & Veizer, 2002; Veizer et al., 1992). However, it is also possible that more radiogenic $^{87}Sr/^{86}Sr$ in marine carbonates (that differ from an expected value for the global ocean) suggest that these carbonates formed either in more restricted coastal/marine settings (e.g. Shao et al., 2018; Vasiliev et al., 2022) and/or have been affected by post-depositional and diagenetic resetting.

As to the variation in the stable strontium isotopes ^{88}Sr with respect to ^{86}Sr (recorded as $\delta^{88/86}Sr$), this novel marine isotope proxy is sensitive to changes in the fluxes or balance between carbonate formation versus dissolution in the ocean, as well as the input of Sr from carbonate weathering (Shao et al., 2021; Vollstaedt et al., 2014). Marine carbonates preferentially uptake the lighter Sr isotope, leaving the fluid or palaeowater isotopically heavy with respect to stable Sr isotopes (Shao et al., 2021; Vollstaedt et al., 2014). When coupled with radiogenic Sr isotopes, felsic (continental) rocks that carry higher $^{87}Sr/^{86}Sr$ relative to mafic (oceanic) rocks or carbonates (Amsellem et al., 2018; Charlier et al., 2012) can be combined with $\delta^{88/86}Sr$ to infer changes in silicate (mafic/felsic) and carbonate weathering

fluxes over time. As such, increased input from felsic, continental sources into the ocean tend to have higher $^{87}Sr/^{86}Sr$ ratios and lighter $\delta^{88/86}Sr$ signatures.

3.4.2 Palaeoenvironmental constraints in the Tonian

There has been a number of studies focused on better constraining the depositional setting of the northern Flinders Ranges during and after the Sturtian glaciation through analysing the key sedimentological and geochemical variations (e.g. Sumartojo & Gostin, 1976; Link & Gostin, 1981; Young & Gostin, 1988; 1991; McKirdy et al., 2001; Giddings & Wallace, 2009; 2009a; Giddings et al., 2009; Fromhold & Wallace, 2011; 2012; Grey et al., 2011; Hood et al., 2011; 2016; 2018; Le Heron et al., 2011; 2011a; 2014; Preiss et al., 2011; Hood & Wallace, 2012; 2014; 2015; Busfield & Le Heron, 2014; Lechte & Wallace, 2015; 2016; Wallace et al., 2015; 2019; Cox et al., 2018; O'Connell et al., 2020; Virgo et al., 2021; Lloyd et al., 2022a). However, there has been considerably less research on the pre-glacial succession (e.g. von der Borch & Lock, 1979; Belperio, 1990; Uppill, 1990; Preiss & Cowley, 1999; Hill & Walter, 2000; Frank & Fielding, 2003; Preiss et al., 2009; Virgo et al., 2021; O'Connell et al., 2022), which is equally important as the conditions for these critical climatic and geochemical shifts were established during this time. The northern Flinders Ranges has been used as the location for many of these studies due to the widespread exposure of these rocks, providing access to stratigraphy both temporally and spatially. The Tonian succession examined in this paper is located on the western margin of the northern Flinders Ranges. At this location, the pre-glacial succession can be broadly divided into two formations: the Skillogalee Dolomite and Myrtle Springs Formation (Preiss & Cowley, 1999; Virgo et al., in press).

Overall, the Skillogalee Dolomite has been interpreted to represent a marginal marine to carbonate platform environment with stacked shoaling cycles (Preiss, 1973; von der Borch & Lock, 1979; Preiss, 1987; Belperio, 1990; Virgo et al., 2022). The lower half of the formation is represented by clastic dominated interbedded siltstone, sandstone and dolostone (Preiss, 1987; Counts, 2017), indicating a continued transgression from the underlying deltaic deposits of the Copley Quartzite (Virgo et al., 2021). This is interpreted to represent a low to moderate energy productive setting (Preiss, 1973; 1987), such as an intertidal to lagoonal inner platform environment (Virgo et al., 2021). The upper unit is characterised by several regressive parasequences, represented by cyclical deposition of intraclastic magnesite ($MgCO_3$), black chert, layered microbialites, and minor clastic material (Preiss, 1987; Belperio, 1990; Frank & Fielding, 2003; Counts, 2017; Virgo et al., 2021). This is interpreted to reflect an inner platform supratidal to lagoonal setting (Virgo et al., 2021). The very top of the Skillogalee Dolomite is marked by the microbialite *Baicalia burra* (Preiss, 1973; Belperio, 1990; Grey et al., 2011), possibly corresponding to a transgression to an outer platform stromatolitic buildup (Virgo et al., 2021). As discussed in Chapter 2, elemental geochemistry from this formation records weakly negative Ce/Ce* (0.95), high Eu/Eu* (2.47), low Y/Ho (34.90) and slight LREE depletion (Nd_{PASS}/Yb_{PASS} = 0.74), representing a semi-restricted, dysoxic water column fed by oxic shallow waters and anoxic deeper marine waters (e.g. Wallace et al., 2017; Shuster et al., 2018), as well as continental freshwaters (Virgo et al., 2021). Isotopic geochemistry, including $\delta^{18}O$ and $\delta^{13}C$, reveal a range of values that appears to be facies dependant (Veizer & Compston, 1974; 1976; Schidlowski et al., 1975; Veizer & Hoefs, 1976; Burke et al., 1982;

Veizer et al., 1983; Belperio, 1990; Frank & Fielding, 2003). Layered microbialite and dolostone samples are the most isotopically homogenous, with $\delta^{18}O$ values ranging between -2.25‰ and +0.25‰, and $\delta^{13}C$ scattering between +2.70‰ and +5.75‰, which seems to support an evaporative and biologically productive marine to coastal setting (Frank & Fielding, 2003). The measured $\delta^{18}O$ values are heavier than marine dolostones of the same age, possibly due to evaporation induced $\delta^{18}O$ enrichment, while $\delta^{13}C$ values are comparable (or heavier) to marine carbonates of the time (Schidlowski et al., 1975; Belperio, 1990; Jacobsen & Kaufman, 1999; Frank & Fielding, 2003). The overall positive $\delta^{13}C$ values for dolostone samples in the Skillogalee Dolomite are recorded at four locations: (1) at this study location (Frank & Fielding, 2003); (2) along strike to the NW in the Willouran Ranges (Belperio, 1990); (3) further NW in the Peak and Denison Ranges (Grey et al., 2011); and (4) towards the south in the Southern Flinders Ranges (Grey et al., 2011). Intraclastic magnesite samples exhibit more isotopic variability, with the highest $\delta^{13}C$ values of up to +6.30‰ recorded in magnesite clasts (Frank & Fielding, 2003). Comparatively heavy $\delta^{13}C$ values (up to +7.27‰) were also recorded from intraclastic magnesite samples along strike to the north (Belperio, 1990). Organic carbon and Sr isotopic analyses from the section in the Willouran Ranges can potentially be used as a proxy for water chemistry conditions at this study location. Microbial successions, including layered microbialites and stromatolitic samples, record the highest total organic carbon (TOC) content (up to 1.38 wt%), while intraclastic magnesite samples record the lowest TOC values (Belperio, 1987; 1990). Several microbialite and magnesite samples have $^{87}Sr/^{86}Sr$ values of 0.709 that are comparable to global seawater $^{87}Sr/^{86}Sr$ values at that time, while mudstone samples are considerably more radiogenic (0.741; Belperio, 1990). The latter was interpreted to result from the input from non-marine sources and/or post-depositional diagenetic alteration and possible detrital contamination (Belperio, 1990).

The overlying Myrtle Spring Formation is characterised by siltstone, sandstone, dolomite and stromatolitic successions (Coats, 1973; Murrel, 1977), interpreted to reflect a subtidal to marginal marine/carbonate platform settings (Preiss, 1987, Virgo et al., 2021). The base of the formation is marked by a transgression that resulted in deposition of basinal silts (Virgo et al., 2021). This succession records high Y/Ho (35.66) and significant LREE depletion (Nd_{PASS}/Yb_{PASS} = 0.49), interpreted to indicate more open seawater conditions relative to the underlying Skillogalee Dolomite (Virgo et al., 2021). The middle portion of the Myrtle Springs Formation is characterised by stromatolitic buildups interbedded with carbonates and sandstones. This part of the succession is interpreted to represent a regression from the outer platform reef, through the lagoon to an intertidal setting (Virgo et al., 2021). It coincides with decreasing LREE depletion (Nd_{PASS}/Yb_{PASS} = 1.03), and lower Y/Ho and Eu/Eu* (30.24 and 1.93), which is interpreted to reflect increased continental input, and a more restricted (less reducing) water column, respectively (Lawrence et al., 2006; Bolhar & Van Kranendonk, 2007; Frimmel, 2009; Corkeron et al., 2012; Wallace et al., 2017; Shuster et al., 2018; Virgo et al., 2021). The top of the formation is represented by coarsening-up cycles from dolostones to siltstones and stromatolitic facies, characterising outer to inner platform settings (Virgo et al., 2021). This regression is mirrored by the elemental geochemistry, which is comparable to the underlying regression (low LREE depletion, Y/Ho, Ce/Ce* and Eu/Eu*) (Virgo et al., 2021).

There does not appear to be any previous literature on isotopic analyses for the Myrtle Springs Formation, highlighting the importance of the data from this study.

3.5 Methods

3.5.1 Sample selection

Tonian carbonate samples (dolostone and magnesite) were collected from outcrops located 2 km southwest of Copley township in the northern Flinders Ranges, SA (Figure 1). Sampling resolution varied, and was determined by the availability of outcrop, as well as lithology and rock quality. This was determined by the degree of weathering, identification of secondary alteration (e.g. veining), and proximity to siliciclastic units - fresh, unaltered rocks without clastic interbeds were preferred, as they are less likely to be contaminated or reset. The best successions were sampled in 20 cm intervals, while lower quality outcrops were targeted at a metre scale. A detailed sedimentary log through this section, with a comprehensive facies analysis, interpreted depositional environments and sequence stratigraphy, is outlined in Virgo et al. (2021).

3.5.2 Backscattered Electron (BSE) Imaging and Mineral Liberation Analysis (MLA) Maps

A total of three samples were selected from carbonate-bearing formations (Skillogalee Dolomite and Myrtle Springs Formation) in the study location and represent the key carbonate lithologies present within the section (magnesite, dolomite and dolomitic siltstone). These samples were imaged for their key mineral assemblage, mineral associations, and textural properties, where attention was directed to primary carbonate mineralogy and microcrystalline textures. A Hitachi SU3800 Automated Mineralogy Scanning Electron Microscope (SEM) at Adelaide Microscopy was used to collect Backscattered Electron (BSE) images and Mineral Liberation Analysis (MLA) maps via SEM-EDS for the selected samples, following Subarkah et al. (2022). Mineral identification and quantification of samples were processed using AMICS Automated Mineralogy software package.

3.5.3 C and O isotope analysis

A total of 83 samples with carbonate lithologies were analysed for their C and O isotope values. Samples were micro-drilled along laminations to target the carbonate matrix, and the analysis of C and O isotopes followed the procedure addressed in Spötl & Vennemann (2003) and Cox et al. (2016). Briefly, the drilled rock powder was weighted into glass septa vials and cleansed with He. Samples were then purged with phosphoric acid to release CO_2, which was collected through cryogenic extraction. Isotopic ratios of C and O from the resultant gas were measured using a Nu Dual Inlet Isotope Ratio Mass Spectrometer (DI-IRMS) with attached Fisons Isocarb Carbonate Preparation Systems at the University of Adelaide, to correct for fractionation effects. Samples were calibrated to Vienna Pee Dee Belemnite (VPDB) values using house standards, with errors of ~0.05‰ (1 SD) for $\delta^{13}C$ and $\delta^{18}O$.

3.5.4 Sr isotopic analysis

Samples analysed from the best-preserved horizons in the Skillogalee Dolomite and Myrtle Springs Formation were selected for $^{87}Sr/^{86}Sr$ and $\delta^{88/86}Sr$ analysis via TIMS and double-spike (see Shao et al., 2021). The sample selection was based on REE patterns that reflect primary conditions and excursions in C and O isotopes (Virgo et al., 2021). In total, 15 samples were analysed for $^{87}Sr/^{86}Sr$ and five samples for $\delta^{88/86}Sr$ analysis.

Methods outlined by Shao et al. (2018; 2021) were followed for coupled $^{87}Sr/^{86}Sr$ and $\delta^{88/86}Sr$ analyses. Briefly, to determine $\delta^{88/86}Sr$ values, two aliquots were taken from each sample, and one was spiked using $^{87}Sr/^{84}Sr$ double spike solution while the other was processed unspiked. Both samples or aliquots were then purified for Sr fraction via Sr-Spec columns using ion chromatography and loaded onto a single non-zone-refined rhenium filament. For $^{87}Sr/^{86}Sr$ analysis, a single aliquot was purified and loaded onto a filament. The purified Sr fractions were analysed by thermal ionisation mass spectrometry (TIMS) using a Phoenix Isotopx instrument at the University of Adelaide. A multi-dynamic peak-hopping method was employed for $^{87}Sr/^{86}Sr$, with a typical ^{88}Sr beam of around 6 Volts. For stable Sr analysis, three isotopic ratios were collected: $^{87}Sr/^{86}Sr$, $^{86}Sr/^{88}Sr$ and $^{84}Sr/^{86}Sr$ from the spiked sample aliquots. The $^{87}Sr/^{86}Sr$ ratios were corrected based on internal normalisation of instrumental mass-dependent fractionation effects using $^{86}Sr/^{88}Sr$ value of 0.1194 as a normalising ratio (Nier, 1938). The $^{87}Sr/^{86}Sr$ values have a typical 2SD uncertainty of ±0.0000125 and the $\delta^{88/86}Sr$ values have a 2SD error of ±0.004. These are both based on long-term NBS987, IAPSO (seawater) and JCP-1 (carbonate) standard measurements.

3.6 Results

3.6.1 Mineralogy and Petrography

MLA (SEM-EDS) and BSE imaging identified 16 mineral phases, with two common minerals (quartz and dolomite) present between the three selected samples (Figure 2).

The major mineral phases for sample 037 (magnesite), collected 558 m above the base of the measured section in the Skillogalee Dolomite, are magnesite (90.08 wt%) and talc (6.18 wt%). The magnesite is cryptocrystalline, and forms spherical, sub-rounded to well-rounded pebble sized (up to 2.4 mm) clasts. The intragranular space has been filled with what has been identified as talc, which is grown as <50 µm long fibrous crystals that are randomly oriented. These fibrous talc crystals are also observed growing inside a 350 µm, rounded remnant mineral (Figure 2). Trace minerals include actinolite, phlogopite, quartz, clinochlore and dolomite.

For sample 059 (dolostone), which was collected ~110 m above sample 037 in the Skillogalee Dolomite, the major mineral phases include dolomite (80.8 wt%), calcite (9.32 wt%) and quartz (3.43 wt%). The dolomite has a cryptocrystalline, micritic texture, organising into ~550 µm thick laminae. Dolomite is also associated with clastic laminae, although is slightly less abundant. Secondary calcite is evidenced from <100 µm thick veins that crosscut the primary sedimentary structures and occurs as a weathering surface (Figure 2).

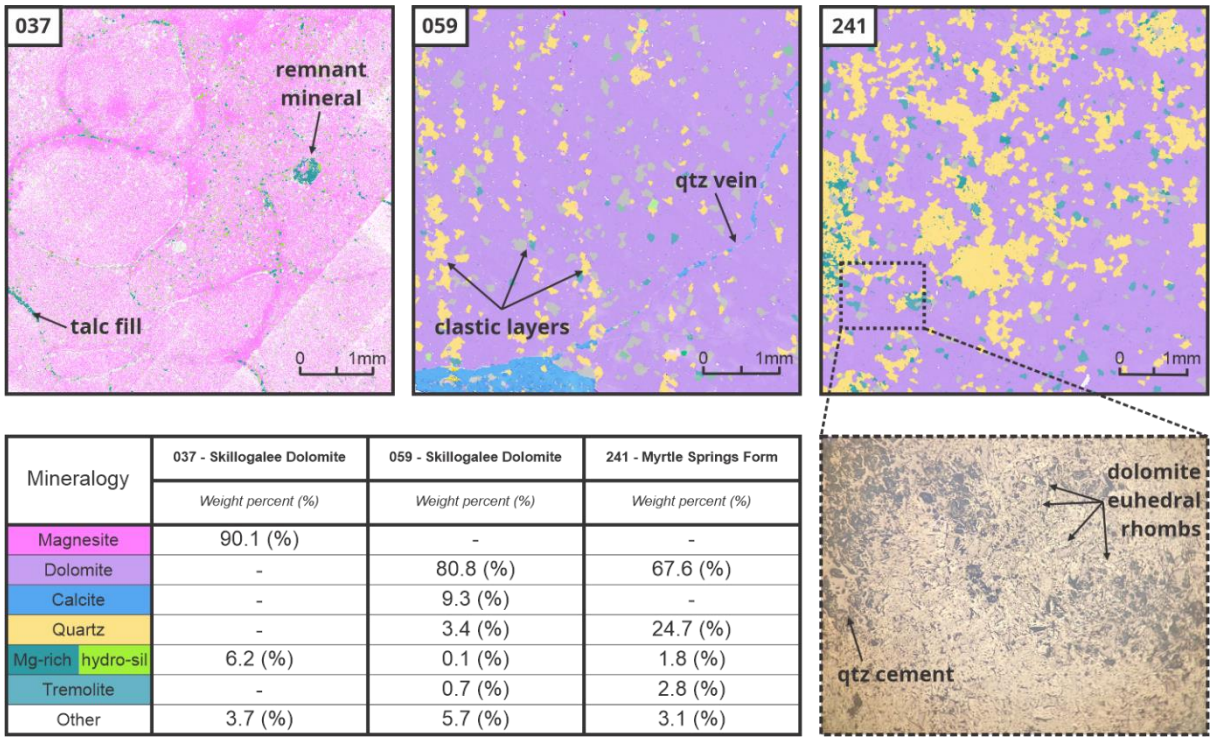

Mineralogy	037 - Skillogalee Dolomite	059 - Skillogalee Dolomite	241 - Myrtle Springs Form
	Weight percent (%)	*Weight percent (%)*	*Weight percent (%)*
Magnesite	90.1 (%)	-	-
Dolomite	-	80.8 (%)	67.6 (%)
Calcite	-	9.3 (%)	-
Quartz	-	3.4 (%)	24.7 (%)
Mg-rich hydro-sil	6.2 (%)	0.1 (%)	1.8 (%)
Tremolite	-	0.7 (%)	2.8 (%)
Other	3.7 (%)	5.7 (%)	3.1 (%)

Figure 2: BSE images overlain by spectral reflectance MLA maps for selected samples. Sample 037 from a magnesite sample in the Skillogalee Dolomite. Sample 059 from a dolomitic siltstone in the Skillogalee Dolomite. Sample 241 from a crystalline dolostone sample in the Myrtle Springs Formation. Included is insert microscope reflected light image displaying mineral textures. Table of corrected mineral weight percents for each sample.

Quartz grows as spherical, sub-angular to sub-rounded interlocking grains, which range from 30 µm to 100 µm, and are concentrated in clastic laminae. There is a suite of trace mineral phases deposited as detritus within clastic layers (Figure 2). These include ilmenite, hematite, orthoclase, rutile, apatite, zircon and phlogopite, iron oxides (in particular hematite) appear as ~20 µm nodules; orthoclase crystals are subhedral to anhedral (elongate to spherical, sub-angular to sub-rounded); rutile occurs as <70 µm subhedral prisms; apatite is very angular, ranging in size from 20 µm to 65 µm, where some of the larger grains have calcite centres; zircons are ~25 µm in size and form both broken and subhedral prisms.

In the Myrtle Springs Formation, 1872 m from the base of the logged section, sample 241 (dolostone) has major mineral phases of dolomite (67.63 wt%) and quartz (24.73 wt%), with tremolite (2.80 wt%) and a magnesium-rich hydrosilicate (1.78 wt%). Dolomite appears as ca. 100 µm diameter euhedral rhombs, which are surrounded by an interstitial quartz cement (Figure 2). These likely represent interlocking cements where dolomite formation preceded quartz formation, as quartz is seen wrapping around dolomite crystals. We also observe peloid shaped areas of high quartz concentration and an associated magnesium-rich hydrosilicate mineral (Figure 2), which could be remnant of a magnesium-rich clast (potentially magnesite).

3.6.1.1 Screening for secondary overprints

Geochemical and isotope data were screened for detrital input and diagenetic overprints, focusing on samples that display limited post-depositional chemical alteration.

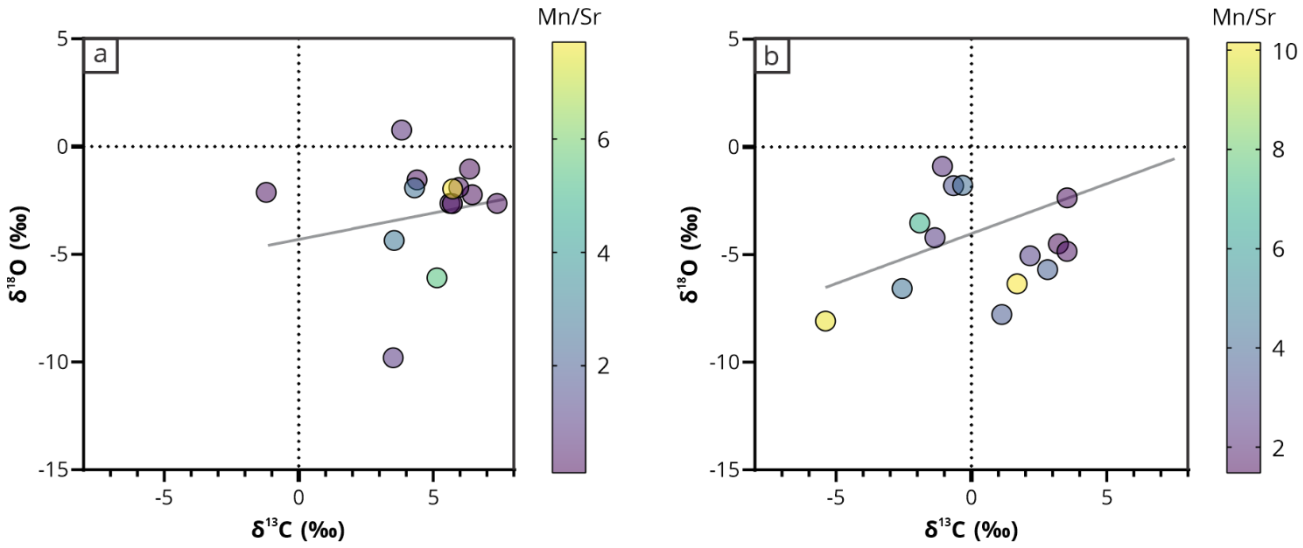

Figure 3: $\delta^{13}C$ and $\delta^{18}O$ cross plot with Mn/Sr data (represented by colour gradient) that tests for secondary alteration from diagenetic processes. $\delta^{13}C$ and $\delta^{18}O$ are calibrated to Vienna Pee Dee Belemnite (VPDB). Mn/Sr values are from Virgo et al. (2021) and normalised to PASS (Nance and Taylor, 1976). Linear regression is covariance between two isotope systems. (a) Data from Skillogalee Dolomite. (b) Data from Myrtle Springs Formation.

The correlation between $\delta^{13}C$ and $\delta^{18}O$ values for each carbonate formation were analysed to identify possible patterns to assess if the isotopic signatures have been affected by secondary diagenetic alteration (Figure 3; Allan & Matthews, 1990; Banner & Hanson, 1990). There is no statistically significant correlation between C and O isotopes for samples in the Skillogalee Dolomite (R2 = 0.03844, p-value = 0.3174), and a weak correlation for samples in the Myrtle Springs Formation (R2 = 0.09757, p-value = 0.0289). These observations are also consistent with MLA data, which demonstrates an increasing trend to secondary carbonate minerals, increased detrital input and recrystallised textures up-section from the Skillogalee Dolomite to the Myrtle Springs Formation.

To test if this weak covariance between C and O isotope data in the Myrtle Springs Formation is the result of interference from secondary diagenesis, we measured the interplay between these isotopic systems and Mn/Sr (Figure 3), the latter being a proxy for post-depositional alteration from meteoric waters (Brand & Veizer, 1980; Banner & Hanson, 1990; Kaufman & Knoll, 1995; Bartley et al., 2001; Peral et al., 2007; Frimmel, 2010, Hua et al., 2013). The weak positive covariance from Myrtle Springs Formation samples is anchored by a sample that has a distinctly elevated Mn/Sr ratio of 9.94. When this anomalous value is excluded, the resulting linear regression becomes statistically insignificant (R2 = 0.07808, p-value = 0.0544). Therefore, with this sample removed, the geochemical record in the pre-glacial succession at

this site is interpreted to reflect primary or close-to-primary isotope signals imparted during the original/authigenic carbonate precipitation and/or syn-sedimentary dolomitisation of studied carbonates.

3.6.1.2 Stratigraphic trends in isotopic data

Overall, samples in the Skillogalee Dolomite are represented by relatively consistent, positive $\delta^{13}C$ values, ranging between 2.38‰ and 7.49‰ (Figure 4). These values are paired with weakly negative $\delta^{18}O$ values that vary between -6.81‰ and 0.76‰. However, a rather light $\delta^{13}C$ value of -1.21‰ and a $\delta^{18}O$ value of -9.81‰ are recorded from a layered microbialite sample and a magnesite sample at stratigraphic depths of 648 m and 672 m, respectively. The $^{87}Sr/^{86}Sr$ values appear to increase up-section from 0.708 to 0.718. There is an inverse trend between $\delta^{13}C$ and $^{87}Sr/^{86}Sr$ values, where $\delta^{13}C$ decreases from 6.78‰ to -1.21‰ up-section across this same interval (Figure 4). The $\delta^{88/86}Sr$ values from samples of the Skillogalee Dolomite vary slightly with the stratigraphy, oscillating between lighter and heavier values up-section (i.e. 0.14‰ to 0.21‰, and 0.16‰ to 0.21‰). The heaviest values (0.21‰) were recorded from a conglomeratic magnesite and stromatolitic microbialite sample, while the lightest value (0.14‰) was from a dolostone sample.

Unlike the Skillogalee Dolomite, samples in the Myrtle Springs Formation are represented by an overall positive $\delta^{13}C$ excursion up-section with a magnitude of ~6‰, from -3.02‰ to 3.70‰. This coincides slightly also with $\delta^{18}O$ values, that range from between -8.12‰ and -0.45‰ (Figure 4). There are two negative $\delta^{13}C$ excursions with magnitudes of ~8‰ and ~4.5‰, where values shift from +5.13‰ to -3.02‰ at the base of the formation; and from +1.12‰ to -3.52‰ in the middle of the Myrtle Springs Formation. The horizons that record the most negative values, at depths of 1034 m and 1380 m, correspond to a layered microbialite and a dolomitic siltstone sample, respectively. A marked negative $\delta^{18}O$ excursion of -12.32‰ occurs at the same stratigraphic horizon as the $\delta^{13}C$ excursion in the dolomitic siltstone. Up-section towards the top of the Myrtle Springs Formation, values become more positive, with $\delta^{13}C$ and $\delta^{18}O$ values trending to 3.7‰ and -0.70‰, respectively. A layered microbialite sample at a depth of 1790 m records anomalous and generally very heavy or high $\delta^{13}C$ (7.49‰) and $\delta^{18}O$ (6.22‰) values with respect to the surrounding samples. The increasing $^{87}Sr/^{86}Sr$ values up-section seen in the Skillogalee Dolomite continues in the Myrtle Springs Formation, where samples record an increase from 0.709 to 0.711 (Figure 4). There is a very weak inverse relationship with $\delta^{13}C$, where values decrease from 2.81‰ to 1.61‰. Only one sample in the Myrtle Springs Formation (a stromatolitic microbialite) was analysed for stable Sr isotopes, and this sample recorded $\delta^{88/86}Sr$ value of 0.21‰.

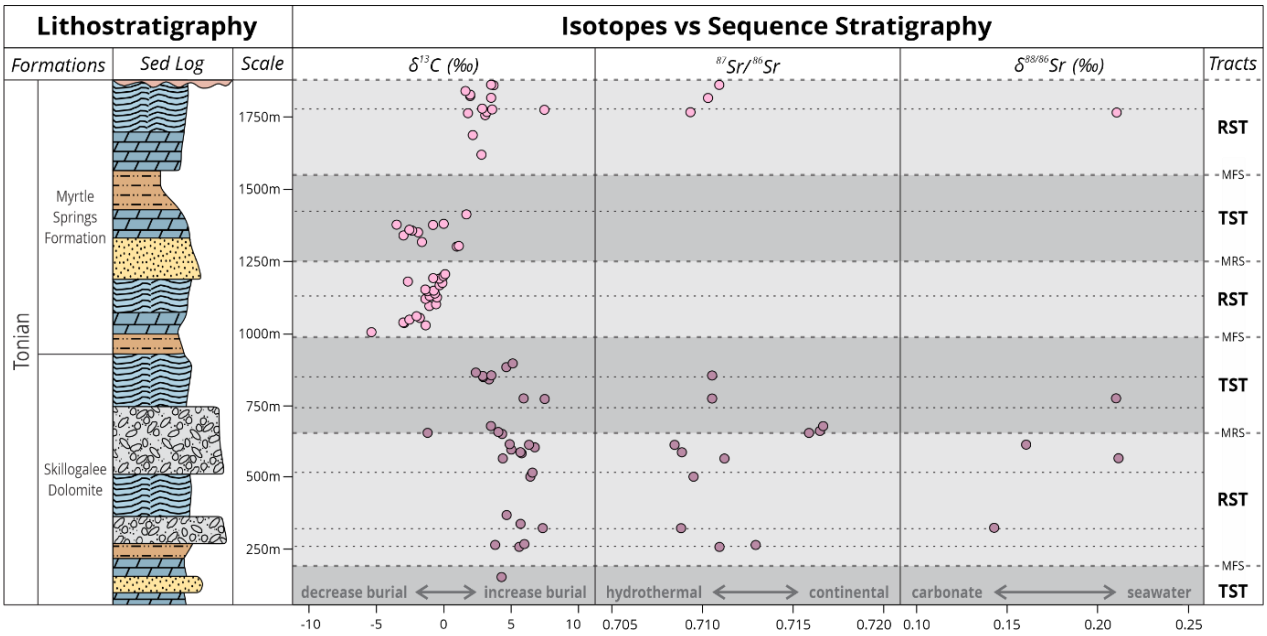

Figure 4: $\delta^{13}C$, $^{87}Sr/^{86}Sr$ and $\delta^{88/86}Sr$ values from carbonate samples in Skillogaee Dolomite (dark pink) and Myrtle Springs Formation (light pink). $^{87}Sr/^{86}Sr$ has 2SD error of ±0.0125 and $\delta^{88/86}Sr$ has 2SD error of ±0.004, based on long-term IAPSO and JCP-1 standard measurements. Vertical axis is stratigraphic thickness. Sequence stratigraphic systems tracts are shaded (TST = dark grey, RST = light grey). Thick dashed lines are sequence boundaries, thin dashed lined are parasequence boundaries. TST = transgressive systems tract, RST = regressive systems tract, MFS = maximum flooding surface, MRS = maximum regressive surface.

3.7 Discussion

3.7.1 Carbon isotope stratigraphy

Carbon isotopes in marine carbonates or organic rich shales are widely used as a chemostratigraphic correlation tool in the Neoproterozoic. This is due to the relatively long residence time of DIC in the ocean (~100,000 years) relative to an average mixing time of the global ocean (~1000 years), and well-mixed nature of C isotopes in seawater coupled with the extreme fluctuations in marine $\delta^{13}C$ recorded in the Neoproterozoic (Halverson et al., 2010; Park et al., 2020). The apparent global synchronicity of the negative $\delta^{13}C$ anomalies in particular has been used to identify sections where base-Sturtian glacial erosion is thought to have not removed 'significant time' of the sedimentary record. The Copley section described here preserves consistently positive $\delta^{13}C$ values in the lower part of the succession (with a lone negative $\delta^{13}C$ value in a Skillogalee Dolomite magnesite bed) (Figure 4). Two prominent negative $\delta^{13}C$ anomalies occur at ca. 1050 m and ca. 1400 m, where values drop to lower than -3 (Figure 4). Park et al. (2020) described a similar two-pronged anomaly separated by similar magnitude positive $\delta^{13}C$ values directly beneath the Sturtian glacial unconformity in Tigray, Ethiopia. The older of these two anomalies was constrained to be ca. 735 Ma (and correlated with the Garvellach anomaly). If this correlation holds up, the top ca. 400m of the Copley section, with weakly positive $\delta^{13}C$ values, correlates with similar sequences in Tigray and the

NW Highlands of Scotland (Park et al., 2020; Fairchild et al., 2017), with little missing stratigraphy at the Tonian–Cryogenian boundary (Ali et al., 2018). To further explore and validate such interpretations for the Copley section in this study, we have also examined the $\delta^{13}C$ record in the context of the sedimentological record, in conjunction with other elemental and isotopic proxies of palaeoenvironmental indicators.

3.7.1 Sequence stratigraphic constraints on isotopic trends

3.7.1.1 Systems Tracts

The logged Skillogalee Dolomite section was interpreted to represent a partial transgressive systems tract (TST), through a complete regressive systems tract (RST) to a second TST (Figure 4), by Virgo et al. (2021). The flat carbonate platform environment was shown to be sensitive to minor flooding and desiccation events, which are recorded by fourth-order parasequences (Virgo et al., 2021). We suggest that these sea-level fluctuations imparted significant perturbations in the isotopic record. Figure 4 demonstrates a weak to moderate stratigraphic correlation between third-order systems tracts and $\delta^{13}C$, where values increase up-section (3.82‰ to 6.78‰) in the RST towards the MRS and decrease (4.34‰ to 2.38‰) through the TST towards the MFS. Values likely become heavier in the RST due to increased evaporation and productivity in the shallow-water, restricted carbonate platform (Frimmel, 2010), and become lighter in the TST due to increased ^{12}C inputs and/or decreased burial efficiency of organic matter at greater depths (Sarmiento et al., 2013). Consequently, the RST intervals are associated with the deposition of supratidal to intertidal carbonates (magnesite mud), while the TST intervals have increasingly subtidal carbonate (stromatolitic microbialite) deposition. The $^{87}Sr/^{86}Sr$ values are on average higher (~0.714) through the TST compared to the RST (~0.710), which is largely due to a cluster of very radiogenic values recorded at the base of the TST that correlate with the RST-TST boundary (Figure 4). Due to the limited number of $\delta^{88/86}Sr$ values analysed, it is challenging to determine a robust correlation of the stable Sr isotope variations with third-order sequences. Nevertheless, it is evident that $\delta^{88/86}Sr$ values in the TST (~0.21‰) are overall heavier than for the RST (0.17‰). This is possibly linked to an increase in carbonate precipitation/deposition and elevated salinity that resulted from increased seawater input during the rise in relative sea level (Krabbenhoeft et al., 2010; Fruchter et al., 2017; Shao et al., 2021).

The Myrtle Springs Formation is represented by three complete third order systems tracts (two RST and one TST), and it includes the top of the uppermost TST in the underlying Skillogalee Dolomite (Figure 4). These sequence stratigraphic cycles appear to closely correlate with stratigraphic trends in isotopic data. There is a trend in $\delta^{13}C$ through the TST, where values decrease up-section from 0.97‰ to -3.52‰. Like the TSTs in the Skillogalee Dolomite, this likely resulted from decreased burial efficiency and increased input of a deep-water flux enriched in lighter ^{12}C. There may also be a role of remineralised organic carbon during transgression. Further, a clear increase in $\delta^{13}C$ up-section through the RSTs is present, where values increase from -3.02‰ to -0.03‰ and 2.16‰ to 3.71‰ (Figure 4). The lower RST records the strongest correlation trend, which was likely due to more extreme fluctuation in relative sea level during early deposition of the Myrtle Springs Formation (Virgo et al., 2021).

The isotopically light or lower $\delta^{13}C$ signatures in the basinal shale and dolostone interval at the bottom of RST, just above the MFS was likely the result of an influx of ^{12}C enriched deeper waters. In contrast, the much heavier or higher $\delta^{13}C$ values in the inner platform microbialite carbonates at the top of RST, near the MRS, resulted from ^{12}C drawdown and eventual C burial in the shallow-water setting where there was increased bioproductivity and subsequently enhanced carbonate deposition (Kump & Arthur, 1999; Bastow et al., 2002; Frimmel, 2010; Sarmiento et al., 2013). The RST in the top of the Skillogalee Dolomite is paired with an increasing $^{87}Sr/^{86}Sr$ trend (values increasing from 0.709 to 0.711, Figure 4), as such, the increasingly radiogenic trend is interpreted to reflect enhanced continental input with decreasing water depth.

3.7.1.2 Sequence Boundaries

The C isotopic trends in the Skillogalee Dolomite correspond well with sequence boundaries (Figure 4). The TST-RST boundary is marked by a maximum flooding surface (MFS), while the RST-TST boundary is represented by a maximum regressive surface (MRS). An anonymously light $\delta^{13}C$ value (-1.21‰) was collected from 1 m above the MRS (Figure 4), which marks an overall low in relative sea level. This intertidal to lagoonal layered microbialite sample also records a very radiogenic $^{87}Sr/^{86}Sr$ value of 0.716, which is significantly higher or more radiogenic than the samples stratigraphically below the regressive surface (Figure 4). Consequently, this drop in relative sea level appears matched by a large input of continental (riverine) water, producing a more radiogenic signal, and consistent with a landward shift in facies. This is also supported by the presence of soft sediment deformation structures at this horizon that developed from liquefaction due to rapid sedimentation (Postma, 1983; Stromberg & Bluck, 1998; Moretti et al., 2001), which was likely the result of high riverine discharge. Further, the input from isotopically light riverine carbon likely resulted in a temporary shift in $\delta^{13}C$ to negative values (Kump & Arthur, 1999). This excursion recovers rapidly back to positive values as a response to enhanced organic carbon burial and reduced riverine input, as evidenced by decreasing $^{87}Sr/^{86}Sr$ values.

Perturbations in the C isotopic record for the Myrtle Springs Formation appears to correlate with parasequence boundaries (PB), which represent flooding surfaces forming a minor and abrupt shift from shallow to deep-water deposition (Catuneanu, 2006). An anomalously heavy $\delta^{13}C$ (7.49‰) and $\delta^{18}O$ (6.22‰) was recorded from a supratidal to intertidal layered microbialite sample directly below the PB (Figure 4). This interval represents an overall low in relative sea level before a minor flooding event. Due to the simultaneous increase in $\delta^{13}C$ and $\delta^{18}O$, this was likely the result of enhanced water evaporation in the basin (Frimmel, 2010), which seems to be also supported by the sedimentological data with the deposition of carbonates with tepee structures that form from fracturing/crustal cracking during desiccation (Asserto & Kendall, 1977; Kendall & Warren, 1987; Belperio, 1990; Frank & Fielding, 2003; Tucker & Wright, 2009; O'Connell et al., 2020).

3.7.2 Isotopic relationship with REE proxies

Two REE elements, Ce and Eu, are sensitive to redox conditions and can thus provide insights into the oxygenation of ancient water columns. The Ce anomaly (Ce/Ce*) becomes increasingly negative under oxygen-rich conditions (German & Elderfield, 1990; Ling et al., 2013; Tostevin et al., 2016; Wallace et al., 2017; Shuster et al., 2018; Liu et al., 2019), while the Eu anomaly (Eu/Eu*) becomes more positive under anoxic conditions (Bau, 1991; Hood & Wallace, 2015). Further, the Eu anomaly can also be used as a proxy for input from continentally weathered feldspar-rich rocks (Verdel et al., 2018), or deep marine hydrothermal fluids (Derry & Jacobsen, 1990; Olivarez & Owen, 1991).

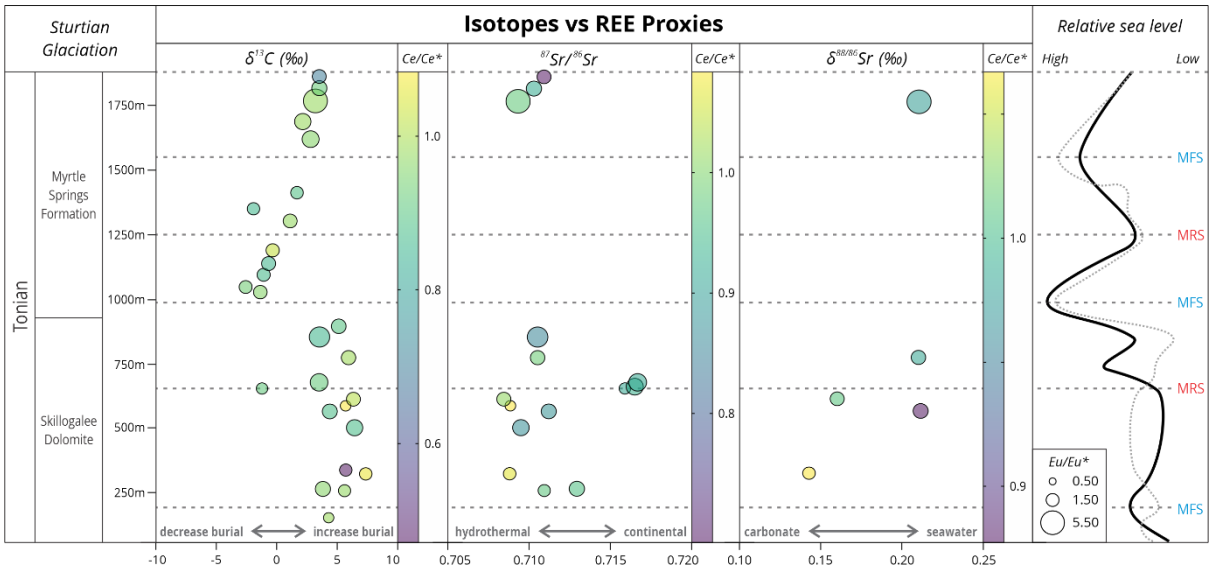

Figure 5: $\delta^{13}C$, $^{87}Sr/^{86}Sr$ and $\delta^{88/86}Sr$ values from carbonate samples in Skillogaee Dolomite and Myrtle Springs Formation. Ce/Ce* data are represented by colour gradient and Eu/Eu* data are represented by the circle size. Ce/Ce* = cerium anomaly. Eu/Eu* = europium anomaly. REE data are from Virgo et al. (2021) and normalised to PASS (Nance and Taylor, 1976). Vertical axis is stratigraphic thickness. Thick dashed lines ae sequence boundaries. The solid relative sea level curve is from Virgo et al. (2021), dotted relative sea level curve is from Preiss (2000).

3.7.2.1 *C isotopes and REE*

The Skillogalee Dolomite has overall positive $\delta^{13}C$ values (ca. 5‰), paired with weakly negative Ce/Ce* (~0.92) and low Eu/Eu* (~2.2) values (Figure 5). The heavy or more positive $\delta^{13}C$ suggests enhanced biological productivity, which is indicated by the thick accumulation of carbonates (Preiss et al., 2010; Virgo et al., 2021; in press). The Ce and Eu anomalies reflect dysoxic redox conditions, which we suggest represents the mixing of deep anoxic water with shallow oxic water and is accentuated by a redox stratified Proterozoic ocean (Preiss, 1987; Giddings & Wallace, 2009; Hood & Wallace, 2015; Counts, 2017; Wallace et al., 2017; Ward et al., 2019). We suggest that the correlation of less oxic water proxies with parasequence boundaries supports this interpretation with anoxic deep waters periodically flooding more oxic carbonate platform top environments.

The $\delta^{13}C$ values in the Myrtle Springs Formation appear to have a weak relationship with Eu/Eu* and Ce/Ce*. The lighter δ13C values (ca. -3.02‰) correspond to lower Eu/Eu* (~1.73) and less negative Ce/Ce* (~0.92), while heavier $\delta^{13}C$ (ca. 3.70‰) corresponds to a larger and positive Eu/Eu* (2.45) and more negative Ce/Ce* (0.69; Figure 5). The former conditions correspond to a less productive, anoxic environment, typical of a deeper water setting in the stratified ocean (Giddings & Wallace, 2009; Hood & Wallace, 2015; Wallace et al., 2017; Ward et al., 2019). The latter is consistent with bioproductive, oxic conditions with increased continental input, that was likely the result of decreasing water depth and increased proximity to continental sources.

3.7.2.2 Sr isotopes and REE

In the Skillogalee Dolomite, the $^{87}Sr/^{86}Sr$ values record two clusters (at ca. 0.710 and 0.718) that reflect two sets of conditions or Sr sources; specifically (i) more juvenile and hydrothermally sourced material versus (ii) more radiogenic and continent derived Sr sources, respectively. This supports the notion of a mixed water column, which is sourced from both deep seawater that record lower $^{87}Sr/^{86}Sr$ values, and riverine water or 'freshwater plume' in shallower settings that record more radiogenic values (McLennan et al., 1990; Shields & Veizer, 2002; Banner, 2004; Kuznetsov et al., 2018). The lower $^{87}Sr/^{86}Sr$ values are recorded from successions that coincide with weakly negative Ce/Ce* (ca. 0.98; Figure 5). This supports the above interpretation involving input from deeper anoxic waters dominated by juvenile and less radiogenic Sr into the shallow platform setting. The more radiogenic values coincide with the MRS and deposition of interbedded carbonate and clastic rocks, and record anomalously heavy Eu/Eu* (>4). As this horizon represents an overall low in relative sea level and preferential input from evolved, continental material, this Eu/Eu* anomaly likely reflects the input from continentally weathered feldspathic rocks (Verdel et al., 2018).

The clear shift in $^{87}Sr/^{86}Sr$ values from 0.709 to 0.711 in the RST at the top of the Myrtle Springs Formation correlates with more negative Ce/Ce* and Eu/Eu* up-section, from ca. 0.98 to 0.69 and ca. 5.77 to 1.93, respectively (Figure 5). The $^{87}Sr/^{86}Sr$ values becomes larger due to increased inputs from evolved, continental material, which is likely facilitated by decreasing water depth and proximity to continental sources. This shallower water is interpreted to be associated with more oxygenated conditions, as a result of the stratified redox conditions in the ocean, which drives the Ce/Ce* to more negative values (Hood & Wallace, 2015; Wallace et al., 2017; Ward et al., 2019). Further, the decreasing input from anoxic, hydrothermally sourced, anoxic deep waters would correspond with the decreasing Eu anomaly (Hood & Wallace, 2015; Ward et al., 2019).

Similar to $^{87}Sr/^{86}Sr$, the stable Sr isotope data ($\delta^{88/86}Sr$) in the Skillogalee Dolomite also records two separate clusters (Figure 5), one with generally lighter or lower values (ca. 0.15‰) and the other with heavier or systematically higher values (0.21‰), the latter likely recording precipitation from a heavier water column or palaeo-seawater. This variability in $\delta^{88/86}Sr$ data likely corresponds to changing Sr inputs related to water depth and basin restriction or local depositional settings. Briefly, the lighter $\delta^{88/86}Sr$ values are recorded from carbonates deposited in a more proximal intertidal setting with more continental input, while the heavier $\delta^{88/86}Sr$

values are recorded from carbonates deposited in a subtidal setting with presumably more dominant seawater inputs (Krabbenhoeft et al., 2010; Vollstaedt et al., 2014; Amsellem et al., 2018). These Sr isotope data complement the $\delta^{13}C$ record, where the lightest $\delta^{88/86}Sr$ values coincides with the heaviest $\delta^{13}C$ values and vice versa (Figure 5). The former thus likely represents intervals with enhanced bioproductivity that correspond with shallower water depths (Kump &
Arthur, 1999; Bastow et al., 2002; Frimmel, 2010). Furthermore, the heavier $\delta^{88/86}Sr$ values tend to have more negative Ce/Ce* anomalies, indicating more oxygenated marine conditions corresponding with the increased bioproductivity (Wallace et al., 2017).

3.7.3 Global context of data from the Adelaide Superbasin

The pre-glacial succession studied here is constrained to being younger than 788 ± 6 Ma (the age of the basal Burra Group Boucaut Volcanics, Armistead et al., 2021) and older than 684 ± 37 Ma, the age of shales within the Sturt Formation in the Stuart Shelf (Lloyd et al., 2022a). The pre-glacial succession is likely older than 717.43 ± 0.14 Ma, based on an interpretation of the age-equivalence of the Sturtian glaciation globally (Rooney et al., 2015), and constrained by a maximum depositional age for the base of the Sturtian glaciation in Laurentia (Macdonald et al., 2010). Based on these age constraints, global seawater $^{87}Sr/^{86}Sr$ from ca. 788–719 Ma yield values between 0.7061 and 0.7073 (Park et al., 2020 and references therein). These values are systematically lower than those presented in this study (0.7084 to 0.7182), which indicates a possible basin restriction with relatively less hydrothermal (marine) input and an enhanced continental (riverine) input at the studied palaeo-location (see also Halverson et al., 2007a). The more radiogenic and 'non-marine' $^{87}Sr/^{86}Sr$ values in studied samples thus support the notion that these carbonates were precipitated in a marginal marine environment that is influenced by considerable continental run-off into the Adelaide Superbasin.

Further, the $\delta^{88/86}Sr$ values from this study record much lighter or lower values (0.14‰ to 0.21‰) relative to those reported from a Tonian carbonate section in the Mackenzie Mountains, Canada (0.30‰ to 0.51‰), which have been interpreted to be marine in origin (Sarvian et al., 2019). As seen in Figure 6, the light values recorded in this study are close to modern day marine carbonate values (ca. 0.21‰), while the marine carbonates from Canada yield values closer to modern seawater (ca. 0.386‰). As $\delta^{88/86}Sr$ acts as a tracer for mixing between Sr derived from riverine weathering of carbonates versus Sr from seawater or marine brines, the lighter values recorded at this location (in South Australia) indicate a possible enhanced input of continental riverine water sources into restricted settings, leading to formation of carbonates with isotopically lighter Sr values than contemporaneous seawater (Krabbenhoeft et al., 2010; Vollstaedt et al., 2014).

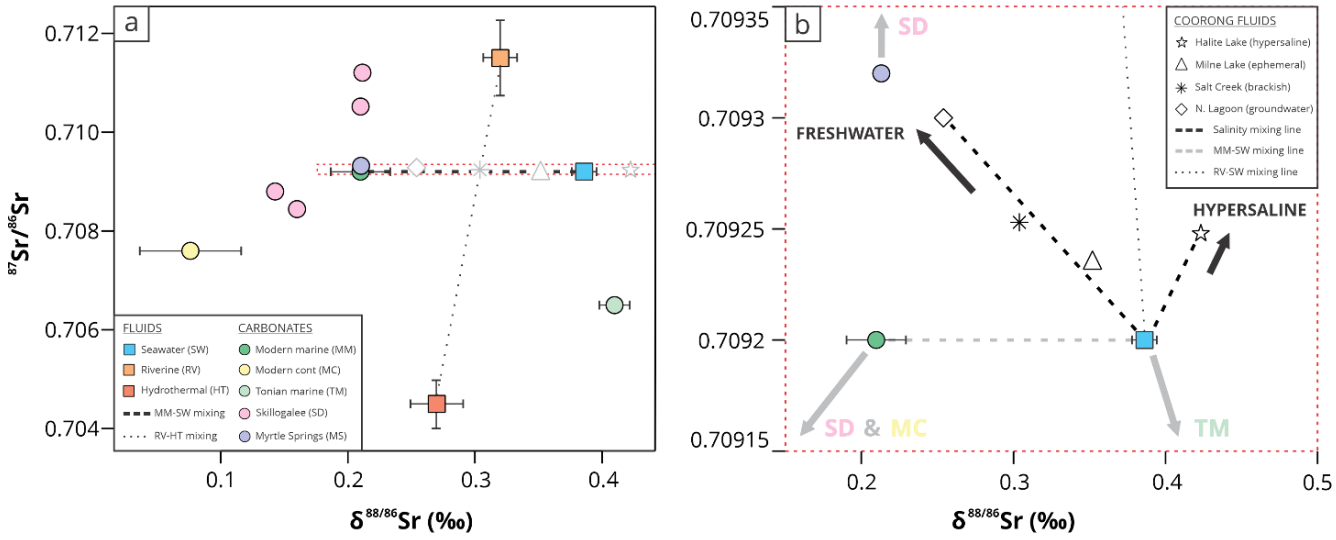

Figure 6: $^{87}Sr/^{86}Sr$ and $\delta^{88/86}Sr$ cross plot adapted from Krabbenhöft et al. (2010). (a) Includes sample in Skillogalee Dolomite and Myrtle Springs Formation (this study), Tonian marine carbonates (Sarvian et al., 2019), modern continental carbonates (Shalev et al., 2017), modern Coorong waters (Shao et al., 2021), and modern marine carbonates, seawater, hydrothermal and riverine fluids (Krabbenhöft et al., 2010). Dashed line represents seawater-carbonate fractionation mixing line. Dotted line represents water-source mixing. (b) Insert from smaller interval in graph (a). Includes modern marine carbonate and seawater (Krabbenhöft et al., 2010) and Coorong water columns with varying salinity (Shao et al., 2021). Grey arrows indicate direction to other carbonates not pictured from graph (a). Grey dashed line represents seawater-carbonate fractionation mixing line. Black dashed line represents salinity mixing line. Dotted line represents mixing of riverine and seawater.

3.7.3.1 Modern analogue for semi-restricted coastal marine/lagoon setting

The Coorong Lagoon in southern South Australia is a semi-restricted and elongated depositional system or lagoon environment that runs parallel to the coast of the Southern Ocean (Shao et al., 2021; Priestley et al., 2022). This unique depositional and hydrological setting, in particular its ephemeral lakes, has long been used as a possible modern analogue for the facies of the Skillogalee Dolomite and associated magnesite-rich lithologies (von der Borch & Lock, 1979; Belperio, 1990; Uppill, 1990; Preiss, 2000). Although the Coorong Lagoon provides an explanation for such carbonate formations, including interbedded dolomite and magnesite, other authors have suggested that the lateral extent of magnesite beds and palaeocurrent data from the Skillogalee Dolomite is better explained by deposition in a marine tidal flat system rather than localised lagoon and ephemeral lake settings (Frank & Fielding, 2003). Regardless of the specific depositional setting, the Sr isotopic data from the Coorong Lagoon measured in waters and carbonates (Shao et al., 2021) provide a first-order and unique insight into the strikingly radiogenic and light $\delta^{88/86}Sr$ values acquired from samples in this study.

Specifically, the fresh groundwater entering the Coorong has the highest $^{87}Sr/^{86}Sr$ values (ca. 0.7093, Figure 6) and lightest $\delta^{88/86}Sr$ (ca. 0.254‰) values (Shao et al., 2021), (Figure 6), which is closest to carbonate values in this study. In contrast, brackish waters have $^{87}Sr/^{86}Sr$ values of

0.7092 and $\delta^{88/86}$Sr of 0.31‰, and the ephemeral and hypersaline systems have values of >0.7092 and 0.352‰, which are along the mixing line between fresh and marine water sources. Assuming stable Sr isotope fractionation between a fluid and carbonate of -0.21‰, based on the data from modern seawater and skeletal calcite, a brackish and ephemeral waters with $\delta^{88/86}$Sr values of 0.31‰ and 0.35‰ would precipitate carbonates with $\delta^{88/86}$Sr of 0.1‰ and 0.14‰, respectively. Although the carbonates that formed brackish waters in the Coorong Lagoon are isotopically lighter than the $\delta^{88/86}$Sr values for Neoproterozoic carbonates measured in this study, the carbonates from ephemeral and restricted coastal waters have the same Sr isotope value as some samples in the Skillogalee Dolomite. These isotopically lighter Sr isotope data provide a plausible explanation for the shift to lighter $\delta^{88/86}$Sr values in studied carbonates from presumably restricted marine settings, if compared to carbonate data from 'open marine' settings at that time.

With that said, it is unlikely that the Sr isotope fractionation factor for the ancient marine system (fluid-carbonate) would be the same as today due to differences in chemical composition of the oceans, marine carbonate chemistry and palaeoenvironments. This is evidenced by the preferential precipitation of Mg-rich carbonates, including marine dolomites and magnesites, over calcite or limestones during the Neoproterozoic. These differences might thus impact the stable Sr isotope fractionation between waters and carbonates. Consequently, it is very difficult to infer the stable Sr isotope composition of palaeo-seawater based on the $\delta^{88/86}$Sr data recorded in ancient marine carbonates. Further research into the Sr isotope fractionation between Mg-rich carbonates and fluids, including ephemeral/brackish waters in the Coorong, would be useful as a tool to better understand the Neoproterozoic system and coeval carbonate archives.

3.8 Conclusions

This study builds upon the previous findings in Chapter 2 that highlighted the sedimentology, sequence stratigraphy, and elemental geochemistry for a Tonian succession near Copley. Chaper 3 illustrates the interactions and close links between C and Sr isotopic systems, sequence stratigraphy and redox conditions recorded in marine carbonates during the Tonian, which sheds light on the depositional conditions necessary for the precipitation of these Mg-rich carbonates. Specifically, the Skillogalee Dolomite records overall heavy δ^{13}C values, and two distinct clusters of ^{87}Sr/^{86}Sr and $\delta^{88/86}$Sr data, which indicate a setting that was biologically productive and received significant fresh, riverine input in semi-restricted marine or coastal settings. This corresponds to a TST-RST-TST cycle in an overall inner platform setting that was fed by both anoxic deep waters and oxic shallow waters. The Myrtle Springs Formation marks a transition to more variable δ^{13}C values that appear to overall increase up-section. The Sr isotope values collected at the top of the formation record an increasing radiogenic ^{87}Sr/^{86}Sr trend up-section and heavy $\delta^{88/86}$Sr values. Overall. These data might reflect a setting with increasing biological productivity and organic carbon burial and increasing continental input and local carbonate production. The sequence stratigraphic and REE data preserve multiple RST-TST cycles that correspond to a transition from an anoxic, deeper water subtidal setting to a dysoxic inner platform supratidal setting.

Two major negative $\delta^{13}C$ anomalies occur in the pre-glacial section of the Copley section (Figure 4), which are similar to those reported from other near-conformable Tonian–Cryogenian successions (Fairchild et al., 2017; Park et al., 2020). At Copley, both C isotope excursions occur at times of near maximum flooding, or during transgression, suggesting that they are more likely to reflect seawater than other parts of the section (Figure 4). This begs the question as to whether the negative C isotopic anomalies reflect a single, stratigraphically more extensive excursion modulated by regressive cycles restricting the global ocean signal, or whether these truly reflect two global excursions.

The $^{87}Sr/^{86}Sr$ and $\delta^{88/86}Sr$ data from this study are both considerably more radiogenic and lighter, respectively, compared to recently reported marine values from more 'open ocean' settings at that time (Sarvian et al., 2019). The more radiogenic Sr isotope values from the Flinders Ranges are interpreted to indicate a semi-restricted marine or coastal/lagoonal settings that was impacted by significantly higher inputs from continental riverine weathering and/or other non-marine Sr sources. When compared to the modern Coorong Lagoon of South Australia, water columns with increasing freshwater input have also more radiogenic Sr signatures and isotopically light $\delta^{88/86}Sr$ values that could thus provide an explanation for the data observed in this study. Consequently, further investigations into this or other modern analogue depositional systems could provide an insight into complex Tonian carbonate archives and their isotope signatures, which were deposited in the northern Flinders Ranges during such a fascinating but poorly understood time in Earth's history. In parallel, we propose that coupling a sequence stratigraphic analysis with both elemental and multiple isotopic analysis is important to interpret the significance of any chemical/isotope proxy, and especially to unravel global seawater signals from local basins and/or coeval depositional systems.

3.9 Supplementary Material

Supplementary material is freely available as XLSX on Figshare.

Isotope dataset: https://doi.org/10.6084/m9.figshare.23640912.v1

3.10 Acknowledgments

We acknowledge that this research is conducted on the ancestral lands of the Kuyani peoples. We acknowledge and respect their deep feelings of attachment and spiritual relationship to Country, and that their cultural and heritage beliefs are still as important to the living people today. This project was supported by funding from the Geological Survey of South Australia, and an Australian Government Research Training Program (RTP) Scholarship awarded to Virgo. We are very grateful to Jack Ward (The University of Queensland) and Jarred Lloyd (The University of Adelaide) for their field assistance in 2018 and 2019, respectively. We thank David Bruce, Dr Tony Hall and Dr Robert Klaebe (The University of Adelaide) for their guidance and technical support with sample preparation and analysis. The authors acknowledge the instruments and scientific and technical assistance of Microscopy Australia at Adelaide Microscopy, The University of Adelaide, a facility that is funded by the University, and State and Federal Governments.

3.11 References

Ali, D. O., Spencer, A. M., Fairchild, I. J., Chew, K. J., Anderton, R., Levell, B. K., Hambrey, M. J., Dove, D. & Le Heron, D. P. (2018). Indicators of relative completeness of the glacial record of the Port Askaig Formation, Garvellach Islands, Scotland. Precambrian Research 319: 65-78. https://doi.org/10.1016/j.precamres.2017.12.005

Allan, J. R. & Matthews, R. K. (1990). Isotope signatures associated with early meteoric diagenesis. Carbonate Diagenesis, 197-217. https://doi.org/10.1002/9781444304510.ch16

Amsellem, E., Moynier, F., Day, J. M., Moreira, M., Puchtel, I. S. & Teng, F. Z. (2018). The stable strontium isotopic composition of ocean island basalts, mid-ocean ridge basalts, and komatiites. Chemical Geology 483: 595-602. https://doi.org/10.1016/j.chemgeo.2018.03.030

Armistead, S. E., Collins, A. S., Buckman, S. & Atkins, R. (2020). Age and geochemistry of the Boucaut Volcanics in the Neoproterozoic Adelaide Rift Complex, South Australia. Australian Journal of Earth Sciences: 1-10. https://doi.org/10.1080/08120099.2021.1840435

Assereto, R. L. & Kendall, C. G. ST C. (1977). Nature, origin and classification of peritidal tepee structures and related breccias. Sedimentology 24(2): 153-210. https://doi.org/10.1111/j.1365-3091.1977.tb00254.x

Banner, J. L. (2004). Radiogenic isotopes: systematics and applications to earth surface processes and chemical stratigraphy. Earth-Science Reviews 65(3-4): 141-194. https://doi.org/10.1016/S0012-8252(03)00086-2

Banner, J. L. & Hanson, G. N. (1990). Calculation of simultaneous isotopic and trace element variations during water-rock interaction with applications to carbonate diagenesis. Geochimica et Cosmochimica Acta 54(11): 3123-3137. https://doi.org/10.1016/0016-7037(90)90128-8

Barovich, K. & Foden, J. (2000). A Neoproterozoic flood basalt province in southern-central Australia: geochemical and Nd isotope evidence from basin fill. Precambrian Research 100(1-3): 213-234. https://doi.org/10.1016/S0301-9268(99)00075-3

Bartley, J. K., Semikhatov, M. A., Kaufman, A. J., Knoll, A. H., Pope, M. C. & Jacobsen, S. B. (2001). Global events across the Mesoproterozoic–Neoproterozoic boundary: C and Sr isotopic evidence from Siberia. Precambrian Research 111(1-4): 165-202. https://doi.org/10.1016/S0301-9268(01)00160-7

Bastow, T. P., Jackson, G. & Edmonds, J. S. (2002). Elevated salinity and isotopic composition of fish otolith carbonate: stock delineation of pink snapper, Pagrus auratus, in Shark Bay, Western Australia. Marine Biology 141(5): 801-806. https://doi.org/10.1007/s00227-002-0884-8

Bau, M. (1991). Rare-earth element mobility during hydrothermal and metamorphic fluid-rock interaction and the significance of the oxidation state of europium. Chemical Geology 93(3-4): 219-230. https://doi.org/10.1016/0009-2541(91)90115-8

Belperio, A. (1990). Palaeoenvironmental interpretations of the Late Proterozoic Skillogalee Dolomite in the Willouran Ranges, South Australia. The Evolution of a Late Precambrian–Early Palaeozoic Rift Complex: The Adelaide Geosyncline. Geol. Soc. Aust. Spec. Publ 16: 85-104.

Belperio, A. P. (1987). Mineralogical, chemical, isotopic and source-rock anlayses of Burra Group (Adelaidean) sedimentary rocks from the Willouran Ranges. Report Book, Department of Mines and Energy, South Australia. 87/40: 1-17.

Berkner, L. V. & Marshall, L. (1965). On the origin and rise of oxygen concentration in the Earth's atmosphere. Journal of Atmospheric Sciences 22(3): 225-261. https://doi.org/10.1175/1520-0469(1965)022<0225:OTOARO>2.0.CO;2

Bolhar, R. & Van Kranendonk, M. J. (2007). A non-marine depositional setting for the northern Fortescue Group, Pilbara Craton, inferred from trace element geochemistry of stromatolitic carbonates. Precambrian Research 155(3-4): 229-250. https://doi.org/10.1016/j.precamres.2007.02.002

Brand, U. & Veizer, J. (1980). Chemical diagenesis of a multicomponent carbonate system; 1, Trace elements. Journal of Sedimentary Research 50(4): 1219-1236. https://doi.org/10.1306/212F7BB7-2B24-11D7-8648000102C1865D

Brocks, J. J., Jarrett, A. J., Sirantoine, E., Hallmann, C., Hoshino, Y. & Liyanage, T. (2017). The rise of algae in Cryogenian oceans and the emergence of animals. Nature 548(7669): 578-581. https://doi.org/10.1038/nature23457

Burke, W. H., Denison, R. E., Hetherington, E. A., Koepnick, R. B., Nelson, H. F. & Otto, J. B. (1982). Variation of seawater 87Sr/86Sr throughout Phanerozoic time. Geology 10(10): 516-519. https://doi.org/10.1130/0091-7613(1982)10<516:VOSSTP>2.0.CO;2

Busfield, M. & Le Heron, D. (2014). Sequencing the Sturtian icehouse: dynamic ice behaviour in South Australia. Journal of the Geological Society 171(3): 443-456. https://doi.org/10.1144/jgs2013-067

Butterfield, N. J. (2000). Bangiomorpha pubescens n. gen., n. sp.: implications for the evolution of sex, multicellularity, and the Mesoproterozoic/Neoproterozoic radiation of eukaryotes. Paleobiology 26(3): 386-404. Doi:10.1666/0094-8373(2000)0262.0.CO;2

Canfield, D. E. & Teske, A. (1996). Late Proterozoic rise in atmospheric oxygen concentration inferred from phylogenetic and sulphur-isotope studies. Nature 382(6587): 127-132. https://doi.org/10.1038/382127a0

Catuneanu, O. (2006). Principles of sequence stratigraphy. Elsevier.

Charlier, B. L. A., Nowell, G. M., Parkinson, I. J., Kelley, S. P., Pearson, D. G. & Burton, K. W. (2012). High temperature strontium stable isotope behaviour in the early solar system and planetary bodies. Earth and Planetary Science Letters 329: 31-40. https://doi.org/10.1016/j.epsl.2012.02.008

Chen, X., Zhou, Y. & Shields, G. A. (2022). Progress towards an improved Precambrian seawater 87Sr/86Sr curve. Earth-Science Reviews 224: 103869. https://doi.org/10.1016/j.earscirev.2021.103869

Coats, R. (1973). Copley, South Australia. Geological Survey of South Australia, Geological Series Explanatory Notes: 54-59.

Collins, A. S., Blades, M. L., Merdith, A. S. & Foden, J. D. (2021), Closure of the Proterozoic Mozambique Ocean was instigated by a late Tonian plate reorganization event. Communications Earth & Environment, 2(1). https://doi.org/10.1038/s43247-021-00149-z

Collins, A. S. & Pisarevsky, S. A. (2005), Amalgamating eastern Gondwana: The evolution of the Circum-Indian Orogens. Earth-Science Reviews, 71(3), 229-270. https://doi.org/10.1016/j.earscirev.2005.02.004

Corkeron, M., Webb, G. E., Moulds, J. & Grey, K. (2012). Discriminating stromatolite formation modes using rare earth element geochemistry: Trapping and binding versus in situ precipitation of stromatolites from the Neoproterozoic Bitter Springs Formation, Northern Territory, Australia. Precambrian Research 212: 194-206. https://doi.org/10.1016/j.precamres.2012.04.019

Counts, J. W. (2017). The Adelaide Rift Complex in the Flinders Ranges: Geologic history, past investigations and relevant analogues. Department of the Premier and Cabinet, South Australia, Adelaide, Report Book 16: 42.

Cox, G. M., Halverson, G. P., Stevenson, R. K., Vokaty, M., Poirier, A., Kunzmann, M., Li, Z. X., Denyszyn, S. W., Strauss, J. V. & Macdonald, F. A. (2016). Continental flood basalt weathering as a trigger for Neoproterozoic Snowball Earth. Earth and Planetary Science Letters 446: 89-99. https://doi.org/10.1016/j.epsl.2016.04.016

Cox, G. M., Isakson, V., Hoffman, P. F., Gernon, T. M., Schmitz, M. D., Shahin, S., Collins, A. S., Preiss, W., Blades, M. L., Mitchell, R. N. & Nordsvan, A. (2018). South Australian U-Pb zircon (CA-ID-TIMS) age supports globally synchronous Sturtian deglaciation. Precambrian Research 315: 257-263. https://doi.org/10.1016/j.precamres.2018.07.007

Dalziel, I. W. D. (1997), Neoproterozoic-Paleozoic geography and tectonics: Review, hypothesis, environmental speculation. Geol Soc Am Bull, 109(1), 16-42. https://doi.org/10.1130/0016-7606(1997)109<0016:ONPGAT>2.3.CO;2

Derry, L. A. & Jacobsen, S. B. (1988). The Nd and Sr isotopic evolution of Proterozoic seawater. Geophysical Research Letters 15(4): 397-400. https://doi.org/10.1029/GL015i004p00397

Derry, L. A. & Jacobsen, S. B. (1990). The chemical evolution of Precambrian seawater: evidence from REEs in banded iron formations. Geochimica et Cosmochimica Acta 54(11): 2965-2977. https://doi.org/10.1016/0016-7037(90)90114-Z

El Meknassi, S., Dera, G., De Rafélis, M., Brahmi, C., Lartaud, F., Hodel, F., Jeandel, C., Menjot, L., Mounic, S., Henry, M. & Besson, P. (2020). Seawater 87Sr/86Sr ratios along continental margins: Patterns and processes in open and restricted shelf domains. Chemical Geology 558: 119874. https://doi.org/10.1016/j.chemgeo.2020.119874

Fairchild, I. J., Spencer, A.M., Ali, D.O., Anderson, R.P., Anderton, R., Boomer, I., Dove, D., Evans, J.D., Hambrey, M.J., Howe, J. & Sawaki, Y. (2017). Tonian-Cryogenian boundary sections of Argyll, Scotland. Precambrian Research, 319, 37-64. https://doi.org/10.1016/j.precamres.2017.09.020

Fanning, C. M., Ludwig, K. R., Forbes, B. G. & Preiss, W. V. (1986). Single and multiple grain U–Pb zircon analyses for the early Adelaidean Rook Tuff, Willouran Ranges, South Australia. Geological Society of Australia Abstracts.

Foden, J., Elburg, M., Turner, S., Clark, C., Blades, M.L., Cox, G., Collins, A.S., Wolff, K. & George, C. (2020). Cambro-Ordovician magmatism in the Delamerian orogeny: Implications for tectonic development of the southern Gondwanan margin. Gondwana Research 81: 490-521. https://doi.org/10.1016/j.gr.2019.12.006

Foden, J., Elburg, M. A., Dougherty-Page, J. & Burtt, A. (2006). The timing and duration of the Delamerian Orogeny: correlation with the Ross Orogen and implications for Gondwana assembly. The Journal of Geology 114(2): 189-210. https://doi.org/10.1086/499570

Frank, T. D. & Fielding, C. R. (2003). Marine origin for Precambrian, carbonate-hosted magnesite? Geology 31(12): 1101-1104. https://doi.org/10.1130/G20101.1

Frimmel, H. E. (2009). Trace element distribution in Neoproterozoic carbonates as palaeoenvironmental indicator. Chemical Geology 258(3-4): 338-353. https://doi.org/10.1016/j.chemgeo.2008.10.033

Frimmel, H. E. (2010). On the reliability of stable carbon isotopes for Neoproterozoic chemostratigraphic correlation. Precambrian Research 182(4): 239-253. https://doi.org/10.1016/j.precamres.2010.01.003

Fromhold, T. & Wallace, M. (2011). Nature and significance of the Neoproterozoic Sturtian–Marinoan Boundary, Northern Adelaide Geosyncline, South Australia. Australian

Journal of Earth Sciences 58(6): 599-613. https://doi.org/10.1080/08120099.2011.579624
Fromhold, T. & Wallace, M. (2012). Regional recognition of the Neoproterozoic Sturtian–Marinoan boundary, northern and central Adelaide Geosyncline, South Australia. Australian Journal of Earth Sciences 59(4): 527-546. https://doi.org/10.1080/08120099.2012.673507
Fruchter, N., Lazar, B., Nishri, A., Almogi-Labin, A., Eisenhauer, A., Shlevin, Y. B. E. & Stein, M. (2017). 88Sr/86Sr fractionation and calcite accumulation rate in the Sea of Galilee. Geochimica et Cosmochimica Acta 215: 17-32. https://doi.org/10.1016/j.gca.2017.07.026
German, C. R. & Elderfield, H. (1990). Application of the Ce anomaly as a paleoredox indicator: the ground rules. Paleoceanography 5(5): 823-833. https://doi.org/10.1029/PA005i005p00823
Giddings, J. A., Wallace, M. W. & Woon, E. M. (2009). Interglacial carbonates of the Cryogenian Umberatana Group, northern Flinders Ranges, South Australia. Australian Journal of Earth Sciences 56(7): 907-925. https://doi.org/10.1080/08120090903005378
Giddings, J. A. & Wallace, M. W. (2009a). Facies-dependent δ13C variation from a Cryogenian platform margin, South Australia: Evidence for stratified Neoproterozoic oceans? Palaeogeography, Palaeoclimatology, Palaeoecology 271(3-4): 196-214. https://doi.org/10.1016/j.palaeo.2008.10.011
Giddings, J. A. & M. W. Wallace (2009). Sedimentology and C-isotope geochemistry of the 'Sturtian'cap carbonate, South Australia. Sedimentary Geology 216(1-2): 1-14. https://doi.org/10.1016/j.sedgeo.2009.01.007
Grey, K., Hill, A. C. & Calver, C. (2011). Biostratigraphy and stratigraphic subdivision of Cryogenian successions of Australia in a global context. Geological Society, London, Memoirs 36(1): 113-134. https://doi.org/10.1144/M36.8
Halverson, G. P., Dudás, F. Ö., Maloof, A. C. & Bowring, S. A. (2007). Evolution of the 87Sr/86Sr composition of Neoproterozoic seawater. Palaeogeography, Palaeoclimatology, Palaeoecology 256(3-4): 103-129. https://doi.org/10.1016/j.palaeo.2007.02.028
Halverson, G. P., Hoffman, P. F., Schrag, D. P., Maloof, A. C. & Rice, A. H. N. (2005). Toward a Neoproterozoic composite carbon-isotope record. GSA Bulletin 117(9-10): 1181-1207. https://doi.org/10.1130/B25630.1
Halverson, G. P., Hurtgen, M. T., Porter, S. M. & Collins, A. S. (2009). Neoproterozoic-Cambrian biogeochemical evolution. Developments in Precambrian geology 16: 351-365. https://doi.org/10.1016/S0166-2635(09)01625-9
Halverson, G. P., Wade, B. P., Hurtgen, M. T. & Barovich, K. M. (2010). Neoproterozoic chemostratigraphy. Precambrian Research 182(4): 337-350. https://doi.org/10.1016/j.precamres.2010.04.007
Hill, A. & Walter, M. (2000). Mid-Neoproterozoic (~ 830–750 Ma) isotope stratigraphy of Australia and global correlation. Precambrian Research 100(1-3): 181-211. https://doi.org/10.1016/S0301-9268(99)00074-1
Hoffman, P. F., Abbot, D.S., Ashkenazy, Y., Benn, D.I., Brocks, J.J., Cohen, P.A., Cox, G.M., Creveling, J.R., Donnadieu, Y., Erwin, D.H. & Fairchild, I.J. (2017). Snowball Earth climate dynamics and Cryogenian geology-geobiology. Science Advances 3(11): e1600983. 10.1126/sciadv.1600983
Hoffman, P. F., Kaufman, A. J., Halverson, G. P. & Schrag, D. P. (1998). A Neoproterozoic snowball earth. Science 281(5381): 1342-1346. 10.1126/science.281.5381.1342

Hoffman, P. F. & Schrag, D. P. (2002). The snowball Earth hypothesis: testing the limits of global change. Terra Nova 14(3): 129-155. https://doi.org/10.1046/j.1365-3121.2002.00408.x

Hood, A. v.S., Wallace, M. W., Reed, C. P., Hoffmann, K. H. & Freyer, E. E. (2015). Enigmatic carbonates of the Ombombo Subgroup, Otavi Fold Belt, Namibia: a prelude to extreme Cryogenian anoxia? Sedimentary Geology 324: 12-31. https://doi.org/10.1016/j.sedgeo.2015.04.007

Hood, A. v.S, Planavsky, N. J., Wallace, M. W., Wang, X., Bellefroid, E. J., Gueguen, B. & Cole, D. B. (2016). Integrated geochemical-petrographic insights from component-selective δ238U of Cryogenian marine carbonates. Geology 44(11): 935-938. https://doi.org/10.1130/G38533.1

Hood, A. vS., Wallace, M. W. & Drysdale, R. N. (2011). Neoproterozoic aragonite-dolomite seas? Widespread marine dolomite precipitation in Cryogenian reef complexes. Geology 39(9): 871-874. https://doi.org/10.1130/G32119.1

Hood, A. v.S. & Wallace, M. W. (2012). Synsedimentary diagenesis in a Cryogenian reef complex: Ubiquitous marine dolomite precipitation. Sedimentary Geology 255: 56-71. https://doi.org/10.1016/j.sedgeo.2012.02.004

Hood, A. v.S. & Wallace, M. W. (2015). Extreme ocean anoxia during the Late Cryogenian recorded in reefal carbonates of Southern Australia. Precambrian Research 261: 96-111.

Hua, G., Yuansheng, D., Lian, Z., Jianghai, Y., Hu, H., Min, L. & Yuan, W. (2013). Trace and rare earth elemental geochemistry of carbonate succession in the Middle Gaoyuzhuang Formation, Pingquan Section: Implications for Early Mesoproterozoic ocean redox conditions. Journal of Palaeogeography 2(2): 209-221. https://doi.org/10.3724/SP.J.1261.2013.00027

Jacobsen, S. B. & Kaufman, A. J. (1999). The Sr, C and O isotopic evolution of Neoproterozoic seawater. Chemical Geology 161(1-3): 37-57. https://doi.org/10.1016/S0009-2541(99)00080-7

Kaufman, A. J. & Knoll, A. H. (1995). Neoproterozoic variations in the C-isotopic composition of seawater: stratigraphic and biogeochemical implications. Precambrian Research 73(1-4): 27-49. https://doi.org/10.1016/0301-9268(94)00070-8

Keeman, J., Turner, S., Haines, P.W., Belousova, E., Ireland, T., Brouwer, P., Foden, J. & Wörner, G. (2020). New U-Pb, Hf and O isotope constraints on the provenance of sediments from the Adelaide Rift Complex–documenting the key Neoproterozoic to early Cambrian succession. Gondwana Research. https://doi.org/10.1016/j.gr.2020.02.005

Kendall, C. G. S. C. & Warren, J. (1987). A review of the origin and setting of tepees and their associated fabrics. Sedimentology 34(6): 1007-1027.

Kirschvink, J. L. (1992).”Late Proterozoic low-latitude global glaciation: the snowball Earth. https://resolver.caltech.edu/CaltechAUTHORS:20130117-100718783

Knoll, A., Hayes, J. M., Kaufman, A. J., Swett, K. & Lambert, I. B. (1986). Secular variation in carbon isotope ratios from Upper Proterozoic successions of Svalbard and East Greenland. Nature 321(6073): 832. https://doi.org/10.1038/321832a0

Knoll, A. H. (1992). The early evolution of eukaryotes: a geological perspective. Science 256(5057): 622-627. 10.1126/science.1585174

Krabbenhöft, A., Fietzke, J., Eisenhauer, A., Liebetrau, V., Böhm, F. & Vollstaedt, H. (2009). Determination of radiogenic and stable strontium isotope ratios (87 Sr/86 Sr; δ 88/86 Sr) by thermal ionization mass spectrometry applying an 87 Sr/84 Sr double spike. Journal of Analytical Atomic Spectrometry 24(9): 1267-1271. 10.1039/B906292K

Krabbenhöft, A., Eisenhauer, A., Böhm, F., Vollstaedt, H., Fietzke, J., Liebetrau, V., Augustin, N., Peucker-Ehrenbrink, B., Müller, M. N., Horn, C. and Hansen, B. T. (2010). Constraining the marine strontium budget with natural strontium isotope fractionations (87Sr/86Sr∗, δ88/86Sr) of carbonates, hydrothermal solutions and river waters. Geochimica et Cosmochimica Acta, 74(14), 4097-4109. https://doi.org/10.1016/j.gca.2010.04.009

Kump, L. R. & Arthur, M. A. (1999). Interpreting carbon-isotope excursions: carbonates and organic matter. Chemical Geology 161(1-3): 181-198. https://doi.org/10.1016/S0009-2541(99)00086-8

Kuznetsov, A., Semikhatov, M. A. & Gorokhov, I. M. (2018). Strontium isotope stratigraphy: principles and state of the art. Stratigraphy and Geological Correlation 26(4): 367-386. https://doi.org/10.1134/S0869593818040056

Lawrence, M. G., Greig, A., Collerson, K. D. & Kamber, B. S. (2006). Rare earth element and yttrium variability in South East Queensland waterways. Aquatic Geochemistry 12(1): 39-72. https://doi.org/10.1007/s10498-005-4471-8

Le Heron, D. P., Busfield, M. E. & Collins, A. S. (2014). Bolla Bollana boulder beds: A Neoproterozoic trough mouth fan in South Australia? Sedimentology 61(4): 978-995. https://doi.org/10.1111/sed.12082

Le Heron, D. P., Cox, G., Trundley, A. & Collins, A. (2011). Sea ice− free conditions during the Sturtian glaciation (early Cryogenian), South Australia. Geology 39(1): 31-34. https://doi.org/10.1130/G31547.1

Le Heron, D. P., Cox, G., Trundley, A. & Collins, A. S. (2011a). Two Cryogenian glacial successions compared: Aspects of the Sturt and Elatina sediment records of South Australia. Precambrian Research 186(1-4): 147-168. https://doi.org/10.1016/j.precamres.2011.01.014

Lechte, M. & Wallace, M. (2016). Sub–ice shelf ironstone deposition during the Neoproterozoic Sturtian glaciation. Geology 44(11): 891-894. https://doi.org/10.1130/G38495.1

Lechte, M. A. & Wallace, M. W. (2015). Sedimentary and tectonic history of the Holowilena Ironstone, a Neoproterozoic iron formation in South Australia. Sedimentary Geology 329: 211-224. https://doi.org/10.1016/j.sedgeo.2015.09.014

Lenton, T. M., Boyle, R. A., Poulton, S. W., Shields-Zhou, G. A. & Butterfield, N. J. (2014). Co-evolution of eukaryotes and ocean oxygenation in the Neoproterozoic era. Nature Geoscience 7(4): 257-265. https://doi.org/10.1038/ngeo2108

Li, Z.-X., Bogdanova, S., Collins, A.S., Davidson, A., De Waele, B., Ernst, R.E., Fitzsimons, I.C.W., Fuck, R.A., Gladkochub, D.P., Jacobs, J. & Karlstrom, K.E. (2008). Assembly, configuration, and break-up history of Rodinia: a synthesis. Precambrian Research 160(1-2): 179-210. https://doi.org/10.1016/j.precamres.2007.04.021

Ling, H.-F., Chen, X., Li, D. A., Wang, D., Shields-Zhou, G. A. & Zhu, M. (2013). Cerium anomaly variations in Ediacaran–earliest Cambrian carbonates from the Yangtze Gorges area, South China: implications for oxygenation of coeval shallow seawater. Precambrian Research 225: 110-127. https://doi.org/10.1016/j.precamres.2011.10.011

Link, P. K. & Gostin, V. A. (1981). Facies and paleogeography of Sturtian glacial strata (late Precambrian), South Australia. American Journal of Science 281(4): 353-374. https://doi.org/10.2475/ajs.281.4.353

Liu, X.-M., Hardisty, D. S., Lyons, T. W. & Swart, P. K. (2019). Evaluating the fidelity of the cerium paleoredox tracer during variable carbonate diagenesis on the Great Bahamas Bank. Geochimica et Cosmochimica Acta 248: 25-42. https://doi.org/10.1016/j.gca.2018.12.028

Lloyd, J. C., Blades, M.L., Counts, J.W., Collins, A.S., Amos, K.J., Wade, B.P., Hall, J.W., Hore, S., Ball, A.L., Shahin, S. & Drabsch, M. (2020). Neoproterozoic geochronology and provenance of the Adelaide Superbasin. Precambrian Research 350: 105849. https://doi.org/10.1016/j.precamres.2020.105849

Lloyd, J. C., Collins, A. S., Blades, M. L., Gilbert, S. E. & Amos, K. J. (2022). Early Evolution of the Adelaide Superbasin, Geosciences, 12(4). https://doi.org/10.3390/geosciences12040154

Lloyd, J. C., Preiss, W. V., Collins, A. S., Virgo, G. M., Blades, M. L., Gilbert, S. E., Subarkah, D., Krapf, C. B. E. & Amos, K. J. (2022a). Geochronology and formal stratigraphy of the Sturtian Glaciation in the Adelaide Superbasin, Geological Magazine. https://doi.org/10.31223/X50G9N

Macdonald, F. A., Schmitz, M.D., Crowley, J.L., Roots, C.F., Jones, D.S., Maloof, A.C., Strauss, J.V., Cohen, P.A., Johnston, D.T. & Schrag, D.P. (2010). Calibrating the cryogenian. Science 327(5970): 1241-1243. 10.1126/science.1183325

Marais, D. J. D., Strauss, H., Summons, R. E. & Hayes, J. M. (1992). Carbon isotope evidence for the stepwise oxidation of the Proterozoic environment. Nature 359(6396): 605-609. https://doi.org/10.1038/359605a0

McKirdy, D. M., Burgess, J.M., Lemon, N.M., Yu, X., Cooper, A.M., Gostin, V.A., Jenkins, R.J. & Both, R.A. (2001). A chemostratigraphic overview of the late Cryogenian interglacial sequence in the Adelaide Fold-Thrust Belt, South Australia. Precambrian Research 106(1-2): 149-186. https://doi.org/10.1016/S0301-9268(00)00130-3

McLennan, S., Taylor, S. R., McCulloch, M. T. & Maynard, J. B. (1990). Geochemical and Nd/Sr isotopic composition of deep-sea turbidites: crustal evolution and plate tectonic associations. Geochimica et Cosmochimica Acta 54(7): 2015-2050. https://doi.org/10.1016/0016-7037(90)90269-Q

Meert, J. G. (2003). A synopsis of events related to the assembly of eastern Gondwana. Tectonophysics, 362(1-4), 1-40. https://doi.org/10.1016/S0040-1951(02)00629-7

Merdith, A. S., Collins, A.S., Williams, S.E., Pisarevsky, S., Foden, J.D., Archibald, D.B., Blades, M.L., Alessio, B.L., Armistead, S., Plavsa, D. & Clark, C. (2017). A full-plate global reconstruction of the Neoproterozoic. Gondwana Research 50: 84-134. https://doi.org/10.1016/j.gr.2017.04.001

Merdith, A. S., Williams, S. E., Muller, R. D. & Collins, A. S. (2017a). Kinematic constraints on the Rodinia to Gondwana transition. Precambrian Research, 299, 132-150. https://doi.org/10.1016/j.precamres.2017.07.013

Merdith, A. S., Williams, S. E., Brune, S., Collins, A. S. & Müller, R. D. (2019). Rift and plate boundary evolution across two supercontinent cycles. Global and Planetary Change 173: 1-14. https://doi.org/10.1016/j.gloplacha.2018.11.006

Merdith, A. S., Williams, S.E., Collins, A.S., Tetley, M.G., Mulder, J.A., Blades, M.L., Young, A., Armistead, S.E., Cannon, J., Zahirovic, S. & Müller, R.D. (2021). Extending full-plate tectonic models into deep time: Linking the Neoproterozoic and the Phanerozoic. Earth-Science Reviews 214: 103477. https://doi.org/10.1016/j.earscirev.2020.103477

Micheels, A. & Montenari, M. (2008). A snowball Earth versus a slushball Earth: Results from Neoproterozoic climate modeling sensitivity experiments. Geosphere, 4(2): 401-410. https://doi.org/10.1130/GES00098.1

Moretti, M., Soria, J. M., Alfaro, P. & Walsh, N. (2001). Asymmetrical soft-sediment deformation structures triggered by rapid sedimentation in turbiditic deposits (Late Miocene, Guadix Basin, Southern Spain). Facies 44(1): 283-294. https://doi.org/10.1007/BF02668179

Murrell, B. (1977). Stratigraphy and tectonics across the Torrens Hinge Zone between Andamooka and Marree, South Australia, University of Adelaide, Department of Geology. https://hdl.handle.net/2440/21084

Nier, A. O. (1938). Variations in the relative abundances of the isotopes of common lead from various sources. Journal of the American Chemical Society 60(7): 1571-1576.

O'Connell, B., Wallace, M. W., Hood, A. v.S, Lechte, M. A. & Mahon, E. M. (2022). Nearshore environments before the evolution of land plants. Precambrian Research 382: 106883. https://doi.org/10.1016/j.precamres.2022.106883

O'Connell, B., Wallace, M. W., Hood, A. v.S, Lechte, M. A. & Planavsky, N. J. (2020). Iron-rich carbonate tidal deposits, Angepena Formation, South Australia: a redox-stratified Cryogenian basin. Precambrian Research 342: 105668. https://doi.org/10.1016/j.precamres.2020.105668

Olivarez, A. M. & Owen, R. M. (1991). The europium anomaly of seawater: implications for fluvial versus hydrothermal REE inputs to the oceans. Chemical Geology 92(4): 317-328. https://doi.org/10.1016/0009-2541(91)90076-4

Park, Y., Swanson-Hysell, N.L., MacLennan, S.A., Maloof, A.C., Gebreslassie, M., Tremblay, M.M., Schoene, B., Alene, M., Anttila, E.S., Tesema, T. & Haileab, B. (2020). The lead-up to the Sturtian Snowball Earth: Neoproterozoic chemostratigraphy time-calibrated by the Tambien Group of Ethiopia. Bulletin 132(5-6): 1119-1149. https://doi.org/10.1130/B35178.1

Peral, L. E. G., Poiré, D. G., Strauss, H. & Zimmermann, U. (2007). Chemostratigraphy and diagenetic constraints on Neoproterozoic carbonate successions from the Sierras Bayas Group, Tandilia System, Argentina. Chemical Geology 237(1-2): 109-128. https://doi.org/10.1016/j.chemgeo.2006.06.022

Postma, G. (1983). Water escape structures in the context of a depositional model of a mass flow dominated conglomeratic fan-delta (Abrioja Formation, Pliocene, Almeria Basin, SE Spain). Sedimentology 30(1): 91-103. https://doi.org/10.1111/j.1365-3091.1983.tb00652.x

Preiss, W. (2000). The Adelaide Geosyncline of South Australia and its significance in Neoproterozoic continental reconstruction. Precambrian Research 100(1-3): 21-63. https://doi.org/10.1016/S0301-9268(99)00068-6

Preiss, W. & Cowley, W. (1999). Genetic stratigraphy and revised lithostratigraphic classification of the Burra Group in the Adelaide Geosyncline. MESA Journal 14: 30-40.

Preiss, W. V. (1973). Palaeoecological interpretations of South Australian Precambrian stromatolites. Journal of the Geological Society of Australia 19(4): 501-532.

Preiss, W. V. (1987). The Adelaide Geosyncline: Late Proterozoic stratigraphy, sedimentation, palaeontology and tectonics, Department of Mines and Energy.

Preiss, W. V., Drexel, J. F. & Reid, A. J. (2009). Definition and age of the Kooringa Member of the Skillogalee Dolomite: host for Neoproterozoic (c. 790 Ma) porphyry related copper mineralisation at Burra. MESA Journal 55: 19-33.

Preiss, W. V., Gostin, V. A., McKirdy, D. M., Ashley, P. M., Williams, G. E. & Schmidt, P. W. (2011). The glacial succession of Sturtian age in South Australia: the Yudnamutana Subgroup. Geological Society, London, Memoirs 36(1): 701-712. https://doi.org/10.1144/M36.69

Priestley, S. C. C., Tyler, J., Liebelt, S.R., Mosley, L.M., Wong, W.W., Shao, Y., Woolston, Z., Farrell, M., Welsh, D.T., Brookes, J.D. & Collins, A.S. (2022). N and C Isotope Variations Along an Extreme Eutrophication and Salinity Gradient in the Coorong Lagoon, South Australia. Front Earth Sc-Switz, 9. https://doi.org/10.3389/feart.2021.727971

Rooney, A. D., Strauss, J. V., Brandon, A. D. & Macdonald, F. A. (2015). A Cryogenian chronology: Two long-lasting synchronous Neoproterozoic glaciations, Geology, 43(5), 459-462. https://doi.org/10.1130/G36511.1

Runnegar, B. (1991). Precambrian oxygen levels estimated from the biochemistry and physiology of early eukaryotes. Palaeogeography, Palaeoclimatology, Palaeoecology 97(1-2): 97-111. https://doi.org/10.1016/0031-0182(91)90186-U

Sarmiento, J. L. (2013). Ocean biogeochemical dynamics. Ocean Biogeochemical Dynamics, Princeton University Press. https://doi.org/10.1515/9781400849079

Sarvian, N. L., Hurtgen, M.T., Jacobsen, A.D. & Maloof, A.C. (2019). Stable Strontium Isotope (δ88/86Sr) Record of pre-Sturtian Carbonate Rocks Spanning a Large δ13C Anomaly. Goldschmidt2021. Virtual.

Schidlowski, M. (1988). A 3,800-million-year isotopic record of life from carbon in sedimentary rocks. Nature 333(6171): 313-318. https://doi.org/10.1038/333313a0

Schidlowski, M., Eichmann, R. & Junge, C. E. (1975). Precambrian sedimentary carbonates: carbon and oxygen isotope geochemistry and implications for the terrestrial oxygen budget. Precambrian Research 2(1): 1-69. https://doi.org/10.1016/0301-9268(75)90018-2

Shao, Y., Farkaš, J., Holmden, C., Mosley, L., Kell-Duivestein, I., Izzo, C., Reis-Santos, P., Tyler, J., Törber, P., Frýda, J. & Taylor, H. (2018). Calcium and strontium isotope systematics in the lagoon-estuarine environments of South Australia: Implications for water source mixing, carbonate fluxes and fish migration. Geochimica et Cosmochimica Acta 239: 90-108. https://doi.org/10.1016/j.gca.2018.07.036

Shao, Y., Farkaš, J., Mosley, L., Tyler, J., Wong, H., Chamberlayne, B., Raven, M., Samanta, M., Holmden, C., Gillanders, B.M. & Kolevica, A. (2021). Impact of salinity and carbonate saturation on stable Sr isotopes (δ88/86Sr) in a lagoon-estuarine system. Geochimica et Cosmochimica Acta 293: 461-476. https://doi.org/10.1016/j.gca.2020.11.014

Shields-Zhou, G. & Och, L. (2011). The case for a Neoproterozoic oxygenation event: geochemical evidence and biological consequences. GSA Today 21(3): 4-11. http://dx.doi.org/10.1130/GSATG102A.1

Shields, G. & Veizer, J. (2002). Precambrian marine carbonate isotope database: Version 1.1. Geochemistry, Geophysics, Geosystems 3(6): 1 of 12-12 of 12. https://doi.org/10.1029/2001GC000266

Shuster, A. M., Wallace, M. W., Hood, A. v.S. & Jiang, G. (2018). The Tonian Beck Spring Dolomite: Marine dolomitization in a shallow, anoxic sea. Sedimentary Geology 368: 83-104. https://doi.org/10.1016/j.sedgeo.2018.03.003

Spötl, C. & Vennemann, T. W. (2003). Continuous-flow isotope ratio mass spectrometric analysis of carbonate minerals. Rapid communications in mass spectrometry 17(9): 1004-1006. https://doi.org/10.1002/rcm.1010

Stromberg, S. G. & Bluck, B. (1998). Turbidite facies, fluid-escape structures and mechanisms of emplacement of the Oligo-Miocene Aljibe Flysch, Gibraltar Arc, Betics, southern Spain. Sedimentary Geology 115(1-4): 267-288. https://doi.org/10.1016/S0037-0738(97)00096-1

Sumartojo, J. & Gostin, V. (1976). Geochemistry of the late Precambrian Sturt Tillite, Flinders Ranges, South Australia. Precambrian Research 3(3): 243-252. https://doi.org/10.1016/0301-9268(76)90011-5

Swanson-Hysell, N. L., Rose, C. V., Calmet, C. C., Halverson, G. P., Hurtgen, M. T. & Maloof, A. C. (2010). Cryogenian glaciation and the onset of carbon-isotope decoupling. Science 328(5978): 608-611. 10.1126/science.1184508

Thomson, B., Coats, R. P., Mirams, R. C., Forbes, B. G., Dalgarno, C. R. & Johnson, J. E. (1964). Precambrian rock groups in the Adelaide Geosyncline: a new subdivision. Quarterly Journal of the Geological Survey of South Australia 9: 1-19.

Tostevin, R., Shields, G. A., Tarbuck, G. M., He, T., Clarkson, M. O. & Wood, R. A. (2016). Effective use of cerium anomalies as a redox proxy in carbonate-dominated marine settings. Chemical Geology, 438, 146-162. https://doi.org/10.1016/j.chemgeo.2016.06.027

Tucker, M. E. & Wright, V. P. (2009). Carbonate sedimentology. John Wiley & Sons.

Uppill, R. K. (1990). Sedimentology of a dolomite-magnesite-sandstone sequence in the late Precambrian Mundallio Subgroup, South Australia. The evolution of a late Precambrian–early Paleozoic rift complex: The Adelaide geosyncline: Geological Society of Australia Special Publication 16: 105-128.

Vasiliev, I., Stoica, M., Grothe, A., Lazarev, S., Palcu, D. V., van Baak, C., De Leeuw, A., Sangiorgi, F., Reichart, G. J., Davies, G. R. & Krijgsman, W. (2021). Hydrological Changes in Restricted Basins: Insights From Strontium Isotopes on Late Miocene-Pliocene Connectivity of the Eastern Paratethys (Dacian Basin, Romania). Geochemistry, Geophysics, Geosystems, 22(7), e2020GC009369. https://doi.org/10.1029/2020GC009369

Veizer, J. (1983). Chemical diagenesis of carbonates: theory and application. Stable isotopes in sedimentary geology 10: 3-100. https://doi.org/10.2110/scn.83.01.0000

Veizer, J. & Compston, W. (1974). 87Sr/86Sr composition of seawater during the Phanerozoic. Geochimica et Cosmochimica Acta 38(9): 1461-1484. https://doi.org/10.1016/0016-7037(74)90099-4

Veizer, J. & Compston, W. (1976). 87Sr/86Sr in Precambrian carbonates as an index of crustal evolution. Geochimica et Cosmochimica Acta 40(8): 905-914. https://doi.org/10.1016/0016-7037(76)90139-3

Veizer, J. & Hoefs, J. (1976). The nature of O18/O16 and C13/C12 secular trends in sedimentary carbonate rocks. Geochimica et Cosmochimica Acta 40(11): 1387-1395. https://doi.org/10.1016/0016-7037(76)90129-0

Veizer, J., Plumb, K. A., Clayton, R. N., Hinton, R. W. & Grotzinger, J. P. (1992). Geochemistry of Precambrian carbonates: V. late Paleoproterozoic seawater. Geochimica et Cosmochimica Acta 56(6): 2487-2501. https://doi.org/10.1016/0016-7037(92)90204-V

Verdel, C., Phelps, B. & Welsh, K. (2018). Rare earth element and 87Sr/86Sr step-leaching geochemistry of central Australian Neoproterozoic carbonate. Precambrian Research 310: 229-242. https://doi.org/10.1016/j.precamres.2018.02.014

Virgo, G. M., Collins, A. S., Amos, K. J., Farkaš, J., Blades, M. L. & Subarkah, D. (2021). Descending into the "snowball": High resolution sedimentological and geochemical analysis across the Tonian to Cryogenian boundary in South Australia. Precambrian Research 367: 106449. https://doi.org/10.1016/j.precamres.2021.106449

Vollstaedt, H., Eisenhauer, A., Wallmann, K., Böhm, F., Fietzke, J., Liebetrau, V., Krabbenhöft, A., Farkaš, J., Tomašových, A., Raddatz, J. & Veizer, J. (2014). The Phanerozoic δ88/86Sr record of seawater: New constraints on past changes in oceanic carbonate fluxes. Geochimica et Cosmochimica Acta 128: 249-265. https://doi.org/10.1016/j.gca.2013.10.006

Von der Borch, C. & Lock, D. (1979). Geological significance of Coorong dolomites. Sedimentology 26: 813-824. https://doi.org/10.1111/j.1365-3091.1979.tb00974.x

Wallace, M. W., Shuster, A., Greig, A., Planavsky, N. J. & Reed, C. P. (2017). Oxygenation history of the Neoproterozoic to early Phanerozoic and the rise of land plants. Earth and Planetary Science Letters 466: 12-19. https://doi.org/10.1016/j.epsl.2017.02.046

Wallace, M. W., Hood, A. v.S, Fayle, J., Hordern, E. S. & O'Hare, T. F. (2019). Neoproterozoic marine dolomite hardgrounds and their relationship to cap dolomites. Precambrian Research 328: 269-286. https://doi.org/10.1016/j.precamres.2019.04.026

Wallace, M. W., Hood, A. v.S, Woon, E. M., Giddings, J. A. & Fromhold, T. A. (2015). The Cryogenian Balcanoona reef complexes of the Northern Flinders Ranges: implications for Neoproterozoic ocean chemistry. Palaeogeography, Palaeoclimatology, Palaeoecology 417: 320-336. https://doi.org/10.1016/j.palaeo.2014.09.028

Walter, M., Veevers, J. J., Calver, C. R., Gorjan, P. & Hill, A. C. (2000). Dating the 840–544 Ma Neoproterozoic interval by isotopes of strontium, carbon, and sulfur in seawater, and some interpretative models. Precambrian Research 100(1-3): 371-433. https://doi.org/10.1016/S0301-9268(99)00082-0

Ward, J. F., Verdel, C., Campbell, M. J., Leonard, N. & Nguyen, A. D. (2019). Rare earth element geochemistry of Australian Neoproterozoic carbonate: Constraints on the Neoproterozoic oxygenation events. Precambrian Research 335: 105471. https://doi.org/10.1016/j.precamres.2019.105471

Young, G. & Gostin, V. (1988). Stratigraphy and sedimentology of Sturtian glacigenic deposits in the western part of the North Flinders Basin, South Australia. Precambrian Research 39(3): 151-170. https://doi.org/10.1016/0301-9268(88)90040-X

Young, G. & Gostin, V. (1991). Late Proterozoic (Sturtian) succession of the North Flinders Basin, South Australia: an example of temperate glaciation in an active rift setting. Glacial Marine Sedimentation: Paleoclimatic Significance 261: 207-222.

Chapter 4: Tectonic, eustatic and climate controls on facies architecture during the transition to the Neoproterozoic icehouse in the Adelaide Superbasin, Australia

Accepted for publication in peer-reviewed journal *Sedimentologika:*

Georgina M. Virgo[a,b,*], Alan S. Collins[b], Morgan L. Blades[b], Kathryn J. Amos[a]

Statement of Authorship

Title of Paper	Tectonic, eustatic and climate controls on facies architecture during the transition to the Neoproterozoic icehouse in the Adelaide Superbasin, Australia
Publication Status	☐ Published ☑ Accepted for Publication ☐ Submitted for Publication ☐ Unpublished and Unsubmitted work written in manuscript style
Publication Details	Virgo, G. M., Collins, A. S., Blades, M. L., Amos, K. J. (2023). Tectonic, eustatic and climate controls on facies architecture during the transition to the Neoproterozoic icehouse in the Adelaide Superbasin, Australia. Sedimentologika

Principal Author

Name of Principal Author (Candidate)	Georgina Virgo
Contribution to the Paper	All manuscript text and figure drafting; data collection, processing and analysis; methodology; interpretations; field investigation
Overall percentage (%)	90%
Certification:	This paper reports on original research I conducted during the period of my Higher Degree by Research candidature and is not subject to any obligations or contractual agreements with a third party that would constrain its inclusion in this thesis. I am the primary author of this paper.
Signature	Date 07/07/2023

Co-Author Contributions

By signing the Statement of Authorship, each author certifies that:

i. the candidate's stated contribution to the publication is accurate (as detailed above);
ii. permission is granted for the candidate in include the publication in the thesis; and
iii. the sum of all co-author contributions is equal to 100% less the candidate's stated contribution.

Name of Co-Author	Alan Collins
Contribution to the Paper	Reviews and commentary; assistance with methodology
Signature	Date 07/07/2023

Name of Co-Author	Morgan Blades
Contribution to the Paper	Reviews and commentary
Signature	Date 07/07/2023

Please cut and paste additional co-author panels here as required.

Name of Co-Author	Kathryn Amos		
Contribution to the Paper	Reviews and commentary		
Signature		Date	07/07/2023

4.1 Abstract

The Tonian to Cryogenian (ca. 1000–635 Ma) marks a crucial turning point in Earth's history, where tectonic reorganisation and fluctuating oceanic and atmospheric geochemistry plunged the globe into icehouse conditions. This was followed by a postglacial warming period that delivered large volumes of nutrients to the oceans and stimulated eukaryotic evolution. The Adelaide Superbasin in South Australia hosts a thick repository of Neoproterozoic and lower Cambrian sedimentary successions that preserve the depositional conditions during this unique time.

In this study, detailed sedimentological data were collected from over 8,350 m of measured section at seven locations across the northern Flinders Ranges. Tonian deposits reveal a carbonate platform setting, where deposition was controlled by basin geometry and proximity to uplifted source areas. In the early Cryogenian, sedimentary successions were affected by the Sturtian glaciation, characterised by two glacial advance-retreat phases that coincide with climatically driven regression. The end of the Sturtian glaciation was marked by basin subsidence and widespread transgression into a more distal subaqueous environment.

Despite the lithostratigraphic and sequence stratigraphic similarity between Tonian–Cryogenian successions globally, their correlation remains contentious. The influence of local tectonic regimes during the Tonian created a potential oceanic restriction between developing basins, which challenges the chemostratigraphic correlation between these deposits. Further, limited geochronological ages and opposing interpretations of glacial cyclicity puts into question the timing and extent of the Sturtian glaciation. Conversely, the post glacial transgression appears to be the most globally consistent as it results from climatically controlled sea level rise that was driven by melting ice sheets.

4.2 Introduction

The Neoproterozoic (ca. 1000 to 539 Ma) was one of the most dynamic eras in Earth's history and is marked by significant tectonic, biological, atmospheric, and climatic events. These include a supercontinent cycle, with the breakup of Rodinia and amalgamation of Gondwana (Li et al., 2008; Merdith et al., 2017; 2019; 2021); evolution from a prokaryote- to a eukaryotic-dominated biosphere (Butterfield, 2011; Lenton et al., 2014; Brocks et al., 2017); the Neoproterozoic Oxygenation Event (Shields-Zhou & Och, 2011); and vast low-latitude glaciations that have been referred to as "Snowball Earth" (Kirschvink, 1992; Hoffman et al., 1998; 2017b). These global shifts facilitated the development of a suite of depositional settings under vastly contrasting conditions, from warm shallow carbonate-rich seas to cold, ice-covered continents (Hoffman et al., 1998; 2017b; Halverson et al., 2009; Brocks et al., 2017). Palaeoenvironments varied not only on a global scale, but also at a local level within the confines of sedimentary basins. The Adelaide Superbasin in South Australia (Lloyd et al., 2020), preserves thick successions of these Neoproterozoic sedimentary rocks, recording the temporal and spatial variability and distribution of environments through the Tonian (ca. 1000–720 Ma), Cryogenian (ca. 720–635 Ma), Ediacaran (ca. 635–539 Ma), and Cambrian (ca. 539–485 Ma).

Literature from early studies in South Australia provide a foundation for the stratigraphy and tectonic evolution of the Adelaide Superbasin (e.g., Howchin, 1929; Segnit, 1939; Mawson & Sprigg, 1950; Preiss, 1987; Preiss et al., 1993), while contemporary sedimentological research presents more detailed analyses of specific formations and locations within the basin (Hill & Walter, 2000; McKirdy et al., 2001; Frank & Fielding, 2003; Giddings et al., 2009; Giddings & Wallace, 2009a, 2009b; Preiss et al., 2009, 2011; Fromhold & Wallace, 2011, 2012; Grey et al., 2011; Hood et al., 2011, 2016, 2018; Hood & Wallace, 2012, 2014, 2015; Le Heron et al., 2011, 2011a, 2014; Busfield & Le Heron, 2014; Lechte & Wallace, 2015, 2016; Wallace et al., 2015; Counts et al., 2016; Cox et al., 2018; Corkeron & Slezak, 2020; O'Connell et al., 2020; Virgo et al., 2021). In addition, advances in understanding the chronostratigraphy and provenance of the superbasin have established a firmer temporal framework and tectonic setting for the evolving basin (Cox et al., 2018; Armistead et al., 2020; Lloyd et al., 2020; 2022). Although these studies have contributed immensely to our understanding of Neoproterozoic palaeoenvironments and stratigraphic evolution through this time, they have not captured the wider facies architecture across the basin. In particular, basin-scale architecture within the context of sequence stratigraphic changes related to active rifting and climatically driven sea level fluctuations, which resulted from the breakup of Rodinia and the Cryogenian glaciations.

Further, there have been a number of notable studies through Neoproterozoic strata at other sites globally, including Namibia (Frimmel et al., 1996; Hoffman & Halverson, 2008; Le Heron et al., 2013; Miller, 2013; Hood et al., 2015; Lechte & Wallace, 2016; Hoffman et al., 2017a; 2021; Lamothe et al., 2019), northern Ethiopia (Alene et al., 2006; Avigad et al., 2007; Miller et al., 2009; 2011; Swanson-Hysell et al., 2015; Park et al., 2020), Scotland (Spencer & Spencer, 1972; Glover & Winchester, 1989; Smith et al., 1999; Anderson et al., 2013; Stephenson et al., 2013; Fairchild et al., 2017; Ali et al., 2018), Svalbard (i.e., Norway, Halverson et al., 2004; 2011; 2017; 2022; Maloof et al., 2006; Hoffman et al., 2012; 2017a; Kunzmann et al., 2015; Fairchild et al., 2016; 2016a; Millikin et al., 2022), western USA (Crittenden et al., 1983; Link et al., 1994; Lund et al., 2003; Fanning & Link, 2004; Link & Christie- Blick, 2011; Keeley et al., 2012; Balgord et al., 2013; Busfield & Le Heron, 2016; Le Heron & Busfield, 2016; Le Heron et al., 2020; Nelson et al., 2020; 2021), northern Canada (Chartrand & Brown, 1985; Eisbacher, 1985; Park & Jefferson, 1991; Narbonne et al., 1994; Narbonne & Aitken, 1995; Batten et al., 2004; Long & Turner, 2013; Milton et al., 2017) and south China (Wang & Li, 2001; Li et al., 2003; Zhang et al., 2008; Zhang et al., 2011; Lan et al., 2015; Busigny et al., 2018). These studies have investigated the lithostratigraphic variation across each respective basin, and the subsequent relationship with shifting climate and tectonic regimes. Although many of these changes are local, global climatic fluctuations and tectonic reorganisation could also be responsible for the major temporal and spatial variability in stratigraphy, potentially providing a platform from which these sections may be correlated globally.

In this study, we use detailed sedimentological data collected from multiple sites across the northern Flinders Ranges to construct a sequence stratigraphic framework and correlate facies across the width of the Adelaide Superbasin during the Neoproterozoic. This is achieved

through extensive analyses of grain sizes, sedimentary structures, bedding thicknesses, and palaeocurrent directions, followed by lithostratigraphic correlations and the interpretation of sequence stratigraphic boundaries and palaeoenvironmental settings. The temporal and spatial distributions of depositional environments can subsequently be correlated to other basins across the globe in order to better differentiate local vs. global influence in tectonic and palaeoclimatic regimes during the Tonian and Cryogenian. As one of the most well-preserved and understudied Precambrian basins in the world, the Adelaide Superbasin therefore provides a window into an important and unique time in Earth's past.

4.3 Geological Setting

The Adelaide Rift Complex (Figure 1) lies within the Adelaide Superbasin and forms a thick repository of sedimentary rocks that preserve a record of Earth surface systems throughout the Neoproterozoic and early Cambrian. The northern part of this ~750 km north–south trending basin started as a half graben fault-controlled rift basin that initiated during the breakup of Rodina as Laurentia rifted from Australia-east Antarctica (Merdith et al., 2019). The basin then developed into an aulacogen (continentward of a passive margin) during the late Proterozoic (Lloyd et al., 2022). Tonian sediments were transported into the basin from the surrounding rift shoulders, which were focused at the time along a NW–SE rift valley that formed the present day Willouran Ranges (Figure 1; Preiss, 2000; Lloyd et al., 2020). The start of the Cryogenian was characterised by widespread erosion across the basin during the Sturtian glaciation, followed by a second period of sedimentation focused in the northwest and sourced from the reactivated rift shoulders (Lloyd et al., 2020). Deposition was terminated at the onset of the Delamerian Orogeny (ca. 514 Ma; Preiss, 2000; Foden et al., 2006; 2020), and the subsequent folding, uplift and erosion exposed the Neoproterozoic rocks as the modern Flinders Ranges of South Australia (Figure 1).

The Neoproterozoic sedimentary rocks are divided lithostratigraphically into the Callana, Burra, Umberatana, and Wilpena groups (Thomson et al., 1964; Preiss et al., 1998; Preiss & Cowley, 1999; Preiss, 2000; Preiss et al., 2011; Lloyd et al., 2020), where deposits of the Tonian and Cryogenian periods correspond to the Burra and Umberatana groups, respectively (Figure 1; Mawson & Sprigg, 1950; Thomson et al., 1964; Lloyd et al., 2020). Formation nomenclature varies across the basin and largely arises from the locally derived classification of type sections (Preiss & Cowley, 1999). Overall, the Burra Group in the northern Flinders Ranges can be subdivided into three units. There is a basal quartzite, which has several designations that corresponds to the location of the measured sections and reflects an overall deltaic environment (Preiss, 1987). This transitions into the Skillogalee Dolomite, a carbonate (magnesite and dolomite) dominated succession with minor clastic interbeds that is interpreted to represent a paralic/ marginal marine setting (Belperio, 1990; Frank & Fielding, 2003). The top of the Burra Group in the northern Flinders Ranges is marked by the Myrtle Springs Formation, a dominantly fine-grained clastic unit with minor carbonate interbeds, which reflect deposition in a subtidal to marginal marine environment (Preiss, 1987, 2000). The base of the Umberatana Group corresponds to the Sturtian glaciation and is represented by diamictite successions that are separated by finer-grained clastic beds that represent an overall glaciomarine setting (Link and Gostin, 1981; Young & Gostin 1988; 1990; 1991).

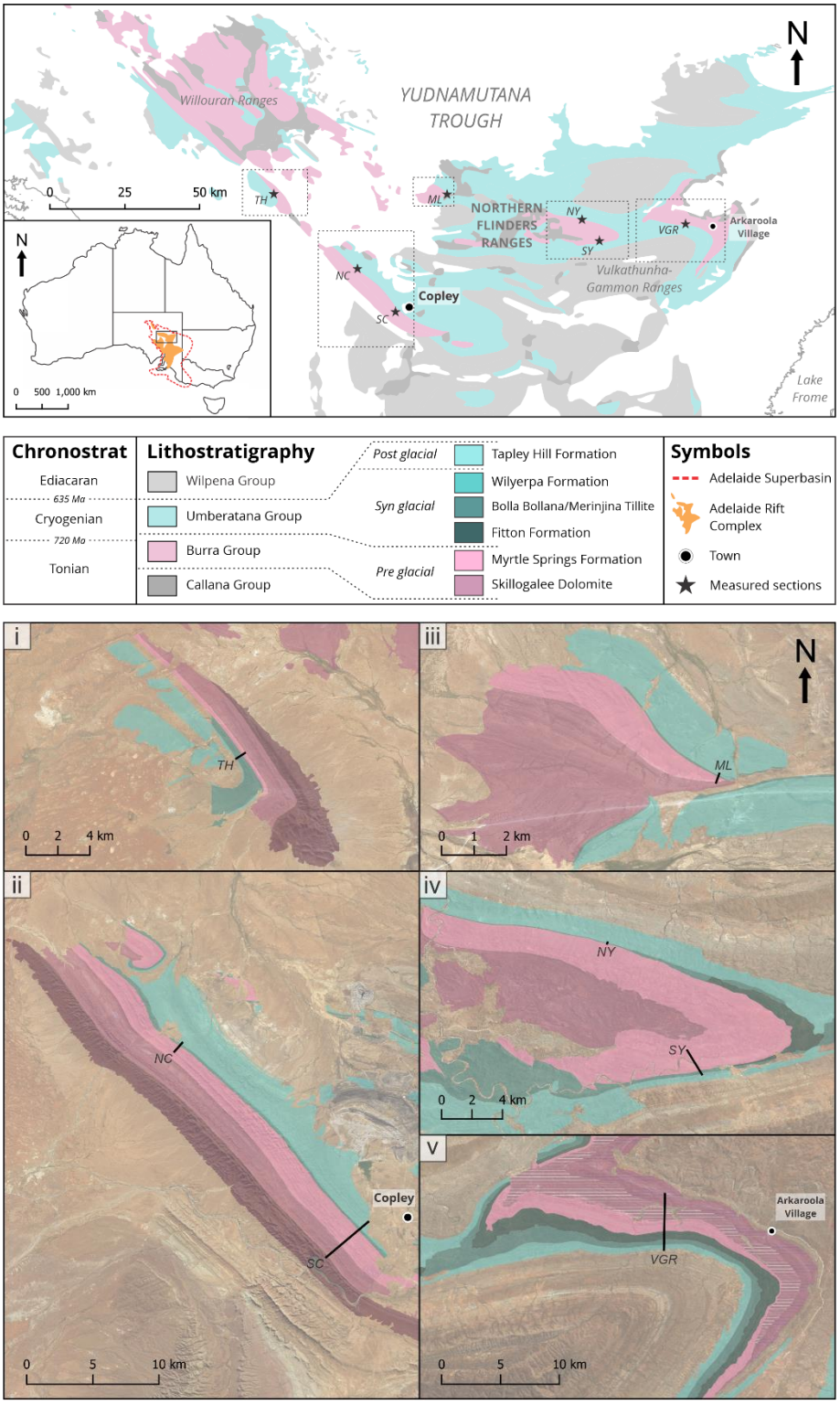

Figure 1: Geological map of Neoproterozoic lithostratigraphic groups in the Adelaide Rift Complex, northern Flinders Ranges, South Australia. Insert shows position of Adelaide Rift Complex within Australia. Satellite images of fieldwork locations overlain by stratigraphic formations. Black line denotes the location of the section measured. (i) TH = Termination Hill (ii) NC = North Copley, SC = South Copley (iii) ML = Mount Lyndhurst (iv) NY = North Yankaninna, SY = South Yankaninna (v) VGR = Vulkathunha-Gammon Ranges.

Young & Gostin 1988; 1990; 1991). Several of these diamictite successions have tillite nomenclature that are in the process of being synthesized and reclassified to the Sturt Formation (Lloyd et al., 2023). This is overlain by the Wilyerpa/Lyndhurst Formation, which defines the onset of deglacial conditions and is dominated by fine-grained clastic lithofacies that are dropstone rich, reflecting deposition in a proglacial setting. This is succeeded by an extensive post-glacial carbonate and shale unit that is termed the Tapley Hill Formation and represents a shift to a slope to basinal environment (Preiss, 1987). This formation includes a basal shale member, Tindelpina Shale Member, which directly overlies glaciogenic rocks (Thomson et al., 1964; Preiss, 1987). The Tapley Hill Formation and its basal member are widespread and were deposited not only in the northern Flinders Ranges but across the basin.

Chronostratigraphic constraints are provided by U–Pb zircon ages from tuffs and volcanic units as well as from the youngest zircons preserved in detrital sedimentary units. Age constraints on the Tonian succession are provided by a maximum depositional age (MDA) of 893 ± 9 Ma from the basal unit in the Callana Group (Lloyd et al., 2022). This complements the 802 ± 10 Ma depositional age of the Rook Tuff in the Willouran Ranges (Fanning et al., 1986), which sits stratigraphically below the Burra Group (Preiss et al., 2009; Lloyd et al., 2020). Igneous zircon grains from the base of the overlying Burra Group have been dated and provide depositional ages of 788 ± 6 Ma (Boucaut Volcanics, Armistead et al., 2020) and 794 ± 4 Ma (Kooringa Member, Preiss et al., 2009). These are stratigraphically equivalent to the base of the Skillogalee Dolomite Formation in this study (Lloyd et al., 2020). In the Cryogenian, a new in-situ Rb-Sr age of 684 +/- 37 Ma dates deposition of the interglacial shales within the Sturt Formation (Lloyd et al., 2023). The Wilyerpa Formation of the Umberatana Group is constrained from a precise tuff age of 663.03 ± 0.76 Ma (zircon U–Pb CA-ID-TIMS; Cox et al., 2018) collected from the South Copley section. The base of the Wilpena Group is constrained by an MDA of 654 ± 11 Ma (Seacliff Sandstone, van der Wolff, pers. comms., 2020) from the Southern Mount Lofty Ranges, which is stratigraphically equivalent to the “cap carbonate” (Nuccaleena Formation) of the Marinoan glaciation in the northern Flinders Ranges (Lloyd et al., 2020). Up-section, an MDA of 630 +/- 16 Ma (ABC Range Quartzite, Lloyd et al., 2020) collected from the Willouran Ranges defines the middle of the Wilpena Group.

4.4 Methods

This study encompasses several field sites located across the northern Flinders Ranges (Figure 1). Site selection was based on previous geological mapping (Coats, 1973), access to site location, geographic spread, and stratigraphic thickness. Coordinates for each section were recorded with a handheld GPS and the stratigraphy was measured bed by bed at approximately one metre-resolution using a tape measure. Detailed descriptions of grain size, sedimentary structures, bedding thicknesses and palaeocurrent direction were recorded (Supplementary Figures 1–7).

Sedimentary logs produced in the field were digitised using EasyCore software and palaeocurrent data were analysed with the software Stereonet. Lithofacies were classified based on grain size and sedimentary structures (Table 1). The lithofacies were then grouped into facies associations (Table 2), which were determined by the stacking pattern of facies. Each

facies association represents multiple depositional processes in a genetically related interval (Catuneanu, 2006). All these elements were used together to interpret the depositional environments throughout each section. Lithofacies, facies associations and interpreted depositional environment are presented within the sedimentary logs in Supplementary Figures 1–7.

The spatial and temporal distribution of depositional environments across the northern Flinders Ranges was incorporated into a sequence stratigraphic model based on lithofacies stacking patterns and stratigraphic relationships. Interpretations were then made as to the controls on sedimentary architecture within the basin (e.g., variations in accommodation and sediment input, driven by fluctuations in tectonism (i.e., subsidence or uplift), eustacy, and sediment supply; Catuneanu, 2006).

4.5 Results

4.5.1 Sedimentary Logs

Summary graphic sedimentary logs for each of the measured sections are presented in Figure 2 and have a collective total stratigraphic thickness of 8,350 m. There are considerable variations in stratigraphic thicknesses and lithologies across the northern Flinders Ranges (Figure 2). However, the base of the measured sections was arbitrarily chosen, so thicknesses of the pre-glacial rocks do not reflect complete thicknesses of preserved stratigraphy.

On the western margin of the basin, the measured Skillogalee Dolomite intervals at Termination Hill (TH) and South Copley (SC) sections are 380 m and 925 m thick, respectively. This is represented by a carbonate-dominated succession of magnesite, dolomite and microbial lithologies with interbedded clastics. In the north-central zone of the basin at Mount Lyndhurst (ML), the stromatolite-dominated Skillogalee Dolomite unit is 48 m thick. In the east of the basin, in the Vulkathunha-Gammon Ranges (VGR), the 1040 m thick Skillogalee Dolomite unit records a shift to clastic-dominated deposition, characterised by siltstone and sandstone with minor dolostone and microbial carbonates. The overlying Myrtle Springs Formation varies in thickness from 80 m, 502 m, 966 m, 103 m, 21 m, and 848 m between the Termination Hill (TH), North Copley (NC), South Copley (SC), Mount Lyndhurst (ML), North Yankaninna (NY) and South Yankaninna (SY) sections, respectively. These are characterised by a suite of clastic and carbonate lithofacies, including siltstone, sandstone, dolostone and microbialites. In the Vulkathunha-Gammon Ranges (VGR), the Myrtle Springs Formation is marked by 477 m of interbedded siltstone and sandstone with minor dolostone lithofacies towards the top.

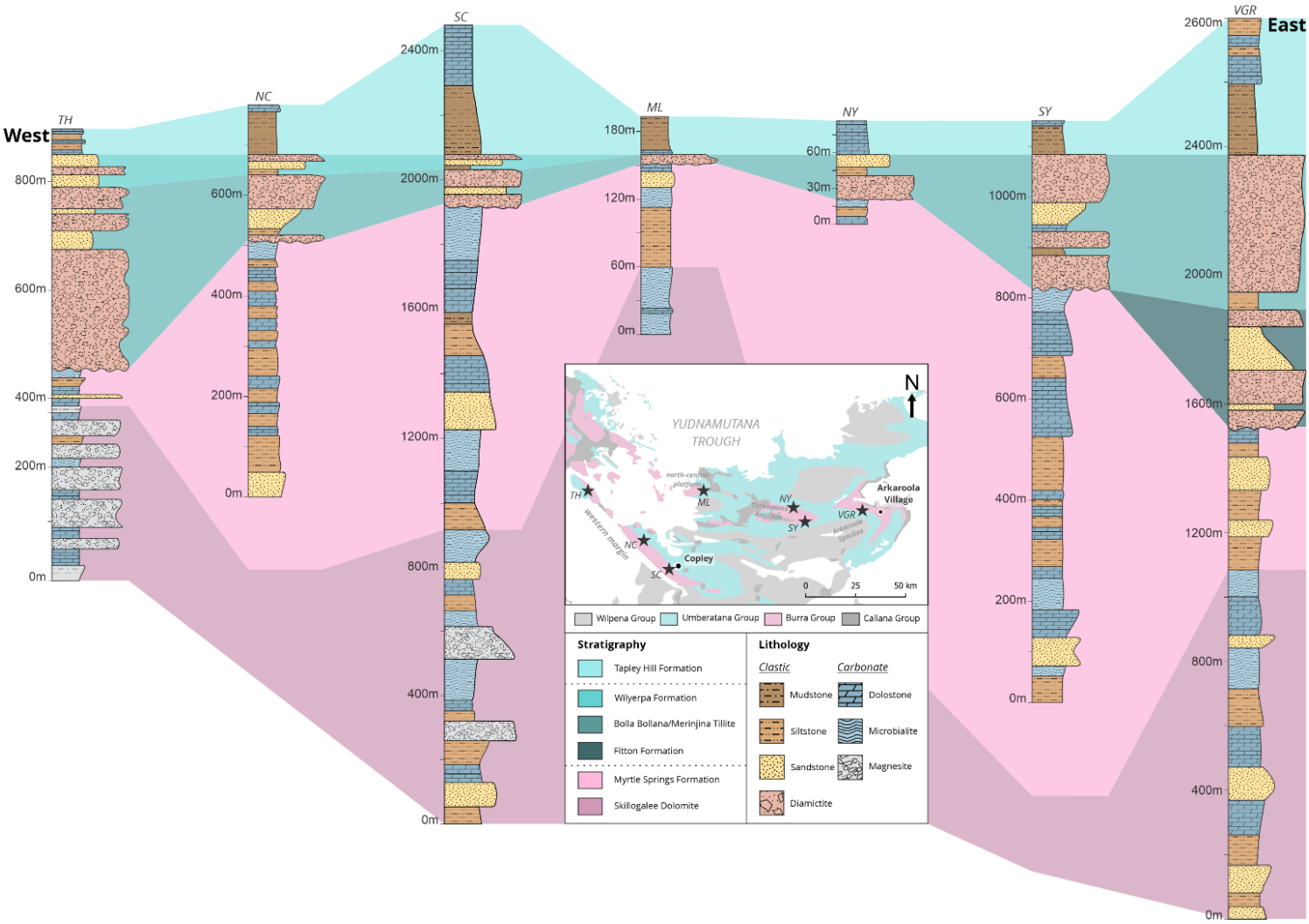

Figure 2: Generalised sedimentary logs through Tonian–Cryogenian sections across the northern Flinders Ranges, South Australia. Coloured panels indicate correlation of stratigraphic formations between sections. TH = Termination Hill, NC = North Copley, SC = South Copley, ML = Mount Lyndhurst, NY = North Yankaninna, SY = South Yankaninna, VGR = Vulkathunha-Gammon Ranges.

The measured syn-glacial successions unconformably overlie Tonian rocks and represent the true stratigraphic thicknesses throughout the region. The syn-glacial interval in the Vulkathunha-Gammon Ranges is divided into the 413 m thick Fitton Formation and 424 m thick Bolla Bollana Tillite, which is composed of coarse-grained lithofacies, including diamictites with sandy and conglomeratic interbeds. In the south-central part of the basin, North Yankaninna (38 m) and South Yankaninna (256 m) sections are characterised by diamictites with mudstone and siltstone interbeds. At the Mount Lyndhurst section, towards the north-east, the equivalent Merinjina Tillite is incredibly thin (~5 m), and records only diamictite lithofacies. On the western margin, the Bolla Bollana Tillite thins towards the south from 324 m at Termination Hill, through 126 m at North Copley to 112 m at South Copley. These sections are represented by diamictites with thin siltstone, sandstone and conglomerate interbeds. The overlying Wilyerpa Formation consists of interbedded shale, siltstone and sandstone with frequent dropstones, and demonstrates the same pinching geometry to the south, from 57 m at Termination Hill, to 52 m at North Copley, to 44 m at South Copley.

The post-glacial intervals are lithologically consistent across the basin, recording deposition of fine clastic and carbonate lithofacies. A cap carbonate is exposed in the Termination Hill, Mount Lyndhurst and North Yankaninna sections. Conversely, the North Copley, South Copley, South Yankaninna and Vulkathunha-Gammon Ranges sections do not appear to have a cap carbonate but instead are clastic-dominated at the base of the post-glacial succession. This shale-dominated interval represents the Tindelpina Shale Member of the Tapley Hill Formation. The measured sections only capture the base of Tapley Hill Formation (between 30m and 400 m thick), while the entirety of this formation can reach stratigraphic thicknesses over 2000 m in the northern Flinders Ranges (Preiss, 1987).

4.5.2 Lithofacies Descriptions

Eleven clastic and seven carbonate facies were classified resulting in a total of 18 lithofacies (Table 1). The pre-glacial successions encompass a mix of both clastic and carbonate lithologies, while the syn-glacial successions comprise exclusively clastic lithofacies. The post-glacial sequences characterise a shift to interbedded clastic and carbonate lithologies. Three carbonate platform and three glaciomarine facies associations were interpreted (Table 2). Photographic excerpts from each facies association are presented in Figures 3 – 8, detailing the key lithofacies and sedimentary structures. Depositional processes within facies associations were used to identify eleven specific depositional environments throughout the section (Table 2; see also Supplementary Figures).

4.5.2.1 Inner platform

Inner platform deposits are characterised by mixed siliciclastic and carbonate lithologies, including laminated siltstone (LF2), laminated sandstone (LF5), laminated dolostone (LF12), cross-stratified dolostone (LF13), massive dolostone (LF14), and layered microbialites (LF15). There are also minor cross-stratified siltstone (LF3), heterolithic strata (LF4), cross-stratified sandstone (LF6), massive sandstone (LF7), micritic magnesite (LF17), and conglomeratic magnesite (LF18). Laminated beds are planar to wavy and range from millimetre- to centi-metre-scale thicknesses. Shrinkage cracks are commonly recognised on bedding surfaces for both clastic and carbonate lithofacies, represented by partially connected branches, polygons (Figure 3a), branching spindles, and sinuous and curlicue cracks in ripple troughs (Figure 3b). Rippled beds are represented by straight-crested symmetrical (Figure 3b) and interference ripples while cross-stratified beds are represented by small (1 cm to 15 cm foresets) hummocky swaley cross-laminations, large (40 cm foresets) tabular cross-stratification, supercritical (60° climb angle) climbing ripples, and unimodal and bimodal ripple cross-laminations with rare reactivation surfaces and mud drapes. Heterolithic strata are marked by flaser, wavy and lenticular bedding that deposited bidirectional and unidirectional ripples (Figure 3c). Many carbonate lithofacies present tepee structures (Figure 3d; 1 cm to 10 cm) that occasionally comprise brecciated material and chert replacement in the space under tepee crests. Microbialite lithofacies are characterised by thin (mm- to cm-scale) stratiform and undulating laminations with rare pseudocolumnar structures. Intraformational conglomeratic magnesite beds (Figure 3e) are frequently graded (inverse and normal). Some of these beds show undulating top surfaces. Further, these inner platform lithofacies are also characterised by rare

scour and graded fill structures with intraclasts, and soft sediment deformation structures expressed as convolute bedding, simple load casts and flame structures.

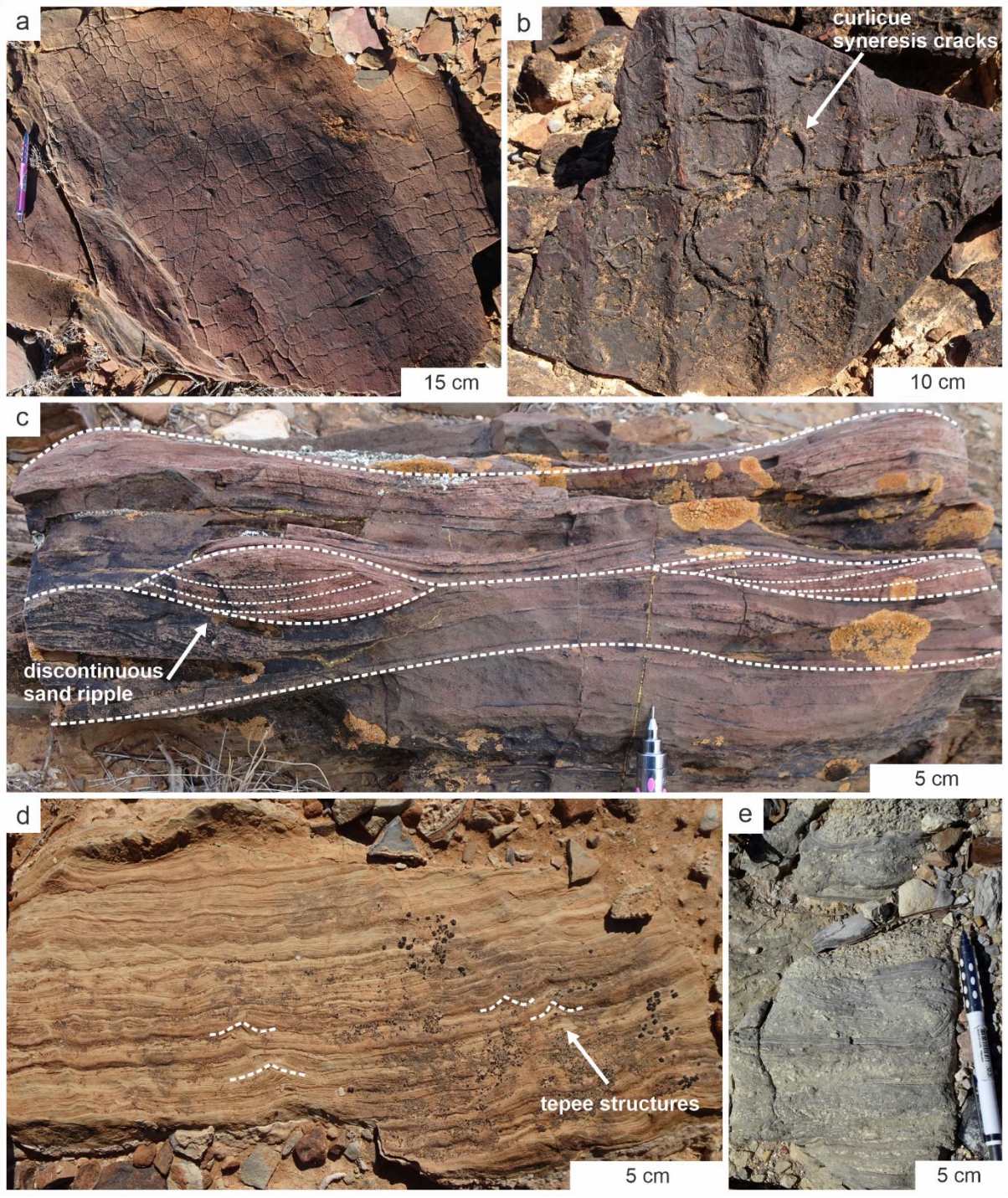

Figure 3: Key lithofacies and sedimentary structures in inner platform setting. (a) Laminated siltstone, LF2. Polygonal shrinkage cracks on bedding surface. North Copley section. (b) Rippled dolostone, LF13. Bedding surface with curlicue shrinkage cracks deposited in troughs of straight ripple sets. North Copley section. (c) Heterolithic siltstone and sandstone, LF4. Lenticular bedding with discontinuous and continuous sandstone ripples. South Yankaninna section. (d) Layered microbialite, LF15. Undulating dolomite and mudstone laminations with tepee structures. Mount Lyndhurst section. (e) Intraclastic magnesite and laminated dolostone, LF18 and LF12. Crudely (convolute) interbedded carbonate layers. South Copley section.

Table 1: Lithofacies and their subsequent characteristics and depositional processes and occurrence throughout the measured section. LF = lithofacies. *SC* = South Copley, *NC* = North Copley, *TH* = Termination Hill, *ML* = Mount Lyndhurst, *NY* = North Yankaninna, *SY* = South Yankaninna, V*GR* = Vulkathunha-Gammon Ranges

Lithofacies	**Descriptions**	**Depositional Processes**	**Occurrence**
LF1 Laminated mudstone	Fresh medium grey to dark brown/blue; weathered red, pink, purple, blue green and white; planar and wavy laminated (mm to cm scale); occasional inverse grading, mud to very fine silty mud; occasionally dolomitic (SY, VGR); rare crude laminations (mm scale) to massive (*SC, SY*); rare dropstones (gravel to cobble clasts), soft sediment deformation (convolute, simple load cast and flame structures), subcritical (15° climb) climbing ripples (~20 cm stoss, 5 cm foresets) (*SC*)	Fine grained material - settled out of suspension, lower flow regime, slow sedimentation rate (Boggs, 2014; Yawar & Schieber, 2017); ice-rafted debris - transported in floating ice and deposited as rainout (e.g. Link & Gostin, 1981; Young & Gostin, 1988; 1991; Powell, 2002; Eyles et al., 2007; Preiss et al., 2011; Boggs, 2014; Le Heron et al., 2013; 2014; 2021; Le Heron & Busfield, 2016); soft sediment deformation - liquefaction induced from rapid sedimentation (Postma, 1983; Stromberg & Bluck, 1998; Moretti et al., 2001); convolute laminations - bottom current reworking (Shanmugam, 1997), earthquakes (Shanmugam, 2017), or submarine slumping (Stow & Mayall, 2000; Stracchan, 2008); simple load casts and flame structures - formed in response to differential sediment densities or lateral loading during liquefaction (Owen, 2003); subcritical climbing ripples - deceleration of turbulent current activity and net deposition (high sediment supply and rapid sedimentation rate), stoss-side erosion and bedform migration (Ashley et al., 1982; Young & Gostin, 1988; Baas et al., 2000; Jobe et al., 2012; Boggs, 2014; Le Heron & Busfield, 2016; Maciaszek et al., 2019)	*SC, NY, SY, VGR*
LF2 Laminated siltstone	Fresh light grey/blue/purple to dark brown; weathered white, yellow, orange, pink, red; planar and wavy laminated (mm to cm scale); occasionally crude planar laminated (mm scale) and massive; occasional normal and inverse grading, silt to very fine sandy silt; occasionally dolomitic; soft sediment deformation (convolute, load and fold and drag structures) (*SC, VGR*); rare gravel lags in base of bed (*SC*); rare shrinkage cracks, connected branches and polygons (*NC*); debrite breccia, randomly orientated angular boulder clasts of well-laminated silt	Fine grained material – *same as LF1*; soft sediment deformation – *same as LF1*; gravel lag - winnowing unidirectional flows, high sediment supply and rapid deposition (Boggs, 2014); connected branches and polygons - subaqueous shrinkage of cohesive sediment caused by compaction during burial, filled with overlying coarse sediment (Plummer & Gostin, 1981; Tanner, 1998; Pfluger, 1999; McMahon et al., 2016); breccia – gravitational debris flow (Thomson et al., 2014; Wallace et al., 2015; Thorie et al., 2020)	All sections

LF3 Rippled and cross-stratified siltstone	Light grey/purple to green; very fine silt; thin laminations (mm to cm scale), occasionally black minerals (VGR); occasionally dolomitic (*NC, SY, VGR*); concave-down (hummock) and concave-up (swale) ripple cross laminations (1 cm to 15 cm scale foresets), cross sets marked by curved erosional surfaces, occasionally bimodal (*SY*); occasional reactivation surfaces (*SY, VGR*) and mud drapes (*SY*); rare supercritical (60° climb) climbing ripples (~3 cm stoss, 5 cm foresets) (*NC*); rare straight crested symmetrical ripples (cm scale wavelengths) (*VGR*), and shrinkage cracks, connected branches and polygons (*NC*), and branching spindles (*VGR*)	Hummocky and swaley cross stratification - suspended load, decreasing flow regime (storm activity), waning combined unidirectional and oscillatory flow (Nottvedt & Kreisa, 1987; Arnott & Southard, 1990; Cheel, 1991; Duke et al., 1991; Cheel & Leckie, 1993; Dumas & Arnott, 2006; Reading, 2009; Basilici et al., 2012; Boggs, 2014); bimodal ripple cross lamination – lower flow regime, unidirectional tidal flow, downcurrent migration of small sinuous and catenary ripples (Ashley, 1990; Colquhoun, 1995; Chakrabarti, 2005; Reading, 2009; Daidu, 2013; Davis, 2013; Boggs, 2014; Thomson et al., 2014; Momta et al., 2015; Jorissen et al., 2018); reactivation surfaces – foreset erosion due to changing flow conditions (Mowbray & Visser, 1984; Daidu, 2013; Davis, 2013); mud drapes - settle out of suspension during slackwater (Reineck & Wunderlich, 1968; Bhattacharya, 1997; Daidu, 2013; Davis, 2013; Boggs, 2014); supercritical climbing ripples – *same as LF1*, stoss-side preservation, increasing rate of suspension sedimentation and decreasing bedform migration (Jobe et al., 2012); symmetrical ripples - traction transport as bedload, lower flow regime, oscillatory flow (Reading, 2009; Boggs, 2014; Counts et al., 2016); connected branches and polygons - desiccation during exposure (Plummer & Gostin, 1981; Boggs, 2014); branching spindles – *same as LF2* (Donovan & Foster, 1972)	*SC, NC, ML, SY, VGR*
LF4 Heterolithic siltstone and sandstone	Fresh light grey/yellow/brown; weathered white, orange, purple to dark brown/red/black; feldspathic and quartzitic; normal and inverse grading, silt and fine sand; bifurcated wavy connected and disconnected mud flasers, mm thickness (flaser bedding), concavely and convexly bowed, fill sand ripple troughs and overlie sand ripple crests (*CQ*), both curve crested current ripples and bidirectional ripples (*SY*); mud layer drapes complete sand ripples (wavy bedding) (*SY, VGR*); mud layer drapes discontinuous and continuous bidirectional sand ripples, cm thickness (lenticular bedding) (*VGR*); mud layer drapes connected	Bedload and suspended load, alternating high and low energy flows, rippled sand deposited from energetic turbulent flow, mud drapes settle out of suspension during slackwater (Reineck & Wunderlich, 1968; Bhattacharya, 1997; Daidu, 2013; Davis, 2013; Boggs, 2014; Maciaszek et al., 2019); flaser bedding – highest energy flows, unidirectional and bidirectional (tidal and wave currents); wavy bedding – moderate energy flows, unidirectional (tidal current); lenticular bedding – lowest energy flows, bidirectional and unidirectional (tidal and wave currents); partially connected branches and polygons – *same as LF3*	*SY, VGR*

	unidirectional sand ripples, up to 3 cm thickness (*SY*); rare shrinkage cracks, partially connected branches and rectangular to hexagonal polygons, multiple generations (*SY, VGR*)		
LF5 Laminated sandstone	Fresh light grey/yellow/brown; weathered white, orange, green, purple to dark brown/red/black; feldspathic and quartzitic; normal and inverse grading, very fine to fine sand; planar and wavy laminated (mm to cm scale), occasional thin black laminations (*NC*); occasional crude laminations to massive; rare small (5 cm to 15 cm scale) scour and fill structure (*SY, VGR*); rare dropstones (pebble to boulder clasts) (*SY, VGR*); soft sediment deformation (convolute, simple load cast structures) (*VGR*); rare gravel lags in base (*VGR*); rare shrinkage cracks, partially connected branches (*VGR*)	Planar laminated - traction transport as bedload, upper flow regime, unidirectional laminar flow (Cheel, 1990; Bridge, 2009; Boggs, 2014; Jorissen et al., 2018); wavy laminations - bedload and suspended load, lower flow regime, unidirectional flow (Colquhoun, 1995; Bridge, 2009; Boggs, 2014; Momta et al., 2015; Jorissen et al., 2018); scour and fill structure - erosion from high velocity flow, filled by coarse material during waning stage of flow (Fielding, 2006; Bridge, 2009; Boggs, 2014); ice-rafted debris – *same as LF1*; soft sediment deformation – *same as LF1*; gravel lags - *same as LF2*; partially connected branches - *same as LF3*	All sections
LF6 Rippled and cross-stratified sandstone	Light grey/yellow/orange/brown to dark brown; weathered white, orange, purple to dark brown/red; feldspathic and quartzitic; normal and inverse grading, very fine to coarse sand; occasional thin black laminations (*NC, SY, VGR*); concave-down (hummock) and concave-up (swale) ripple cross laminations (10 cm foresets), cross sets marked by curved erosional surfaces, occasional mud drapes on foresets (10 cm foresets) (*NC, SC, VGR*); occasional small trough cross stratification (cm scale foresets), occasionally bimodal (*NC, SY, VGR*); occasional sand lenses (cm scale), rare tabular cross stratified (40 cm foresets) (*VGR*); rare symmetrical rippled (~10 cm scale wavelengths) and shrinkage cracks (*SY, VGR*); rare interference rippled (cm scale wavelengths), symmetrical and asymmetrical (*SC*)	Hummocky and swaley cross stratification – *same as LF3*; ripple cross lamination and mud drapes – *same as LF3*; trough - bedload and suspended load, lower flow regime, unidirectional flow, downcurrent migration of small scale ripples (Ashley, 1990; Bridge, 2009; Boggs, 2014; Momta et al., 2015); tabular - traction transport as bedload, lower flow regime, unidirectional flow, downcurrent migration of straight crested dunes (Ashley, 1990; Bridge, 2009; Boggs, 2014; Momta et al., 2015); symmetrical ripples – *same as LF3*; straight to bifurcating and terminating crests - decreasing flow velocities (Nelson & Voulgaris, 2014); interference ripples - lower flow regime, bidirectional and unidirectional flow (Colquhoun, 1995; Bridge, 2009; Boggs, 2014; Momta et al., 2015; Jorissen et al., 2018), two sets of current directions intersecting at high angles (Gough, 2020)	*SC, NC, SY, VGR*
LF7 Massive sandstone	Light grey/yellow/brown/blue to dark red; quartzitic; occasionally immature, lithics, angular to sub-rounded, fine sand to gravel; massive; occasional thin planar and wavy laminations; rare normal and inverse grading, very fine to coarse sand; rare scoured base (*SC*); rare thin, heavy	Hyperconcentrated debris flows, rapid deposition; normal grading – high density turbidity current (Lowe, 1982; Kneller, 1995; Shanmugam, 2000; Winsemann et al., 2009; Talling et al., 2012; Le Heron & Busfield, 2016), inverse grading – kinetic sieving (Legros, 2002; Talling et al., 2012; Le Heron et	*SC, NC, TH, NY, SY, VGR*

	mineral trough cross-laminations (*SC*); rarely dolomitic with silty matrix (*TH*)	al., 2014); scoured base – same as LF5; cross-laminations – *same as LF3* OR low density turbidity current (Shanmugam, 1997; Talling et al., 2012)	
LF8 Ortho-conglomerate	Fresh light grey/brown/grey/green/blue, weathered dark grey/blue/black; clast supported (50% to 80% clasts); very coarse sand to cobble clasts (sub-angular to well-rounded), granite/quartzite/carbonate boulders, quartzite cobbles, carbonate pebbles; medium to coarse sand matrix; massive, inverse and normal grading; occasionally interlaminated or interbedded with silt (*SY, NY*); occasionally pierces top surface (*SC*); rare scoured base (*SY*)	Subaqueous hyperconcentrated debris flows, rapid deposition, non-cohesive, laminar flows (Lowe, 1982; Kneller, 1995; Shanmugam, 2000; Winsemann et al., 2009; Talling et al., 2012; Le Heron & Busfield, 2016); scoured base – *same as LF5*	*SC, NC, NY, SY, VGR*
LF9 Stratified diamictite	Light blue/purple/green/brown/red; thin (cm scale) planar laminations; silt to fine sand matrix; often clast-poor (<15% clasts); quartzite/carbonate/conglomerate boulder, quartzite/carbonate/basaltic cobbles and quartzite/sand gravel, casts; occasionally clast-rich (30-60% clasts), granite/quartzite boulders/cobbles, carbonate pebbles and sand pebbles/cobbles, casts (*SC, NY, VGR*); rare inverse and normal grading (SC, *VGR*); rare scoured base (*NY, SY*); rarely carbonaceous (*TH*)	Subaqueous sediment gravity flow (Young & Gostin, 1988; Anderson, 1989; Eyles et al., 2007; Le Heron et al., 2013; 2014); stratification - sorting through clast settling (Anderson, 1989) OR current reworking (Boggs, 2014); scoured base – *same as LF7*	*SC, TH, NY, SY, VGR*
LF10 Massive diamictite	Light grey/green/yellow/brown/red; matrix to clast supported (<5% - 60% clasts); quartzite/granite/carbonate/sandstone boulders (up to 1.5 m), quartzite/carbonate/sandstone/granite cobbles/pebbles, conglomerate fragments, and casts; mud to fine sand matrix; inverse and normal grading; occasionally dolomitic (*VGR, TH*)	Slow deposition directly from the ice as melt-out (Link & Gostin, 1981; Young & Gostin, 1988; Preiss et al., 2011) OR cohesive debris flows, moderate to high strength (Talling et al., 2012); rapid deposition (Young & Gostin, 1988; Anderson, 1989; Eyles et al., 2007; Le Heron et al., 2013; 2014), kinetic sieving during flows (Legros, 2002; Talling et al., 2012; Le Heron et al., 2014)	All sections
LF11 Massive dolostone	Fresh brown/blue/grey, weathered white/yellow/pink/red; elephant skin weathering style; occasional laminated weathering style (NC, *TH, SY*); rarely ferruginous (*SY*); rare shrinkage cracks, multiple generations (*NC*)	Authigenic precipitation from the water column, due to chemical, salinity or temperature fluctuations (Tucker, 1982; Tucker & Wright, 2009; Flugel, 2013) OR syn-sedimentary dolotimisation (mimetic replacement), carbonates retain primary textures and water column geochemical signatures (Hood et al., 2011; 2018; Hood & Wallace, 2012; 2014; Shuster et al., 2018); shrinkage cracks – *same as LF3*	*SC, NC, TH, SY, VGR*

LF12 Laminated dolostone	Fresh light yellow/brown/blue/grey, weathered white/yellow/orange/pink/red; fine crystalline texture; elephant skin weathering style; normal and inverse grading, thinly (mm to cm scale) planar laminated with fine (mud to silt) clastic material; occasionally wavy laminated and massive; small (cm scale) tepee structures, chert and breccia fills space under tepee crests (*SC, VGR*); rare thin black laminations (*VGR*); occasional soft sediment deformation (convolute structures) (*VGR*)	Dolostone material – *same as LF11* OR secondary diagenetic recrystallisation (non-mimetic replacement), poorly preserves original carbonate textures (Tucker & Wright, 2009; Flugel, 2013); interlaminated clastic material - transported as suspended load, low energy tidal currents (O'Connell et al., 2020) or higher energy storm activity (Hoffman, 1976; Wanless et al., 1988; Tucker & Wright, 2009; Jahnert & Collins, 2012; Chiarella et al., 2017; Kunzmann et al., 2019; O'Connell et al., 2020); tepee structures - fracturing/crustal cracking, periods of desiccation (Asserto & Kendall, 1977; Kendall & Warren, 1987; Belperio, 1990; Frank & Fielding, 2003; Tucker & Wright, 2009; O'Connell et al., 2020); soft sediment deformation – *same as LF1*	All sections
LF13 Rippled and cross stratified dolostone	Grey/blue/black, weathered white/yellow/brown; thinly wavy laminated; fine crystalline texture; elephant skin weathering style; occasional dolostone layer drapes discontinuous and complete unidirectional sand ripples, cm thickness (lenticular and wavy bedding) (*SY, VGR*); rare large (8 cm wavelength, 3 cm height) (*NY*) and small (3 cm wavelength, 1 cm height) (*NC*) symmetrical ripples; rare ripple cross-laminations (5 cm foresets), obliquely stacked in opposing directions (*NC, SC,* ML); rare soft sediment deformation (convolute and buckled structures) (*VGR*); shrinkage cracks, partially connected branches (*SY*) and polygons (*NC*); shrinkage cracks, sinuous and curlicue cracks deposited in troughs of straight ripple sets (*NC, VGR*)	Dolostone material – *same as LF11 and LF12*; heterolithic stratification – *same as LF4*; symmetrical ripples – *same as LF3*; ripple cross-laminations – *same as LF3*; soft sediment deformation – *same as LF1*; partially connected branches and polygons – *same as LF3*; sinuous and curlicue cracks – *same as LF2* (Gehling, 2000)	*SC, NC, ML, SY, VGR*
LF14 Massive dolostone	Fresh light blue/grey, weathered white/yellow/purple; crystalline texture; normal and inverse grading, fine to very coarsely crystalline; occasional thin (cm) planar laminated weathering style (*SC, NC, ML*); occasional faint wavy laminations (*VGR*); occasionally quartz rich and brecciated (*VGR*); rare concretions (nodular anhydrite?) (*VGR*); rare shrinkage cracks (*NC*)	Dolostone material – *same as LF12*; interlaminated clastic material – *same as LF12*; shrinkage cracks – *same as LF2*	*SC, NC, TH, ML, SY, VGR*

LF15 Layered microbialite	Fresh light blue/grey/yellow, weathered white; thin (mm to cm scale) stratiform and undulating dolomite laminations, interlaminated mud; rare thin black laminations (*SY*); occasional (1 cm to 10 cm scale) tepee structures (*SY, TH, ML, VGR*), brecciated material and chert replacement fills space under tepee crests (*SC*); occasional soft sediment deformation (convolute) (*VGR*), small (1 cm) load and flame structures (*SC*); occasional ripple cross-stratified and buckled (*SY, ML*); rare pseudocolumnar structures (*SC*); rare inverse grading, very finely to medium crystalline (*SC, SY*)	Microbial material - precipitated in-situ (authigenic) (Tucker, 1982; Tucker & Wright, 2009; Flugel, 2013); clastic material - trapped and bound by microbial material (Wright, 1984; Tucker & Wright, 2009; O'Connell et al., 2020); stratiform microbialite - suspended load, low flow regime, gentle current action (Hoffman, 1976; Wanless et al., 1988; Tucker & Wright, 2009; Jahnert & Collins, 2012; Chiarella et al., 2017; Kunzmann et al., 2019 O'Connell et al., 2020); small tepee structures – *same as LF12*; large tepee structures - crystallisation expansion in carbonate-supersaturated subaqueous conditions (Shinn, 1969; Kendall & Warren, 1987; O'Connell et al., 2020); soft sediment deformation – *same as LF1*; ripple cross-laminations – *same as LF3*	All sections
LF16 Microbialite buildup	Fresh light blue/grey to white/yellow; thin (cm scale) columnar and domical dolomite laminations, interlaminated (mud to silt) clastic material; hemispherical (*SC, NC, ML*), bulbous (ML) and nodular (SC, *NC, TH, ML*) domical buildup, cm scale; occasional domical and columnar bioherms (*SC*); rare columnar buildup, cm scale (*SC*); rare convex conical buildup (*SC, ML*), cm scale; rare brecciated material and chert replacement in domical buildups (*SC*); rarely mottled (*SC, NC*); rare inverse grading, very finely to medium crystalline (*SC*)	Microbial material – *same as LF15*; clastic material – *same as LF15*; microbialite buildup - suspended load, higher energy storm activity (Hoffman, 1976; Wanless et al., 1988; Tucker & Wright, 2009; Jahnert & Collins, 2012; Chiarella et al., 2017; Kunzmann et al., 2019 O'Connell et al., 2020)	*SC, NC, ML*
LF17 Magnesite mudstone	Light grey/cream to white; micritic; massive to laminated (cm scale); rare small (cm scale) tepee structures (*SC*); rare soft sediment deformation (convolute) (*TH*)	Magnesite material - precipitated in-situ, evaporative magnesium-rich water column (Mur & Urpinell, 1987; Warren, 1990; Melezhik et al., 2001); small tepee – *same as LF12*; soft sediment deformation – *same as LF1*	*SC, TH*
LF18 Intraclastic magnesite	Light grey/cream to white; massive to crudely laminated (cm scale); occasionally conglomerate (clast-rich), sub-angular to rounded clasts, mud to sand sized matrix; normal and inverse grading, gravel to very coarse-grained; rare undulating top surfaces and soft sediment deformation (convolute) (*SC*)	Magnesite material – *same as LF17*; conglomerate - reworked sedimentary magnesite (Uppill, 1980; Belperio, 1990; Preiss, 2000; Frank & Fielding, 2003; Counts, 2017); soft sediment deformation – *same as LF1*	*SC, TH*

Table 2: Facies associations and their constituent lithofacies and depositional environments. LF = lithofacies.

Facies Association	Constituent lithofacies	Depositional Environment
Carbonate Platform		
A – Inner platform	Major: LF2, LF5, LF12, LF13, LF14, LF15 Minor: LF3, LF4, LF6, LF7, LF17, LF18	A1 – Supratidal to intertidal A2 – Intertidal to subtidal
B – Outer platform	Major: LF2, LF12, LF16 Minor: LF1, LF5, LF13, LF14, LF15	B1 – Shallow subtidal B2 – Platform margin reef
C – Slope to basin	Major: LF1, LF2, LF12, LF13 Minor: LF3, LF11, LF14	C1 – Slope C2 – Basin
Glaciomarine		
D – Ice-margin	Major: LF10 Minor: LF9	D1 – Terrestrial to grounding zone D2 – Proximal subaqueous
E – Proximal proglacial	Major: LF2, LF5, LF6, LF7, LF10 Minor: LF3, LF8, LF9	E1 – Subaqueous glacial outwash E2 – Subaqueous channel
F – Distal proglacial	Major: LF1, LF2, LF14 Minor: LF5, LF6, LF7, LF8, LF9, LF10, LF12	F1 – Subaqueous fan

4.5.2.2 Outer platform

Laminated siltstone (LF2), laminated dolostone (LF12) and microbialite buildup (LF16) dominate the outer platform facies association. Minor lithofacies include laminated mudstone (LF1), laminated sandstone (LF5), cross-stratified dolostone (LF13), massive dolostone (LF14) and layered microbialite (LF15). The frequent thinly (mm to cm thick) laminated lithofacies are commonly planar with minor wavy laminae (Figure 4a), forming both inverse and normally graded beds. Occasionally, these beds contain soft sediment deformation (convolute) structures (Figure 4b). Microbialite lithofacies are frequently represented by domical (hemispherical, bulbous, nodular) buildups (Figure 4c), domical and columnar bioherms (Figure 4d), with rare columnar and conical (convex) buildups (Figure 4e and 4f). These beds, as well as massive dolostone successions, are commonly inverse graded, coarsening from a fine to coarse crystalline texture.

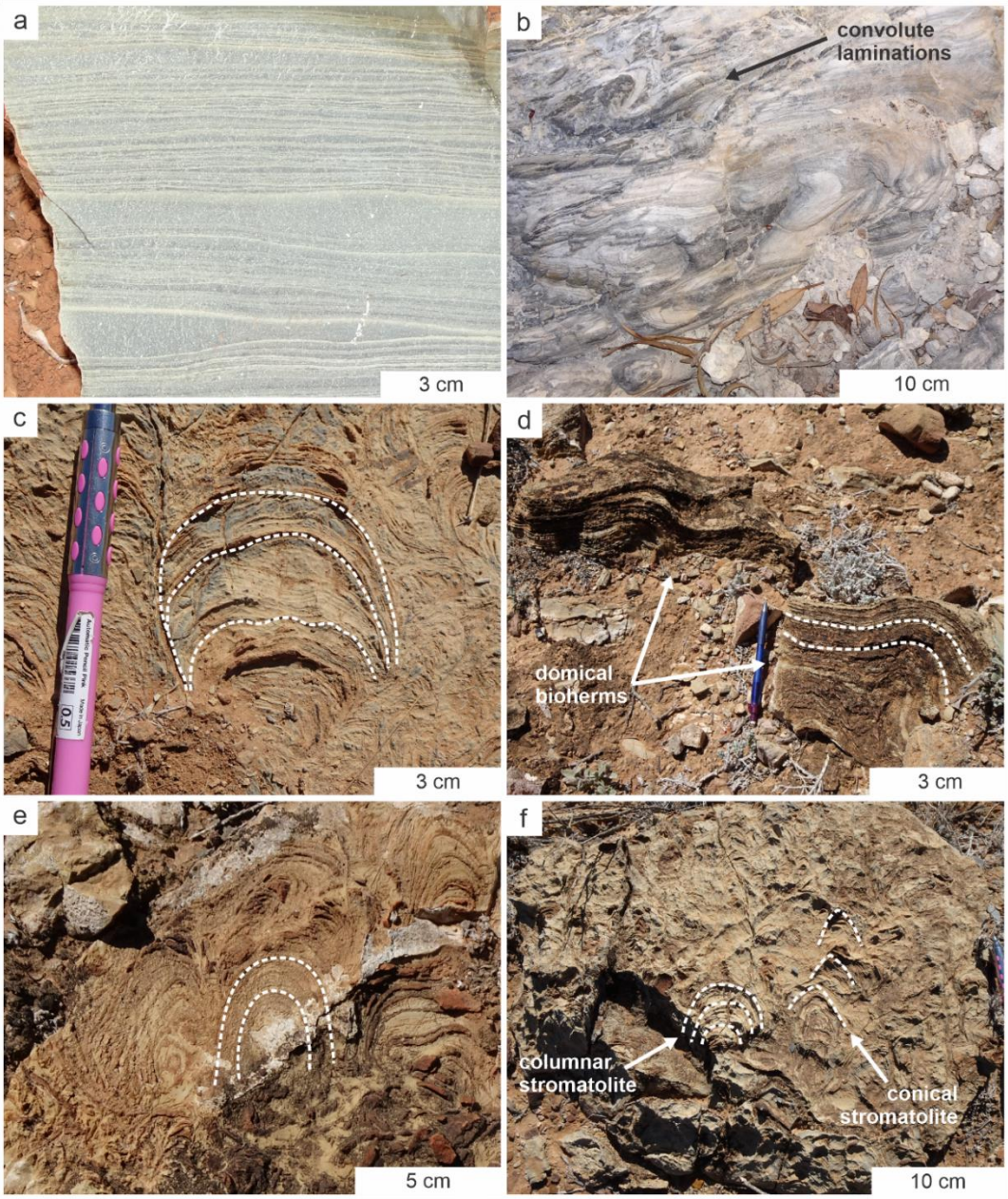

Figure 4: Key lithofacies and sedimentary structures in outer platform setting. (a) Laminated siltstone, LF2. Very thinly (mm scale) planar laminated. South Copley section. (b) Laminated siltstone, LF2. Convolute soft sediment deformation. South Copley section. (c) Stromatolitic microbialite, LF16. Domical bioherm. South Copley section. (d) Stromatolitic microbialite, LF16. Hemispherical domical buildup. Mount Lyndhurst section. (e) Stromatolitic microbialite, LF16. Columnar buildup. South Copley section. (f) Stromatolitic microbialite, LF16. Columnar buildup and convex conical buildup. Mount Lyndhurst section.

4.5.2.3 Slope to basin

Slope to basinal successions are mainly composed of laminated mudstone (LF1), siltstone (LF2), dolostone (LF12) and cross-stratified dolostone (LF13). Cross-stratified siltstone (LF3), massive dolostone (LF11) and laminated dolostone (LF14) occur as minor lithofacies. Ripple cross laminations (Figure 5a) and small (15 cm foresets) hummocky swaley cross laminations (Figure 5b) are common in cross-stratified successions. Slope packages are also characterised by convolute beds (Figure 5c) and associated rare breccia beds of randomly oriented, boulder-

sized angular blocks comprising well-laminated rocks (Figure 5d. Fine-grained deposits are massive (Figure 5e) or planar to wavy laminated at millimetre to centimetre scale.

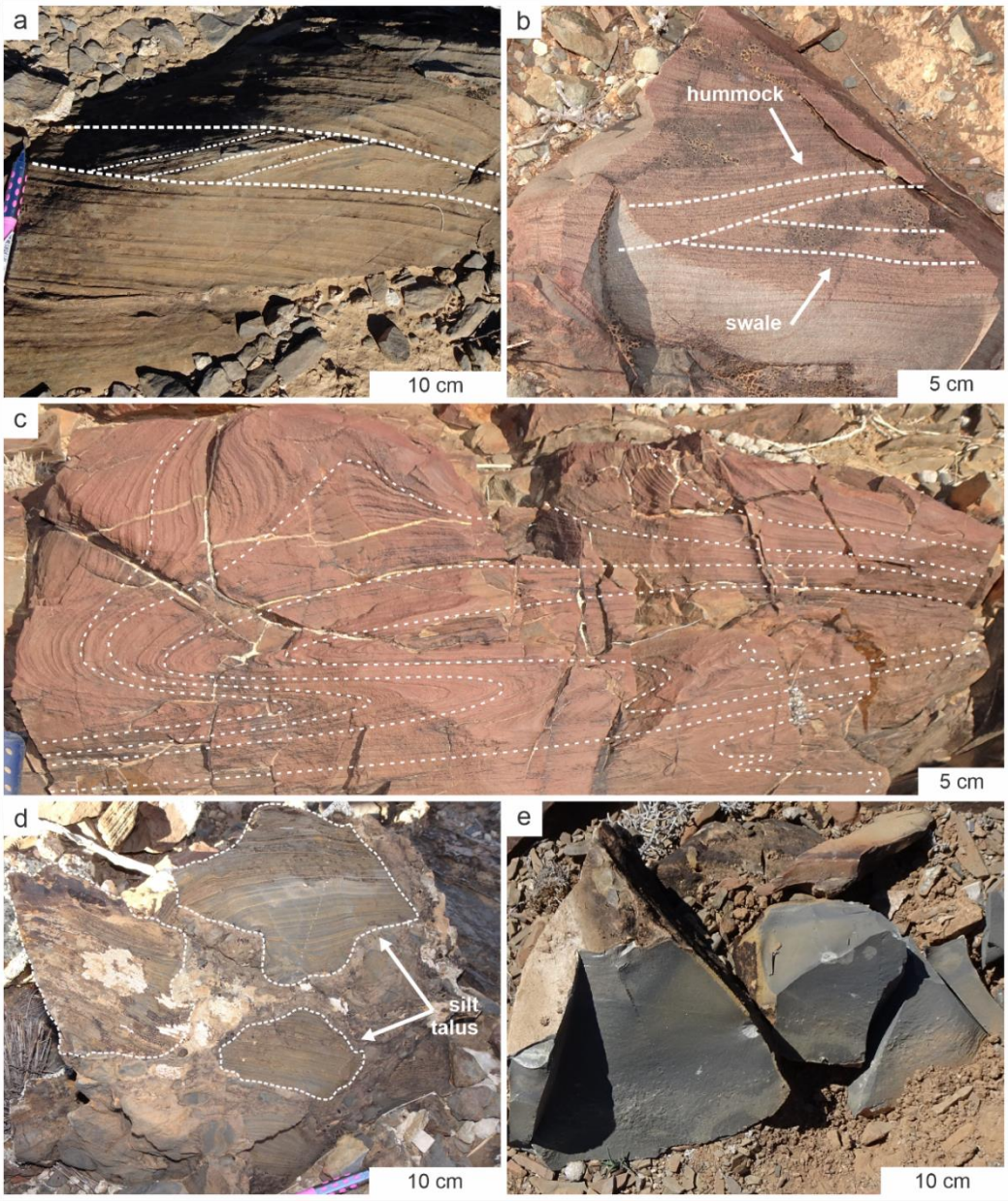

Figure 5: Key lithofacies and sedimentary structures in slope to basin setting. (a) Cross stratified siltstone, LF3. Unidirectional ripple cross lamination. Vulkathunha-Gammon Ranges section. (b) Cross stratified siltstone, LF3. Hummock (concave-down) and swale (concave-up) ripple cross lamination. South Copley section. (c) Laminated siltstone, LF2. Convolute soft sediment deformation. Vulkathunha-Gammon Ranges section. (d) Laminated siltstone, LF2. Debrite breccia with randomly oriented angular boulder clasts of well-laminated siltstone. Vulkathunha-Gammon Ranges section. (e) Massive dolostone, LF11. South Copley section.

4.5.2.4 Ice margin

Massive diamictite (LF10) lithofacies dominate the grounded ice-margin facies association, with minor deposition of stratified diamictite (LF9). Both diamictite lithofacies are inverse and normally graded. The massive diamictites are matrix supported (<5% to 20% clasts), incorporating sub-angular to well-rounded pebble to boulder-sized clasts.

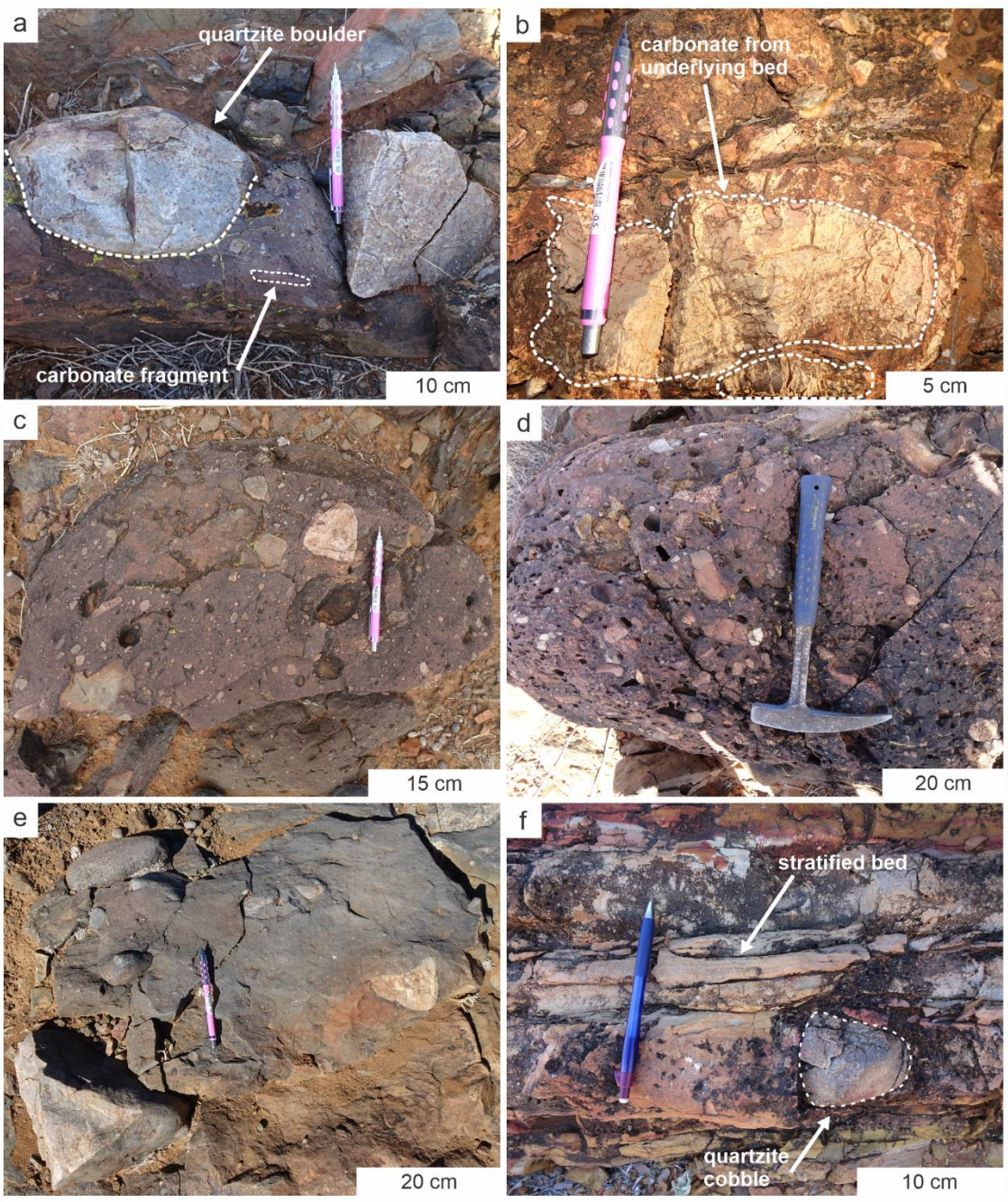

Figure 6: Key lithofacies and sedimentary structures in ice-margin setting. (a) Stratified diamictite, LF9. Clast-poor diamictite with quartzite cobble. South Copley section. (b) Massive diamictite, LF10. Clast-rich diamictite with carbonate cobble from underlying bed. Termination Hill section. (c) Massive diamictite, LF10. Clast-rich diamictite with pebble to cobble sized clasts in mudstone matrix. Vulkathunha-Gammon Ranges section. (d) Massive diamictite, LF10. Clast-rich diamictite with pebble sized clasts in mudstone matrix. South Yankaninna section. (e) Massive diamictite, LF10. Clast-poor diamictite with angular quartzite boulder in mudstone matrix. Vulkathunha-Gammon Ranges section. (f) Massive diamictite, LF10. Clast-rich diamictite with rounded quartzite bounder in mudstone matrix. South Yankaninna section.

These include sandstone, quartzite, carbonate, granite and conglomerate fragments (Figure 6a–e). The matrix is mudstone to fine-grained sandstone and occasionally dolomitic. Stratified diamictite beds are often clast-poor (<15% clasts), comprising gravel to boulder-sized clasts in a siltstone to fine sandstone matrix (Figure 6f).

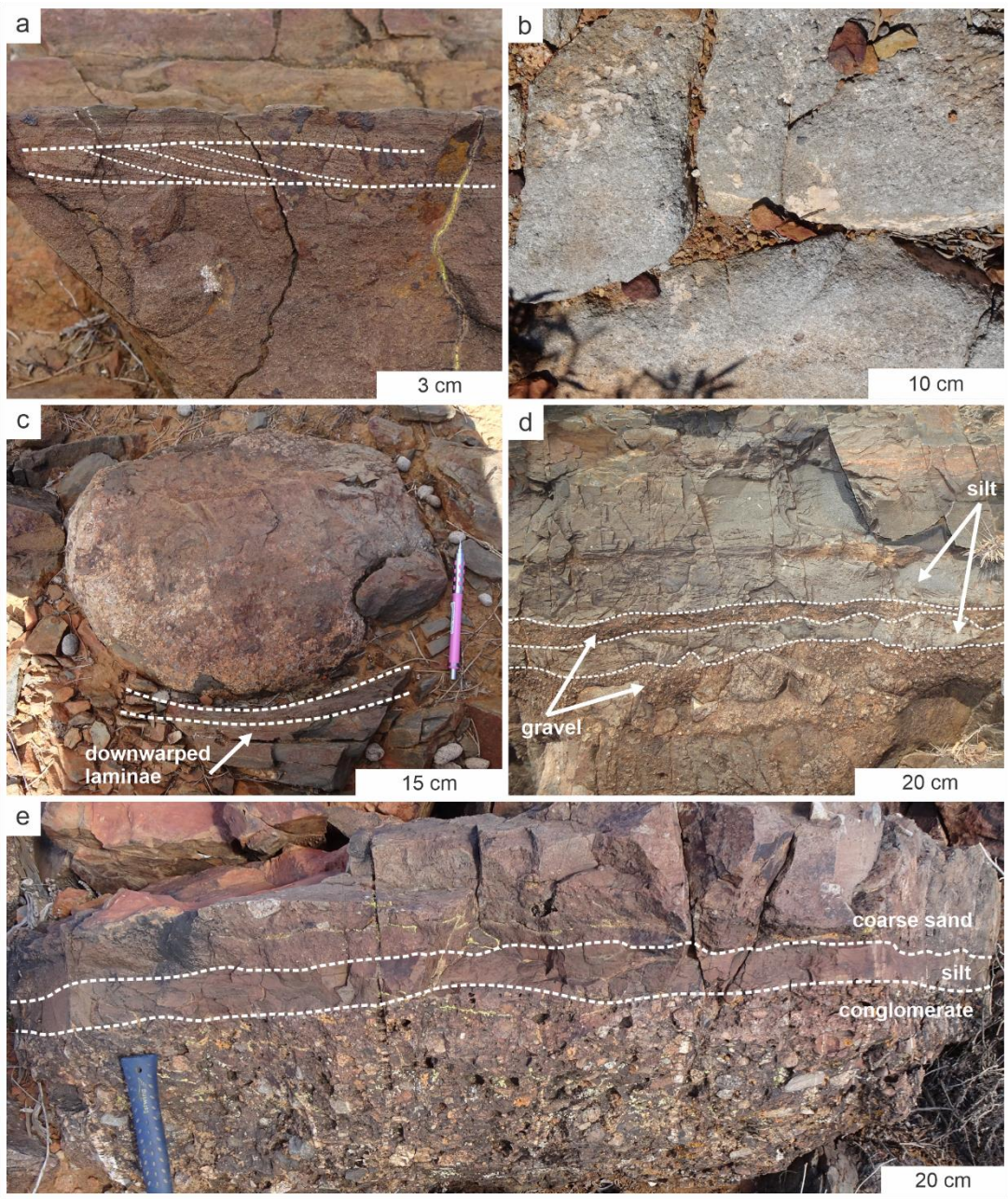

Figure 7: Key lithofacies and sedimentary structures in proximal proglacial setting. (a) Laminated siltstone and orthoconglomerate, LF2 and LF8. Interbedded laminated siltstone with gravel conglomerate with scoured bases. Vulkathunha-Gammon Ranges section. (b) Laminated sandstone, LF5. Rounded boulder dropstone downwarping underlying sandstone laminations. Vulkathunha-Gammon Ranges section. (c) Cross stratified sandstone, LF6. Unidirectional trough cross laminations. Vulkathunha-Gammon Ranges section. (d) Massive sandstone, LF7. Graded bed with angular to sub-rounded clasts. South Copley section. (e) Laminated siltstone and orthoconglomerate, LF2 and LF8. Interbedded massive siltstone with clast-rich conglomerate and coarse sandstone beds. South Yankaninna section.

4.5.2.5 Proximal proglacial

Proximal proglacial deposits are characterised by laminated siltstone (LF2), laminated sandstone (LF5), ripple and cross-stratified sandstone (LF6), massive sandstone (LF7) and massive diamictite (LF10). Minor lithofacies include cross-stratified siltstone, orthoconglomerates (LF8) and stratified diamictites (LF9).

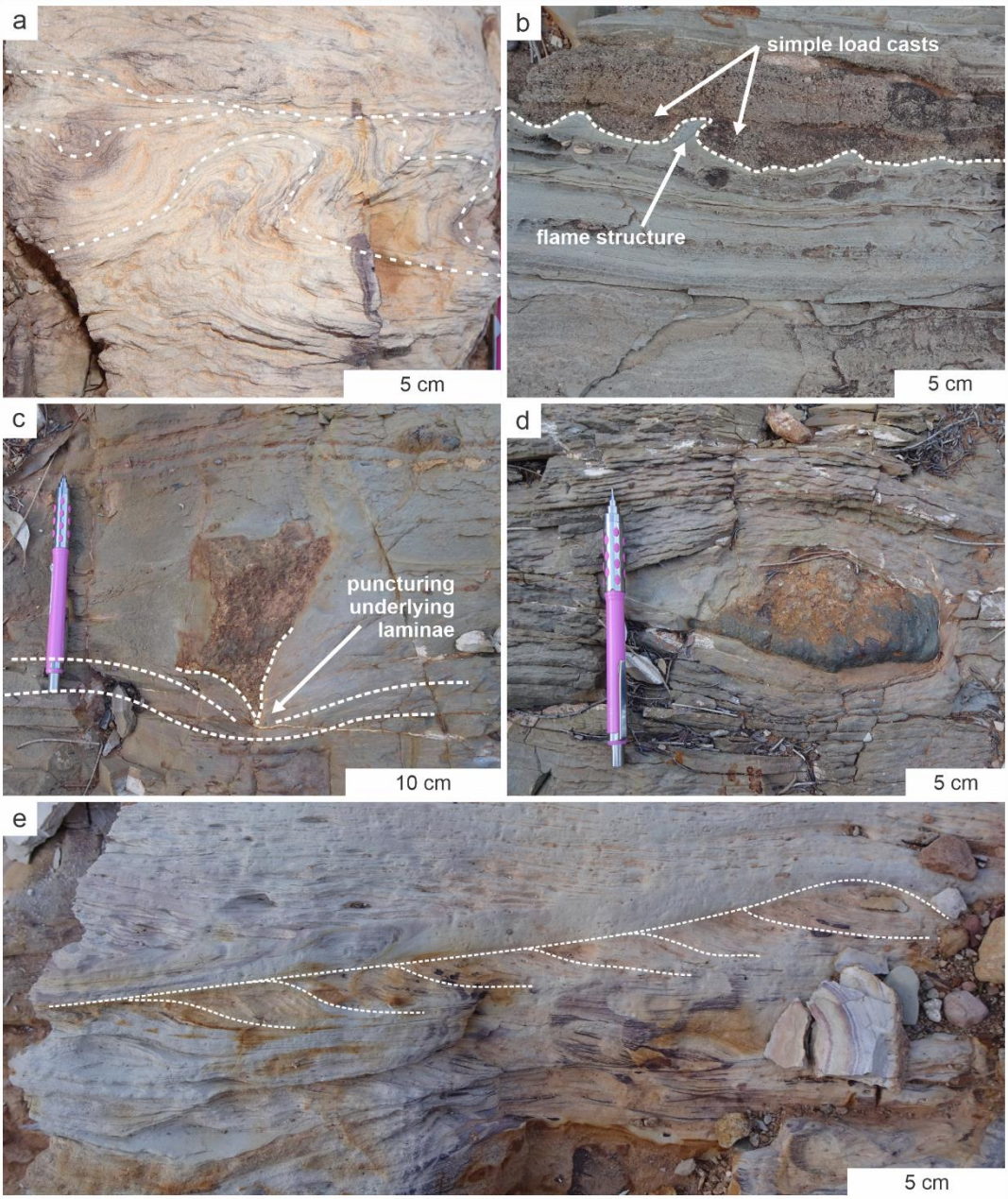

Figure 8: Key lithofacies and sedimentary structures in distal proglacial setting. (a) Laminated mudstone, LF1. Very angular cobble dropstone that punctures and deforms the underlying mudstone laminations. South Copley section. (b) Laminated mudstone, LF1. Sub-rounded dropstone that downwarps the underlying mudstone laminations and is draped by the overlying mudstone laminations. South Copley section. (c) Laminated mudstone, LF1. Subcritical unidirectional climbing ripples. South Copley section. (d) Laminated mudstone and laminated sandstone, LF1 and LF5. Simple load cast and flame structure soft sediment deformation at contact between sandstone and underlying mudstone bed. South Copley section. (e) Laminated mudstone, LF1. Convolute soft sediment deformation. South Copley section.

Unidirectional, small (<5 cm foresets) ripple cross-stratification is representative of the cross-stratified lithofacies (Figure 7a), where foresets are often composed of dark, heavy minerals. Massive sandstone beds are frequently graded (inverse and normal) and immature, characterised by angular to sub-rounded fine sandstone to gravel (Figure 7b). Diamictite lithofacies are marked by frequent clast-poor (<5% to 15%) beds, incorporating sand, quartzite, carbonate and granite gravel to boulder-sized clasts in a siltstone to fine sandstone matrix

(Figure 7c). These diamictite beds occasionally have scoured bases. Clast-supported (40% to 80%) orthoconglomerates comprise medium sandstone to boulder-sized, sub- to well-rounded sand, quartz, carbonate and granite clasts. These orthoconglomerate beds are occasionally thinly interbedded with siltstone (Figure 7d, e), graded (inverse and normal), and/or have scoured bases.

4.5.2.6 Distal proglacial

Fine-grained lithofacies dominate the distal proglacial facies association, including laminated mudstone (LF1), laminated siltstone (LF2) and massive dolostone (LF14). There is a suite of more minor lithofacies, including laminated sandstone (LF5), cross-stratified sandstone (LF6), massive sandstone (LF7), orthoconglomerate (LF8), stratified (LF9) and massive (LF10) diamictite, and laminated dolostone (LF12). A number of fine- and coarse-grained distal proglacial deposits fine-up within beds and in packages. Laminated lithofacies comprise millimetre to centimetre-thick planar and wavy laminations, where mudstone and siltstone are commonly interlaminated. Mudstone beds occasionally contain soft sediment deformation structures, including convolute bedding (Figure 8a), simple load casts and flame structures (Figure 8b). There are also rare dropstones (Figure 8c, d), ranging from sand, quartzite, carbonate and conglomeratic gravel to boulders, and subcritical (15° climb angle) climbing ripples (Figure 8e). Cross-stratified sands are represented by thin, heavy mineral ripple cross-stratifications. Diamictite lithofacies are commonly clast-poor (<20%), with minor laminated successions in siltstone to very fine-sandstone matrices. Rare orthoconglomerate beds, composed of up to 70% very coarse sandstone to cobble clasts, pierce overlying fine-grained beds.

4.6 Discussion

4.6.1 Facies Association A: Inner platform

4.6.1.1 Sedimentary Processes

The presence of minor wave action is evidenced by the deposition of symmetrical ripples, which were likely deposited from lower flow regime oscillatory flows (Reading, 2009; Boggs, 2014; Counts et al., 2016). Small hummocky and swaley cross-laminations provide evidence for combined waning unidirectional and oscillatory flow (Nøttvedt & Kreisa, 1987; Arnott & Southard, 1990; Cheel, 1991; Duke et al., 1991; Cheel & Leckie, 1993; Dumas & Arnott, 2006; Reading, 2009; Basilici et al., 2012; Boggs, 2014). The suite of unidirectional cross-stratified structures represents downcurrent migration of small sinuous and catenary crested ripples and straight crested dunes from low and high-energy flows, respectively (Ashley, 1990; Colquhoun, 1995; Chakrabarti, 2005; Bridge, 2009; Reading, 2009; Daidu, 2013; Boggs, 2014; Thomson et al., 2014; Momta et al., 2015; Jorissen et al., 2018). The presence of bimodal cross-stratified foresets, reactivation surfaces and mud-drapes indicate tidal influence (Ashley, 1990; Colquhoun, 1995; Reading, 2009; Daidu, 2013; Boggs, 2014; Momta et al., 2015). Further, the presence of heterolithic strata deposited as bedload and suspended load during alternating high and low energy flows are also tidally induced structures (Reineck & Wunderlich, 1968; Bhattacharya, 1997; Daidu, 2013; Boggs, 2014; Maciaszek et al., 2019). Microbialite material likely reflects authigenic precipitation and/or capture, where clastic material was transported

under low energy flow regimes, then trapped and bound the microbial layers (Wright, 1984; Tucker & Wright, 2009; O'Connell et al., 2020). This in-situ precipitation could also have been responsible for the accumulation of magnesite mudstone, although developing in more of an evaporative magnesium-rich water column (Mur & Urpinell, 1987; Warren, 1990; Melezhik et al., 2001), and graded, intraformational conglomeratic magnesite beds were likely reworked by secondary current processes (Uppill, 1980; Belperio, 1990; Preiss, 2000; Frank & Fielding, 2003; Counts, 2017). Tepee structures are common in carbonate lithofacies, likely resulting from expansion-related fracturing due to mineral precipitation in peritidal conditions (Asserto & Kendall, 1977; Kendall & Warren, 1987; Belperio, 1990; Frank & Fielding, 2003; Tucker & Wright, 2009; O'Connell et al., 2020). Other desiccation features include branching and polygonal shrinkage cracks (Plummer & Gostin, 1981; Boggs, 2014). However, other branching, polygonal, curlicue, sinuous and spindle cracks were likely developed from subaqueous shrinkage of cohesive sediment caused by compaction during burial (Donovan & Foster, 1972; Plummer & Gostin, 1981; Tanner, 1998; Pflueger, 1999; Gehling, 2000; McMahon et al., 2017).

4.6.1.2 Environmental Interpretations

The mixed carbonate and clastic lithofacies reflect deposition under dominant tidal influence with minor wave energy, and show evidence for evaporative carbonate precipitation and periodic exposure, which is consistent with deposition in an inner carbonate platform (A) setting (Figure 9; e.g., von der Borch & Lock, 1979; Uppill, 1980; Belperio, 1990; Frank and Fielding, 2003). These inner platform deposits can be further classified into packages reflecting deposition in more of a subaerial or subtidal environment based on the presence of desiccation and current features, respectively. Packages composed of magnesite mudstones, tepee structures and desiccation cracks are interpreted to have been deposited in the supratidal to intertidal zone (A1), while units dominated by current reworking, undisturbed laminations and soft-sediment deformation are characteristic of deposition in the intertidal to subtidal zone (A2), (Figure 9; Belperio, 1990; Powers & Holt, 2000; Frank & Fielding, 2003; Thomson et al., 2014; Kunzmann et al., 2019).

4.6.2 Facies Association B: Outer platform

4.6.2.1 Sedimentary Processes

Thinly laminated siltstone and mudstone intervals were likely deposited in the lower flow regime, settling out of suspension with a slow sedimentation rate (Boggs, 2014; Yawar & Schieber, 2017), while planar laminated sandstone beds represent deposition under upper flow regime conditions (Cheel, 1990; Bridge, 2009; Boggs, 2014; Jorissen et al., 2018). Convolute soft sediment deformation structures could have developed from seismic activity (Shanmugam, 2017). Less crystalline dolomitic material in dolostone lithofacies likely preserve primary carbonate textures and therefore reflect authigenic precipitation or syn-sedimentary dolomitisation (mimetic replacement). Conversely, more crystalline lithofacies likely reflect

secondary diagenetic recrystallisation (non-mimetic replacement) that resulted in the destruction of these primary textures (Tucker, 1985; Tucker & Wright, 2009; Flügel, 2010). Planar and cross-stratified interlaminated clastic material was likely transported as suspended load and deposited from low-energy tidal currents (O'Connell et al., 2020) and higher energy storm activity (Hoffman, 1976; Wanless et al., 1988; Tucker & Wright, 2009; Jahnert & Collins, 2012; Chiarella et al., 2017; Kunzmann et al., 2019; O'Connell et al., 2020), respectively. The same mechanisms were likely responsible for microbialite lithofacies, where microbialite buildups, previously identified as *Baicalia burra* (Preiss, 1973; Belperio, 1990), reflect deposition under lower energy conditions (Hoffman, 1976; Tucker & Wright, 2009; Jahnert & Collins, 2012; Kunzmann et al., 2019).

4.6.2.2 Environmental Interpretations

The deposition of both low-energy fine-grained lithofacies, and higher-energy, inverse-graded carbonate lithofacies are consistent with a setting that experiences both quiescent, subtidal conditions and energetic shoaling (Gómez-Pérez et al., 1999; Grotzinger & James, 2000; Pomar, 2001; Chatalov et al., 2015; Wilmsen et al., 2018; Thorie et al., 2020). This facies association is interpreted as an outer platform (B) (Figure 9), and more specifically a shallow subtidal zone (B1) below fair-weather wave base (e.g., Belperio, 1990; Jahnert & Collins, 2012; Milli et al., 2013; Thomson et al., 2014; Wilmsen et al., 2018; Thorie et al., 2020), and a platform margin reef (B2) where there is evidence for stromatolitic buildups (Figure 9; e.g., Gómez- Pérez et al., 1999; Grotzinger & James, 2000; Pomar, 2001; Chatalov et al., 2015; Thorie et al., 2020). The presence of stromatolitic buildup lithofacies (B2) likely corresponds to a high-relief carbonate platform geometry (Grotzinger, 1988; 1990, 2012; Grotzinger & James, 2000), while outer platform deposits with only shallow subtidal zone lithofacies (B1) may characterise ramp style carbonate platforms (Grotzinger, 1989; Grotzinger & James, 2012).

4.6.3 Facies Association C: Slope to basin

4.6.3.1 Sedimentary Processes

Soft sediment deformation structures, in particular convolute bedding and load structures, likely resulted from submarine slumping (Stow & Mayall, 2000; Stracchan, 2008) or lateral loading during liquefaction (Postma, 1983; Stromberg & Bluck, 1998; Moretti et al., 2001; Owen, 2003), respectively. Brecciated beds are likely deposited as a debrite from gravitational collapse on an unstable and steep slope (e.g., Talling et al., 2012; Thomson et al., 2014; Wallace et al., 2015).

4.6.3.2 Environmental Interpretations

The prevalence of fine-grained lithofacies, storm reworking, soft sediment deformation and debrite breccias are consistent with a slope to basinal (C) setting (Figure 9; Gómez-Pérez et al., 1999; Grotzinger & James, 2000; Thomson et al., 2014; Wallace et al., 2015; Corkeron & Slezak, 2020). Slumped beds and brecciated beds are consistent with rapid deposition from turbidity and debris flows on an unstable slope (C1) (Talling et al., 2012; Thomson et al., 2014; Thorie et al., 2020). From previous literature on slope lithofacies in the north-western Flinders Ranges, the brecciated beds could be forereef debrites that were eroded and transported from a

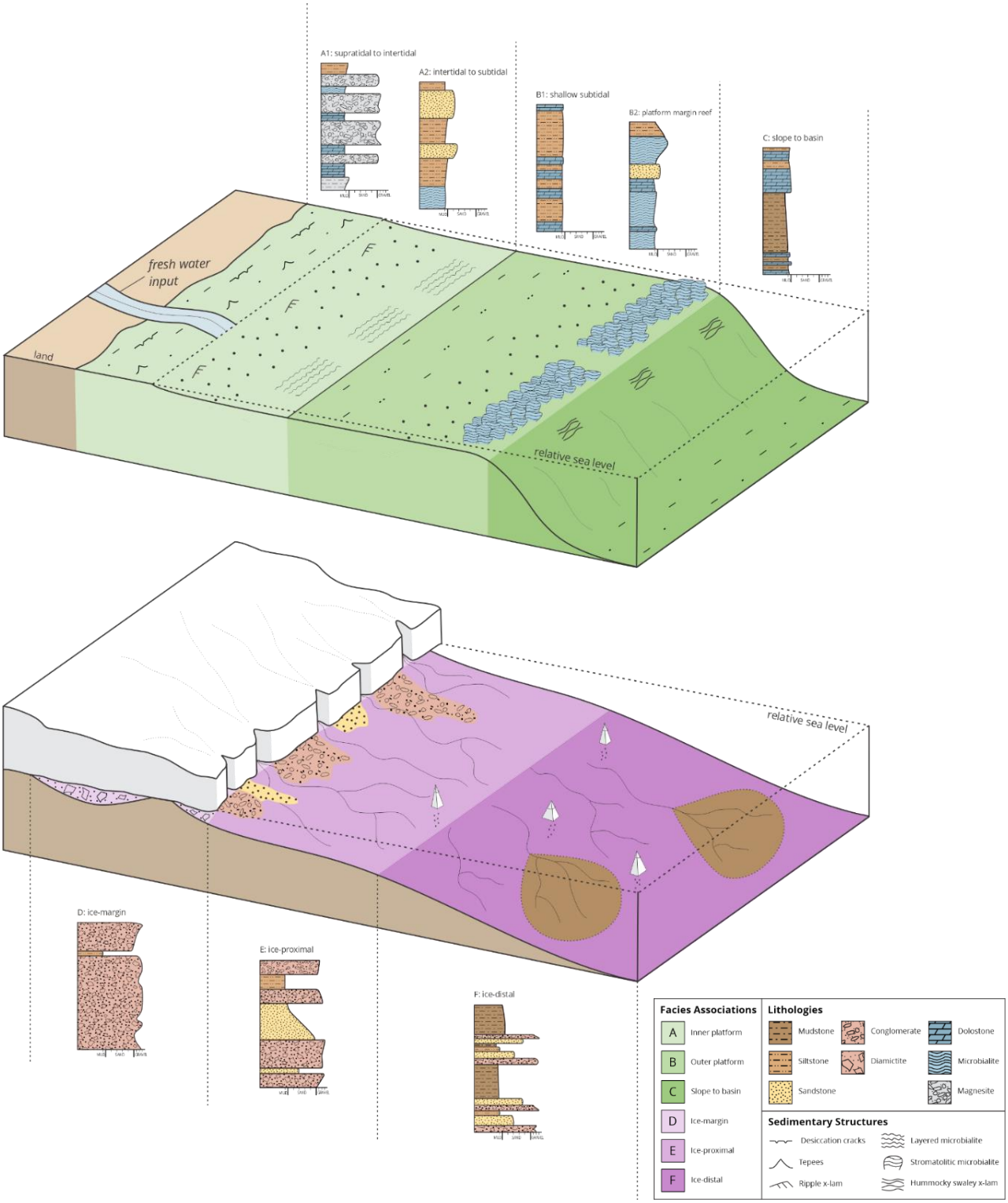

Figure 9: Depositional models for the two key settings during the Tonian–Cryogenian in the northern Flinders Ranges, with representative sedimentary logs for each depositional environment. Carbonate platforms in this study have been interpreted with both high relief and ramp-style geometries. A high relief carbonate platform model is shown here to demonstrate the platform margin reef (B2). Carbonate platform environments are interpreted for the pre-glacial and post-glacial successions, and glaciomarine environment is interpreted for the syn-glacial succession. Legend for symbology in depositional model and sedimentary logs.

regional reef escarpment (e.g., Giddings & Wallace, 2009a; Hood & Wallace, 2012; Wallace et al., 2015; Corkeron & Slezak, 2020) or resulted from more locally derived topography including those on the margins of minibasins and salt domes (Counts et al., 2016). Conversely, well-laminated fine-grained beds support deposition in more of a basinal (C2) environment under very low energy conditions (Figure 9; Thomson et al., 2014; Kunzmann et al., 2019).

4.6.4 Facies Association D: Ice margin

4.6.4.1 Sedimentary Processes

The massive, ungraded diamictites of the grounded ice-margin facies association were likely deposited rapidly from meltwater directly from the ice sheet (Link & Gostin, 1981; Young & Gostin, 1988; Preiss et al., 2011). Stratified diamictites and normally graded beds could reflect slower deposition and sorting through clast settling (Anderson, 1989), while inverse grading likely indicates kinetic sieving during flows (Legros, 2002; Talling et al., 2012; Le Heron et al., 2014).

4.6.4.2 Environmental Interpretations

From previous literature, these thick diamictite successions have been interpreted as melt-out at the ice margin (D), (Figure 9; e.g., Link & Gostin, 1981; Young & Gostin, 1988; 1991; Preiss et al., 2011; Le Heron et al., 2014). Massive diamictite packages support deposition as ice-contact till in the terrestrial and/or grounding zone (D1) (Young & Gostin, 1988; 1991; Virgo et al., 2021), while packages with evidence for reworking (i.e., sorting and stratification) are more closely associated with subaqueous deposition as proximal proglacial till (D2) (Figure 9; Young & Gostin, 1988; 1990; 1991; Anderson, 1989; Eyles et al., 2007; Boggs, 2014; Busfield & Le Heron, 2013; 2016; Le Heron et al., 2013; 2014; Fleming et al., 2016).

4.6.5 Facies Association E: Proximal proglacial

4.6.5.1 Sedimentary Processes

Upper plane beds and ripple cross-stratification are likely deposited from a similar process to that outlined in the inner platform setting (Ashley, 1990; Reading, 2009; Boggs, 2014). However, the unimodal current orientation of flows could indicate deposition from low-density turbidity currents rather than a tidal source (Lowe, 1982; Kneller, 1995; Shanmugam, 1997; 2000; Bridge, 2009; Winsemann et al., 2009; Talling et al., 2012; Momta et al., 2015; Jorissen et al., 2018). High-density turbidity currents could have deposited graded sands and orthoconglomerates with internal structure, while more massive beds could reflect deposition from hyperconcentrated debris flows (Lowe, 1982; Kneller, 1995; Shanmugam, 2000; Winsemann et al., 2009; Talling et al., 2012; Le Heron & Busfield, 2016). Similarly, stratified diamictite beds are more consistent with rapid deposition from subaqueous sediment gravity flows (Young & Gostin, 1988; Anderson, 1989; Eyles et al., 2007; Le Heron et al., 2013; 2014), and massive diamictites could indicate moderate to high strength, cohesive debris flow deposits (Talling et al., 2012). Bed forms with rare, scoured bases likely indicate high-velocity flows that eroded the substrate and subsequently filled any new topography during the waning stage of the same flow (Fielding, 2006; Bridge, 2009; Boggs, 2014).

4.6.5.2 Environmental Interpretations

The mix of structured and massive lithofacies was likely deposited in a subaqueous environment from turbidity and debris flows, respectively (Lowe, 1982; Kneller, 1995; Shanmugam, 1997; 2000; Bridge, 2009; Talling et al., 2012; Boggs, 2014). This is consistent with a proximal proglacial setting (E), (Figure 9; e.g., Powell & Domack, 2002; Winsemann et al., 2009; Le Heron et al., 2013; 2014; Busfield & Le Heron, 2013; 2016), which can be further classified based on the abundance of specific lithofacies and the stratigraphic relationship between them. Immature and massive sands, gravels and diamictites are interpreted to represent deposition from debris flows as glacial outwash (E1), (e.g., Young & Gostin, 1988; 1991; Powell & Domack, 2002; Le Heron et al., 2014; Le Heron & Busfield, 2016), while graded beds with scoured bases and unidirectional structures represent subaqueous turbidite channel deposits (E2), (Figure 9; e.g., Lowe, 1982; Reading & Richards, 1994; Le Heron et al., 2014).

4.6.6 Facies Association F: Distal proglacial

4.6.6.1 Sedimentary Processes

Low-density turbidity currents were likely responsible for depositing fine-grained sediments (Talling et al., 2012; Tinterri et al., 2016). Convolute laminations were likely deposited from bottom current reworking (Dzuynski & Smith, 1963; Shanmugam, 1997), while simple load casts and flame structures reflect liquefaction in response to differential sediment densities or lateral loading (Owen, 2003). Dropstones that deform underlying beds provide evidence for ice-rafted debris that were likely deposited as rainout (e.g., Link & Gostin, 1981; Young & Gostin, 1988; 1991; Powell & Domack, 2002; Eyles et al., 2007; Preiss et al., 2011; Boggs, 2014; Le Heron et al., 2013; 2014; 2021; Le Heron & Busfield, 2016). Subcritical climbing ripples within siltstone beds provide further evidence for decelerating turbidity currents, net deposition and bedform migration (Ashley et al., 1982; Young & Gostin, 1988; Baas et al., 2000; Jobe et al., 2012; Boggs, 2014; Le Heron & Busfield, 2016; Maciaszek et al., 2019).

4.6.6.2 Environmental Interpretations

The repeated emplacement of fine-grained turbidite successions, transitioning from massive sandstone, rippled, cross-stratified and convolute sandstone and siltstone, to laminated mudstone, along with ice-rafted dropstones, have been interpreted as distal proglacial deposits (F), (Figure 9; e.g., Eyles et al., 1983; Powell & Domack, 2002; Le Heron et al., 2014; Busfield & Le Heron, 2016). More specifically, a subaqueous fan (F1) could have provided the large sediment supply and facilitated the slope instability necessary for the development of these turbidity currents (Figure 9; e.g., Bouma, 1964; Middleton & Hampton, 1976; Lowe, 1982; Shanmugam, 1997; 2000; Powell & Domack, 2002; Talling et al., 2012; Boggs, 2014; Le Heron et al., 2014).

4.6.7 Regional Correlation

4.6.7.1 Sequence 1

4.6.7.1.1 Sequence 1.1

The base of the Termination Hill section in the north-west corner of the basin is marked by a 350 m thick succession of supratidal to subtidal magnesite and dolostone with minor microbial

carbonate, siltstone and sandstone (Sequence 1.1; Figure 10). Although this distinct unit was not logged in the North Copley section, it has been recorded near this location from previous studies (i.e., Frank & Fielding, 2003). Sequence 1.1 can be further traced to the South Copley section (Figure 10), increasing in stratigraphic thickness up to 485 m. Deposition of sedimentary magnesite in the northern Flinders Ranges is restricted to the western margin, extending discontinuously across a strike length of ~ 130 km.

4.6.7.1.2 Sequence 1.2

The overlying unit (Sequence 1.2) was only recorded at the South Copley and Mount Lyndhurst sections (Figure 10), ranging in thickness from 157 m to 33 m, respectively. It is represented by platform margin stromatolitic reefs with minor sandstone, dolostone and layered microbialite. It appears to pinch out north-west towards the Termination Hill section (Figure 10), where the magnesite interval (Sequence 1.1) is directly overlain by Sequence 2. The correlation of this stromatolitic unit to North Copley and Yankannina is uncertain as this part of the stratigraphy was not logged at these locations (Figure 10). However, as stratigraphy appears to be continuous along strike between the South Copley and North Copley sections, it is likely that Sequence 1.2 was also deposited in North Copley.

4.6.7.1.3 Sequence 1.3

Sequence 1.3 is deposited in the South Copley section and comprises slope to basinal cross-stratified siltstone (60 m thick). Like Sequence 1.2, this interval was not logged in the North Copley and Yankaninna sections, so correlation to these locations is ambiguous (Figure 10). It is evident that this deepwater unit pinches out further north towards Termination Hill and Mount Lyndhurst and east to the Vulkathunha-Gammon Ranges (Figure 10).

Towards the eastern margin of the basin, this sequence totals 1084 m and is characterised by more siliciclastic rocks, which are lithologically dissimilar to the carbonate-dominated rocks along the western margin. At the Vulkathunha-Gammon Ranges section, this interval is represented by supratidal to intertidal clastic (siltstone and sandstone) and carbonate (dolostone and microbial carbonate) lithofacies, and lagoonal siltstone and dolostone. Due to the variability of the lithologies and depositional settings in the Vulkathunha-Gammon Ranges, it is hard to correlate Sequence 1 with certainty to the stratigraphically equivalent successions at other locations in the central and western part of the northern Flinders Ranges (Figure 10).

4.6.7.2 Sequence 2

At Termination Hill, Sequence 2 is represented by 30 m of intertidal to subtidal dolostone and sandstone (Sequence 1.4; Figure 10). This can be traced along strike to North and South Copley (Figure 10), where it becomes thicker (139 m and 322 m) and includes more clastic lithofacies. In South Yankaninna (Figure 10), Sequence 2 is 254 m thick and includes supratidal layered microbialite and dolostone lithofacies. Although this clastic-rich unit was not logged in North Yankaninna, it has been mapped at this location (Coats, 1973). Sequence 2 can also be correlated to the Vulkathunha-Gammon Ranges (Figure 10), where it is characterised by 476 m of intertidal to subtidal clastics with minor dolostone.

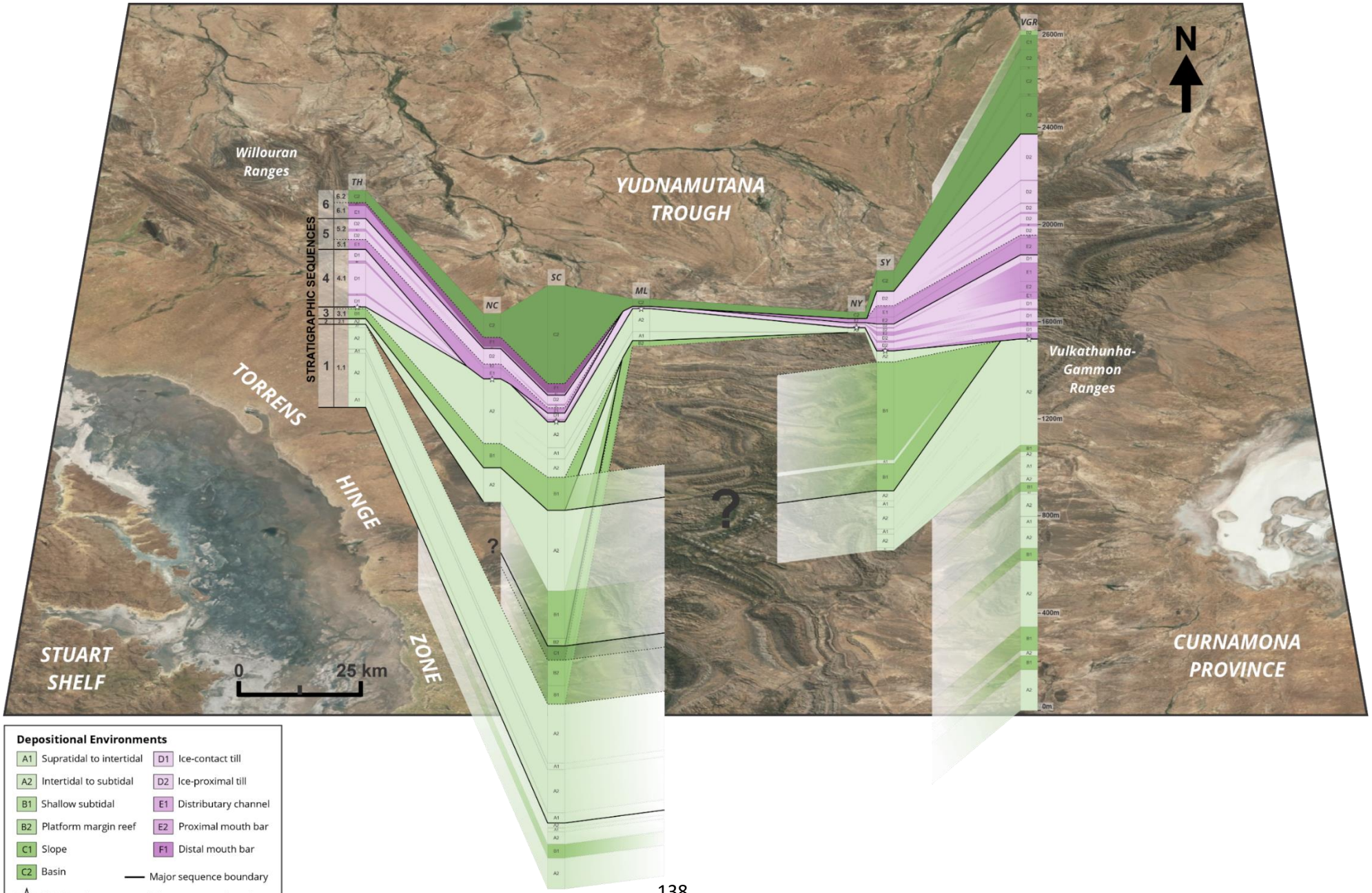
Willouran Ranges
YUDNAMUTANA TROUGH
TORRENS HINGE ZONE
STUART SHELF
CURNAMONA PROVINCE
Vulkathunha-Gammon Ranges
STRATIGRAPHIC SEQUENCES
TH
NC
SC
ML
NY
SY
VGR
0
25 km
N
2600m
2400m
2000m
1600m
1200m
800m
400m
0m
Depositional Environments
A1 Supratidal to intertidal
A2 Intertidal to subtidal
B1 Shallow subtidal
B2 Platform margin reef
C1 Slope
C2 Basin
Field locations
D1 Ice-contact till
D2 Ice-proximal till
E1 Distributary channel
E2 Proximal mouth bar
F1 Distal mouth bar
Major sequence boundary
Minor sequence boundary

Figure 10: Fence diagram with correlation panels between sections across the northern Flinders Ranges. Stratigraphic columns and panels show temporal and spatial distribution of depositional environments. Semi-transparent panels indicate correlations with uncertainty. Thick black lines indicate major sequence boundaries, dashed lines indicate minor sequence boundaries. TH = Termination Hill, NC = North Copley, SC = South Copley, ML = Mount Lyndhurst, NY = North Yankaninna, SY = South Yankaninna, VGR = Vulkathunha-Gammon Ranges

4.6.7.3 Sequence 3

4.6.7.3.1 Sequence 3.1

The base of Sequence 3 is characterised by lagoonal siltstone and dolostone (Sequence 3.1) and can be traced across several sections in the northern Flinders Ranges, with varying stratigraphic thicknesses (Figure 10). It increases in thickness from 44 m at Termination Hill, to 100 m at North Copley and 150 m in South Copley, where it includes minor microbial carbonate lithofacies. This lagoonal unit pinches out in the north-central part of the basin at Mount Lyndhurst but can be correlated to the south-central Yankaninna area (Figure 10). In South Yankaninna, the deposition of Sequence 3.1 is considerably thicker (545 m) and is represented by analogous siltstone and dolostone lithofacies to those on the western margin. Like Sequence 2, this interval was not logged in North Yankaninna. However, the correlation is uncertain as it cannot be constrained from the previous mapping. Sequence 3.1 appears to pinch out towards the east in the Vulkathunha-Gammon Ranges section, where Sequence 2 is directly overlain by the Sturtian glaciogenic deposits.

4.6.7.3.2 Sequence 3.2

The top of Sequence 3 is marked by a microbial-dominated unit that is prevalent in the west and central parts of the northern Flinders Ranges (Sequence 3.2; Figure 10). In North Copley, this 264 m thick interval comprises intertidal to subtidal siltstone, dolostone and microbial carbonates, which can be traced along strike to a 197 m thick succession in South Copley with minor supratidal lithofacies (Figure 10). The unit thins towards Mount Lyndhurst (103 m) and is characterised by comparable inner platform lithofacies, including sandstone interbeds. Sequence 3.2 is the only pre-glacial stratigraphy logged in North Yankaninna (Figure 10), recording a thin (21 m) interval that can be correlated to a thicker (49 m) succession in South Yankaninna.

4.6.7.4 Sequence 4

At the Termination Hill section, a thick (210 m) basal diamictite unit (Sequence 4.1) with minor conglomeratic interbeds is interpreted to reflect ice-contact till and proglacial outwash, respectively. Sequence 4 appears to pinch out at the North Copley section, reappearing again in a thinner interval (36 m) at the base of the South Copley section (Figure 10). Similar lithofacies are identified in South Copley but include additional meltwater channel-graded sandstone interbeds. This basal diamictite is the only glaciogenic unit deposited in Mount Lyndhurst, represented by a thin (5 m), massive, graded diamictite bed interpreted as proximal proglacial till. In the Yankaninna sections, Sequence 4 reflects slightly more proximal deposition of proglacial tills and fine-grained, laminated and scoured meltwater channel interbeds. This basal diamictite thickens towards the south from 22 m in North Yankaninna to

116 m thick in the South Yankaninna section (Figure 10). Towards the east, at the Vulkathunha-Gammon Ranges section, Sequence 4 is much thicker (345 m), with frequent sandy interbeds. This marks the return of interpreted ice-contact tills and proglacial outwash analogous to the basal diamictite succession deposited along the western margin.

4.6.7.5 Sequence 5

4.6.7.5.1 Sequence 5.1

The overlying heterogenous unit (Sequence 5.1) is deposited in all sections along the north-western margin of the basin, but with varying degrees of thickness and representative lithologies (Figure 10). In the north, at Termination Hill, the unit is 36 m thick and characterised by glacial outwash sands and diamictites. These pass into a 65 m thick succession in North Copley, which includes meltwater channel cross-stratified sands. Along strike, at the South Copley section, Sequence 5.1 is lithologically similar but considerably thinner (20 m). The North and South Yankaninna sections record a 17 m thick succession of turbidite channel deposits and a 77 m thick succession of coarse-grained clastic glacial outwash and meltwater channel lithofacies, respectively. Sequence 5.1 can be correlated east to the Vulkathunha-Gammon Ranges section, represented by an 86 m thick succession of comparable lithofacies to those deposited in the South Yankaninna section.

4.6.7.5.2 Sequence 5.2

At Termination Hill, Sequence 5.2 is characterised by 77 m of proximal proglacial massive and crudely stratified diamictite till with proglacial outwash sandstone interbeds. At the North Copley section, the unit is thinner (40 m) and lithologically homogenous, depositing only proximal proglacial massive diamictite facies. Along strike at the South Copley section, Sequence 5.2 is 53 m thick and marked by the return of interbedded proximal proglacial sands, comparable to those deposited in the Termination Hill section. This upper diamictite unit appears to pinch out in the North Yankaninna section but can be traced to the top of the South Yankaninna section (Figure 10). Like North Copley, it is lithologically homogenous and represented by a 50 m thick proximal proglacial diamictite. Deposition of Sequence 5.2 can be correlated to a very thick (406 m) succession over to the east at the Vulkathunha-Gammon Ranges section, where it is similar to Termination Hill and South Copley.

4.6.7.6 Sequence 6

4.6.7.6.1 Sequence 6.1

Sequence 6.1 appears to have more limited deposition, accumulating only at the top of the sections along the north-western margin of the basin (Figure 10). At the Termination Hill section, this unit is characterised by a 57 m thick succession of proximal outwash sandstone and diamictites, overlain by distal fan mudstone, siltstone and sandstone. Sequence 6.1 is correlated to the North and South Copley sections (Figure 10), where it is represented by 45 m and 41 m thick successions, respectively. Although this upper heterogenous unit was not identified in the other sections, it has been recorded at locations in South Yankaninna from previous studies (i.e., Young & Gostin, 1990; 1991), which were correlated to the sections on the north-western margin of the basin (Figure 10).

4.6.7.6.2 Sequence 6.2

On the north-western margin in Termination Hill, the bottom of Sequence 6.2 is marked by a 2 m thick dolostone bed, followed by deposition of basinal siltstone and carbonate. The North Copley and South Copley sections are dominated by the deposition of basinal mudstone, with thin (1 m) carbonate beds increasing in number up-section. This succession in South Copley is of particular significance because it contains a 3 cm tuff layer that has provided an accurate geochronological age for the end of the Sturtian glaciation (663.03 ± 0.11 Ma, Cox et al., 2018). The cap carbonate recorded at Termination Hill is also deposited in the north-central Mount Lyndhurst section, represented by a 4 m thick bed that grades into basinal mudstone with minor thin (1m) carbonate interbeds. Sequence 6.2 in North Yankaninna is the only carbonate-dominated interval, where 30 m of basinal dolostone overlie glaciogenic rocks. The South Yankaninna and Vulkathunha-Gammon Ranges sections are comparable to those in Copley, with mudstone-dominated deposition in the bottom, and increasing carbonate deposition up-section.

4.6.8 Controls on basin architecture

The sequence stratigraphic architecture of the basin, including the variations in depositional environments and stratigraphic thicknesses recorded in this study, results from the interaction of accommodation and sediment input and can be divided into systems tracts (e.g., Catuneanu, 2006; 2017; Catuneanu et al., 2009; 2011; Embry, 2009; Vakarelov & Ainsworth, 2013; Kunzmann et al., 2019; 2020). Accommodation and sedimentation rates are in turn largely controlled by variations in tectonics (subsidence and uplift), eustasy, and climate. In addition, salt tectonics played a critical role in the production of syndepositional topography. This was largely through the formation of salt withdrawal minibasins and diapirs, which correspond to topographic lows and highs, respectively (Rowan et al., 2020).

4.6.8.1 Sequence 1

4.6.8.1.1 Sequence 1.1

The distinctive magnesite succession (Sequence 1.1) is interpreted to have been deposited during a slow transgression (Figure 11) in an arid, low-energy, inner platform environment that was sheltered from marine reworking by barrier reefs (O'Connell et al., 2020). This is evidenced by the limited clastic input and aggradation of shallow-water carbonate deposits (Figure 11). Eustatic sea level rise was likely driving the increase in accommodation during a time of relative tectonic quiescence, demonstrated by the prevalence of fine-grained, carbonate-rich material and lack of source area clastics (Figure 11; Preiss, 1987; Catuneanu, 2006). Due to the tabular geometry of the platform, minor fluctuations in sea level would result in near instantaneous flooding (Preiss, 2000), and it is marked by current-reworked intraclastic magnesite and third-order flooding surfaces (Figure 11). Sequence 1.1 is confined to the western margin of the northern Flinders Ranges because it was restricted to a major rift shoulder on this western boundary of the Adelaide Rift Complex (Lloyd et al., 2020). This resulted in a littoral depositional setting and higher relief relative to other parts of the basin.

4.6.8.1.2 Sequence 1.2

The stromatolitic buildup of Sequence 1.2 indicates deposition as a platform margin microbialite reef during a highstand systems tract (Figure 11), where the reefal growth kept pace with the newly created accommodation space. This accumulation of carbonate material was likely facilitated by earlier transgressions that flooded the rift shoulder platform margins, creating a sediment-starved distal area relative to clastic source areas in the northwest (Catuneanu, 2006; Lloyd et al., 2020). Deposition of these Tonian reefs was recorded in the north-western margin and north central part of the basin (Figure 11), and coincides with the location of later Cryogenian reef complexes (e.g., Balcanoona Formation, Wallace et al., 2015; Corkeron and Slezak, 2020). These likely correspond to long-lasting topographic highs, which were influenced by normal faults along the basin margin in the north-west (Preiss, 2000) and large salt diapirs in Mount Lyndhursrt (Rowan et al., 2020). Further, the deposition of Sequence 1.2 at Copley and Mount Lyndhurst likely corresponds to carbonate platforms with high relief geometries (Wallace et al., 2015), while locations that do not record this sequence (e.g., Yankaninna) probably developed more of a ramp-style geometry.

In contrast, the Vulkathunha-Gammon Ranges section in the north-eastern part of the basin was likely deposited under a very different set of conditions. The thick, clastic-rich succession (Figure 11) is consistent with fault-controlled deposition and proximity to uplifted source areas at the rim of the basin. This is supported by detrital zircon provenance data that demonstrates restricted eastern detrital sources (Lloyd et al., 2020). Deposition likely occurred during a highstand systems tract (Figure 11), as the high supply of clastic material prograded basinward into the high accommodation area generated by tectonic subsidence. Not only could these tectonics be related to the ongoing rifting in the basin, but the nearby formation of the allochthonous salt (e.g., Arkaroola and Tourmaline Hill diapirs) may have also been responsible for the generation of uplifted material and subsidence-induced accommodation. The Arkaroola diapir to the east is defined by a gentler ramp geometry, while the Tourmaline Hill diapir to the north is very steep and continued into the overlying Umberatana Group (Rowan et al., 2020). The latter would have created significant topography and is likely, in part, responsible for the generated uplift and subsidence recognised in the deposition of this sequence in the Vulkathunha-Gammon Ranges section.

4.6.8.1.3 Sequence 1.3

The deep-water siltstone succession of Sequence 1.3 was likely deposited during rapid transgression (Figure 11), resulting in the drowning of the carbonate platform and the shutdown of carbonate productivity. This is represented by backstepping (retrogradational) geometries and is capped by a major flooding surface (MFS; Figure 11). On the western margin, this unit pinches out towards the north, suggesting a more distal setting in Copley (Figure 11). Further, Sequence 1.3 was not deposited in the north-central and eastern sections, supporting a more proximal, shallow environment in these parts of the basin.

4.6.8.2 Sequence 2

The overlying sandstone succession (Sequence 2) is consistent with a highstand systems tract and is capped by a major regressive surface (MRS; Figure 11), reflecting deposition in a

proximal clastic-dominated setting with high sediment input. This was likely in response to pulses of rifting and newly uplifted source regions (Preiss, 1987), which resulted in basinward progradation of clastics and burial of the platform carbonates. The uplift interpreted during the deposition of this unit may also have developed from salt diapirism actively forming across the basin during this time. Complex diapirism in the Willouran Ranges (Hearon et al., 2015; 2015a; Rowan et al., 2020), may have eroded areas close to the diapir (e.g., Termination Hill), which in turn created the lateral thickness variation of Sequence 2 along the western margin. The Burr diapir to the west of the Yankaninnna Anticline formed an apparent flat (Rowan et al., 2020), which would have created high topography responsible for highstand deposition. This succession is recorded across most of the northern Flinders Ranges, except in the Mt Lyndhurst section (Figure 11). There are several possibilities as to why Sequence 2 is not present in the north central portion of the basin. The first is that these locations were too proximal and topographically high to be affected by the rise in base level. The second possibility is that they were restricted from the fluvial sources of sediment input. Thirdly, sediments in these locations may have been subaerially exposed and eroded during the subsequent drop in base level.

4.6.8.3 Sequence 3

4.6.8.3.1 Sequence 3.1

The widespread siltstone and dolostone unit (Sequence 3.1) that succeeds Sequence 2 is consistent with a low energy, lagoonal outer platform setting deposited during a transgression (Figure 11). This rise in base level creates a backstepping geometry as the mixed clastic and carbonate material retrograde over the underlying sandstone unit. The increase in accommodation was largely tectonically controlled (Preiss, 1987), but could also be in part eustatic due to the prevalent deposition of fine-grained sediment across the basin (Figure 11).

4.6.8.3.2 Sequence 3.2

The inner platform microbial succession at the top of Sequence 3 represents deposition during a highstand systems tract (Figure 11), where the accumulated sediment outpaced base-level rise and the carbonate platform aggraded and prograded basinward (Catuneanu, 2006). Like the rest of the pre-glacial succession, the transgressive-regressive cycle likely formed due to pulses of rift-related subsidence (Figure 11; Preiss, 1987). The widespread deposition of this particular succession across the basin could represent a eustatically driven fluctuation in base level. Sequence 3.2 may not have been deposited in the east in the Vulkathunha-Gammon Ranges section because that area was physically separated from the rest of the basin and dominated by the deposition of clastic material (Figure 11).

4.6.8.4 Sequence 4

The basal diamictite in the bottom of Sequence 4 unconformably overlies the pre-glacial successions, which is represented by a sequence boundary (SB; Figure 11). Sequence 4 could have been deposited during a lowstand systems tract and would be capped by an MRS (Figure 11). This was likely driven by climatic fluctuations and glacio-eustatic fall and marked by widespread deposition across the basin during a glacial maximum. Although sediment is typically eroded during drops in eustatic sea level, the predominance of climatic control on deposition during the glaciation prompted a decrease in fluvial discharge and resulted in glacio-

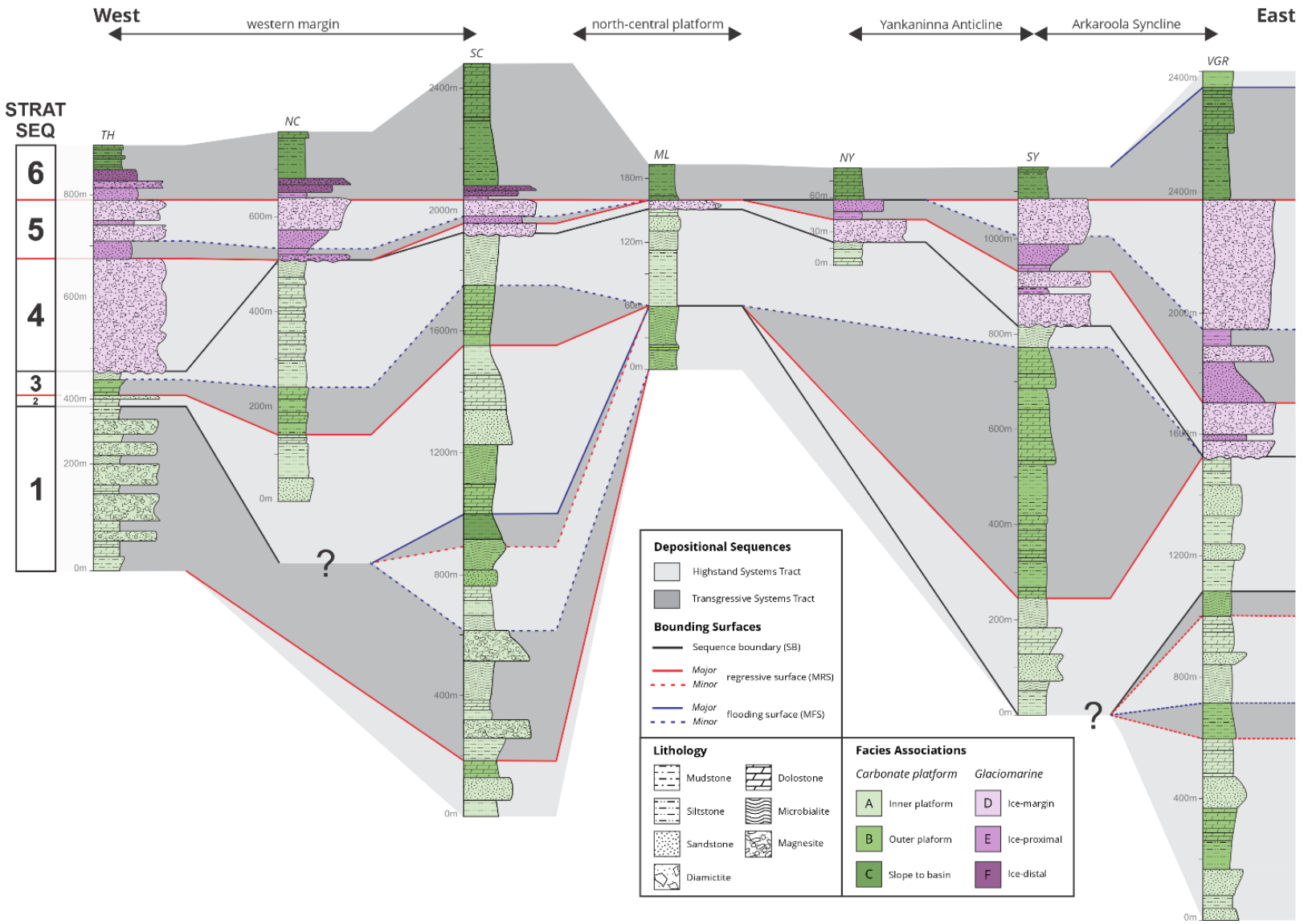

Figure 11: Generalised sedimentary logs through Tonian-Cryogenian sections across the northern Flinders Ranges, South Australia. Colour of logs corresponds to facies associations. Grey panels indicate correlation of systems tracts between sections. Coloured dashed lines indicate correlation of sequence stratigraphic surfaces between sections. STRAT SEQ = Stratigraphic Sequences. TH = Termination Hill, NC = North Copley, SC = South Copley, ML = Mount Lyndhurst, NY = North Yankaninna, SY = South Yankaninna, VGR = Vulkathunha-Gammon Ranges.

fluvial aggradation (e.g., Blum, 1994; 2001; Catuneanu, 2006). Le Heron et al. (2014) suggests that a tectonic mechanism for topography generation may not have been required. However, the extreme thickness variations of Sequence 4 across the basin (Figure 11), and in particular across the Paralana Fault in Arkaroola (Lloyd et al., 2022), suggests that faulting was active during deposition and impacted the topography. Combined glacial scour and coeval faulting was likely the cause for these thickness and lithological variations (Young & Gostin, 1991, Preiss, 2000). The considerably thinner exposure of this unit at Mt Lyndhurst (Figure 11) may have been influenced by contemporaneous uplift of the Lyndhurst Diapir (Preiss, 1987), although Rowan et al. (2020) suggested that allochthonous salt transport was initiated later during the deposition of the overlying Tapley Hill Formation. The complex geometry of this diapir, where it displays evidence of both allochthonous and thrust structures, makes it difficult to unravel both the nature and timing of emplacement (Rowan et al., 2020). On the western margin, a platform geometry may have influenced the deposition of more proximal ice-contact diamictites (Figure 11), where localised deposition in Termination Hill and South Copley may correspond to palaeovalleys that channelled ice flow (Young & Gostin, 1988, 1991). Further, the pronounced variability in depositional thickness between the South Yankaninna and North Yankaninna sections (Figure 11) was likely due to topography generated from contemporaneous faulting (Young & Gostin, 1990) and/or allochthonous salt diapirism associated with the Burr Diapir (Rowan et al., 2020). This diapir occurred less than 10 km to the west within the underlying Skillogalee Dolomite (Sequence 1), where the geometry of its eastern extent was largely influenced by a pre-existing anticlinorium (Rowan et al., 2020), referred to in this study as the Yankaninna Anticline. Uneven glacial incision further to the east could have resulted from active tectonic faulting that created uplift and increased glacial erosion relative to other parts of the basin (Young & Gostin, 1991).

4.6.8.5 Sequence 5

4.6.8.5.1 Sequence 5.1

The overlying fine-grained unit (Sequence 5.1) is consistent with deposition during a transgression (Figure 11), which would similarly have been driven by eustacy and climate. The implication of this sequence is that the Sturtian glaciation likely reflects more of a "slushball" than a hard "snowball" Earth (Lewis et al., 2007). As the grounded ice margin retreated, the increased fluvial discharge from melting ice would have outpaced the rise in sea level, resulting in fluvial erosion (e.g., Blum, 1994; 2001; Catuneanu, 2006). From palaeocurrent data, glacier movement was from the south (Young & Gostin, 1991), producing a backstepping geometry from the Termination Hill section to the South Copley section (Figure 11). Sequence 5.1, and subsequent glaciogenic units, are not present in the north-central zone in Mt Lyndhurst (Figure 11). This was likely due to the topographic high in this area and the possible erosion during the subsequent glacial advance. Coarse deposits included in this lower heterogenous unit in South Yankaninna could reflect local uplift and resedimentation of shedding material related to diapiric movements (Young & Gostin, 1990). Areas that were previously dominated by glacial scour, particularly those in the east, received significant amounts of sediment and resulted in thick deposition (Figure 11; Young & Gostin, 1991). Sequence 5.1 is exposed at the Vulkathunha- Gammon Ranges section and is lithologically dissimilar to other sections in the

basin, likely due to its proximal proglacial location where coarse material continued to deposit despite the glacial recession.

4.6.8.5.2 Sequence 5.2

The ice proximal till of Sequence 5.2 represents deposition during a second basinward prograding package that represents either a highstand and/or lowstand systems tract, capped by an MRS (Figure 11). Like the lower diamictite (Sequence 4), this coincides with a glacial advance and an eustatic sea-level fall. However, this represents slightly more distal, subaqueous deposition relative to the first glacial advance (Young & Gostin, 1988; 1990; 1991). This unit does not appear in the Mt Lyndhurst and North Yankaninna sections (Figure 11). As these sections correlate with a central high (horst) in the basin, Sequence 5.2 may not have been deposited or was potentially eroded.

4.6.8.6 Sequence 6

4.6.8.6.1 Sequence 6.1

Like the lower heterogenous unit (Sequence 5.1), Sequence 6.1 is characterised by transgressive, fine-grained lithofacies (Figure 11), although deposited during widespread deglaciation rather than an ice retreat. This was probably driven by climatic warming following the glacial maximum and eustatic sea level rise, where fine-grained subaqueous sediment backstepped and retrograded landward. Sequence 6.1 is only recorded along the western margin (Figure 11), which could correspond to the tabular geometry here and subsequent susceptibility to flooding.

4.6.8.6.2 Sequence 6.2

The slope to basinal succession of Sequence 6.2 is consistent with deposition during a widespread transgression (Figure 11), where postglacial sediments backstepped over the continental margin. Consequently, this succession is recorded on the adjacent Stuart Shelf in the west and right over the Curnamona province to the Barrier Ranges in New South Wales to the east (Preiss, 1987). The predominance of fine-grained material (Figure 11), and depositional spread and synchronicity across the basin have been used to suggest that post-rift thermal subsidence likely assisted the eustatic rise (Preiss, 1987; Powell, 1994). Deglaciation delivered large amounts of detritus into the marine environment, which resulted in considerable stratigraphic thicknesses of this postglacial succession in the Adelaide Superbasin (Lloyd et al., 2020). This has been hypothesised to have stimulated eukaryote evolution through the flux of detrital bio-essential nutrients (Brocks et al., 2017).

Carbonate rocks (“cap carbonates”) at the base of Sequence 6.2 are recorded in the northern most sections of this study (Figure 11), which could be due to their more restricted setting relative to other locations in the basin. These more restricted settings provide an optimal environment for cap carbonate precipitation due to the increased effect of ocean stratification, low salinity, and greater alkalinity production (Yu et al., 2020). This was likely due to their relative proximity to continental weathering sources.

4.6.9 Global context

4.6.9.1 Stratigraphy

4.6.9.1.1 Pre-glacial

The pre-glacial succession in South Australia was marked by active rifting that created topographic variability and varying sediment supply across the basin. Subsurface allochthonous salt movement during Skillogalee Dolomite Formation (Sequence 1 and 2) times is also documented to have a role in topography creation (Rowan et al., 2020). This regional tectonic control during Tonian deposition has been shown in other sections globally, including key sites in Namibia, Canada, China, Svalbard, Scotland and Ethiopia (Figure 12).

Namibia and northern Canada both underwent episodic cratonic rifting during the Tonian (Figure 12; Narbonne & Aitken, 1995; Frimmel et al., 1996; Hoffman & Halverson, 2008; Miller, 2013; Hood et al., 2015; Milton et al., 2017; Lamothe et al., 2019). These were characterised by deposition of up to 5800 m and 3500 m of coarse clastics, evaporitic to subtidal carbonates, and deep-water shales, representing multiple regressive-transgressive cycles (Chartrand & Brown, 1985; Park & Jefferson, 1991; Narbonne & Aitken, 1995; Batten et al., 2004; Long & Turner, 2013; Hood et al., 2015; Lamothe et al., 2019). In South China, rifting was more consistently active throughout the Tonian (Figure 12; Zhang et al., 2011; Lan et al., 2015; Busigny et al., 2018), and resulted in 200 m to 3500 m thick (Zhang et al., 2008) successions characterised by fine-grained clastic turbidites and minor platform carbonates (Wang & Li, 2001).

Conversely, Svalbard and Scotland appear to be in a post-rift thermal subsidence phase during the Tonian (Figure 12; Smith et al., 1999; Maloof et al., 2006; Stephenson et al., 2013; Halverson et al., 2017). This resulted in the deposition of 1000 m of transgressive-regressive sequences in a carbonate platform setting (Halverson et al., 2017) and up to 15,500 m of cyclical clastics and carbonates in deep to shallow-water settings, respectively (Glover & Winchester, 1989; Smith et al., 1999; Stephenson et al., 2013; Fairchild et al., 2017).

The pre-glacial succession in northern Ethiopia developed in an intra-oceanic back-arc basin (Figure 12; Alene et al., 2006; Miller et al., 2009; 2011; Swanson-Hysell et al., 2015; Park et al., 2020), where slab rollback followed by thermal isostatic subsidence facilitated the deposition of up to 5 km of intertidal carbonate and siliciclastics and subtidal, micritic carbonates, respectively (Alene et al., 2006; Miller et al., 2009; 2011; Swanson-Hysell et al., 2015; Park et al., 2020).

4.6.9.1.2 Syn-glacial

The syn-glacial succession in Australia is characterised by two glacial advance and retreat cycles in a glaciomarine setting, reflecting climatically driven eustatic changes in base level, and coeval faulting that impacted the thickness distribution of the glacial unit across the basin.

Sections in northern Canada (Eisbacher, 1985; Narbonne et al., 1994), California (Busfield & Le Heron, 2016; Le Heron & Busfield, 2016), Idaho and Utah (Crittenden et al., 1983; Link &

Christie-Blick, 2011) all preserve two diamictite packages with interbedded carbonate and clastic units, representing glacial advance and retreat phases in glaciomarine environments, respectively. Although there were significant climate-driven eustatic sea-level fluctuations during the Sturtian glaciation, the deposition of sections in USA and Canada were still largely fault controlled in response to continental rifting (Figure 12; Eisbacher, 1985; Link et al., 1994; Narbonne et al., 1994; Fairchild & Kennedy, 2007; Link & Christie-Blick, 2011; Keeley et al., 2012).

The <2000 m thick syn-glacial successions in South China and Namibia have very thin (20 m and 30 m thick) intervals of mudstone and sandstone between thicker diamictite packages (Zhang et al., 2011; Le Heron et al., 2013; Lan et al., 2015; Buechi et al., 2017; Hoffman et al., 2017a). These have been interpreted as representing a sub-glacial to glaciomarine environment, influenced by both fluctuations in climate-controlled eustasy (Zhang et al., 2011; Le Heron et al., 2013) and tectonic phases (Zhang et al., 2011; Hoffman et al., 2017a; Busigny et al., 2018).

In Scotland, the syn-glacial succession is ~1100 m thick, depositing diamictites with interbedded clastics that represent a glaciomarine environment (Ali et al., 2018; Fairchild et al., 2017). This climatically dynamic succession is interpreted to result from tectonic subsidence, eustatic changes, ice loading and extreme seasonal fluxes (Fairchild et al., 2017; Ali et al., 2018).

Conversely, the deposition of glaciomarine diamictites with shale interbeds in Svalbard is incredibly thin (average 10 m) (Halverson et al., 2011; 2017; 2022; Hoffman et al., 2012; Kunzmann et al., 2015; Fairchild et al., 2016). This was likely due to the decreased accommodation space and/or erosion from reduced subsidence during deposition in the Cryogenian (Halverson et al., 2022), resulting in an unconformity of approximately 10 million years (Millikin et al., 2022).

The syn-glacial succession in northern Ethiopia is consistent with a subglacial to glaciomarine setting (Park et al., 2020). This is represented by ~750 m of massive diamictites with interbedded sandstone, siltstone, micritic carbonate and carbonate breccia (Park et al., 2020), which accumulated during thermal subsidence (Alene et al., 2006). In this scenario, the sediment was able to keep pace with the increasing accommodation space (Park et al., 2020), which maintained a relatively proximal setting.

4.6.9.1.3 Post-glacial

The post-glacial succession in Australia is represented by widespread transgressive to basinal shales and carbonates, a result of de-glacial eustatic sea level rise coupled with thermal sag after rifting (Figure 12).

A transgression to deeper water argillite, carbonates and turbidites has been recorded in North America, where between 200 m and 1000 m of material accumulated in northern Canada

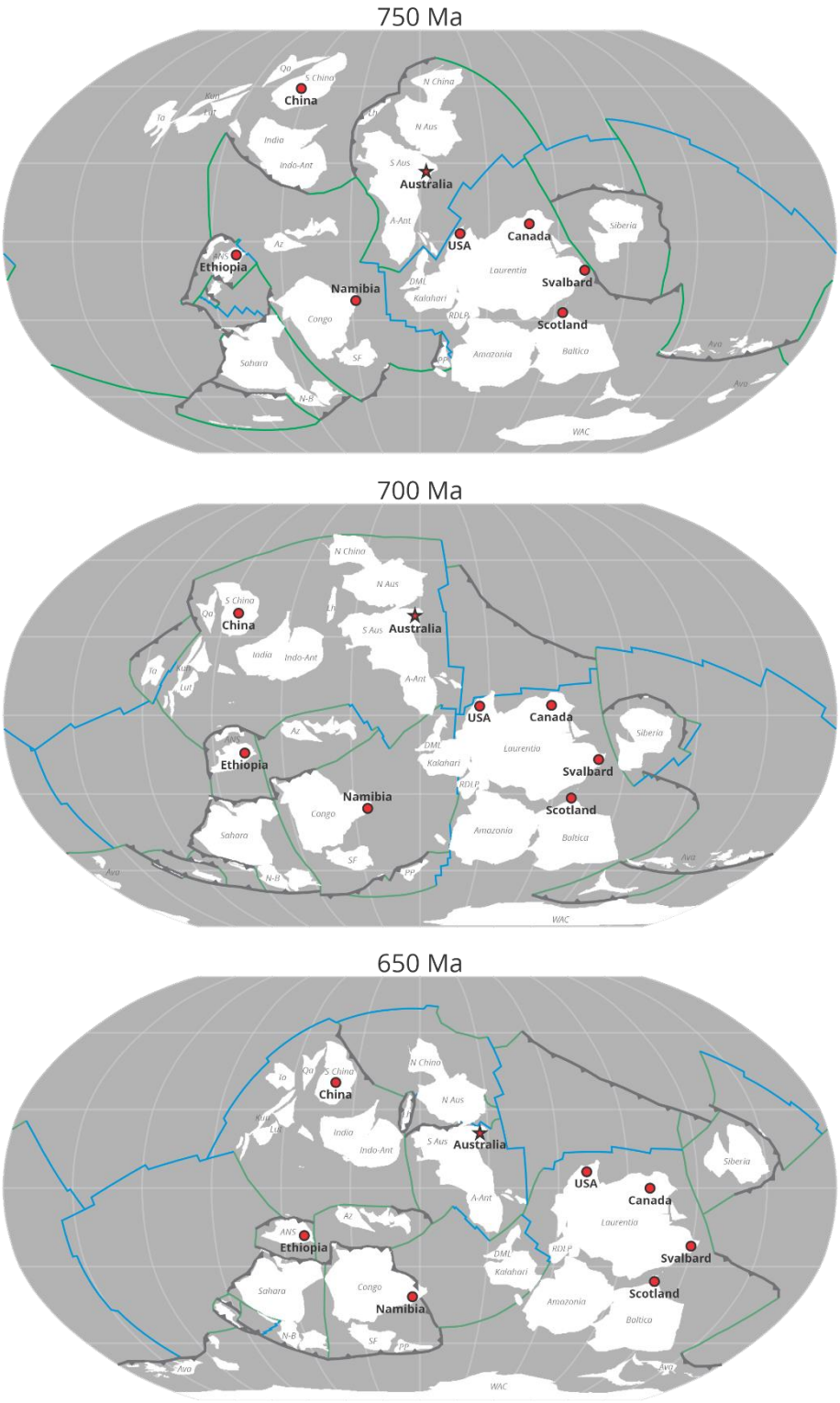

Figure 12: Global plate models with evolving plate boundaries. Models were produced using G-Plates software and files from Merdith et al. (2021). Each model corresponds to key time slice in Tonian or Cryogenian. 750 Ma = pre-glacial. 700 Ma = syn-glacial. 650 Ma = post-glacial. Transform boundary = green line. Divergent boundary = blue line. Convergent boundary = grey line (arrows indicate direction). Key sites marked by red circles. This study marked by red star. Cratons and continents labelled in grey. ANS = Arabian Nubian Shield, Ant = Antarctica, A-Ant = Austral-Antarctica, Aus = Australia, Ava = Avalonia, Az = Azania, DML = Dronning Maud Land, Kun = Kunlun, N-B = Nigeria-Benin, Qa = Qaidam, Lh = Lhasa, PP = Parana Panema, RDLP = Rio de la Plata, SF = Sao Francisco, Ta = Tarim, WAC = West African Craton

(Eisbacher, 1985; Narbonne et al., 1994), California (Nelson et al., 2020; 2021), Idaho (Lund et al., 2003; Fanning & Link, 2004; Link & Christie-Blick, 2011; Keeley et al., 2012), and Utah (Crittenden et al., 1971; Link & Christie-Blick, 2011; Balgord et al., 2013). The accommodation space increase was likely controlled by a combination of eustatic and tectonic factors associated with the developing Pacific margin (Figure 12; Eisbacher, 1985; Narbonne et al., 1994; Link & Christie-Blick, 2011; Keeley et al., 2012; Balgord et al., 2013).

Deep-water successions were also deposited after the Sturtian glaciation in South China and Svalbard. Sections in South China are 12–500 m thick, and deposit basinal muddy clastics and carbonaceous shales (Zhang et al., 2011), while Svalbard is characterised by up to 215 m of offshore marine dolomitic shales and siltstones (Hoffman et al., 2012; 2017a; Fairchild et al., 2016; 2016a). South China was marked by persistent rift-induced subsidence, and deposition transgressed into a restricted shelf setting (Zhang et al., 2011). Conversely, Svalbard was already in a post-rift setting (Figure 12) and exhibited no apparent changes in relative sea level with the underlying diamictite (Halverson et al., 2004; 2011).

Namibia and Scotland form a sharp contrast to the aforementioned post-glacial successions, and record deposition in much shallower settings. The <450 m thick unit in Namibia is characterised by laminated dolostone, turbidites and microbial carbonates, deposited in a shallow-water, platform environment (Hoffman et al., 2017a; 2021). Meanwhile, the post-glacial unit in Scotland is represented by 350 m of shallow subtidal to intertidal clastics and carbonates (Spencer & Spencer, 1972; Anderson et al., 2013; Stephenson et al., 2013; Fairchild et al., 2017; Ali et al., 2018). The shallow platform setting in Namibia was the result of active uplift during deposition at the edge of the basin (Hoffman et al., 2017a; 2021), while Scotland was experiencing steady subsidence that was balanced by high sediment supply (Ali et al., 2018).

4.6.9.2 Correlation and Significance

4.6.9.2.1 Pre-glacial

An overall increase in accommodation space and deposition of marginal marine, interbedded clastic and carbonate successions characterise Tonian deposits globally, including those in Australia, Namibia, northern Canada, South China, Svalbard, Scotland and Ethiopia. The widespread extent of these comparable depositional settings is likely to reflect global signatures, which were then modified by local tectonically driven effects.

The abundant platform carbonates recorded at these locations suggest that the climate during this time was stable, and despite the variability in palaeolatitudes (Figure 12), promoted deposition in warm, shallow seas globally (MacLennan et al., 2020). Further, the correlation of isotopic signatures recorded in these Tonian rocks has often been used to justify that the basins developing during this time were globally connected (Halverson et al., 2005; 2010; Park et al., 2020). As the δ13C signature in carbonates and organic-rich shales is used as a measure of bioproductivity (Knoll et al., 1986; Schidlowski, 1988), and the Proterozoic ocean is widely accepted to have been stratified (i.e., oxic shallow-water and anoxic deep-water; Preiss, 1987;

Giddings & Wallace, 2009a; Hood & Wallace, 2015; Counts, 2017), excursions in the isotope record may correspond to shifts from bioproductive, oxic, shallow-water (positive δ13C values) to biologically inactive, anoxic deep-water (negative δ13C values). Consequently, the preservation and correlation of negative excursions at multiple sites globally could reflect widespread transgressions that, on that scale, likely resulted from eustatic sea level rise.

With that said, the development of basins during the Tonian largely resulted from active tectonism associated with the breakup of supercontinent Rodinia (Merdith et al., 2021), and corresponds to a suite of local tectonic conditions (e.g., rifting, subsidence and slab rollback) that would have influenced the production of accommodation space. These local tectonic controls may modify the lithostratigraphic trends recorded in Tonian successions, and by extension, the chemostratigraphic record.

4.6.9.2.2 Syn-glacial

The Sturtian glaciation is recognised in the stratigraphic record through the deposition of distinct diamictite intervals capped by carbonate rocks, which, accompanied by palaeomagnetic and geochemical data, facilitated the correlation of these deposits globally (Hoffman & Schrag, 2002). However, the stratigraphic thicknesses of these units and the presence or absence of finer-grained interbeds have resulted in contention surrounding the extent and cyclicity of the icehouse.

Although the glacial successions in North America appear to record a very similar two-fold glacial advance-retreat cycle to that in South Australia (Eisbacher, 1985; Link et al., 1994), Le Heron et al. (2020) suggested that these instead represent regional, diachronous glacial cycles. In fact, Le Heron et al. (2020) makes a controversial suggestion that because there have been no direct ages from the Sturtian cryochron in Australia, just ages that bracket the glacial rocks, then perhaps there was no glaciation in Australia between ca. 716 and 663 Ma. However, recent laser Rb–Sr dating of shales in the lower heterogenous unit (Sequence 3.2) in a borehole from the Stuart Shelf yields an age of 684 ± 37 Ma (Lloyd et al., 2023), and instead suggests that the Sturtian cryochron of South Australia had a ca. 58 Ma time span, and represents two major ice advances, one before ca. 684 Ma and a second between ca. 684 and 663 Ma. These data agree with the syn-glacial volcanic ages from Idaho of Lund et al. (2003), demonstrating that the glaciations in North America and Australia were likely synchronous.

Like in Australia and North America, the glacial successions in South China and Namibia have been interpreted as reflecting a glacial retreat phase between two glacial advance episodes in a glaciomarine setting (Zhang et al., 2011; Le Heron et al., 2013; Lan et al., 2015), which was largely controlled by climatic sea level changes (Zhang et al., 2011; Le Heron et al., 2013). However, these sections have also been interpreted to reflect sub-ice deposition during a singular glacial event (Lechte and Wallace, 2016; Buechi et al., 2017; Hoffman et al., 2017a; Busigny et al., 2018), with more emphasis on the influence of changing tectonic phases (Figure 12; Zhang et al., 2011; Hoffman et al., 2017a; Busigny et al., 2018). Further, the thick inter-bedded diamictite and clastic successions in Scotland have been interpreted to represent up to 28 glacial cycles (Ali et al., 2018; Fairchild et al., 2017).

For these reasons, although age constraints and detailed paleoenvironmental interpretations are improving, it is still uncertain whether the Sturtian glacial cycle advances were global (eustatically driven) or happening at different times and at more local scales (tectonically driven).

4.6.9.2.3 Post-glacial

The transgression at the end of the Sturtian glaciation is observed globally and is widely accepted to be a consequence of eustatic sea level rise driven by melting of continental ice sheets (Kaufman et al., 1997; Kennedy et al., 1998; Bold et al., 2016). Not only was there significant eustatic sea level rise and climatic warming, but there is a notable tectonic shift to post-rift subsidence at almost all the sites discussed above, which would further increase accommodation in basins globally. Further, the distinct cap carbonate unit that overlies glaciogenic rocks has been documented at many localities and records a sharp negative δ13C excursion that has long been used as a chemostratigraphic tool to correlate this horizon (Halverson et al., 2005; 2010; Park et al., 2020). Consequently, the post Sturtian-glacial interval is one of the most well constrained and reliably correlated of the Neoproterozoic.

4.7 Conclusions

The Adelaide Superbasin was a dynamic basin influenced by syn-sedimentary tectonics, and climate and environmental changes throughout the Tonian and Cryogenian. This study presents over 8,350 m of measured sedimentary logs through seven sections in an approximately 150 km east–west transect across the northern Flinders Ranges. This includes sites in Termination Hill, Copley, Mount Lyndhurst, Yankaninna and Vulkathunha-Gammon Ranges. From these, 18 lithofacies, 6 facies associations and 11 depositional environments have been classified.

Facies and sequence stratigraphic analyses reveal deposition in a carbonate platform setting for the preglacial succession, where in the western margin a mixed carbonate succession of dolostone and magnesite accumulated under the influence of fluctuations in sea level. A topographic high in the north central portion of the basin at Mount Lyndhurst is characterised by a high-relief platform margin microbialite reef. To the east, at Yankaninna, the preglacial succession is represented by more equal volumes of fine-grained clastic and carbonate facies that were deposited in a ramp-style platform environment. Further east again, clastic rocks dominate the succession. These were sourced locally from contemporaneous fault-created topography, with some possible topography created by salt tectonics. The syn-glacial sequence coincides with a climatically driven regression. This succession is represented by two tillite units and two fine-grained heterogenous units, that represent glacial advance and retreat phases, respectively. The platform geometry of the western margin and subsequent susceptibility to flooding promoted the deposition of ice-contact till and distal fine-grained clastics. Conversely, the central part of the basin was characterised by a number of topographic highs and palaeovalleys, which were marked by a lack of glacial deposition, and a mix of proximal proglacial till and fine-grained sediment, respectively. On the eastern side of the basin, thick tillites and coarse interbedded deposits are interpreted to result from increased glacial erosion in response to syn-depositional fault-created accommodation space and proximity to uplift source areas relative to other parts of the basin. The post-glacial succession in the northern

Flinders Ranges is represented by a widespread transgression following the Sturtian glaciation that was driven by the large volume of melting ice. This promoted the deposition of slope to basinal fine-grained siltstone and dolostone facies at all locations in the study area, with varying proportions of clastic and carbonate deposits.

The lithostratigraphic and sequence stratigraphic correlation of Tonian to Cryogenian successions globally provides insights into the scale and impact of tectonic, eustatic and climate conditions, highlighting whether these changes were occurring on a local level or influencing the global system. Tonian successions in Australia, Ethiopia, Namibia, South China, Canada, Svalbard (Norway), and Scotland are all represented by the deposition of marginal marine clastics and carbonates, indicating stable climatic conditions. Further, these sites have been correlated through chemostratigraphy based on the shared record of carbon isotope excursions, implying global connections between these developing basins. However, the impact of tectonics complicates this correlation, as local tectonic regimes superimpose on litho- and chemo-stratigraphic signatures. Locations in North America (northern Canada, California, Idaho and Utah) are comparable to South Australia during the Sturtian glaciation, as they also preserve two distinct glacial advance-retreat cycles that were deposited during faulting and rifting. However, uncertainty surrounding the timing of these glaciations calls into question the synchronicity of the Sturtian. Further, glacial cyclicity at these sites ranges from one to several dozen, which convolutes our understanding of the global extent of this glaciation. Conversely, the post-glacial transgression is more consistent globally. This interval is marked by distinct litho- chemo- and sequence stratigraphic shifts to deep-water carbonates that record a negative carbon isotope excursion and demonstrate the widespread nature of the Sturtian deglaciation.

This comprehensive sedimentological and sequence stratigraphic analysis presents a facies architecture and stratigraphic framework for the Tonian to Cryogenian across the Adelaide Rift Complex in the northern Flinders Ranges. The study elucidates the temporal and spatial distribution of depositional environments before, during and after the global Sturtian glaciation, and correlates the stratigraphic framework of this basin with others that were developing across the globe during this unique time in Earth's history.

4.8 Supplementary Material

Supplementary material is freely available as PDF on Figshare.

Termination Hill log: https://doi.org/10.6084/m9.figshare.23640924.v1

North Copley log: https://doi.org/10.6084/m9.figshare.23640927.v1

South Copley log: https://doi.org/10.6084/m9.figshare.23640936.v1

Mount Lyndhurst log: https://doi.org/10.6084/m9.figshare.23640939.v1

North Yankaninna log: https://doi.org/10.6084/m9.figshare.23640945.v1

South Yankaninna log: https://doi.org/10.6084/m9.figshare.23640954.v1

Vulkathunda-Gammon Ranges log: https://doi.org/10.6084/m9.figshare.23640960.v1

4.9 Acknowledgments

We acknowledge that this research is conducted on the ancestral lands for the Adnyamathanha people. We acknowledge and respect their deep feelings of attachment and spiritual relationship to Country, and that their cultural and heritage beliefs are still as important to the living people today. We thank reviewers Paula Castillo and John Counts, executive editor Giovanna Della Porta, and associate editor Or Bialik for their valuable insight, comments and advice that greatly improved the quality of this manuscript. This project was supported by funding from the Geological Survey of South Australia, and an Australian Government Research Training Program (RTP) Scholarship awarded to Virgo. We are very grateful to Jack Ward (The University of Queensland) and Jarred Lloyd (The University of Adelaide) for their field assistance in 2018 and 2019, respectively. We would also like to thank the Department for Energy and Water (DEW) for granting us a permit to undertake scientific research in Witchelina (Permit Number: Q26796-1).

4.10 References

Alene, M., Jenkin, G. R., Leng, M. J. & Darbyshire, D. F. (2006). The Tambien Group, Ethiopia: an early Cryogenian (ca. 800–735 Ma) neoproterozoic sequence in the Arabian–Nubian shield. Precambrian Research 147(1-2): 79-99. https://doi.org/10.1016/j.precamres.2006.02.002

Ali, D. O., Spencer, A. M., Fairchild, I. J., Chew, K. J., Anderton, R., Levell, B. K., Hambrey, M. J., Dove, D. & Le Heron, D. P. (2018). Indicators of relative completeness of the glacial record of the Port Askaig Formation, Garvellach Islands, Scotland. Precambrian Research 319: 65-78. https://doi.org/10.1016/j.precamres.2017.12.005

Anderson, J. B. (1989). Antarctica's glacial setting. Glacial-Marine Sedimentation, 9, 11-57. https://doi.org/10.1002/9781118667675.ch3

Anderson, R. P., Fairchild, I. J., Tosca, N. J. & Knoll, A. H. (2013). Microstructures in metasedimentary rocks from the Neoproterozoic Bonahaven Formation, Scotland: Microconcretions, impact spherules, or microfossils? Precambrian Research 233: 59-72. https://doi.org/10.1016/j.precamres.2013.04.016

Armistead, S. E., Collins, A. S., Buckman, S. & Atkins, R. (2020). Age and geochemistry of the Boucaut Volcanics in the Neoproterozoic Adelaide Rift Complex, South Australia. Australian Journal of Earth Sciences: 1-10. https://doi.org/10.1080/08120099.2021.1840435

Arnott, R. W. & Southard, J.B. (1990). Exploratory flow-duct experiments on combined-flow bed configurations, and some implications for interpreting storm-event stratification. Journal of Sedimentary Research 60(2): 211-219. https://doi.org/10.1306/212F9156-2B24-11D7-8648000102C1865D

Ashley, G. M. (1990). Classification of large-scale subaqueous bedforms; a new look at an old problem. Journal of Sedimentary Research 60(1): 160-172. https://doi.org/10.2110/jsr.60.160

Ashley, G. M., Southard, J. B. & BoothRoyd, J. C. (1982). Deposition of climbing-ripple beds: a flume simulation. Sedimentology, 29(1), 67-79. https://doi.org/10.1111/j.1365-3091.1982.tb01709.x

Assereto, R. L. & Kendall, C. G. ST C. (1977). Nature, origin and classification of peritidal tepee structures and related breccias. Sedimentology 24(2): 153-210. https://doi.org/10.1111/j.1365-3091.1977.tb00254.x

Avigad, D., Stern, R. J., Beyth, M., Miller, N. & McWilliams, M. O. (2007). Detrital zircon U–Pb geochronology of Cryogenian diamictites and Lower Paleozoic sandstone in Ethiopia (Tigrai): age constraints on Neoproterozoic glaciation and crustal evolution of the southern Arabian–Nubian Shield. Precambrian Research 154(1-2): 88-106. https://doi.org/10.1016/j.precamres.2006.12.004

Baas, J. H., Van Dam, R. L. & Storms, J. E. A. (2000). Duration of deposition from decelerating high-density turbidity currents. Sedimentary Geology 136(1-2): 71-88. https://doi.org/10.1016/S0037-0738(00)00088-9

Balgord, E. A., Yonkee, W. A., Link, P. K. & Fanning, C. M. (2013). Stratigraphic, geochronologic, and geochemical record of the Cryogenian Perry Canyon Formation, northern Utah: Implications for Rodinia rifting and snowball Earth glaciation. Bulletin 125(9-10): 1442-1467. https://doi.org/10.1130/B30860.1

Basilici, G., de Luca, P. H. V. & Poiré, D. G. (2012). Hummocky cross-stratification-like structures and combined-flow ripples in the Punta Negra Formation (Lower-Middle Devonian, Argentine Precordillera): a turbiditic deep-water or storm-dominated prodelta inner-shelf system? Sedimentary Geology 267: 73-92. https://doi.org/10.1016/j.sedgeo.2012.05.012

Batten, K. L., Narbonne, G. M. & James, N. P. (2004). Paleoenvironments and growth of early Neoproterozoic calcimicrobial reefs: platformal Little Dal Group, northwestern Canada. Precambrian Research 133(3-4): 249-269. https://doi.org/10.1016/j.precamres.2004.05.003

Belperio, A. (1990). Palaeoenvironmental interpretations of the Late Proterozoic Skillogalee Dolomite in the Willouran Ranges, South Australia. The Evolution of a Late Precambrian–Early Palaeozoic Rift Complex: The Adelaide Geosyncline. Geol. Soc. Aust. Spec. Publ 16: 85-104.

Bhattacharya, A. (1997). On the origin of non-tidal flaser bedding in point bar deposits of the river Ajay, Bihar and West Bengal, NE India. Sedimentology 44(6): 973-975. https://doi.org/10.1111/j.1365-3091.1997.tb02172.x

Blum, M. (2001). Importance of falling stage fluvial deposition: Quaternary examples from the Texas Gulf Coastal Plain and Western Europe. Seventh International Conference on Fluvial Sedimentology, Lincoln, August.

Blum, M. D. (1993). Genesis and architecture of incised valley fill sequences: a Late Quaternary example from the Colorado River, Gulf Coastal Plain of Texas: Chapter 10: Recent applications of siliciclastic sequence stratigraphy. M 58: Siliciclastic Sequence Stratigraphy: Recent Developments and Applications: 259-283.

Boggs Jr, S. (2014). Principles of sedimentology and stratigraphy. Pearson Education.

Bold, U., Smith, E. F., Rooney, A. D., Bowring, S. A., Buchwaldt, R., Dudás, F. Ő., Ramezani, J., Crowley, J. L., Schrag, D. P. & Macdonald, F. A. (2016). Neoproterozoic stratigraphy of the Zavkhan terrane of Mongolia: The backbone for Cryogenian and early Ediacaran chemostratigraphic records. American Journal of Science 316(1): 1-63. https://doi.org/10.2475/01.2016.01

Bouma, A. (1964). Turbidites. Developments in Sedimentology, Elsevier. 3: 247-256. https://doi.org/10.1016/S0070-4571(08)70967-1

Bridge, J. S. (2009). Rivers and floodplains: forms, processes, and sedimentary record. John Wiley & Sons.

Brocks, J. J., Jarrett, A. J., Sirantoine, E., Hallmann, C., Hoshino, Y. & Liyanage, T. (2017). The rise of algae in Cryogenian oceans and the emergence of animals. Nature 548(7669): 578-581. https://doi.org/10.1038/nature23457

Buechi, M. W., Frank, S. M., Graf, H. R., Menzies, J. & Anselmetti, F. S. (2017). Subglacial emplacement of tills and meltwater deposits at the base of overdeepened bedrock troughs. Sedimentology 64(3): 658-685. https://doi.org/10.1111/sed.12319

Busfield, M. & Le Heron, D. (2014). Sequencing the Sturtian icehouse: dynamic ice behaviour in South Australia. Journal of the Geological Society 171(3): 443-456. https://doi.org/10.1144/jgs2013-067

Busfield, M. E. & Le Heron, D. P. (2013). Glacitectonic deformation in the Chuos Formation of northern Namibia: implications for Neoproterozoic ice dynamics. Proceedings of the Geologists' Association 124(5): 778-789. https://doi.org/10.1016/j.pgeola.2012.10.005

Busfield, M. E. & Le Heron, D. P. (2016). A Neoproterozoic ice advance sequence, Sperry Wash, California. Sedimentology 63(2): 307-330. https://doi.org/10.1111/sed.12210

Busigny, V., Planavsky, N. J., Goldbaum, E., Lechte, M. A., Feng, L. & Lyons, T. W. (2018). Origin of the Neoproterozoic Fulu iron formation, South China: Insights from iron isotopes and rare earth element patterns. Geochimica et Cosmochimica Acta 242: 123-142. https://doi.org/10.1016/j.gca.2018.09.006

Butterfield, N. J. (2011). Animals and the invention of the Phanerozoic Earth system. Trends in ecology & evolution 26(2): 81-87. https://doi.org/10.1016/j.tree.2010.11.012

Catuneanu, O. (2006). Principles of sequence stratigraphy. Elsevier.

Catuneanu, O. (2017). Sequence stratigraphy: Guidelines for a standard methodology. Stratigraphy & timescales, Elsevier. 2: 1-57. https://doi.org/10.1016/bs.sats.2017.07.003

Catuneanu, O., Abreu, V., Bhattacharya, J. P., Blum, M. D., Dalrymple, R. W., Eriksson, P. G., Fielding, C. R., Fisher, W. L., Galloway, W. E., Gibling, M. R. & Giles, K. A. (2009). Towards the standardization of sequence stratigraphy. Earth-Science Reviews 92(1-2): 1-33. https://doi.org/10.1016/j.earscirev.2008.10.003

Catuneanu, O., Galloway, W. E., Kendall, C. G. St C., Miall, A. D., Posamentier, H. W., Strasser, A. & Tucker M. E. (2011). Sequence stratigraphy: methodology and nomenclature. Newsletters on stratigraphy 44(3): 173-245.

Chakrabarti, A. (2005). Sedimentary structures of tidal flats: A journey from coast to inner estuarine region of eastern India. Journal of earth system science 114(3): 353-368. https://doi.org/10.1007/BF02702954

Chartrand, F. & Brown, A. (1985). The diagenetic origin of stratiform copper mineralization, Coates Lake, Redstone copper belt, NWT, Canada. Economic Geology 80(2): 325-343. https://doi.org/10.2113/gsecongeo.80.2.325

Cheel, R. J. (1990). Horizontal lamination and the sequence of bed phases and stratification under upper-flow-regime conditions. Sedimentology 37(3): 517-529. https://doi.org/10.1111/j.1365-3091.1990.tb00151.x

Cheel, R. J. (1991). Grain fabric in hummocky cross-stratified storm beds; genetic implications. Journal of Sedimentary Research 61(1): 102-110. https://doi.org/10.1306/D426769A-2B26-11D7-8648000102C1865D

Cheel, R. J. & Leckie, D. A. (1993). Hummocky cross-stratification. Sedimentology review 1, Blackwell Scientific Publications Oxford. 1: 103-122.

Chiarella, D., Longhitano, S. G. & Tropeano, M. (2017). Types of mixing and heterogeneities in siliciclastic-carbonate sediments. Marine and Petroleum Geology 88: 617-627. https://doi.org/10.1016/j.marpetgeo.2017.09.010

Coats, R. (1973). Copley, South Australia. Geological Survey of South Australia, Geological Series Explanatory Notes: 54-59.

Collins, A. S., Blades, M. L., Merdith, A. S. & Foden, J. D. (2021). Closure of the Proterozoic Mozambique Ocean was instigated by a late Tonian plate reorganization event.

Communications Earth & Environment 2(1): 1-7. https://doi.org/10.1038/s43247-021-00149-z

Colquhoun, G. P. (1995). Siliciclastic sedimentation on a storm-and tide-influenced shelf and shoreline: the Early Devonian Roxburgh Formation, NE Lachlan Fold Belt, southeastern Australia. Sedimentary Geology 97(1-2): 69-98. https://doi.org/10.1016/0037-0738(94)00142-H

Corkeron, M. L. & Slezak, P. R. (2020). Stromatolite framework builders: ecosystems in a Cryogenian interglacial reef. Australian Journal of Earth Sciences, 67(6), 833-856. https://doi.org/10.1080/08120099.2020.1732464

Counts, J. W., Rarity, F., Ainsworth, R. B., Amos, K. J., Lane, T., Moron, S., Trainor, J., Valenti, C. & Nanson, R. (2016). Sedimentological interpretation of an Ediacaran delta: Bonney Sandstone, South Australia. Australian Journal of Earth Sciences, 63(3), 257-273. https://doi.org/10.1080/08120099.2016.1180322

Counts, J. W. (2017). The Adelaide Rift Complex in the Flinders Ranges: Geologic history, past investigations and relevant analogues. Department of the Premier and Cabinet, South Australia, Adelaide, Report Book 16: 42.

Cox, G. M., Isakson, V., Hoffman, P. F., Gernon, T. M., Schmitz, M. D., Shahin, S., Collins, A. S., Preiss, W., Blades, M. L., Mitchell, R. N. & Nordsvan, A. (2018). South Australian U-Pb zircon (CA-ID-TIMS) age supports globally synchronous Sturtian deglaciation. Precambrian Research 315: 257-263. https://doi.org/10.1016/j.precamres.2018.07.007

Crittenden Jr, M. D., Christie-Blick, N. & Karl Link, P. (1983). Evidence for two pulses of glaciation during the late Proterozoic in northern Utah and southeastern Idaho. Geological Society of America Bulletin 94(4): 437-450. https://doi.org/10.1130/0016-7606(1983)94<437:EFTPOG>2.0.CO;2

Crittenden Jr, M. D., Schaeffer, F. E., Trimble, D. E. & Woodward, L. A. (1971). Nomenclature and correlation of some upper Precambrian and basal Cambrian sequences in western Utah and southeastern Idaho. Geological Society of America Bulletin 82(3): 581-602. https://doi.org/10.1130/0016-7606(1971)82[581:NACOSU]2.0.CO;2

Daidu, F., Yuan, W. & Min, L. (2013). Classifications, sedimentary features and facies associations of tidal flats. Journal of Palaeogeography 2(1): 66-80. https://doi.org/10.3724/SP.J.1261.2013.00018

Donovan, R. N. & Foster, R. J. (1972). Subaqueous shrinkage cracks from the Caithness Flagstone Series (middle Devonian) of northeast Scotland. Journal of Sedimentary Research 42(2): 309-317. https://doi.org/10.1306/74D72531-2B21-11D7-8648000102C1865D

Duke, W. L., Arnott, R. W. C. & Cheel, R. J. (1991). Shelf sandstones and hummocky cross-stratification: new insights on a stormy debate. Geology 19(6): 625-628. https://doi.org/10.1130/0091-7613(1991)019<0625:SSAHCS>2.3.CO;2

Dumas, S. & Arnott, R. (2006). Origin of hummocky and swaley cross-stratification—The controlling influence of unidirectional current strength and aggradation rate. Geology 34(12): 1073-1076. https://doi.org/10.1130/G22930A.1

Dzuynski, S. & Smith, A. J. (1963). Convolute lamination, its origin, preservation, and directional significance. Journal of Sedimentary Research 33(3): 616-627. https://doi.org/10.1306/74D70ED4-2B21-11D7-8648000102C1865D

Eisbacher, G. (1985). Late Proterozoic rifting, glacial sedimentation, and sedimentary cycles in the light of Windermere deposition, western Canada. Palaeogeography, Palaeoclimatology, Palaeoecology 51(1-4): 231-254. https://doi.org/10.1016/0031-0182(85)90087-2

Embry, A. (2009). Practical sequence stratigraphy. Canadian Society of Petroleum Geologists 81: 79.

Eyles, C. H., Eyles, N. & Grey, K. (2007). Palaeoclimate implications from deep drilling of Neoproterozoic strata in the Officer Basin and Adelaide Rift Complex of Australia; a marine record of wet-based glaciers. Palaeogeography, Palaeoclimatology, Palaeoecology 248(3-4): 291-312. https://doi.org/10.1016/j.palaeo.2006.12.008

Fairchild, I. J., Bonnand, P., Davies, T., Fleming, E. J., Grassineau, N., Halverson, G. P., Hambrey, M. J., McMillan, E. M., McKay, E., Parkinson, I. J. & Stevenson, C. T. (2016). The Late Cryogenian warm interval, NE Svalbard: chemostratigraphy and genesis. Precambrian Research 281: 128-154. https://doi.org/10.1016/j.precamres.2016.05.013

Fairchild, I. J., Fleming, E. J., Bao, H., Benn, D. I., Boomer, I., Dublyansky, Y. V., Halverson, G. P., Hambrey, M. J., Hendy, C., McMillan, E. A. & Spötl, C. (2016a). Continental carbonate facies of a Neoproterozoic panglaciation, north-east Svalbard. Sedimentology 63(2): 443-497. https://doi.org/10.1111/sed.12252

Fairchild, I. J. & Kennedy, M. J. (2007). Neoproterozoic glaciation in the Earth System. Journal of the Geological Society 164(5): 895-921. https://doi.org/10.1144/0016-76492006-191

Fairchild, I. J., Spencer, A. M., Ali, D. O., Anderson, R. P., Anderton, R., Boomer, I., Dove, D., Evans, J. D., Hambrey, M. J., Howe, J. & Sawaki, Y. (2017). Tonian-Cryogenian boundary sections of Argyll, Scotland. Precambrian Research. https://doi.org/10.1016/j.precamres.2017.09.020

Fanning, C. M., Ludwig, K. R., Forbes, B. G. & Preiss, W. V. (1986). Single and multiple grain U–Pb zircon analyses for the early Adelaidean Rook Tuff, Willouran Ranges, South Australia. Geological Society of Australia Abstracts.

Fanning, C. M. & Link, P. K. (2004). U-Pb SHRIMP ages of Neoproterozoic (Sturtian) glaciogenic Pocatello Formation, southeastern Idaho. Geology, 32(10), 881-884. https://doi.org/10.1130/G20609.1

Fielding, C. R. (2006). Upper flow regime sheets, lenses and scour fills: extending the range of architectural elements for fluvial sediment bodies. Sedimentary Geology 190(1-4): 227-240. https://doi.org/10.1016/j.sedgeo.2006.05.009

Fleming, E. J., Benn, D. I., Stevenson, C. T., Petronis, M. S., Hambrey, M. J. & Fairchild, I. J. (2016). Glacitectonism, subglacial and glacilacustrine processes during a Neoproterozoic panglaciation, north-east Svalbard. Sedimentology 63(2): 411-442. https://doi.org/10.1111/sed.12251

Flügel, E. (2010). Microfacies of carbonate rocks: analysis, interpretation and application. Springer Science & Business Media.

Foden, J., Elburg, M., Turner, S., Clark, C., Blades, M. L., Cox, G., Collins, A. S., Wolff, K. & George, C. (2020). Cambro-Ordovician magmatism in the Delamerian orogeny: Implications for tectonic development of the southern Gondwanan margin. Gondwana Research 81: 490-521. https://doi.org/10.1016/j.gr.2019.12.006

Foden, J., Elburg, M. A., Dougherty-Page, J. & Burtt, A. (2006). The timing and duration of the Delamerian Orogeny: correlation with the Ross Orogen and implications for Gondwana assembly. The Journal of Geology 114(2): 189-210. https://doi.org/10.1086/499570

Frank, T. D. & Fielding, C. R. (2003). Marine origin for Precambrian, carbonate-hosted magnesite? Geology 31(12): 1101-1104. https://doi.org/10.1130/G20101.1

Frimmel, H. E., Klötzli, U. S. & Siegfried, P. R. (1996). New Pb-Pb single zircon age constraints on the timing of Neoproterozoic glaciation and continental break-up in Namibia. The Journal of Geology 104(4): 459-469. https://doi.org/10.1086/629839

Fromhold, T. & Wallace, M. (2011). Nature and significance of the Neoproterozoic Sturtian–Marinoan Boundary, Northern Adelaide Geosyncline, South Australia. Australian Journal of Earth Sciences 58(6): 599-613. https://doi.org/10.1080/08120099.2011.579624

Fromhold, T. & Wallace, M. (2012). Regional recognition of the Neoproterozoic Sturtian–Marinoan boundary, northern and central Adelaide Geosyncline, South Australia. Australian Journal of Earth Sciences 59(4): 527-546. https://doi.org/10.1080/08120099.2012.673507

Gehling, J. (2000). Environmental interpretation and a sequence stratigraphic framework for the terminal Proterozoic Ediacara Member within the Rawnsley Quartzite, South Australia. Precambrian Research 100(1-3): 65-95. https://doi.org/10.1016/S0301-9268(99)00069-8

Giddings, J. A., Wallace, M. W. & Woon, E. M. (2009). Interglacial carbonates of the Cryogenian Umberatana Group, northern Flinders Ranges, South Australia. Australian Journal of Earth Sciences 56(7): 907-925. https://doi.org/10.1080/08120090903005378

Giddings, J. A. & Wallace, M. W. (2009a). Facies-dependent δ13C variation from a Cryogenian platform margin, South Australia: Evidence for stratified Neoproterozoic oceans? Palaeogeography, Palaeoclimatology, Palaeoecology 271(3-4): 196-214. https://doi.org/10.1016/j.palaeo.2008.10.011

Giddings, J. A. & Wallace, M. W. (2009). Sedimentology and C-isotope geochemistry of the 'Sturtian'cap carbonate, South Australia. Sedimentary Geology 216(1-2): 1-14. https://doi.org/10.1016/j.sedgeo.2009.01.007

Gough, A. (2020). Sedimentary Structures. In D. Alderton, & N. Lancaster (Eds.), Encyclopaedia of Geology Elsevier.

Glover, B. & Winchester, J. (1989). The Grampian group: a major Late Proterozoic clastic sequence in the Central Highlands of Scotland. Journal of the Geological Society 146(1): 85-96. https://doi.org/10.1144/gsjgs.146.1.0085

Gómez-Pérez, I., Fernández-Mendiola, P. A. & García-Mondéjar, J. (1999). Depositional architecture of a rimmed carbonate platform (Albian, Gorbea, western Pyrenees). Sedimentology 46(2): 337-356. https://doi.org/10.1046/j.1365-3091.1999.00217.xr

Grey, K., Hill, A. C. & Calver, C. (2011). Biostratigraphy and stratigraphic subdivision of Cryogenian successions of Australia in a global context. Geological Society, London, Memoirs 36(1): 113-134. https://doi.org/10.1144/M36.8

Grotzinger, J. P. & James, N. P. (2000). Precambrian carbonates: evolution of understanding.

Grotzinger, J. P. (1990). Geochemical model for Proterozoic stromatolite decline. American Journal of Science, v 290-A, p 80-103

Grotzinger, J. P. (1989). Facies and evolution of Precambrian carbonate depositional systems emergence ofthe modern platform archetype. Controls on Carbonate Platform and Basin Development, SEPM Special Publication 44, p. 79-106. https://doi.org/10.2110/pec.89.44.0079

Grotzinger, J. P. (1988). Introduction to Precambrian reefs. Reefs Canada and Adjacent Areas Canadian Society of Petroleum Geologists Memoir 13, p, 30-37

Halverson, G. P., Shen, C., Davies, J. H. & Wu, L. (2022). A Bayesian Approach to Inferring Depositional Ages Applied to a Late Tonian Reference Section in Svalbard. Front. Earth Sci 10: 798739. https://doi.org/10.3389/feart.2022.798739

Halverson, G. P. (2011). Glacial sediments and associated strata of the Polarisbreen Group, northeastern Svalbard. Geological Society, London, Memoirs 36(1): 571-579. http://hdl.handle.net/10214/9436

Halverson, G. P., Kunzmann, M., Strauss, J. V. & Maloof, A. C. (2017). The Tonian-Cryogenian transition in Northeastern Svalbard. Precambrian Research. https://doi.org/10.1016/j.precamres.2017.12.010

Halverson, G. P., Wade, B. P., Hurtgen, M. T. & Barovich, K. M. (2010). Neoproterozoic chemostratigraphy. Precambrian Research, 182(4), 337-350. https://doi.org/10.1016/j.precamres.2010.04.007

Halverson, G. P., Hurtgen, M. T., Porter, S. M. & Collins, A. S. (2009). Neoproterozoic-Cambrian biogeochemical evolution. Developments in Precambrian geology, 16, 351-365. https://doi.org/10.1016/S0166-2635(09)01625-9

Halverson, G. P., Hoffman, P. F., Schrag, D. P., Maloof, A. C. & Rice, A. H. N. (2005). Toward a Neoproterozoic composite carbon-isotope record. GSA bulletin, 117(9-10), 1181-1207. https://doi.org/10.1130/B25630.1

Halverson, G. P., Maloof, A. C. & Hoffman, P. F. (2004). The Marinoan glaciation (Neoproterozoic) in northeast Svalbard. Basin Research 16(3): 297-324. https://doi.org/10.1111/j.1365-2117.2004.00234.x

Hearon IV, T. E., Rowan, M. G., Lawton, T. G., Hannah, P. T. & Giles, K. A. (2015). Geology and tectonics of Neoproterozoic salt diapirs and salt sheets in the eastern Willouran Ranges, South Australia. Basin Research, 27(2), 183–207. https://doi.org/10.1111/bre.12067

Hearon IV, T. E., Rowan, M. G., Giles, K. A., Kernen, R. A., Gannaway, C. E., Lawton, T. F. & Fiduk, J. C. (2015a). Allochthonous salt initiation and advance in the northern Flinders and eastern Willouran ranges, South Australia: Using outcrops to test subsurface-based models from the northern Gulf of Mexico. AAPG Bulletin, 99, 293–331. https://doi.org/10.1306/08111414022

Hill, A. & Walter, M. (2000). Mid-Neoproterozoic (~ 830–750 Ma) isotope stratigraphy of Australia and global correlation. Precambrian Research 100(1-3): 181-211. https://doi.org/10.1016/S0301-9268(99)00074-1

Hoffman, P. (1976). Environmental diversity of Middle Precambrian stromatolites. Developments in Sedimentology, Elsevier. 20: 599-611. https://doi.org/10.1016/S0070-4571(08)71161-0

Hoffman, P. & Halverson, G. (2008). Otvi Group of the Western Northern Platform, the Eastern Kaoko Zone and the Western Northern Margin Zone. The Geology of Namibia, 2008, pp.69-136. https://hdl.handle.net/2440/54299

Hoffman, P. F. & Schrag, D. P. (2002). The snowball Earth hypothesis: testing the limits of global change. Terra nova, 14(3), 129-155. https://doi.org/10.1046/j.1365-3121.2002.00408.x

Hoffman, P. F., Abbot, D. S., Ashkenazy, Y., Benn, D. I., Brocks, J. J., Cohen, P. A., Cox, G. M., Creveling, J. R., Donnadieu, Y., Erwin, D. H. & Fairchild, I. J. (2017). Snowball Earth climate dynamics and Cryogenian geology-geobiology. Science Advances 3(11): e1600983. 10.1126/sciadv.1600983

Hoffman, P. F., Halverson, G. P., Domack, E. W., Maloof, A. C., Swanson-Hysell, N. L. & Cox, G. M. (2012). Cryogenian glaciations on the southern tropical paleomargin of Laurentia (NE Svalbard and East Greenland), and a primary origin for the upper Russøya (Islay) carbon isotope excursion. Precambrian Research 206: 137-158. https://doi.org/10.1016/j.precamres.2012.02.018

Hoffman, P. F., Halverson, G. P., Schrag, D. P., Higgins, J. A., Domack, E. W., Macdonald, F. A., Pruss, S. B., Blättler, C. L., Crockford, P. W., Hodgin, E. B. & Bellefroid, E. J. (2021). Snowballs in Africa: sectioning a long-lived Neoproterozoic carbonate platform and its bathyal foreslope (NW Namibia). Earth-Science Reviews 219: 103616. https://doi.org/10.1016/j.earscirev.2021.103616

Hoffman, P. F., Kaufman, A. J., Halverson, G. P. & Schrag, D. P. (1998). A Neoproterozoic snowball earth. Science 281(5381): 1342-1346. 10.1126/science.281.5381.1342

Hoffman, P. F., Lamothe, K. G., LoBianco, S. J., Hodgskiss, M. S., Bellefroid, E. J., Johnson, B. W., Hodgin, E. B. & Halverson, G. P. (2017a). Sedimentary depocenters on snowball Earth: Case studies from the Sturtian Chuos Formation in northern Namibia. Geosphere 13(3): 811-837. https://doi.org/10.1130/GES01457.1

Hood, A. v.S., Planavsky, N. J., Wallace, M. W. & Wang, X. (2018). The effects of diagenesis on geochemical paleoredox proxies in sedimentary carbonates. Geochimica et Cosmochimica Acta, 232, 265-287. https://doi.org/10.1016/j.gca.2018.04.022

Hood, A. v.S, Wallace, M. W., Reed, C. P., Hoffmann, K. H. & Freyer, E. E. (2015). Enigmatic carbonates of the Ombombo Subgroup, Otavi Fold Belt, Namibia: a prelude to extreme Cryogenian anoxia? Sedimentary Geology 324: 12-31. https://doi.org/10.1016/j.sedgeo.2015.04.007

Hood, A. v.S, Planavsky, N. J., Wallace, M. W., Wang, X., Bellefroid, E. J., Gueguen, B. & Cole, D. B. (2016). Integrated geochemical-petrographic insights from component-selective δ238U of Cryogenian marine carbonates. Geology 44(11): 935-938. https://doi.org/10.1130/G38533.1

Hood, A. v.S. & Wallace, M. W. (2014). Marine cements reveal the structure of an anoxic, ferruginous Neoproterozoic ocean. Journal of the Geological Society 171(6): 741-744. https://doi.org/10.1144/jgs2013-099

Hood, A. v.S. & Wallace, M. W. (2012). Synsedimentary diagenesis in a Cryogenian reef complex: Ubiquitous marine dolomite precipitation. Sedimentary Geology, 255, 56-71. https://doi.org/10.1016/j.sedgeo.2012.02.004

Hood, A. v.S, Wallace, M. W. & Drysdale, R. N. (2011). Neoproterozoic aragonite-dolomite seas? Widespread marine dolomite precipitation in Cryogenian reef complexes. Geology 39(9): 871-874. https://doi.org/10.1130/G32119.1

Howchin, W. (1929). Geology of South Australia, Govt. Printer, Adelaide.

Jahnert, R. J. & Collins, L. B. (2012). Characteristics, distribution and morphogenesis of subtidal microbial systems in Shark Bay, Australia. Marine Geology 303: 115-136. https://doi.org/10.1016/j.margeo.2012.02.009

Jobe, Z. R., Lowe, D. R. & Morris, W. R. (2012). Climbing-ripple successions in turbidite systems: depositional environments, sedimentation rates and accumulation times. Sedimentology 59(3): 867-898. https://doi.org/10.1111/j.1365-3091.2011.01283.x

Jorissen, E. L., de Leeuw, A., van Baak, C. G., Mandic, O., Stoica, M., Abels, H. A. & Krijgsman, W. (2018). Sedimentary architecture and depositional controls of a Pliocene river-dominated delta in the semi-isolated Dacian Basin, Black Sea. Sedimentary Geology 368: 1-23. https://doi.org/10.1016/j.sedgeo.2018.03.001

Kaufman, A. J., Knoll, A. H. & Narbonne, G. M. (1997). Isotopes, ice ages, and terminal Proterozoic earth history. Proceedings of the National Academy of Sciences 94(13): 6600-6605. https://doi.org/10.1073/pnas.94.13.6600

Keeley, J. A., Link, P. K., Fanning, C. M. & Schmitz, M. D. (2013). Pre-to synglacial rift-related volcanism in the Neoproterozoic (Cryogenian) Pocatello Formation, SE Idaho: New SHRIMP and CA-ID-TIMS constraints. Lithosphere 5(1): 128-150. https://doi.org/10.1130/L226.1

Kendall, C. G. S. C. & Warren, J. (1987). A review of the origin and setting of tepees and their associated fabrics. Sedimentology 34(6): 1007-1027.

Kennedy, M. J., Runnegar, B., Prave, A. R., Hoffmann, K. H. & Arthur, M. A. (1998). Two or four Neoproterozoic glaciations? Geology 26(12): 1059-1063. https://doi.org/10.1111/j.1365-3091.1987.tb00590.x

Kirschvink, J. L. (1992). Late Proterozoic low-latitude global glaciation: the snowball Earth. The Proterozoic biosphere : a multidisciplinary study. Cambridge University Press , New York, pp. 51-52. ISBN 9780521366151. https://resolver.caltech.edu/CaltechAUTHORS:20130117-100718783

Kneller, B. (1995). Beyond the turbidite paradigm: physical models for deposition of turbidites and their implications for reservoir prediction. Geological Society, London, Special Publications 94(1): 31-49. https://doi.org/10.1144/GSL.SP.1995.094.01.04

Knoll, A. H., Hayes, J. M., Kaufman, A. J., Swett, K. & Lambert, I. B. (1986). Secular variation in carbon isotope ratios from Upper Proterozoic successions of Svalbard and East Greenland. Nature, 321(6073), 832-838. https://doi.org/10.1038/321832a0

Kunzmann, M., Crombez, V., Catuneanu, O., Blaikie, T. N., Barth, G. & Collins, A. S. (2020). Sequence stratigraphy of the ca. 1730 Ma Wollogorang Formation, McArthur Basin, Australia. Marine and Petroleum Geology 116: 104297. https://doi.org/10.1016/j.marpetgeo.2020.104297

Kunzmann, M., Halverson, G. P., Scott, C., Minarik, W. G. & Wing, B. A. (2015). Geochemistry of Neoproterozoic black shales from Svalbard: Implications for oceanic redox conditions spanning Cryogenian glaciations. Chemical Geology 417: 383-393. https://doi.org/10.1016/j.chemgeo.2015.10.022

Kunzmann, M., Schmid, S., Blaikie, T. N. & Halverson, G. P. (2019). Facies analysis, sequence stratigraphy, and carbon isotope chemostratigraphy of a classic Zn-Pb host succession: The Proterozoic middle McArthur Group, McArthur Basin, Australia. Ore Geology Reviews 106: 150-175. https://doi.org/10.1016/j.oregeorev.2019.01.011

Lamothe, K. G., Hoffman, P. F., Greenman, J. W. & Halverson, G. P. (2019). Stratigraphy and isotope geochemistry of the pre-Sturtian Ugab Subgroup, Otavi/Swakop Group, northwestern Namibia. Precambrian Research 332: 105387. https://doi.org/10.1016/j.precamres.2019.105387

Lan, Z., Li, X. H., Zhang, Q. & Li, Q. L. (2015). Global synchronous initiation of the 2nd episode of Sturtian glaciation: SIMS zircon U–Pb and O isotope evidence from the Jiangkou Group, South China. Precambrian Research 267: 28-38. https://doi.org/10.1016/j.precamres.2015.06.002

Le Heron, D. P., Busfield, M. E. & Kettler, C. (2021). Ice-rafted dropstones in “postglacial” Cryogenian cap carbonates. Geology 49(3): 263-267. https://doi.org/10.1130/G48208.1

Le Heron, D. P. & Busfield, M. E. (2016). Pulsed iceberg delivery driven by Sturtian ice sheet dynamics: An example from Death Valley, California. Sedimentology 63(2): 331-349. https://doi.org/10.1111/sed.12225

Le Heron, D. P., Busfield, M. E. & Collins, A. S. (2014). Bolla Bollana boulder beds: A Neoproterozoic trough mouth fan in South Australia? Sedimentology 61(4): 978-995. https://doi.org/10.1111/sed.12082

Le Heron, D. P., Busfield, M. E. & Kamona, F. (2013). An interglacial on snowball Earth? Dynamic ice behaviour revealed in the Chuos Formation, Namibia. Sedimentology 60(2): 411-427. https://doi.org/10.1111/j.1365-3091.2012.01346.x

Le Heron, D. P., Cox, G., Trundley, A. & Collins, A. (2011). Sea ice− free conditions during the Sturtian glaciation (early Cryogenian), South Australia. Geology 39(1): 31-34. https://doi.org/10.1130/G31547.1

Le Heron, D. P., Cox, G., Trundley, A. & Collins, A. S. (2011a). Two Cryogenian glacial successions compared: Aspects of the Sturt and Elatina sediment records of South Australia. Precambrian Research 186(1-4): 147-168. https://doi.org/10.1016/j.precamres.2011.01.014

Le Heron, D. P., Eyles, N. & Busfield, M. E. (2020). The Laurentian Neoproterozoic Glacial Interval: reappraising the extent and timing of glaciation. Austrian Journal of Earth Sciences 113(1): 59-70. https://doi.org/10.17738/ajes.2020.0004

Lechte, M. & Wallace M. (2016). Sub–ice shelf ironstone deposition during the Neoproterozoic Sturtian glaciation. Geology 44(11): 891-894. https://doi.org/10.1130/G38495.1

Lechte, M. A. & Wallace M. (2015). Sedimentary and tectonic history of the Holowilena Ironstone, a Neoproterozoic iron formation in South Australia. Sedimentary Geology 329: 211-224. https://doi.org/10.1016/j.sedgeo.2015.09.014

Legros, F. (2002). Can dispersive pressure cause inverse grading in grain flows? Journal of Sedimentary Research 72(1): 166-170. https://doi.org/10.1306/041301720166

Lenton, T. M., Boyle, R. A., Poulton, S. W., Shields-Zhou, G. A. & Butterfield, N. J. (2014). Co-evolution of eukaryotes and ocean oxygenation in the Neoproterozoic era. Nature Geoscience 7(4): 257-265. https://doi.org/10.1038/ngeo2108

Lewis, J. P., Weaver, A. J. & Eby, M. (2007). Snowball versus slushball Earth: Dynamic versus nondynamic sea ice?. Journal of Geophysical Research: Oceans, 112(C11). https://doi.org/10.1029/2006JC004037

Li, Z. X., Bogdanova, S., Collins, A. S., Davidson, A., De Waele, B., Ernst, R. E., Fitzsimons, I. C. W., Fuck, R. A., Gladkochub, D. P., Jacobs, J. & Karlstrom, K. E. (2008). Assembly, configuration, and break-up history of Rodinia: a synthesis. Precambrian Research 160(1-2): 179-210. https://doi.org/10.1016/j.precamres.2007.04.021

Li, Z. X., Li, X., Kinny, P., Wang, J., Zhang, S. & Zhou, H. (2003). Geochronology of Neoproterozoic syn-rift magmatism in the Yangtze Craton, South China and correlations with other continents: evidence for a mantle superplume that broke up Rodinia. Precambrian Research 122(1-4): 85-109. https://doi.org/10.1016/S0301-9268(02)00208-5

Link, P. K. & Gostin, V. A. (1981). Facies and paleogeography of Sturtian glacial strata (late Precambrian), South Australia. American Journal of Science 281(4): 353-374. https://doi.org/10.2475/ajs.281.4.353

Link, P. K. (1994). Glacial-marine facies in a continental rift environment: Neoproterozoic rocks of the western United States Cordillera. Earth's Glacial Record, 29-46.

Lloyd, J. C., Blades, M. L., Counts, J. W., Collins, A. S., Amos, K. J., Wade, B. P., Hall, J. W., Hore, S., Ball, A. L., Shahin, S. & Drabsch, M. (2020). Neoproterozoic geochronology and provenance of the Adelaide Superbasin. Precambrian Research 350: 105849. https://doi.org/10.1016/j.precamres.2020.105849

Lloyd, J. C., Collins, A. S., Blades, M. L., Gilbert, S. E. & Amos, K. J. (2022). Early Evolution of the Adelaide Superbasin. Geosciences 12(4): 154. https://doi.org/10.3390/geosciences12040154

Lloyd, J. C., Preiss, W. V., Collins, A. S., Virgo, G. M., Blades, M. L., Gilbert, S. E. & Amos, K. J. (2023). Geochronology and formal stratigraphy of the Sturtian Glaciation in the Adelaide Superbasin. Geological Magazine: 1-24. https://doi. org/10.1017/S0016756823000390

Long, D. & Turner, E. (2013). Formal definition of the Neoproterozoic Mackenzie Mountains Supergroup (Northwest Territories), and formal stratigraphic nomenclature for terrigenous clastic units of the Katherine Group. Geological Survey of Canada.

Lowe, D. R. (1982). Sediment gravity flows; II, Depositional models with special reference to the deposits of high-density turbidity currents. Journal of Sedimentary Research 52(1): 279-297. https://doi.org/10.1306/212F7F31-2B24-11D7-8648000102C1865D

Lund, K., Aleinikoff, J. N., Evans, K. V. & Fanning, C. M. (2003). SHRIMP U-Pb geochronology of Neoproterozoic Windermere Supergroup, central Idaho: Implications for rifting of western Laurentia and synchroneity of Sturtian glacial deposits.

Geological Society of America Bulletin 115(3): 349-372. https://doi.org/10.1130/0016-7606(2003)115<0349:SUPGON>2.0.CO;2

Maciaszek, P., Chomiak, L., Wachocki, R. & Widera, M. (2019). The interpretative significance of ripple-derived sedimentary structures within an upper Neogene fluvial succession of central Poland. Geologos 25. 10.2478/logos-2019-0001

Maloof, A. C., Halverson, G. P., Kirschvink, J. L., Schrag, D. P., Weiss, B. P. & Hoffman, P. F. (2006). Combined paleomagnetic, isotopic, and stratigraphic evidence for true polar wander from the Neoproterozoic Akademikerbreen Group, Svalbard, Norway. Geological Society of America Bulletin 118(9-10): 1099-1124. https://doi.org/10.1130/B25892.1

Mawson, D. & Sprigg, R. (1950). Subdivision of the Adelaide system. Australian Journal of Science 13(3): 69-72.

McKirdy, D. M., Burgess, J. M., Lemon, N. M., Yu, X., Cooper, A. M., Gostin, V. A., Jenkins, R. J. & Both, R. A. (2001). A chemostratigraphic overview of the late Cryogenian interglacial sequence in the Adelaide Fold-Thrust Belt, South Australia. Precambrian Research 106(1-2): 149-186. https://doi.org/10.1016/S0301-9268(00)00130-3

McMahon, Hood, A. v.S. & McIlroy, D. (2017). The origin and occurrence of subaqueous sedimentary cracks. Geological Society, London, Special Publications 448(1): 285-309. https://doi.org/10.1144/SP448.15

Melezhik, V. A., Fallick, A. E., Medvedev, P. V. & Makarikhin, V. V. (2001). Palaeoproterozoic magnesite: lithological and isotopic evidence for playa/sabkha environments. Sedimentology 48(2): 379-397. https://doi.org/10.1046/j.1365-3091.2001.00369.x

Merdith, A. S., Collins, A. S., Williams, S. E., Pisarevsky, S., Foden, J. D., Archibald, D. B., Blades, M. L., Alessio, B. L., Armistead, S., Plavsa, D. & Clark, C. (2017). A full-plate global reconstruction of the Neoproterozoic. Gondwana Research 50: 84-134. https://doi.org/10.1016/j.gr.2017.04.001

Merdith, A. S., Williams, S. E., Brune, S., Collins, A. S. & Müller, R. D. (2019). Rift and plate boundary evolution across two supercontinent cycles. Global and planetary change 173: 1-14. https://doi.org/10.1016/j.gloplacha.2018.11.006

Merdith, A. S., Williams, S. E., Collins, A. S., Tetley, M. G., Mulder, J. A., Blades, M. L., Young, A., Armistead, S. E., Cannon, J., Zahirovic, S. & Müller, R. D. (2021). Extending full-plate tectonic models into deep time: Linking the Neoproterozoic and the Phanerozoic. Earth-Science Reviews 214: 103477. https://doi.org/10.1016/j.earscirev.2020.103477

Middleton, G. V. (1976). Subaqueous sediment transport and deposition by sediment gravity flows. Marine sediment transport and environment management.

Miller, N. R., Avigad, D., Stern, R. J. & Beyth, M. (2011). The Tambien Group, Northern Ethiopia (Tigre). Geological Society, London, Memoirs 36(1): 263-276. https://doi.org/10.1144/M36.21

Miller, N. R., Stern, R. J., Avigad, D., Beyth, M. & Schilman, B. (2009). Cryogenian slate-carbonate sequences of the Tambien Group, Northern Ethiopia (I): Pre-“Sturtian” chemostratigraphy and regional correlations. Precambrian Research 170(3-4): 129-156. https://doi.org/10.1016/j.precamres.2008.12.004

Miller, R. M. (2013). Comparative stratigraphic and geochronological evolution of the Northern Damara Supergroup in Namibia and the Katanga Supergroup in the Lufilian Arc of Central Africa. Geoscience Canada 40(2): 118-140. http://dx.doi.org/10.12789/geocanj.2013.40.007

Millikin, A. E., Strauss, J. V., Halverson, G. P., Bergmann, K. D., Tosca, N. J. & Rooney, A. D. (2022). Calibrating the Russøya excursion in Svalbard, Norway, and implications for Neoproterozoic chronology. Geology. https://doi.org/10.1130/G49593.1

Milton, J. E., Hickey, K. A., Gleeson, S. A. & Friedman, R. M. (2017). New U-Pb constraints on the age of the Little Dal Basalts and Gunbarrel-related volcanism in Rodinia. Precambrian Research 296: 168-180. https://doi.org/10.1016/j.precamres.2017.04.030

Momta, P. S., Omoboh, J. O. & Odigi, M. I. (2015). Sedimentology and depositional environment of D2 sand in part of greater ughelli depobelt, onshore Niger Delta, Nigeria. American Journal of Engineering and Applied Sciences 8(4): 556.

Moretti, M., Soria, J. M., Alfaro, P. & Walsh, N. (2001). Asymmetrical soft-sediment deformation structures triggered by rapid sedimentation in turbiditic deposits (Late Miocene, Guadix Basin, Southern Spain). Facies, 44(1), 283-294. https://doi.org/10.1007/BF02668179

De Mowbray, T. & Visser, M. J. (1984). Reactivation surfaces in subtidal channel deposits, Oosterschelde, southwest Netherlands. Journal of Sedimentary Research, 54(3), 811-824. https://doi.org/10.1306/212F8503-2B24-11D7-8648000102C1865D

Mur, J. P. & Urpinell, M. I. (1987). Magnesite formation in recent playa lakes, Los Monegros, Spain. Geological Society, London, Special Publications 36(1): 119-122. https://doi.org/10.1144/GSL.SP.1987.036.01.10

Narbonne, G. M. & Aitken, J. D. (1995). Neoproterozoic of the mackenzie mountains, Northwestern Canada. Precambrian Research 73(1-4): 101-121. https://doi.org/10.1016/0301-9268(94)00073-Z

Narbonne, G. M., Kaufman, A. J. & Knoll, A. H. (1994). Integrated chemostratigraphy and biostratigraphy of the Windermere Supergroup, northwestern Canada: Implications for Neoproterozoic correlations and the early evolution of animals. Geological Society of America Bulletin 106(10): 1281-1292. https://doi.org/10.1130/0016-7606(1994)106<1281:ICABOT>2.3.CO;2

Nelson, L. L., Ahm, A. S. C., Macdonald, F. A., Higgins, J. A. & Smith, E. F. (2021). Fingerprinting local controls on the Neoproterozoic carbon cycle with the isotopic record of Cryogenian carbonates in the Panamint Range, California. Earth and Planetary Science Letters 566: 116956. https://doi.org/10.1016/j.epsl.2021.116956

Nelson, L. L., Smith, E. F., Hodgin, E. B., Crowley, J. L., Schmitz, M. D. & Macdonald, F. A. (2020). Geochronological constraints on Neoproterozoic rifting and onset of the Marinoan glaciation from the Kingston Peak Formation in Death Valley, California (USA). Geology 48(11): 1083-1087. https://doi.org/10.1130/G47668.1

Nøttvedt, A. & Kreisa, R. (1987). Model for the combined-flow origin of hummocky cross-stratification. Geology 15(4): 357-361. https://doi.org/10.1130/0091-7613(1987)15<357:MFTCOO>2.0.CO;2

O'Connell, B., Wallace, M. W., Hood, A. v.S, Lechte, M. A. & Planavsky, N. J. (2020). Iron-rich carbonate tidal deposits, Angepena Formation, South Australia: A redox-stratified Cryogenian basin. Precambrian Research, 342, 105668. https://doi.org/10.1016/j.precamres.2020.105668

O'Connell, B., Wallace, M. W., Hood, A. v.S, Lechte, M. A. & Mahon, E. M. (2022). Nearshore environments before the evolution of land plants. Precambrian Research 382: 106883. https://doi.org/10.1016/j.precamres.2022.106883

Owen, G. (2003). Load structures: gravity-driven sediment mobilization in the shallow subsurface. Geological Society, London, Special Publications, 216(1), 21-34. https://doi.org/10.1144/GSL.SP.2003.216.01.03

Park, J. K. & Jefferson, C. W. (1991). Magnetic and tectonic history of the Late Proterozoic Upper Little Dal and Coates Lake groups of northwestern Canada. Precambrian Research 52(1-2): 1-35. https://doi.org/10.1016/0301-9268(91)90011-X

Park, Y., Swanson-Hysell, N. L., MacLennan, S. A., Maloof, A. C., Gebreslassie, M., Tremblay, M. M., Schoene, B., Alene, M., Anttila, E. S., Tesema, T. & Haileab, B. (2020). The lead-up to the Sturtian Snowball Earth: Neoproterozoic chemostratigraphy time-calibrated by the Tambien Group of Ethiopia. Bulletin 132(5-6): 1119-1149. https://doi.org/10.1130/B35178.1

Pflueger, F. (1999). Matground structures and redox facies. Palaios 14(1): 25-39. https://doi.org/10.2307/3515359

Plummer, P. & Gostin, V. (1981). Shrinkage cracks; desiccation or synaeresis? Journal of Sedimentary Research 51(4): 1147-1156. https://doi.org/10.1306/212F7E4B-2B24-11D7-8648000102C1865D

Pomar, L. (2001). Types of carbonate platforms: a genetic approach. Basin Research 13(3): 313-334. https://doi.org/10.1046/j.0950-091x.2001.00152.x

Postma, G. (1983). Water escape structures in the context of a depositional model of a mass flow dominated conglomeratic fan-delta (Abrioja Formation, Pliocene, Almeria Basin, SE Spain). Sedimentology, 30(1), 91-103. https://doi.org/10.1111/j.1365-3091.1983.tb00652.x

Powell, C. M., Preiss, W. V., Gatehouse, C. G., Krapez, B. & Li, Z. X. (1994). South Australian record of a Rodinian epicontinental basin and its mid-Neoproterozoic breakup (~ 700 Ma) to form the Palaeo-Pacific Ocean. Tectonophysics 237(3-4): 113-140. https://doi.org/10.1016/0040-1951(94)90250-X

Powell, R. & Domack, G. W. (2002). Modern glaciomarine environments. Modern and past glacial environments, Elsevier: 361-389. https://doi.org/10.1016/B978-075064226-2/50015-5

Powers, D. W. & Holt, R. M. (2000). The salt that wasn't there: Mudflat facies equivalents to halite of the Permian Rustler Formation, southeastern New Mexico. Journal of Sedimentary Research 70(1): 29-36. https://doi.org/10.1306/2DC408FB-0E47-11D7-8643000102C1865D

Preiss, W. (2000). The Adelaide Geosyncline of South Australia and its significance in Neoproterozoic continental reconstruction. Precambrian Research 100(1-3): 21-63. https://doi.org/10.1016/S0301-9268(99)00068-6

Preiss, W. & Cowley, W. (1999). Genetic stratigraphy and revised lithostratigraphic classification of the Burra Group in the Adelaide Geosyncline. MESA Journal 14: 30-40.

Preiss, W., Dyson, I., Reid, P. & Cowley, W. (1998). Revision of lithostratigraphic classification of the Umberatana Group. MESA Journal, 9, 36-42.

Preiss, W. V. (1973). Palaeoecological interpretations of South Australian Precambrian stromatolites. Journal of the Geological Society of Australia 19(4): 501-532. https://doi.org/10.1080/00167617308728820

Preiss, W. V. (1987). The Adelaide Geosyncline: Late Proterozoic stratigraphy, sedimentation, palaeontology and tectonics. Department of Mines and Energy.

Preiss, W. V., Drexel, J. F. & Parker, A. J. (1993). The Geology of South Australia: The Precambrian (Vol. 1): Mines and Energy, South Australia, Geological Survey of South Australia.

Preiss, W. V., Drexel, J. F. & Reid, A. J. (2009). Definition and age of the Kooringa Member of the Skillogalee Dolomite: host for Neoproterozoic (c. 790 Ma) porphyry related copper mineralisation at Burra. MESA Journal, 55, 19-33.

Preiss, W. V., Gostin, V. A., McKirdy, D. M., Ashley, P. M., Williams, G. E. & Schmidt, P. W. (2011). Chapter 69 The glacial succession of Sturtian age in South Australia: the Yudnamutana Subgroup. Geological Society, London, Memoirs, 36(1), 701-712. https://doi.org/10.1144/M36.69

Reading, H. G. (2009). Sedimentary environments: processes, facies and stratigraphy. John Wiley & Sons.

Reading, H. G. & Richards, M. (1994). Turbidite systems in deep-water basin margins classified by grain size and feeder system. AAPG bulletin 78(5): 792-822. https://doi.org/10.1306/A25FE3BF-171B-11D7-8645000102C1865D

Reineck, H. E. & Wunderlich, F. (1968). Classification and origin of flaser and lenticular bedding. Sedimentology 11(1-2): 99-104. https://doi.org/10.1111/j.1365-3091.1968.tb00843.x

Rowan, M. G., Hearon IV, T. E., Kernen, R. A., Giles, K. A., Gannaway-Dalton, C. E., Williams, N. J., Fiduk, J. C., Lawton, T. F., Hannah, P. T. & Fischer, M. P. (2020). A review of allochthonous salt tectonics in the Flinders and Willouran ranges, South Australia. Australian Journal of Earth Sciences 67(6): 787-813. https://doi.org/10.1080/08120099.2018.1553063

Schidlowski, M. (1988). A 3,800-million-year isotopic record of life from carbon in sedimentary rocks. Nature, 333(6171), 313-318. https://doi.org/10.1038/333313a0

Segnit, R. W. (1939). The Pre-Cambrian-Cambrian Succession: The General and Economic Geology of These Systems, in Portions of South Australia. Frank Trigg, government printer. 10.1086/624923

Shanmugam, G. (1997). The Bouma sequence and the turbidite mind set. Earth-Science Reviews 42(4): 201-229. https://doi.org/10.1016/S0012-8252(97)81858-2

Shanmugam, G. (2000). 50 years of the turbidite paradigm (1950s—1990s): deep-water processes and facies models—a critical perspective. Marine and Petroleum Geology 17(2): 285-342. https://doi.org/10.1016/S0264-8172(99)00011-2

Shanmugam, G. (2017). Global case studies of soft-sediment deformation structures (SSDS): Definitions, classifications, advances, origins, and problems. Journal of Palaeogeography, 6(4), 251-320. https://doi.org/10.1016/j.jop.2017.06.004

Shields-Zhou, G. & Och, L. (2011). The case for a Neoproterozoic oxygenation event: geochemical evidence and biological consequences. GSA Today 21(3): 4-11. http://dx.doi.org/10.1130/GSATG102A.1

Shinn, E. A. (1969). Submarine lithification of Holocene carbonate sediments in the Persian Gulf. Sedimentology, 12(1-2), 109-144. https://doi.org/10.1111/j.1365-3091.1969.tb00166.x

Shuster, A. M., Wallace, M. W., van Smeerdijk Hood, A. & Jiang, G. (2018). The Tonian Beck Spring Dolomite: Marine dolomitization in a shallow, anoxic sea. Sedimentary Geology, 368, 83-104. https://doi.org/10.1016/j.sedgeo.2018.03.003

Smith, M., Robertson, S. & Rollin, K. E. (1999). Rift basin architecture and stratigraphical implications for basement-cover relationships in the Neoproterozoic Grampian Group of the Scottish Caledonides. Journal of the Geological Society 156(6): 1163-1173. https://doi.org/10.1144/gsjgs.156.6.1163

Spencer, A. M. & Spencer, M. O. (1972). The Late Precambrian/Lower Cambrian Bonahaven Dolomite of Islay and its stromatolites. Scottish Journal of Geology 8(3): 269-282. https://doi.org/10.1144/sjg08030269

Stephenson, D., Mendum, J. R., Fettes, D. J. & Leslie, A. G. (2013). The Dalradian rocks of Scotland: an introduction. Proceedings of the Geologists' Association 124(1-2): 3-82. https://doi.org/10.1016/j.pgeola.2012.06.002

Stow, D. A. & Mayall, M. (2000). Deep-water sedimentary systems: New models for the 21st century. Marine and Petroleum Geology, 17(2), 125-135. https://doi.org/10.1016/S0264-8172(99)00064-1

Strachan, L. J. (2008). Flow transformations in slumps: a case study from the Waitemata Basin, New Zealand. Sedimentology, 55(5), 1311-1332. https://doi.org/10.1111/j.1365-3091.2007.00947.x

Stromberg, S. G. & Bluck, B. (1998). Turbidite facies, fluid-escape structures and mechanisms of emplacement of the Oligo-Miocene Aljibe Flysch, Gibraltar Arc, Betics, southern Spain. Sedimentary Geology, 115(1-4), 267-288. https://doi.org/10.1016/S0037-0738(97)00096-1

Swanson-Hysell, N. L., Maloof, A. C., Condon, D. J., Jenkin, G. R., Alene, M., Tremblay, M. M., Tesema, T., Rooney, A. D. & Haileab, B. (2015). Stratigraphy and geochronology of the Tambien Group, Ethiopia: Evidence for globally synchronous carbon isotope change in the Neoproterozoic. Geology 43(4): 323-326. https://doi.org/10.1130/G36347.1

Talling, P. J., Masson, D. G., Sumner, E. J. & Malgesini, G. (2012). Subaqueous sediment density flows: Depositional processes and deposit types. Sedimentology 59(7): 1937-2003. https://doi.org/10.1111/j.1365-3091.2012.01353.x

Tanner, P. (1998). Interstratal dewatering origin for polygonal patterns of sand-filled cracks: a case study from late Proterozoic metasediments of Islay, Scotland. Sedimentology 45(1): 71-89. https://doi.org/10.1046/j.1365-3091.1998.00135.x

Thomson, B. P., Coats, R. P., Mirams, R. C., Forbes, B. G., Dalgarno, C. R. & Johnson, J. E. (1964). Precambrian rock groups in the Adelaide Geosyncline: a new subdivision. Quarterly Journal of the Geological Survey of South Australia 9: 1-19.

Thomson, D., Rainbird, R. H. & Dix, G. (2014). Architecture of a Neoproterozoic intracratonic carbonate ramp succession: Wynniatt Formation, Amundsen basin, Arctic Canada. Sedimentary Geology 299: 119-138. https://doi.org/10.1016/j.sedgeo.2013.11.005

Thorie, A., Mukhopadhyay, A., Mazumdar, P. & Banerjee, T. (2020). Characteristics of a Tonian reef rimmed shelf before the onset of Cryogenian: Insights from Neoproterozoic Kunihar Formation, Simla Group, Lesser Himalaya. Marine and Petroleum Geology, 104393. https://doi.org/10.1016/j.marpetgeo.2020.104393

Tinterri, R., Magalhaes, P. M., Tagliaferri, A. & Cunha, R. S. (2016). Convolute laminations and load structures in turbidites as indicators of flow reflections and decelerations against bounding slopes. Examples from the Marnoso-arenacea Formation (northern Italy) and Annot Sandstones (south eastern France). Sedimentary Geology 344: 382-407. https://doi.org/10.1016/j.sedgeo.2016.01.023

Tucker, M. E. (1982). Precambrian dolomites: petrographic and isotopic evidence that they differ from Phanerozoic dolomites. Geology, 10(1), 7-12. https://doi.org/10.1130/0091-7613(1982)10<7:PDPAIE>2.0.CO;2

Tucker, M. (1985). Shallow-marine carbonate facies and facies models. Geological Society, London, Special Publications 18(1): 147-169. https://doi.org/10.1144/GSL.SP.1985.018.01.08

Tucker, M. E. & Wright, V. P. (2009). Carbonate sedimentology. John Wiley & Sons.

Uppill, R. K. (1980). Sedimentology of the late Precambrian Mundallio Subgroup: a clastic-carbonate (Dolomite, Magnesite) sequence in the Mt. Lofty and Flinders Ranges, South Australia. Doctoral dissertation. https://hdl.handle.net/2440/37784

Vakarelov, B. K. & Ainsworth, R. B. (2013). A hierarchical approach to architectural classification in marginal-marine systems: Bridging the gap between sedimentology and sequence stratigraphyHierarchical Marginal-Marine Architectural Classification. AAPG bulletin 97(7): 1121-1161. https://doi.org/10.1306/11011212024

Virgo, G. M., Collins, A. S., Amos, K. J., Farkaš, J., Blades, M. L. & Subarkah, D. (2021). Descending into the "snowball": High resolution sedimentological and geochemical analysis across the Tonian to Cryogenian boundary in South Australia. Precambrian Research 367: 106449. https://doi.org/10.1016/j.precamres.2021.106449

Von der Borch, C. & Lock, D. (1979). Geological significance of Coorong dolomites. Sedimentology 26: 813-824. https://doi.org/10.1111/j.1365-3091.1979.tb00974.x

Wallace, M. W., Hood, A. v.S, Woon, E. M., Giddings, J. A. & Fromhold, T. A. (2015). The Cryogenian Balcanoona reef complexes of the Northern Flinders Ranges: implications for Neoproterozoic ocean chemistry. Palaeogeography, Palaeoclimatology, Palaeoecology 417: 320-336. https://doi.org/10.1016/j.palaeo.2014.09.028

Wang, J. & Li, Z. X. (2001). Sequence stratigraphy and evolution of the Neoproterozoic marginal basins along southeastern Yangtze Craton, South China. Gondwana Research 4(1): 17-26. https://doi.org/10.1016/S1342-937X(05)70651-1

Wanless, H. R., Tedesco, L. P. & Tyrrell, K. M. (1988). Production of subtidal tubular and surficial tempestites by hurricane Kate, Caicos Platform, British West Indies. Journal of Sedimentary Research 58(4): 739-750. https://doi.org/10.1306/212F8E31-2B24-11D7-8648000102C1865D

Warren, J. K. (1990). Sedimentology and mineralogy of dolomitic Coorong lakes, South Australia. Journal of Sedimentary Research 60(6): 843-858. https://doi.org/10.1306/212F929B-2B24-11D7-8648000102C1865D

Wilmsen, M., Berensmeier, M., Fürsich, F. T., Majidifard, M. R. & Schlagintweit, F. (2018). A Late Cretaceous epeiric carbonate platform: the Haftoman Formation of central Iran. Facies 64(2): 11. https://doi.org/10.1007/s10347-018-0523-6

Winsemann, J., Hornung, J. J., Meinsen, J., Asprion, U., Polom, U., Brandes, C., Bußmann, M. & Weber, C. (2009). Anatomy of a subaqueous ice-contact fan and delta complex, Middle Pleistocene, North-west Germany. Sedimentology 56(4): 1041-1076. https://doi.org/10.1111/j.1365-3091.2008.01018.x

Wright, V. (1984). Peritidal carbonate facies models: a review. Geological Journal 19(4): 309-325. https://doi.org/10.1002/gj.3350190402

Yawar, Z. & Schieber, J. (2017). On the origin of silt laminae in laminated shales. Sedimentary Geology 360: 22-34. https://doi.org/10.1016/j.sedgeo.2017.09.001

Young, G. & Gostin, V. (1988). Stratigraphy and sedimentology of Sturtian glacigenic deposits in the western part of the North Flinders Basin, South Australia. Precambrian Research 39(3): 151-170. https://doi.org/10.1016/0301-9268(88)90040-X

Young, G. & Gostin, V. (1990). Sturtian glacial deposition in the vicinity of the Yankaninna Anticline, north Flinders Basin, south Australia. Australian Journal of Earth Sciences 37(4): 447-458. https://doi.org/10.1080/08120099008727944

Young, G. & Gostin, V. (1991). Late Proterozoic (Sturtian) succession of the North Flinders Basin, South Australia: an example of temperate glaciation in an active rift setting. Glacial Marine Sedimentation: Paleoclimatic Significance 261: 207-222.

Yu, W., Algeo, T. J., Zhou, Q., Du, Y. & Wang, P. (2020). Cryogenian cap carbonate models: A review and critical assessment. Palaeogeography, Palaeoclimatology, Palaeoecology, 552, 109727. https://doi.org/10.1016/j.palaeo.2020.109727

Zhang, Q. R., Chu, X. L. & Feng, L. J. (2011). Neoproterozoic glacial records in the Yangtze Region, China. Geological Society, London, Memoirs 36(1): 357-366.

Zhang, S., Jiang, G. & Han, Y. (2008). The age of the Nantuo Formation and Nantuo glaciation in South China. Terra Nova 20(4): 289-294. https://doi.org/10.1111/j.1365-3121.2008.00819.x

Chapter 5: Tonian chemostratigraphic correlation across the northern Flinders Ranges, South Australia

Unsubmitted manuscript prepared for publication:

Georgina M. Virgo, Alan S. Collins, Juraj Farkaš, Morgan L. Blades, Darwinaji Subarkah

Statement of Authorship

Title of Paper	Tonian chemostratigraphic correlation across the northern Flinders Ranges, South Australia
Publication Status	☐ Published ☐ Accepted for Publication ☐ Submitted for Publication ☑ Unpublished and Unsubmitted work written in manuscript style
Publication Details	Virgo, G. M., Collins, A. S., Farkaš, J., Blades, M. L., & Subarkah, D. (2023). Tonian chemostatigraphic correlation across the northern Flinders Ranges, South Australia

Principal Author

Name of Principal Author (Candidate)	Georgina Virgo		
Contribution to the Paper	All manuscript text and figure drafting; data collection, processing and analysis; methodology; interpretations; field investigation		
Overall percentage (%)	85%		
Certification:	This paper reports on original research I conducted during the period of my Higher Degree by Research candidature and is not subject to any obligations or contractual agreements with a third party that would constrain its inclusion in this thesis. I am the primary author of this paper.		
Signature		Date	07/07/2023

Co-Author Contributions

By signing the Statement of Authorship, each author certifies that:

i. the candidate's stated contribution to the publication is accurate (as detailed above);
ii. permission is granted for the candidate in include the publication in the thesis; and
iii. the sum of all co-author contributions is equal to 100% less the candidate's stated contribution.

Name of Co-Author	Alan Collins		
Contribution to the Paper	Reviews and commentary; assistance with methodology and formal analysis		
Signature		Date	07/07/2023

Name of Co-Author	Juraj Farkas		
Contribution to the Paper	Reviews and commentary		
Signature		Date	07/07/2023

Please cut and paste additional co-author panels here as required.

Name of Co-Author	Morgan Blades		
Contribution to the Paper	Reviews and commentary		
Signature		Date	07/07/2023

Name of Co-Author	Darwinaji Subarkah		
Contribution to the Paper	Reviews and commentary; assistance with methodology and formal analysis		
Signature		Date	07/07/2023

5.1 Abstract

The Tonian to Cryogenian transition, from ca. 800 to 650 Ma, represents a dynamic era in Earth's history, where supercontinent reorganisation and fluctuating geochemistry in the atmosphere and ocean facilitated an intense global icehouse known as the Sturtian glaciation. These shifts are recorded in the lithology and geochemistry of Neoproterozoic basins that were developing in response to the rifting of supercontinent Rodinia. The Adelaide Superbasin in South Australia, developed along the margin between Proterozoic Australia-Antarctica and Laurentia and preserves an extensive archive of these Neoproterozoic rocks. Although this basin is geologically significant, it remains enigmatic due to insufficient contemporary research of the sedimentological and geochemical profile at the onset of the Sturtian glaciation.

Here we present isotopic ($\delta^{13}C$, $\delta^{18}O$), elemental and sequence stratigraphic analyses from 140 carbonate samples collected through a total of 8,350 m of measured Tonian and Cryogenian stratigraphy across a 120 km east–west transect in the northern Flinders Ranges, South Australia. These included sites along the western margin of the basin, in the north-central zone, and in the Yankaninna Anticline. The $\delta^{13}C$ record, rare earth element tracers (Ce/Ce* and Eu/Eu*), and sequence stratigraphy were used to interpret fluctuation in productivity, redox and relative water level and sediment input into the basin. These reveal four depositional conditions that exist during deposition of Tonian stratigraphy in the northern Flinders Ranges: (1) a bioproductive, dysoxic inner platform setting that developed during slow transgression; (2) a bioproductive, suboxic outer platform setting that formed during a highstand systems tract; (3) a biologically inactive inner platform setting, associated with continental progradation during a highstand systems tract; (4) and a biologically inactive, anoxic deep subtidal setting that formed during a transgressive systems tract.

These excursions were then compared with the global $\delta^{13}C$ record to assess if the fluctuating depositional setting in this basin can be correlated to coeval basins. The sharp negative $\delta^{13}C$ excursion (-0.2‰ to -7.75‰) at ~735 Ma that is recorded within the top of the Myrtle Springs Formation in Yankaninna appears to correspond to a major global excursion that is recorded from rocks in Ethiopia, Canada, Scotland and Svalbard (Norway). However, the other excursions recorded from Tonian stratigraphy in the northern Flinders Ranges are not easily correlated to other Neoproterozoic basins. The disparity of the geochemical record in this study, and interpreted restriction of this part of the basin from the global ocean for much of its history, indicates that many of these excursions are likely related to local variations in tectonics, sediment input and climate rather than representative of global fluctuations during the Tonian. Consequently, global signals can only be resolved when these local effects are accounted for.

5.2 Introduction

Neoproterozoic basins, which developed between ca. 1000 to 539 Ma, are archives for the physiochemical changes that occurred during this unique time in Earth's past. These changes include tectonic reorganisation associated with the break-up of supercontinent Rodinia and amalgamation of Gondwana (Li et al., 2008; Merdith et al., 2017; 2019; 2021; Collins et al., 2021); significant changes to the Earth's oxygenation, both in the atmosphere and oceans

(Shields-Zhou & Och, 2011); the biological evolution from a prokaryote- to eukaryote-dominated organisms (Butterfield, 2011; Lenton et al., 2014; Brocks et al., 2017); and an intense icehouse where glaciers extended to low palaeolatitudes (Kirschvink, 1992; Hoffman et al., 1998; 2017). These fluctuations resulted in diverse depositional conditions, including warm, oxygen rich seas, and arid, barren, ice-covered continents. The rocks from these varied environments preserve geochemical signatures that offer a glimpse into how these changes might have occurred.

The Adelaide Superbasin in South Australia offers a thick repository of Neoproterozoic sedimentary rocks that record a suite of depositional environments and provides geochemical insights into the fluctuation in water column chemistry during this unique time in Earth's history. Much of the previous research has focused on particular formations or stratigraphic horizons (e.g. Sumartojo & Gostin, 1976; Belperio, 1990; Hill & Walter, 2000; McKirdy et al., 2001; Frank & Fielding, 2003; Giddings & Wallace, 2009; 2009a; Grey et al., 2011; Hood et al., 2011; 2016; 2018; Hood & Wallace, 2012; 2014; 2015; Lechte & Wallace, 2016; Wallace et al., 2019; O'Connell et al., 2020), while others provide datasets for thick stratigraphic successions or across broad regions (e.g. Barovich & Foden, 2000; Walter et al., 2000; Halverson et al., 2005; Swanson-Hysell et al., 2010; Cox et al., 2016; Wallace et al., 2017; Ward et al., 2019; Virgo et al., 2021). These studies have provided a foundation for our understanding of the palaeoenvironmental conditions through the Neoproterozoic in South Australia. With that said, the disadvantage of the high-resolution studies is the lack of spatial continuity, and the drawback for the broad studies is the lack of temporal resolution. Further, they have not captured the detailed chemostratigraphic architecture across the basin, especially with regard to the sequence stratigraphic changes and how that correlates with other basins globally.

The chemostratigraphy of Neoproterozoic rocks have been studied extensively at many locations across the globe, including those in Ethiopia (Miller et al., 2009; Swanson-Hysell et al., 2015; Park et al., 2020), Svalbard (Norway; Halverson et al., 2007; 2017; Cox et al., 2016), Scotland (Sawaki et al., 2010; Fairchild et al., 2017), Siberia (Bartley et al., 2001; Kuznetsov et al., 2006; Cox et al., 2016), Canada (Asmerom et al., 1991; Halverson et al., 2006; 2007; Jones et al., 2010; Macdonald et al., 2010; Rooney et al., 2014; Cox et al., 2016), Mongolia (Brasier et al., 1996; Bold et al., 2016), Namibia (Halverson et al., 2005; 2007), and Greenland (Cox et al., 2016). These studies have been compiled by Park et al. (2020), which provides a framework for the key trends in the global C isotope record. The comparison of the chemostratigraphy in South Australia presents an opportunity to assess if variations in geochemical condition in South Australia are reflective of tectonic, eustatic and/or climate fluctuations on a global scale.

This study uses elemental geochemistry, C and O isotopic geochemistry of carbonates and sequence stratigraphy from a number of locations across the northern Flinders Ranges to construct a chemostratigraphic framework across the basin during the lead up to the Sturtian glaciation. Samples from carbonate lithologies were collected throughout the successions and screened for indicators of diagenesis, detrital input and secondary overprints. Once samples'

geochemical/isotope signatures were deemed primary, they were investigated for bioproductivity and redox conditions using proxies such as C isotopes and REE tracers, respectively. These datasets were then evaluated against sequence stratigraphy to better constrain how the geochemistry was impacted by fluctuations in tectonic regimes, eustacy and climate. In doing so, we provide a framework for how the Tonian palaeoenvironments responded to geochemical changes through time and across the basin. Further, this was compared to the global chemostratigraphic record to understand if these changes in South Australia are local, or representative of global geochemical variations in the lead up to the Sturtian glaciation.

5.3 Geological Setting

The Adelaide Rift Complex is a ~750 km north–south trending basin that lies within the greater Adelaide Superbasin (Lloyd et al., 2020). This Superbasin developed as the result of rifting between Laurentia and Australia-East Antarctica during the breakup of supercontinent Rodinia, eventually forming an aulocogen in the north that filled with a thick succession of Neoproterozoic sediment (Merdith et al., 2019; Lloyd et al., 2022). At the start of sedimentation during the Tonian, surrounding rift shoulders provided the material that was transported into the basin, particularly along a NW–SE rift valley that became the Willouran Trough (Preiss, 2000; Lloyd et al., 2020). The start of the Cryogenian is represented by the Sturtian glaciation, which saw a transition to a more passive margin and widespread erosion across the basin (Lloyd et al., 2022). The end of the Cryogenian was marked by a second period of rifting during the Ediacaran, where the reactivated rift shoulders and magmatism provided significant material into the basin once more (Lloyd et al., 2020). The Delamerian Orogeny at approximately 500 Ma terminated deposition and resulted in uplift of the basin (Foden et al., 2006; 2020). This Palaeozoic orogeny was followed by Cenozoic orogenesis that exposed these Neoproterozoic rocks in the modern-day Flinders Ranges and Mount Lofty Ranges (Figure 1).

Lithostratigraphically, the Neoproterozoic rocks in the Adelaide Superbasin can be divided into four groups: Callanna, Burra, Umberatana and Wilpena (Figure 1; Thomson et al., 1964; Preiss et al., 1998; Preiss & Cowley, 1999; Preiss, 2000; Preiss et al., 2011; Lloyd et al., 2020). The Tonian period is represented by deposition of the Callanna and Burra group rocks, while the Cryogenian is characterised by the Umberatana Group (Figure 1; Mawson & Sprigg, 1950; Thomson et al., 1964).

5.4 Methods

5.4.1 Field sites

Six field locations located across a 120 km west–east transect were selected across the northern Flinders Ranges, including Termination Hill, Copley, Mount Lyndhurst, and Yankaninna (Figure 1). The sites were chosen based on geological mapping, site accessibility, spatial distribution across the basin, and stratigraphic thickness variability. The coordinates for the locations and through the logged sections were measured using a handheld GPS and the sedimentary log was measured using a tape measure at approximately one metre resolution.

Observations of grain size, sedimentary structures, bedding thicknesses and palaeocurrent directions were recorded for the sedimentary log.

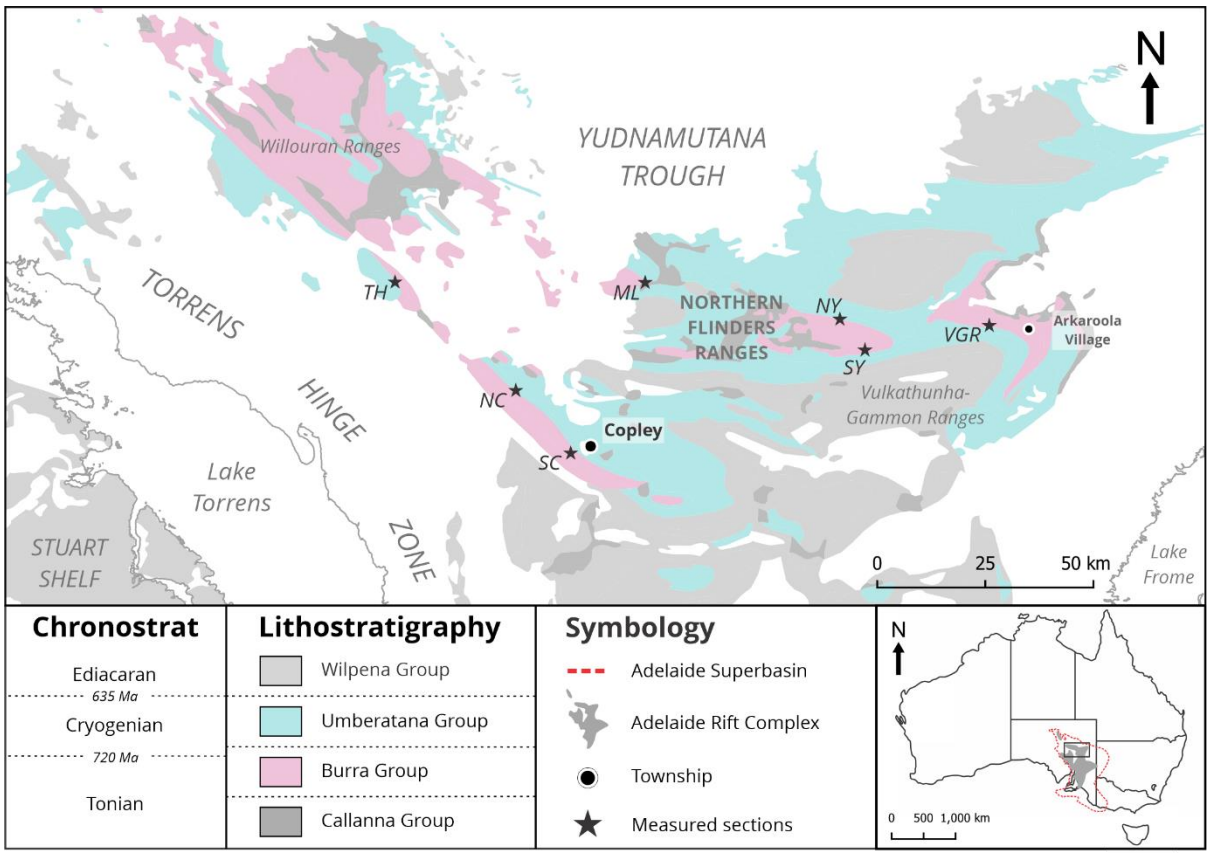

Figure 1: (a) Geological map of Neoproterozoic lithostratigraphy and locations of measured sites across the northern Flinders Ranges, South Australia. Insert shows position of Adelaide Rift Complex within Australia. TH = Termination Hill, NC = North Copley, SC = South Copley, ML = Mount Lyndhurst, NY = North Yankaninna, SY = South Yankaninna, VGR = Vulkathunha-Gammon Ranges.

5.4.2 Sample selection

Tonian and Cryogenian carbonate successions were sampled at locations across the northern Flinders Ranges. The selection criteria for these sections were based on previous geological mapping, site accessibility, and geographic spread. Further, sample selection was based on outcrop exposure, quality and lithology. Well-exposed, thick carbonate successions that appeared to be unaffected by secondary alteration and weathering were sampled at a high resolution (20–40 cm intervals), and lower quality outcrops were sampled at lower resolution (1–2 m scale). Detailed sedimentological descriptions of facies, their interpreted depositional environments and sequence stratigraphic changes, as well as correlation across the northern Flinders Ranges are discussed in Chapter 4 of this thesis.

5.4.3 Major and trace elemental analysis

Concentrations for major, trace and rare earth elements (REE) in carbonate samples were measured via a laser ablation inductive coupled plasma mass spectrometry (LA-ICP-MS) using a spot analysis approach, following Rieger et al. (2022). This was carried out on an Agilent 7900 quadrupole ICP-MS in Adelaide Microscopy, University of Adelaide, where standards NIST612 and NIST614 were used. A 'sample-standard bracketing' approach with a ratio of 20 to 4 was used in this study, which consisted of 20 sample spots followed by 4 spots of standards. An ablation spot size of 110 microns was selected, with 30 seconds of background followed by 40 seconds of ablation during data collection.

A leaching approach followed by solution-based ICP-MS was also applied for a select number of samples to quality control data obtained by LA-ICP-MS. For such solution work, carbonate samples were micro-drilled along laminae, to target the carbonate matrix. The resultant rock powder was washed with ammonium acetate to remove exchangeable cations associated with detrital and clay phases. The powder was further leached twice with acetic acid to extract the carbonate-bearing fraction and minimise non-marine and secondary phases from bulk sediment (Halverson et al., 2010, Kuznetsov et al., 2010; Liu et al., 2014). Next, the supernatant was digested in nitric acid for elemental analysis using an Aligent 8900x triple quad (QQQ) Inductively Coupled Mass Spectrometry (ICP-MS/MS) instrument in Adelaide Microscopy at the University of Adelaide. Typical accuracy and precision on elemental concentration data are within 5% (2 SD).

5.4.4 C and O isotope analysis

Isotopic analysis of $\delta^{13}C$ and $\delta^{18}O$ in carbonate samples followed the procedure from Spötl & Vennemann (2003) and Cox et al., (2016). Briefly, a portion of the micro-drilled rock powder for each sample (i.e. leftover powder from the elemental analysis) was weighed into a glass septa vial. It was then cleansed with He and purged with phosphoric acid. This released CO_2, which could then be collected through cryogenic extraction and analysed for C and O isotopes. Isotopic ratios were measured using a Nu Perspective Dual-Inlet Isotopic Ratio Mass Spectrometer (DI-IRMS) and corrected for fractionation effects using an in-house reference gas. The C and O isotopic ratios were expressed as conventional delta values ($\delta^{13}C$ and $\delta^{18}O$) in per mil (‰), relative to Vienna Pee Dee Belemnite (VPDB) standard, with typical uncertainties on delta values of ~0.05‰ (1 SD).

5.5 Results

5.5.1 Screening for secondary alteration

5.5.1.1 Detrital components

To screen for the contribution by detrital phases, REE parameters were measured against the concentration of Zr in the studied carbonate samples (Figure 2a; Frimmel, 2009; Tostevin et al., 2016; Wallace et al., 2017; Ward et al., 2019). The covariance between Zr and Ce/Ce* and Eu/Eu*, as well as the absolute concentration of Zr, were taken into consideration when marking a particular sample 'contaminated' by detrital components and excluding it from further discussion. From the six sections, a statistically significant but weak correlation trend

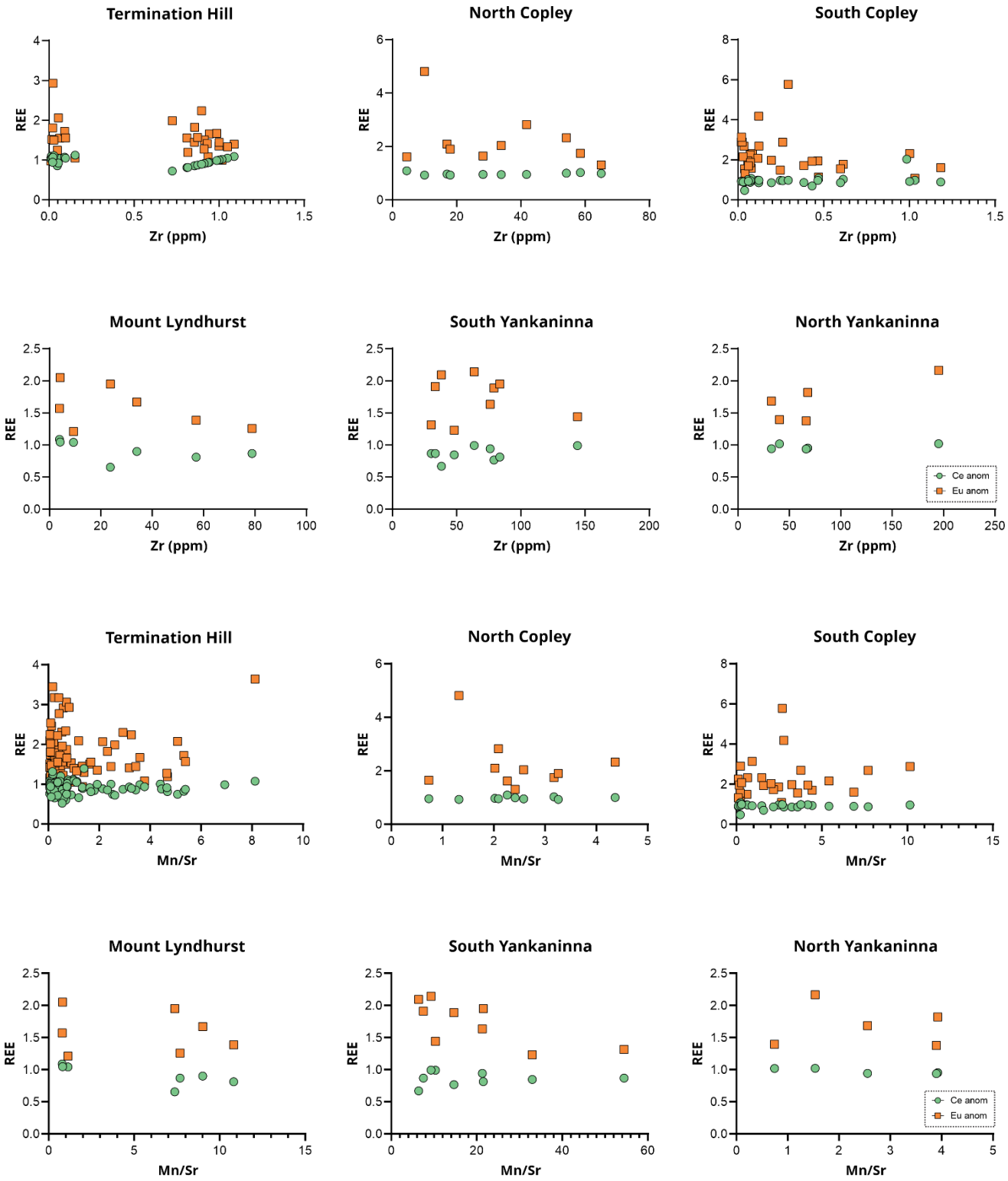

Figure 2: Screening plots for carbonate samples at measured sections across northern Flinders Ranges. REE values are normalised to PAAS (Nance & Taylor, 1976). Ce/Ce* = cerium anomaly. Eu/Eu* = europium anomaly. REE tracers Ce/Ce* (green) and Eu/Eu* (orange). **(a)** Detrital contamination plots, REE tracers were screened against Zr (ppm), where data with anomalously large Zr concentrations were excluded. **(b)** Diagenetic alteration plots, REE tracers were screened against Mn/Sr, where data with anomalously large Mn/Sr ratios or data with a strong covariance were excluded.

is detected between Zr and Ce/Ce* in the Termination Hill section (R^2 = 0.1632, p-value = 0.0242) and between Zr and Eu/Eu* in the South Copley section (R^2 = 0.2429, p-value = 0.0014). This is after excluding a sample with anomalously high REE concentrations (Figure 2a). The Termination Hill section appears to have two populations of Zr concentrations.

Analyses with relatively large Zr concentrations (0.72–1.01 ppm) show a strong covariance between Zr and Ce/Ce* (Figure 2a). Although the correlation between these data sets is strongest at the Termination Hill and South Copley sections, the absolute concentration of Zr at these locations is on average 10 times lower than for the other measured sections (Figure 2a). This may be the result of the preparation of samples, which were systematically leached to isolate carbonate phases and remove detrital contamination (Virgo et al., 2021, and references therein). With that said, there are several samples from the other sections that have anomalously high Zr concentrations that are removed from further interpretation of primary setting as they are likely contaminated by detrital components.

5.5.1.2 Diagenetic alteration

To assess the geochemical overprint from secondary diagenetic or meteoric fluids, the Mn/Sr ratios in carbonate samples was analysed (Figure 2b; Brand & Veizer, 1980; Banner & Hanson, 1990; Kaufman & Knoll, 1995; Bartley et al., 2001; Peral et al., 2007; Frimmel, 2010, Hua et al., 2013). As the Mn/Sr values may be overall higher in Precambrian carbonates due to the solubility of Mn in ancient sweater, the covariance between Mn/Sr and Ce/Ce* and Eu/Eu* was also considered rather than relying on specific thresholds (Hood & Wallace, 2015; Wei et al., 2019). The South Copley and Mount Lyndhurst sections show a statistically significant correlation between Mn/Sr and Ce/Ce* (R^2 = 0.1585, p-value = 0.0133 and R^2 = 0.6251, p-value = 0.0343), while the South Yankaninna section has a significant correlation between Mn/Sr and Eu/Eu* (R^2 = 0.5137, p-value = 0.0298; Figure 2b). The covariance in the South Copley section is formation dependant, where only values in the Skillogalee Dolomite are correlated (R^2 = 0.6058, p-value = 0.0010), however this apparent correlation is anchored by one sample with high Mn/Sr (7.710) that skews the data (Figure 2b). As the Mn/Sr and Ce/Ce* no longer covary if this sample is removed, it is not included in further discussions. The Mount Lyndhurst section constrains two data groups, with the Mn/Sr enriched values possibly indicating alteration from secondary processes (Figure 2b). Conversely, the South Yankaninna section is not defined by distinct populations, but instead it has much larger Mn/Sr ratios compared to the other sections (Figure 2b). There are two samples that have Mn/Sr ratios above 30 and anchor the statistically significant correlation between Mn/Sr and Eu/Eu* (Figure 2b). Further, there is an anomalous value in the Termination Hill section that has considerably larger Mn/Sr (8.12) and Eu/Eu* (3.64) values relative to the other samples from this location (Figure 2b). Consequently, these three samples are excluded from further discussion in this study.

As C and O isotopic systems in carbonates are not affected by detrital input, only the interference from secondary diagenetic or meteoric processes are assessed here (Figure 3). There is a significant correlation between $\delta^{13}C$ and $\delta^{18}O$ data in both the North and South Copley sections (Figure 3). The North Copley sections shows a very strong covariance (R^2 = 0.4490, p-value = 0.0009), however, it is paired by reasonably low Mn/Sr values values (<4.5;

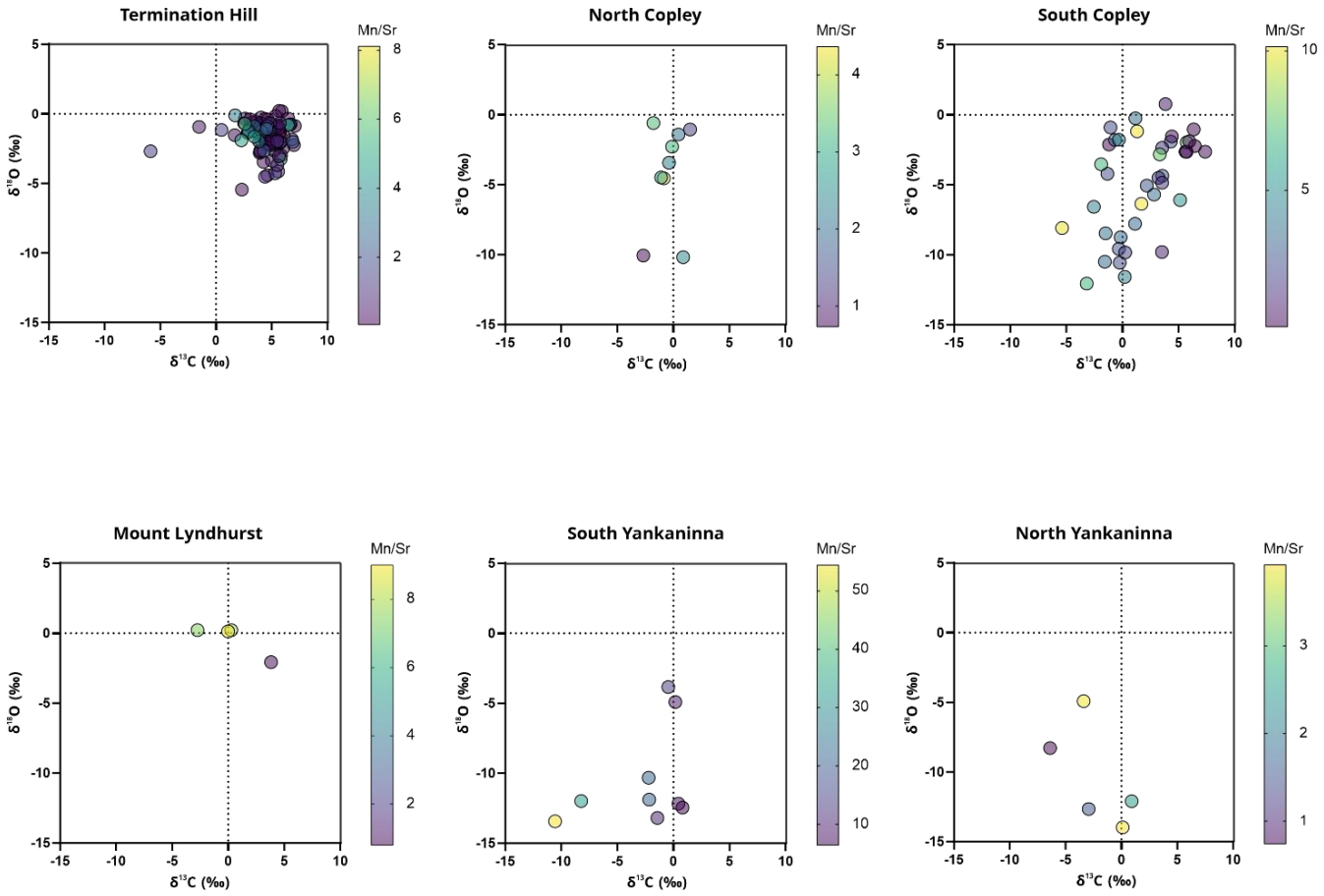

Figure 3: δ^{13}C and δ^{18}O cross plot at measured sections across northern Flinders Ranges. Overlain with Mn/Sr data (represented by colour gradient) that tests for secondary alteration from diagenetic processes. δ^{13}C and δ^{18}O are calibrated to Vienna Pee Dee Belemnite (VPDB). Mn/Sr values are normalised to PASS (Nance & Taylor, 1976).

Figure 3). This could be due to the limited elemental data relative to the isotopic data or resetting of the isotopic systems from another secondary alteration process. There is a less strong, but still statistically significant, correlation (R^2 = 0.2068, p-value = <0.0001) in the South Copley section (Figure 3), which largely corresponds to particular formations. Specifically, the pre-glacial Skillogalee Dolomite does not show a significant correlation between δ^{13}C and δ^{18}O, while the Myrtle Springs Formation at the top of the pre-glacial succession and the post-glacial Tapley Hill Formation show a statistically significant correlation (R^2 = 0.1243, p-value = 0.0140 and R^2 = 0.4036, p-value = <0.0001) that skews the overall data. The strong correlation in the Tapley Hill Formation indicates that the isotopic geochemistry is likely reset and therefore, these samples will not be discussed further in terms of palaeo-seawater signatures. However, the covariance in the Myrtle Springs Formation is weak and is largely anchored by a value with an elevated Mn/Sr ratio (9.94). If this value is excluded, the C and O isotopic systems are no longer statistically correlated. For this reason, this sample will be excluded from interpretations of depositional setting. Further, a sample in the South Yankaninna section that has Mn/Sr of 54.44 and very negative δ^{13}C and δ^{18}O will

also not be discussed further due to its anomalous geochemical signature relative to the other samples from that section (Figure 3).

5.5.2 Stratigraphic trends in isotopic data

5.5.2.1 Western margin

From Figure 4, the lower portion of the Termination Hill section is marked by deposition of the Skillogalee Dolomite. The $\delta^{13}C$ from the base of the measured section shows overall consistent, positive values, ranging from 3.98‰ to 7.06‰. Up-section, a large negative excursion of -9.70‰ is recorded from dolostone samples that are deposited in a succession that is associated with the magnesite ($MgCO_3$) lithologies (Figure 4). The $\delta^{13}C$ record sharply recovers back to positive values (5.66‰), recorded from primarily conglomeratic magnesite samples (Figure 4). This is followed by a trend where values decrease up-section from 6.98‰ to 1.66‰ across an approximately 80 m interval (Figure 4). The top of the formation is marked by the return of heavy $\delta^{13}C$ values (~4.58‰), recorded in dominantly magnesite mud samples (Figure 4). Values from the overlying Myrtle Springs Formation demonstrate an overall negative trend up-section (5.63‰ to 1.70‰; Figure 4). The trend appears to be weaker in the base of the formation (-0.77‰) and becomes sharper towards the top (-4.03‰), coinciding with increased deposition of microbialites and clastic material (Figure 4).

The Myrtle Springs Formation in the base of the measured North Copley section is represented by an overall increase in $\delta^{13}C$ up-section, from -6.32‰ to 3.82‰ (Figure 4). The basal samples that record the heaviest values were recorded from dolostone samples that are thinly (0.5–1 m) interbedded with fine clastics (Figure 4). The lighter values up-section were measured from dolostone samples with frequent desiccation cracks. The $\delta^{13}C$ in the very top of the formation is characterised by a slightly negative trend from 3.82‰ to -1.79‰ and coincides with deposition from dolostone to layered microbialite samples (Figure 4).

Like at Termination Hill, the samples from the base of the Skillogalee Dolomite at South Copley are characterised by generally positive $\delta^{13}C$ values (2.38‰ to 7.49‰; Figure 4). This is overlain by an interval of layered microbialite, magnesite and silt with soft sediment deformation that records a negative excursion of -7.56‰ (Figure 4). These isotopically light $\delta^{13}C$ values recover back to ~3.84‰ and remain consistent throughout the rest of the Skillogalee Dolomite deposition (Figure 4). The transition to the overlying Myrtle Springs Formation is marked by a negative excursion of -8.15‰ (Figure 4). These values increase up-section from -3.02‰ to 1.12‰ and coincide with deposition from siltstone dominated lithologies to fine-grained dolostones (Figure 4). This is followed by a second negative excursion of -4.64‰, which is associated with dolomitic siltstone lithologies (Figure 4). The top of the formation is marked by a return to positive $\delta^{13}C$, which slightly increase up-section from 1.68‰ to 3.71‰ and coincides with deposition from laminated dolostone to stromatolitic carbonates (Figure 4). An anomalously heavy (7.49‰) $\delta^{13}C$ value is recorded from a layered microbialite sample at a stratigraphic depth of 1790 m (Figure 4).

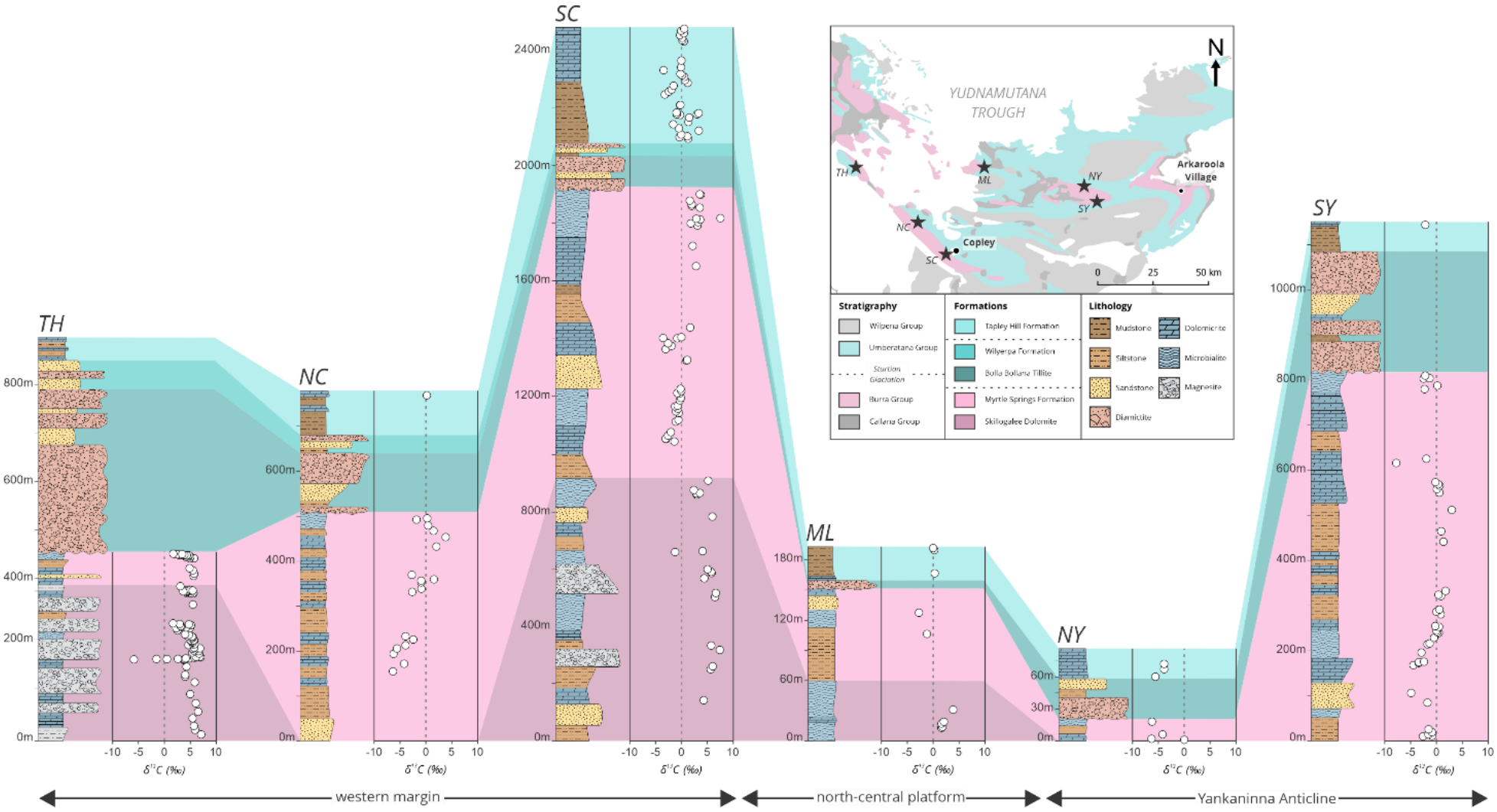

Figure 4: Generalised sedimentary logs and $\delta^{13}C$ values through Tonian–Cryogenian sections across the northern Flinders Ranges, South Australia. Coloured panels indicate correlation of stratigraphic formations between sections. $\delta^{13}C$ values are calibrated to Vienna Pee Dee Belemnite (VPDB). TH = Termination Hill, NC = North Copley, SC = South Copley, ML = Mount Lyndhurst, NY = North Yankaninna, SY = South Yankaninna, VGR = Vulkathunha-Gammon Ranges. Insert shows location of measured sections

5.5.2.2 North-central platform

Samples from the Skillogalee Dolomite at Mount Lyndhurst are represented by a positive $\delta^{13}C$ trend up-section (1.56‰ to 3.82‰; Figure 4). These samples are recorded from samples that transition from stromatolitic buildups to layered microbialites. Although there are only two samples with $\delta^{13}C$ values in the overlying Myrtle Springs Formation, they become slightly heavier up-section from -1.22‰ to -2.75‰ (Figure 4).

5.5.2.3 Yankaninna anticline

Due to the stratigraphically thin measured section at North Yankaninna, there are a limited number of samples. In the Myrtle Springs, the $\delta^{13}C$ record swings from less negative to more negative values up-section; -0.02‰, 6.32‰, -4.18‰, to -6.23‰ (Figure 4). The heavier samples are associated with dolostone lithologies and the lighter samples with layered microbialite lithologies.

At South Yankaninna, the base of the measured section in the Myrtle Springs Formation is characterised by a negative $\delta^{13}C$ excursion of -5.75‰, where values become increasingly negative from -0.86‰ to -4.89‰ (Figure 4). This coincides with the deposition of dolomitic silt with shrinkage cracks to layered microbialites with desiccation cracks (Figure 4). This is followed by a positive $\delta^{13}C$ trend up-section from -4.46‰ in coarse-grained dolostone samples to 2.94‰ in dolomitic siltstone samples. A second and more significant $\delta^{13}C$ negative excursion of -7.75‰ is recorded from a succession dominated by dolostone lithologies (Figure 4). The top of the Myrtle Springs Formation is represented by the return of heavier $\delta^{13}C$ values (-1.62‰) and is marked by deposition of layered microbialite lithofacies (Figure 4

5.6 Discussion

5.6.1 Geochemical proxies and their implications on depositional setting

The $\delta^{13}C$ isotope signature in marine carbonates and organic-rich shales has widely been used as a measure for the bioproductivity (i.e. burial of organic carbon) in past oceanic environments (Knoll et al., 1986; Schidlowski, 1988). This measure is calculated through the C isotope composition of the dissolved inorganic carbon (DIC) pool of a water column, where biological processes and subsequent burial of organic carbon leads to preferential up-take of lighter ^{12}C isotope from the seawater DIC pool, thus enriching the water column (and by inference precipitated marine carbonates) in heavier ^{13}C (Kump & Arthur, 1999; Bastow et al., 2002; Frimmel, 2010). The resultant $\delta^{13}C_{carb}$ trends towards heavier values is thus represented by positive excursions in the marine carbonate $\delta^{13}C$ record. Conversely, negative excursions in the marine carbonate $\delta^{13}C$ record results from the inputs of ^{12}C into the water column, which are associated with decreased burial of organic carbon that is commonly due to remineralisation of isotopically light C sourced from organic matter in the deep ocean (Tziperman et al., 2011; Sarmiento et al., 2013). Another cause for shifts to lower marine $\delta^{13}C$ values is the shutdown of biological productivity in the ocean and/or changes in continental siliciclastic weathering fluxes (Krencker et al., 2020; Andríeu et al., 2022), and associated nutrient inputs, turbidity and salinity changes from weathered and dissolved continental sources (Hallock & Schlager,

1986; Cohen et al., 2004; Follmi et al., 2006; Halfar et al., 2006; Godet et al., 2013; Hermoso & Pellenard, 2014; Them et al., 2017; Deconinck et al., 2020).

In addition to productivity, the redox state of marine palaeo-depositional environments can be measured through redox-sensitive REE tracers. The most common of these is the Ce anomaly (Ce/Ce*), which is particularly sensitive to changes in oxygenation. Due to the low solubility of the oxidised form of cerium, Ce^{4+}, it is adsorbed onto Mn-oxides and depleted in oxygen-rich water columns, leading to more negative Ce/Ce* values (German & Elderfield, 1990; Ling et al., 2013; Wallace et al., 2017; Shuster et al., 2018; Liu et al., 2019). The Eu anomaly (Eu/Eu*) is another REE tracer that can be used to assess redox, as well as inputs from hydrothermal and continental sources. Contrary to cerium, europium has a more reduced state, Eu^{2+}, which is highly compatible with feldspar due to substitution of Eu^{2+} for double-charged alkaline earth metals such as Ca^{2+}. Thus, in anoxic waters that preferentially retain Eu (Bau, 1991; Hood & Wallace, 2015), the input from weathered feldspar-rich continental rocks (Verdel et al., 2018), or hydrothermal fluids with abundant leached Eu-rich minerals (Derry & Jacobsen, 1990; Olivarez & Owen, 1991), will lead to positive Eu/Eu* values.

Both the productivity and redox state of the ancient water column can be influenced by changes in relative water depth and material input fluxes into the system. The latter two parameters can be partly constrained through sequence stratigraphy, which results from the interaction between accommodation space and sediment supply in a basin (Catuneanu, 2006; 2017; Catuneanu et al., 2009; 2011; Embry, 2009; Vakarelov & Ainsworth, 2013; Kunzmann et al., 2019; 2020). The three factors that control these variations are tectonics (subsidence versus uplift), eustacy and climate (Catunaenu, 2006).

5.6.2 Relationship between productivity, redox and sequence stratigraphy

5.6.2.1 Positive $\delta^{13}C$ values - scenario 1

The preservation of heavy $\delta^{13}C$ values in Neoproterozoic marine carbonates exposed in the northern Flinders Ranges are often recorded from intervals that are dominated by interbedded carbonate lithologies, including dolostone and magnesite, with minor fine-grained clastics. This indicates a setting with steady carbonate production and both inorganic (DIC) and organic carbon burial and bioproductivity (Kump & Arthur, 1999; Bastow et al., 2002), as well as water evaporation where there is evidence of desiccation cracks and tepee structures (Frimmel, 2010; Virgo et al., 2021). Such a setting corresponds with the sequence stratigraphic interpretation of deposition during a slow transgressive systems tract (TST) in a sheltered inner platform setting (Virgo et al., 2023, accepted), with active and continuous aggradation of carbonate material that was able to keep pace with base level rise (Virgo et al., 2023, accepted). The Ce/Ce* anomaly through these intervals is often negligible (~0.96; Figure 5), indicating that redox conditions were neither strongly anoxic (Ce/Ce* > 1) or oxic (Ce/Ce* < 1). This could be reflective of a dysoxic water column, facilitated by the mixing of both oxic shallow waters and anoxic deep waters, which is consistent with the stratified ocean model during the Proterozoic (Preiss, 1987; Giddings & Wallace, 2009; Hood & Wallace, 2015; Counts, 2017; Wallace et al., 2017; Ward et al., 2019; Virgo et al., 2021). Due to the geometry of these carbonate

platforms, periodic flooding would be common (Virgo et al., 2023, accepted), and likely facilitated the input of these anoxic deep waters. Further, these intervals coincide with low Eu/Eu* values (~1.57; Figure 5), which suggests there was limited input from hydrothermal and/or evolved continental sources (Derry & Jacobsen, 1990; Bau, 1991; Olivarez & Owen, 1991; Hood & Wallace, 2015; Verdel et al., 2018). This would be expected in a restricted platform setting and supports an active carbonate factory that could produce thick accumulations of carbonate material (Krencker et al., 2020; Andríeu et al., 2022), without input from anoxic hydrothermal fluids and/or siliciclastic continental material.

5.6.2.2 Positive $\delta^{13}C$ values - scenario 2

Conversely, positive $\delta^{13}C$ values are also marked by outer platform microbial buildups deposited during highstand systems tracts (HST; Figure 5). Here, the slow rise in base level allowed carbonate production to outpace the accommodation creation, facilitating carbonate aggradation (Catuneanu, 2006). Like scenario 1, this bioproductive setting supports efficient burial of organic carbon, which generates the heavy $\delta^{13}C$ values (Kump & Arthur, 1999; Bastow et al., 2002). However, values from the previous case record overall more positive values (Figure 5), which could be due to additional CO_2 evasion from evaporation during periodic exposure (Frimmel, 2010; Virgo et al., 2021) or volcanic outgassing (Kump & Arthur, 1999). The prevalence of microbialite lithofacies indicates there was likely a sufficient supply of fine-grained clastic material into the system. This is demonstrated by the larger Eu/Eu* values (~3.01; Figure 5), which may have resulted from trapping and binding of feldspar-rich continental material within the stromatolitic structure. The Ce/Ce* is slightly more negative (~0.91; Figure 5), which could reflect less input from anoxic bottom waters or driven by the elevated bioproductive environment. This may have been facilitated by relative restriction provided by the topography of a high relief platform, which more effectively minimised deep-water input.

5.6.2.3 Negative $\delta^{13}C$ values - scenario 1

There are several negative $\delta^{13}C$ excursions throughout deposition of Tonian carbonates in the northern Flinders Ranges (Figure 5). However, two scenarios can be distinguished based on the litho- and chemo-stratigraphic variations. The first scenario is characterised by deposition of inner platform carbonates and sufficient interbedded clastic material. These intervals stratigraphically overlie a maximum regressive surface (MRS) marked by deposition of deltaic sandstone (Figure 5). Due to the prevalence of siliciclastic intervals, and stratigraphic proximity to a continental progradation, the recorded negative $\delta^{13}C$ values likely resulted from the shutdown of the carbonate factory, and subsequent bioproductivity, due to the input from continental material (Krencker et al., 2020). The presence of soft sediment deformation and scour and fill structures further support this interpreted continental progradation, and likely developed from liquefaction due to rapid sedimentation (Postma, 1983; Stromberg & Bluck, 1998; Moretti et al., 2001) and erosion (Fielding, 2006; Bridge, 2009; Boggs, 2014) during high velocity riverine discharge. This event is also recorded in the Ce/Ce* data, which shifts to slightly more negative values (~0.91). This would be expected in a setting with ^{13}C enriched surface waters and input of isotopically light riverine water (Kump & Arthur, 1999; Bastow et al., 2002; Frimmel, 2010). Interestingly, there is not a notable variation in Eu/Eu* (~1.81;

Figure 5), which would be expected to increase during periods of enhanced continental input (Verdel et al., 2018). We speculate that this might be due to the mineralogy of the source material, which mainly delivered quartz rich sandstones with minimal detrital feldspars.

5.6.2.4 Negative $\delta^{13}C$ values - scenario 2

The final scenario is represented by platform microbialites and dolostones that were deposited during HST, which indicates normal regression as base level rise is outpaced by sediment supply (Catuneanu, 2006). For these intervals, the negative $\delta^{13}C$ anomaly often follows a transgression to a deeper water setting and demonstrates $\delta^{13}C$ values that increase up-section through the HST (Figure 5). This is supported by the distribution of lithofacies, where carbonate content increases up-section as depositional conditions shift from anoxic bottom waters enriched in ^{12}C due to organic matter mineralisation to oxic shallower waters enriched in ^{13}C, leading to enhanced organic carbon burial linked to bioproductivity (Kump & Arthur, 1999; Bastow et al., 2002; Frimmel, 2010; Tziperman et al., 2011; Sarmiento et al., 2013). The Ce/Ce* values decrease up-section (Figure 5), from 2.32 to 1.64 and 0.95 to 0.86, respectively. This is reflective of a redox shift from more anoxic to oxic conditions, which would be expected during regression in a stratified ocean (Preiss, 1987; Giddings & Wallace, 2009; Hood & Wallace, 2015; Counts, 2017; Wallace et al., 2017; Ward et al., 2019; Virgo et al., 2021).

5.6.3 Correlation of Tonian Carbon Isotope Excursions

5.6.2.1 Northern Flinders Ranges

The overall positive $\delta^{13}C$ values in the base of the Skillogalee Dolomite in both the Termination Hill and South Copley sections (Figure 5) are characterised by interbedded fine-grained clastics and various carbonate lithologies, including dolostones and magnesite. This represents a restricted, dysoxic, bioproductive inner platform setting that was deposited during slow transgression. This platform was pervasive and can likely be traced across the entire western margin but was not recorded in North Copley as this stratigraphic interval is below the base of the North Copley measured section (Figure 5).

The overlying negative $\delta^{13}C$ excursion also appears to correlate in the Termination Hill and South Copley sections (Figure 5), recorded by inner platform dolostone, intraclastic magnesite and clastics with evidence of soft sediment deformation and scour and fill structures. These are consistent with deposition during a highstand systems tract, where continental progradation shutdown the carbonate factory, reducing bioproductivity and contributing isotopically light riverine water to the marginal marine environment (Kump & Arthur, 1999; Bastow et al., 2002; Frimmel, 2010). Again, this stratigraphic horizon was not measured in North Copley (Figure 5), but it is likely that it persisted across the western margin of the basin.

The return to positive $\delta^{13}C$ values in the top of the Skillogalee Dolomite can be correlated at three locations across the northern Flinders Ranges (Figure 5). In the north-west corner of the basin at Termination Hill, this interval is represented by interbedded carbonates and shales that correspond to deposition in an inner platform setting. Conversely, further south at South Copley and in the north-central platform at Mount Lyndhurst, deposition is characterised by outer

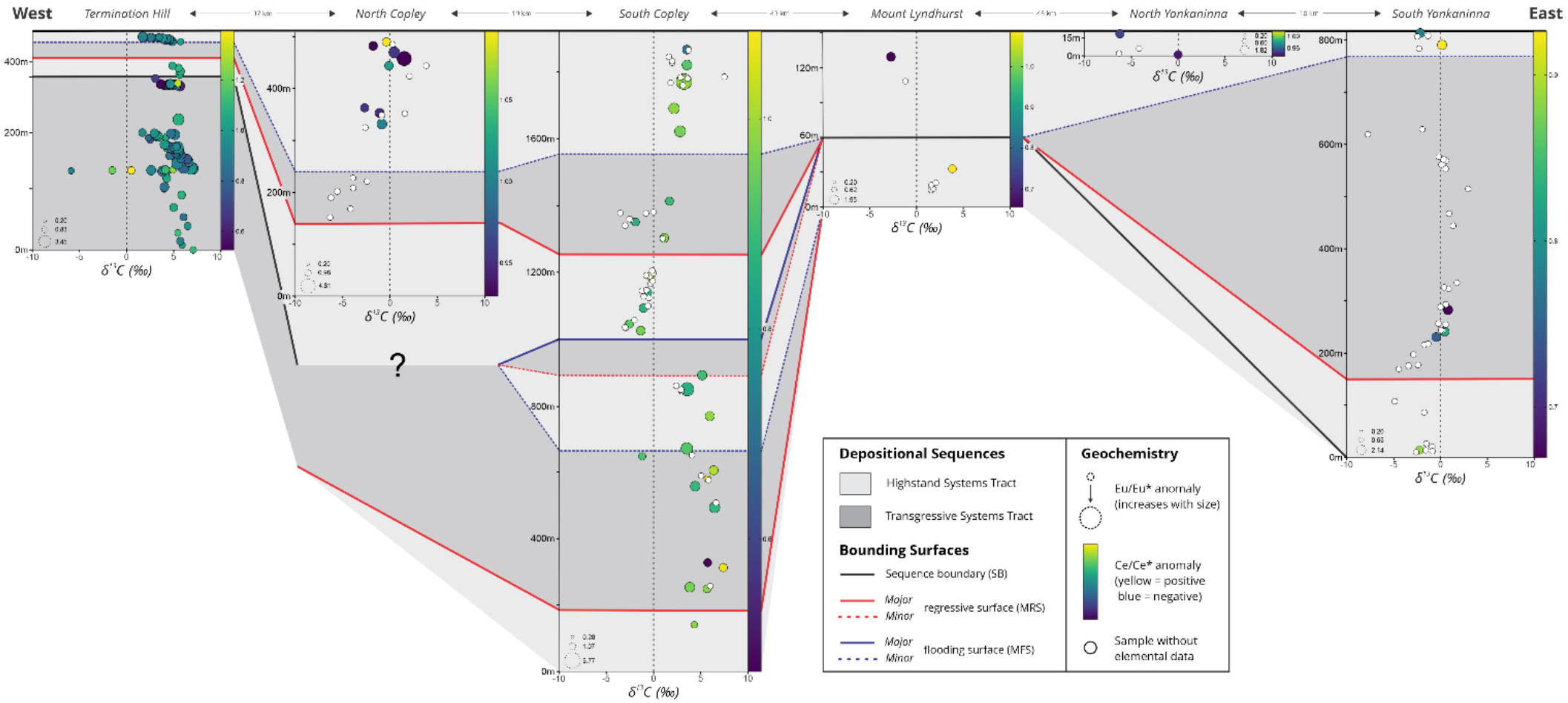

Figure 5: Tonian $\delta^{13}C$ values from carbonate samples in sections across the northern Flinders Ranges. Ce/Ce* data are represented by colour gradient and Eu/Eu* data are represented by the circle size. Ce/Ce* = cerium anomaly. Eu/Eu* = europium anomaly. REE data normalised to PASS (Nance & Taylor, 1976). Vertical axis is stratigraphic thickness. Light grey panels are highstand systems tracts (HST), dark grey panels are transgressive systems tracts (TST). Coloured lines indicate bounding surfaces, solid lines are major sequences and dashed lines are minor sequences.

platform microbial buildups. Although the lithofacies vary across the basin, this interval represents a dyosoxic, bioproductive platform setting during transgression. Relative depositional settings between these locations likely correspond to varying topographies controlled by local tectonics, sediment supply and salt diapirism (Virgo et al., 2023, accepted).

Ongoing transgression into the overlying Myrtle Springs Formation is recorded in the South Copley section, where the maximum flooding surface (MFS) is marked by deep-water siltstones (Figure 5; Virgo et al., 2021). In South Copley and South Yankaninna, this is overlain by platformal microbialites and dolostones that record a positive $\delta^{13}C$ trend up-section through an HST (Figure 5). These increasingly heavy $\delta^{13}C$ values, along with more negative Ce/Ce* up-section, marks the shallowing from an anoxic deep-water environment that had low bioproductivity and burial efficiency, to a more oxic platformal setting that regenerated the carbonate factory. The considerable distance between the South Copley and South Yankaninna section implies that the underlying transgression was persistent across the basin and may have resulted from changes in sediment supply or a period of basin subsidence (Preiss, 1987).

This HST is capped by a maximum regressive surface (MRS), which is represented by the deposition of thick deltaic sandstones that are present in the North Copley, South Copley and South Yankaninna sections (Figure 5). Above this is a TST, represented by a second positive $\delta^{13}C$ trend up-section (Figure 5), and the deposition of inner platform carbonates interbedded with siliciclastic material. This differs from the underlying excursion as it is marked by decreasing continental input rather than significant changes in water depth. In this scenario, the reduction in continental input restarts the carbonate factory, and is accompanied by enhanced organic carbon burial efficiency and bioproductivity, resulting in heavier $\delta^{13}C$. The prevalence of the deltaic sandstone deposition in multiple measured sections indicates that continental progradation was widespread, marking a drop in base level across the northern Flinders Ranges. This likely resulted from increased sediment input into the basin that was sourced from either increased precipitation or rifting and subsequent uplift of the surrounding rift shoulders (Preiss, 1987).

A second HST in the Myrtle Springs is interpreted for all sections across the basin (Figure 5). This marks the return to positive $\delta^{13}C$ values for all sections except Mount Lyndhurst and Yankaninna, which retains a weakly negative $\delta^{13}C$ signatures (Figure 5). Despite the slight variability in carbon isotope values, this interval represents an overall productive, dysoxic to suboxic, inner platform environment, dominated by deposition of layered microbialites. The widespread nature of this carbonate succession (Figure 5), and the preferential deposition under quiescent conditions (Hoffman, 1976; Wanless et al., 1988; Tucker & Wright, 2009; Jahnert & Collins, 2012; Chiarella et al., 2017; Kunzmann et al., 2019; O'Connell et al., 2020), elucidates a potential stasis in basin tectonics (uplift and/or subsidence) and sediment input, facilitating the thick accumulation of microbialite lithofacies (Virgo et al., 2023, accepted).

5.6.2.2 Global marine $\delta^{13}C$ record

One of the major limitations of the studied Neoproterozoic carbonate depositional system in South Australia is the limited number of geochronological constraints, particularly for the Tonian stratigraphy. Consequently, it has been challenging to fit Tonian deposition within the northern Flinders Ranges reliably into the global context. Chemostratigraphic correlations of characteristic negative $\delta^{13}C$ excursions in marine carbonates present an opportunity to constrain the position of the Adelaide Superbasin within the global record and can place indirect age constraints to the section in South Australia due to the robust chronostratigraphic record at other key Neoproterozoic sites.

Data compiled by Park et al. (2020) provides a detailed composite of $\delta^{13}C$ data collected from coeval sites in Ethiopia (Miler et al., 2009; Swanson-Hysell et al., 2015; Park et al., 2020), Canada (Asmerom et al., 1991; Halverson et al., 2006; 2007; Macdonald et al., 2010; Jones et al., 2010; Rooney et al., 2014; Cox et al., 2016), Scotland (Sawaki et al., 2010), Svalbard (Halverson et al., 2007; Cox et al., 2016) and Australia (Swanson-Hysell et al., 2010; Cox et al., 2016). This C isotope dataset, along with precise U–Pb ID-TIMS dates from zircons in tuff beds (Swanson-Hysell et al., 2015; MacLennan et al., 2018; Park et al., 2020), can be considered as one of the most temporally well-constrained chemostratigraphic data sets for the Tonian–Cryogenian period.

From Figure 6, it appears there is reasonable correlation between the $\delta^{13}C$ record in South Australia with the coeval global record. Without the chronostratigraphic constraints, negative excursions were used as an anchor to align the data sets. Data collected from Ethiopia, Svalbard and Canada demonstrate overall positive values during deposition from 790–740 Ma (Figure 6), which coincides with deposition of interbedded carbonates and shales in a shallow-water setting (Jones et al., 2010; Halverson et al., 2017; Park et al., 2020). This is comparable to the setting for the equivalent intervals in this study.

Several negative $\delta^{13}C$ excursions are recorded throughout this interval in the northern Flinders Ranges. The negative trend from Skillogalee Dolomite samples in the Termination Hill and South Copley sections occurs at a similar stratigraphic horizon (purportedly at ~774 Ma) as an anomalously negative value recorded from micritic carbonates in the Ethiopian section (Figure 6). The Park et al. (2020) study acknowledges the scatter in $\delta^{13}C$ data through this interval but does not consider this to be a true negative excursion. This interpretation also applies to several negative values recorded from recrystallised carbonates that occur at 764 Ma and 750 Ma, which overlap with the two negative excursions recorded in the bottom of the Myrtle Springs Formation (Figure 6). These negative intervals in Ethiopia were considered to be the result of secondary diagenetic processes, rather than true primary marine signatures (Park et al., 2020). Further, the negative $\delta^{13}C$ trend in the North Yankaninna section at proposed depositional age of ~725 Ma appears to correspond to several light $\delta^{13}C$ values recorded from presumably coeval micritic carbonates in Ethiopia (Figure 6). Again, these values were considered to be the result of alteration processes, related to the proximity to interbedded siliciclastics that did not act to buffer the carbonate from these secondary fluids (Park et al., 2020).

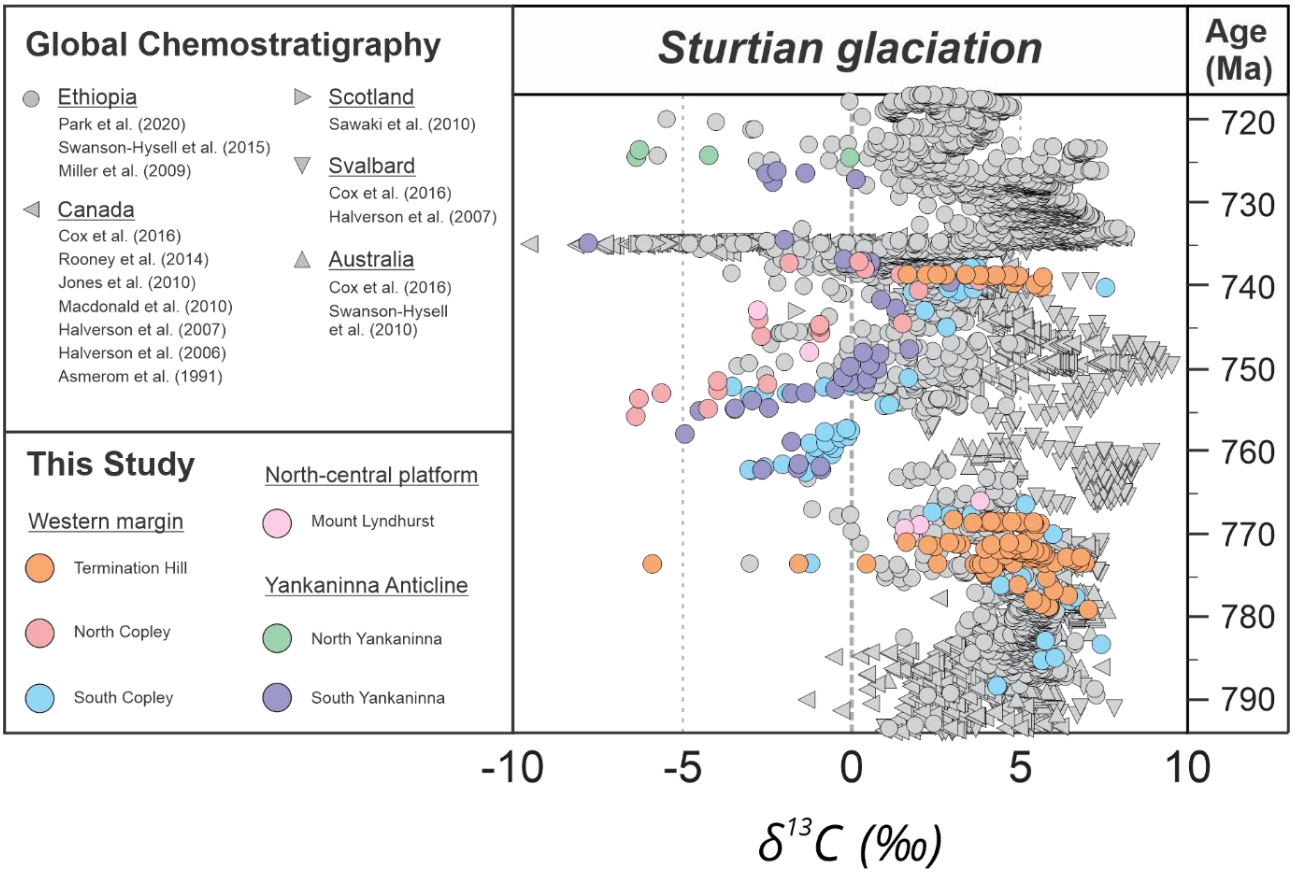

Figure 6: Global Tonian $\delta^{13}C$ chemostratigraphic composite with samples from North America, Africa, Europe and Australia (grey). Overlain with $\delta^{13}C$ data from this study (various colours). Vertical axis is estimated geochronological age, constrained using depositional ages collected from various global locations (Park et al., 2020, and references therein).

The significant $\delta^{13}C$ negative shift recorded in the South Yankaninna section aligns with a major excursion in the global record at ca. 735 Ma (Figure 6), which is commonly referred to in literature as the Islay anomaly. This same sharp $\delta^{13}C$ excursion has been documented from sections in Ethiopia (Swanson-Hysell et al., 2015; MacLennan et al., 2018; Park et al., 2020), Canada (Halverson, 2006), Scotland (Sawaki et al., 2010) and Svalbard (Halverson et al., 2007b; Hoffman et al., 2012), and has been suggested to be global due to the synchroneity of its occurrence in several coeval basins. However, some authors acknowledge the possibility that this excursion may have resulted from local secondary alteration, and therefore, does not reflect a global shift in the $\delta^{13}C$ record (Park et al., 2020).

Interestingly, it appears that the overall $\delta^{13}C$ values recorded in carbonate samples in the Myrtle Springs Formation are on average more negative than those recorded in the global record, which are as heavy as +10‰ in Svalbard (Figure 6). The comparatively lighter $\delta^{13}C$ values in the northern Flinders Ranges could be a response to local controls on bioproductivity, due to the impact of continental progradation mentioned previously. As these processes are linked with either regional climate regimes or tectonics (i.e. faulting and uplift of the rift shoulders; Preiss, 1987), it may have resulted in a unique $\delta^{13}C$ signature in South Australia that is

dissimilar to the global record. Further, this may be reflective of the relative restriction of the northern Flinders Ranges during the Tonian. Global chemostratigraphic correlations are built on the assumption that coeval basins are connected to the global ocean, therefore recording contemporaneous fluctuations in C isotope signatures (Halverson et al., 2005; 2010). Due to the geometry of the evolving Adelaide Superbasin during the Tonian, the north of the basin was likely more distal to the Palaeo-Pacific Ocean that was developing between Australia and Laurentia (Merdith et al., 2019; although note that the Tonian palaeogeography to the north of the Adelaide Superbasin is not known). This meant that the northern Flinders Ranges was less likely to be connected to the open ocean, and thus record water chemistries specific to this purportedly more restricted part of the basin.

5.7 Conclusions

The Adelaide Superbasin is a Neoproterozoic sedimentary system that preserves distinct fluctuations in lithology and geochemistry associated with both global atmospheric, biological, and climatic shifts as well as global and local tectonic effects. This study covered over 8000 m of Tonian and Cryogenian stratigraphy across a 120 km east–west transect in the northern Flinders Ranges, South Australia. These included sites along the western margin of the basin (Termination Hill, North and South Copley), in the north-central zone (Mount Lyndhurst), and in the Yankaninna Anticline (North and South Yankaninna).

To address the relationship between productivity, redox and variations in water depth and sediment supply, the $\delta^{13}C$ record of studied carbonates (that were triaged to avoid samples affected by diagenetic alteration or detrital phases) was compared with elemental geochemical tracers (Ce/Ce* and Eu/Eu*) and sequence stratigraphic changes. These parameters elucidate four depositional conditions that existed within the northern Flinders Ranges during the Tonian, including:

(1) bioproductive, dysoxic inner platform setting that developed during slow transgression;
(2) bioproductive, suboxic outer platform setting that formed during a highstand systems tract;
(3) biologically inactive inner platform setting, associated with continental progradation during a highstand systems tract;
(4) a biologically inactive, anoxic deep subtidal setting that formed during a transgressive systems tract.

These depositional conditions were then correlated between the measured sections across the northern Flinders Ranges. The western margin records heavy carbonate $\delta^{13}C$ values throughout the base of the Skillogalee Dolomite, which is consistent with depositional condition (1) listed above. The overlying negative $\delta^{13}C$ excursion is also recorded in sections along the western margin of the basin and indicates a shift to depositional condition (3). The return of positive $\delta^{13}C$ values in the top of the Skillogalee Dolomite marks the transition to deposition condition (2) and is recorded along the western margin and in the north-central zone. This likely corresponds to topographic highs that were controlled by local tectonism, sediment input and salt diapirism.

The negative $\delta^{13}C$ values recorded in the base of the overlying Myrtle Springs Formation along the western margin and in Yankaninna is consistent with depositional condition (4). Due to the spread of this system across the basin, the transgression could have resulted from a period of basin subsidence or one of eustatic sea-level rise. The overlying transition into deposition condition (3) is also recorded along the western margin of the basin and in Yankaninna and is marked by a distinct negative $\delta^{13}C$ excursion. The prevalence of deltaic sandstone deposition across the basin indicates that the continental sediment that prograded into the basin was likely sourced from active rifting of the surrounding rift shoulders. A shift to more positive $\delta^{13}C$ values is preserved in all sections besides North Yankaninna. This is consistent with depositional condition (2), and likely resulted from a phase of tectonic quiescence. The overlying sharp negative $\delta^{13}C$ excursion, represented by deposition condition (4), was only preserved in the North Yankaninna section. This is due to the uncomfortable contact with Sturtian glacial deposits in other parts of the basin. The record of this anomaly in Yankaninna suggests that this location was either not eroded by the Cryogenian glacials or had sufficient accommodation space. The top of the Myrtle Springs Formation is consistent with shift to depositional condition (3) and is recorded at both Yankaninna sections.

These excursions were then compared with the global $\delta^{13}C$ record of coeval Neoproterozoic marine carbonates from sites in Ethiopia, Canada, Scotland, Svalbard (Norway) and other parts of Australia. Although many of the negative $\delta^{13}C$ excursions from the Tonian in the northern Flinders Ranges appear to overlap with those from Ethiopia, these negative $\delta^{13}C$ values are not considered to represent primary marine DIC signals and are often the result of diagenetic resetting. However, the sharp negative $\delta^{13}C$ excursion at ~735 Ma corresponds to a major global excursion that has been documented in many coeval basins. This suggests that the changes in depositional condition at this stratigraphic horizon may have resulted from more broad, global environmental fluctuations. With that said, there is uncertainty regarding global chemostratigraphic correlations, as evidenced by the overall more negative $\delta^{13}C$ values recorded from Tonian carbonates in this study relative to marine carbonates from other time-equivalent basins. Further, the interpreted punctuated restriction from the global ocean inferred from data from the northern Flinders Ranges during this time suggests that the excursions in the C isotopic record from this study represent a complex mix of local phenomena and global effects. The two can only be unentwined by integrating sedimentological and sequence stratigraphic data with geochemistry and isotope data as has been attempted here.

5.8 Supplementary Material

Supplementary material is freely available as XLSX on Figshare.

Northern Flinders Ranges sample list: https://doi.org/10.6084/m9.figshare.23640963.v1

Isotope dataset: https://doi.org/10.6084/m9.figshare.23640966.v1

5.9 Acknowledgements

We acknowledge that this research is conducted on the ancestral lands for the Adnyamathanha and Kuyani people. We acknowledge and respect their deep feelings of attachment and spiritual relationship to Country, and that their cultural and heritage beliefs are still as important to the living people today. This project was supported by funding from the Geological Survey of South Australia, and an Australian Government Research Training Program (RTP) Scholarship awarded to Virgo. We are very grateful to Jack Ward (The University of Queensland) and Jarred Lloyd (The University of Adelaide) for their field assistance in 2018 and 2019, respectively. We thank David Bruce and Dr Robert Klaebe (The University of Adelaide) for their guidance and technical support with sample preparation and analysis. The authors acknowledge the instruments and scientific and technical assistance of Microscopy Australia at Adelaide Microscopy, The University of Adelaide, a facility that is funded by the University, and State and Federal Governments.

5.10. References

Andríeu, S., Krencker, F. N. & Bodin, S. (2022). Anatomy of a platform margin during a carbonate factory collapse: implications for the sedimentary record and sequence stratigraphic interpretation of poisoning events. Journal of the Geological Society, 179(6), jgs2022-005. https://doi.org/10.1144/jgs2022-005

Asmerom, Y., Jacobsen, S. B., Knoll, A. H., Butterfield, N. J. & Swett, K. (1991). Strontium isotopic variations of Neoproterozoic seawater: implications for crustal evolution. Geochimica et Cosmochimica Acta, 55(10), 2883-2894. https://doi.org/10.1016/0016-7037(91)90453-C

Banner, J. L. & Hanson, G. N. (1990). Calculation of simultaneous isotopic and trace element variations during water-rock interaction with applications to carbonate diagenesis. Geochimica et Cosmochimica Acta 54(11): 3123-3137. https://doi.org/10.1016/0016-7037(90)90128-8

Barovich, K. & Foden, J. (2000). A Neoproterozoic flood basalt province in southern-central Australia: geochemical and Nd isotope evidence from basin fill. Precambrian Research 100(1-3): 213-234. https://doi.org/10.1016/S0301-9268(99)00075-3

Bartley, J. K., Semikhatov, M. A., Kaufman, A. J., Knoll, A. H., Pope, M. C. & Jacobsen, S. B. (2001). Global events across the Mesoproterozoic–Neoproterozoic boundary: C and Sr isotopic evidence from Siberia. Precambrian Research 111(1-4): 165-202. https://doi.org/10.1016/S0301-9268(01)00160-7

Bastow, T. P., Jackson, G. & Edmonds, J. S. (2002). Elevated salinity and isotopic composition of fish otolith carbonate: stock delineation of pink snapper, Pagrus auratus, in Shark Bay, Western Australia. Marine Biology 141(5): 801-806. https://doi.org/10.1007/s00227-002-0884-8

Bau, M. (1991). Rare-earth element mobility during hydrothermal and metamorphic fluid-rock interaction and the significance of the oxidation state of europium. Chemical geology, 93(3-4), 219-230. https://doi.org/10.1016/0009-2541(91)90115-8

Belperio, A. (1990). Palaeoenvironmental interpretations of the Late Proterozoic Skillogalee Dolomite in the Willouran Ranges, South Australia. The Evolution of a Late Precambrian–Early Palaeozoic Rift Complex: The Adelaide Geosyncline. Geol. Soc. Aust. Spec. Publ, 16, 85-104.

Boggs Jr, S. (2014). Principles of sedimentology and stratigraphy. Pearson Education.

Bold, U., Smith, E. F., Rooney, A. D., Bowring, S. A., Buchwaldt, R., Dudás, F. Ő., Ramezani, J., Crowley, J. L., Schrag, D. P. & Macdonald, F. A. (2016). Neoproterozoic stratigraphy of the Zavkhan terrane of Mongolia: The backbone for Cryogenian and early Ediacaran chemostratigraphic records. American Journal of Science 316(1): 1-63. https://doi.org/10.2475/01.2016.01

Brand, U. & Veizer, J. (1980). Chemical diagenesis of a multicomponent carbonate system; 1, Trace elements. Journal of Sedimentary Research 50(4): 1219-1236. https://doi.org/10.1306/212F7BB7-2B24-11D7-8648000102C1865D

Brasier, M. D., Shields, G., Kuleshov, V. N. & Zhegallo, E. A. (1996). Integrated chemo-and biostratigraphic calibration of early animal evolution: Neoproterozoic–early Cambrian of southwest Mongolia. Geological Magazine, 133(4), 445-485. Bridge, J. S. (2009). Rivers and floodplains: forms, processes, and sedimentary record, John Wiley & Sons. doi:10.1017/S0016756800007603

Brocks, J. J., Jarrett, A. J., Sirantoine, E., Hallmann, C., Hoshino, Y. & Liyanage, T. (2017). The rise of algae in Cryogenian oceans and the emergence of animals. Nature, 548(7669), 578-581. https://doi.org/10.1038/nature23457

Butterfield, N. J. (2011). Animals and the invention of the Phanerozoic Earth system. Trends in ecology & evolution, 26(2), 81-87. https://doi.org/10.1016/j.tree.2010.11.012

Catuneanu, O. (2006). Principles of sequence stratigraphy. Elsevier.

Catuneanu, O. (2017). Sequence stratigraphy: Guidelines for a standard methodology. Stratigraphy & timescales, Elsevier. 2: 1-57. https://doi.org/10.1016/bs.sats.2017.07.003

Catuneanu, O., Abreu, V., Bhattacharya, J. P., Blum, M. D., Dalrymple, R. W., Eriksson, P. G., Fielding, C. R., Fisher, W. L., Galloway, W. E., Gibling, M. R. & Giles, K. A. (2009). Towards the standardization of sequence stratigraphy. Earth-Science Reviews 92(1-2): 1-33. https://doi.org/10.1016/j.earscirev.2008.10.003

Catuneanu, O., Galloway, W. E., Kendall, C. G. St C., Miall, A. D., Posamentier, H. W., Strasser, A. & Tucker M. E. (2011). Sequence stratigraphy: methodology and nomenclature. Newsletters on stratigraphy 44(3): 173-245.

Cohen, A. S., Coe, A. L., Harding, S. M. & Schwark, L. (2004). Osmium isotope evidence for the regulation of atmospheric CO2 by continental weathering. Geology, 32(2), 157-160. https://doi.org/10.1130/G20158.1

Collins, A. S., Blades, M. L., Merdith, A. S. & Foden, J. D. (2021). Closure of the Proterozoic Mozambique Ocean was instigated by a late Tonian plate reorganization event. Communications Earth & Environment, 2(1), 75. https://doi.org/10.1038/s43247-021-00149-z

Counts, J. W. (2017). The Adelaide Rift Complex in the Flinders Ranges: Geologic history, past investigations and relevant analogues. Department of the Premier and Cabinet, South Australia, Adelaide, Report Book 16: 42.

Cox, G. M., Halverson, G. P., Stevenson, R. K., Vokaty, M., Poirier, A., Kunzmann, M., Li, Z. X., Denyszyn, S. W., Strauss, J. V. & Macdonald, F. A. (2016). Continental flood basalt weathering as a trigger for Neoproterozoic Snowball Earth. Earth and Planetary Science Letters 446: 89-99. https://doi.org/10.1016/j.epsl.2016.04.016

Deconinck, J. F., Gómez, J. J., Baudin, F., Biscay, H., Bruneau, L., Cocquerez, T., Mathieu, O., Pellenard, P. & Santoni, A. L. (2020). Diagenetic and environmental control of the clay mineralogy, organic matter and stable isotopes (C, O) of Jurassic (Pliensbachian-lowermost Toarcian) sediments of the Rodiles section (Asturian Basin, Northern Spain). Marine and Petroleum Geology, 115, 104286. https://doi.org/10.1016/j.marpetgeo.2020.104286

Derry, L. A. & Jacobsen, S. B. (1990). The chemical evolution of Precambrian seawater: evidence from REEs in banded iron formations. Geochimica et Cosmochimica Acta, 54(11), 2965-2977. https://doi.org/10.1016/0016-7037(90)90114-Z

Embry, A. (2009). Practical sequence stratigraphy. Canadian Society of Petroleum Geologists 81: 79.

Fairchild, I. J., Spencer, A. M., Ali, D. O., Anderson, R. P., Anderton, R., Boomer, I., Dove, D., Evans, J. D., Hambrey, M. J., Howe, J. & Sawaki, Y. (2017). Tonian-Cryogenian boundary sections of Argyll, Scotland. Precambrian Research. https://doi.org/10.1016/j.precamres.2017.09.020

Fielding, C. R. (2006). Upper flow regime sheets, lenses and scour fills: extending the range of architectural elements for fluvial sediment bodies. Sedimentary Geology 190(1-4): 227-240. https://doi.org/10.1016/j.sedgeo.2006.05.009

Foden, J., Elburg, M., Turner, S., Clark, C., Blades, M. L., Cox, G., Collins, A. S., Wolff, K. & George, C. (2020). Cambro-Ordovician magmatism in the Delamerian orogeny: Implications for tectonic development of the southern Gondwanan margin. Gondwana Research 81: 490-521. https://doi.org/10.1016/j.gr.2019.12.006

Foden, J., Elburg, M. A., Dougherty-Page, J. & Burtt, A. (2006). The timing and duration of the Delamerian Orogeny: correlation with the Ross Orogen and implications for Gondwana assembly. The Journal of Geology 114(2): 189-210. https://doi.org/10.1086/499570

Föllmi, K. B., Godet, A., Bodin, S. & Linder, P. (2006). Interactions between environmental change and shallow water carbonate buildup along the northern Tethyan margin and their impact on the Early Cretaceous carbon isotope record. Paleoceanography, 21(4). https://doi.org/10.1029/2006PA001313

Frank, T. D. & Fielding, C. R. (2003). Marine origin for Precambrian, carbonate-hosted magnesite? Geology 31(12): 1101-1104. https://doi.org/10.1130/G20101.1

Frimmel, H. E. (2009). Trace element distribution in Neoproterozoic carbonates as palaeoenvironmental indicator. Chemical Geology 258(3-4): 338-353. https://doi.org/10.1016/j.chemgeo.2008.10.033

Frimmel, H. E. (2010). On the reliability of stable carbon isotopes for Neoproterozoic chemostratigraphic correlation. Precambrian Research 182(4): 239-253. https://doi.org/10.1016/j.precamres.2010.01.003

German, C. R. & Elderfield, H. (1990). Application of the Ce anomaly as a paleoredox indicator: the ground rules. Paleoceanography 5(5): 823-833. https://doi.org/10.1029/PA005i005p00823

Giddings, J. A. & Wallace, M. W. (2009). Facies-dependent δ13C variation from a Cryogenian platform margin, South Australia: Evidence for stratified Neoproterozoic oceans? Palaeogeography, Palaeoclimatology, Palaeoecology 271(3-4): 196-214. https://doi.org/10.1016/j.palaeo.2008.10.011

Giddings, J. A. & Wallace, M. W. (2009a). Sedimentology and C-isotope geochemistry of the 'Sturtian'cap carbonate, South Australia. Sedimentary Geology 216(1-2): 1-14. https://doi.org/10.1016/j.sedgeo.2009.01.007

Godet, A., Föllmi, K. B., Spangenberg, J. E., Bodin, S., Vermeulen, J., Adatte, T., Bonvallet, L. & Arnaud, H. (2013). Deciphering the message of Early Cretaceous drowning surfaces from the Helvetic Alps: What can be learnt from platform to basin correlations?. Sedimentology, 60(1), 152-173. https://doi.org/10.1111/sed.12008

Grey, K., Hill, A. C. & Calver, C. (2011). Biostratigraphy and stratigraphic subdivision of Cryogenian successions of Australia in a global context. Geological Society, London, Memoirs 36(1): 113-134. https://doi.org/10.1144/M36.8

Halfar, J., Godinez-Orta, L., Mutti, M., Valdez-Holguin, J. E. & Borges, J. M. (2006). Carbonates calibrated against oceanographic parameters along a latitudinal transect in the Gulf of California, Mexico. Sedimentology, 53(2), 297-320. https://doi.org/10.1111/j.1365-3091.2005.00766.x

Hallock, P. & Schlager, W. (1986). Nutrient excess and the demise of coral reefs and carbonate platforms. Palaios: 389-398. https://doi.org/10.2307/3514476

Halverson, G. P., Dudás, F. Ö., Maloof, A. C. & Bowring, S. A. (2007). Evolution of the 87Sr/86Sr composition of Neoproterozoic seawater. Palaeogeography, Palaeoclimatology, Palaeoecology, 256(3-4), 103-129. https://doi.org/10.1016/j.palaeo.2007.02.028

Halverson, G. P., Hoffman, P. F., Schrag, D. P., Maloof, A. C. & Rice, A. H. N. (2005). Toward a Neoproterozoic composite carbon-isotope record. GSA Bulletin 117(9-10): 1181-1207. https://doi.org/10.1130/B25630.1

Halverson, G. P., Kunzmann, M., Strauss, J. V. & Maloof, A. C. (2017). The Tonian-Cryogenian transition in Northeastern Svalbard. Precambrian Research. https://doi.org/10.1016/j.precamres.2017.12.010

Halverson, G. P., Maloof, A. C., Schrag, D. P., Dudás, F. Ö. & Hurtgen, M. (2007). Stratigraphy and geochemistry of a ca 800 Ma negative carbon isotope interval in northeastern Svalbard. Chemical Geology, 237(1-2), 5-27. https://doi.org/10.1016/j.chemgeo.2006.06.013

Halverson, G. P., Wade, B. P., Hurtgen, M. T. & Barovich, K. M. (2010). Neoproterozoic chemostratigraphy. Precambrian Research, 182(4), 337-350. https://doi.org/10.1016/j.precamres.2010.04.007

Hermoso, M. & Pellenard, P. (2014). Continental weathering and climatic changes inferred from clay mineralogy and paired carbon isotopes across the early to middle Toarcian in the Paris Basin. Palaeogeography, Palaeoclimatology, Palaeoecology, 399, 385-393. https://doi.org/10.1016/j.palaeo.2014.02.007

Hill, A. C. & Walter, M. R. (2000). Mid-Neoproterozoic (~ 830–750 Ma) isotope stratigraphy of Australia and global correlation. Precambrian Research, 100(1-3), 181-211. https://doi.org/10.1016/S0301-9268(99)00074-1

Hoffman, P. (1976). Environmental diversity of Middle Precambrian stromatolites. In Developments in sedimentology (Vol. 20, pp. 599-611). Elsevier. https://doi.org/10.1016/S0070-4571(08)71161-0

Hoffman, P. F., Halverson, G. P., Domack, E. W., Maloof, A. C., Swanson-Hysell, N. L. & Cox, G. M. (2012). Cryogenian glaciations on the southern tropical paleomargin of Laurentia (NE Svalbard and East Greenland), and a primary origin for the upper Russøya (Islay) carbon isotope excursion. Precambrian Research 206: 137-158. https://doi.org/10.1016/j.precamres.2012.02.018

Hoffman, P. F., Kaufman, A. J., Halverson, G. P. & Schrag, D. P. (1998). A Neoproterozoic snowball earth. Science 281(5381): 1342-1346. 10.1126/science.281.5381.1342

Hoffman, P. F., Lamothe, K. G., LoBianco, S. J., Hodgskiss, M. S., Bellefroid, E. J., Johnson, B. W., Hodgin, E. B. & Halverson, G. P. (2017). Sedimentary depocenters on snowball Earth: Case studies from the Sturtian Chuos Formation in northern Namibia. Geosphere 13(3): 811-837. https://doi.org/10.1130/GES01457.1

Hood, A. v.S., Wallace, M. W., Reed, C. P., Hoffmann, K. H. & Freyer, E. E. (2015). Enigmatic carbonates of the Ombombo Subgroup, Otavi Fold Belt, Namibia: a prelude to extreme Cryogenian anoxia? Sedimentary Geology 324: 12-31. https://doi.org/10.1016/j.sedgeo.2015.04.007

Hood, A. v.S. & Wallace, M. W. (2012). Synsedimentary diagenesis in a Cryogenian reef complex: Ubiquitous marine dolomite precipitation. Sedimentary Geology 255: 56-71. https://doi.org/10.1016/j.sedgeo.2012.02.004

Hood, A. v.S. & Wallace, M. W. (2015). Extreme ocean anoxia during the Late Cryogenian recorded in reefal carbonates of Southern Australia. Precambrian Research 261: 96-111.

Hood, A. v.S, Planavsky, N. J., Wallace, M. W., Wang, X., Bellefroid, E. J., Gueguen, B. & Cole, D. B. (2016). Integrated geochemical-petrographic insights from component-selective δ238U of Cryogenian marine carbonates. Geology 44(11): 935-938. https://doi.org/10.1130/G38533.1

Hood, A. v.S. & Wallace, M. W. (2014). Marine cements reveal the structure of an anoxic, ferruginous Neoproterozoic ocean. Journal of the Geological Society, 171(6), 741-744. https://doi.org/10.1144/jgs2013-099

Hood, A. vS., Wallace, M. W. & Drysdale, R. N. (2011). Neoproterozoic aragonite-dolomite seas? Widespread marine dolomite precipitation in Cryogenian reef complexes. Geology 39(9): 871-874. https://doi.org/10.1130/G32119.1

Hua, G., Yuansheng, D., Lian, Z., Jianghai, Y., Hu, H., Min, L. & Yuan, W. (2013). Trace and rare earth elemental geochemistry of carbonate succession in the Middle Gaoyuzhuang Formation, Pingquan Section: Implications for Early Mesoproterozoic ocean redox conditions. Journal of Palaeogeography 2(2): 209-221. https://doi.org/10.3724/SP.J.1261.2013.00027

Jahnert, R. J. & Collins, L. B. (2012). Characteristics, distribution and morphogenesis of subtidal microbial systems in Shark Bay, Australia. Marine Geology, 303, 115-136. https://doi.org/10.1016/j.margeo.2012.02.009

Jones, D. S., Maloof, A. C., Hurtgen, M. T., Rainbird, R. H. & Schrag, D. P. (2010). Regional and global chemostratigraphic correlation of the early Neoproterozoic Shaler Supergroup, Victoria Island, northwestern Canada. Precambrian Research, 181(1-4), 43-63. https://doi.org/10.1016/j.precamres.2010.05.012

Kaufman, A. J. & Knoll, A. H. (1995). Neoproterozoic variations in the C-isotopic composition of seawater: stratigraphic and biogeochemical implications. Precambrian Research 73(1-4): 27-49. https://doi.org/10.1016/0301-9268(94)00070-8

Kirschvink, J. L. (1992)."Late Proterozoic low-latitude global glaciation: the snowball Earth. https://resolver.caltech.edu/CaltechAUTHORS:20130117-100718783

Knoll, A., Hayes, J. M., Kaufman, A. J., Swett, K. & Lambert, I. B. (1986). Secular variation in carbon isotope ratios from Upper Proterozoic successions of Svalbard and East Greenland. Nature 321(6073): 832. https://doi.org/10.1038/321832a0

Krencker, F. N., Fantasia, A., Danisch, J., Martindale, R., Kabiri, L., El Ouali, M. & Bodin, S. (2020). Two-phased collapse of the shallow-water carbonate factory during the late Pliensbachian–Toarcian driven by changing climate and enhanced continental weathering in the Northwestern Gondwana Margin. Earth-Science Reviews, 208, 103254. https://doi.org/10.1016/j.earscirev.2020.103254

Kump, L. R. & Arthur, M. A. (1999). Interpreting carbon-isotope excursions: carbonates and organic matter. Chemical Geology 161(1-3): 181-198. https://doi.org/10.1016/S0009-2541(99)00086-8

Kunzmann, M., Crombez, V., Catuneanu, O., Blaikie, T. N., Barth, G. & Collins, A. S. (2020). Sequence stratigraphy of the ca. 1730 Ma Wollogorang Formation, McArthur Basin, Australia. Marine and Petroleum Geology, 116, 104297. https://doi.org/10.1016/j.marpetgeo.2020.104297

Kunzmann, M., Schmid, S., Blaikie, T. N. & Halverson, G. P. (2019). Facies analysis, sequence stratigraphy, and carbon isotope chemostratigraphy of a classic Zn-Pb host succession: The Proterozoic middle McArthur Group, McArthur Basin, Australia. Ore Geology Reviews, 106, 150-175. https://doi.org/10.1016/j.oregeorev.2019.01.011

Kuznetsov, A. B., Melezhik, V. A., Gorokhov, I. M., Melnikov, N. N., Konstantinova, G. V., Kutyavin, E. P. & Turchenko, T. L. (2010). Sr isotopic composition of Paleoproterozoic 13C-rich carbonate rocks: the Tulomozero Formation, SE Fennoscandian Shield. Precambrian Research, 182(4), 300-312. https://doi.org/10.1016/j.precamres.2010.05.006

Kuznetsov, A. B., Semikhatov, M. A., Maslov, A. V., Gorokhov, I. M., Prasolov, E. M., Krupenin, M. T. & Kislova, I. V. (2006). New data on Sr-and C-isotopic chemostratigraphy of the Upper Riphean type section (Southern Urals). Stratigraphy and Geological Correlation, 14, 602-628. https://doi.org/10.1134/S0869593806060025

Lechte, M. & Wallace M. (2016). Sub–ice shelf ironstone deposition during the Neoproterozoic Sturtian glaciation. Geology 44(11): 891-894. https://doi.org/10.1130/G38495.1

Lenton, T. M., Boyle, R. A., Poulton, S. W., Shields-Zhou, G. A. & Butterfield, N. J. (2014). Co-evolution of eukaryotes and ocean oxygenation in the Neoproterozoic era. Nature Geoscience 7(4): 257-265. https://doi.org/10.1038/ngeo2108

Li, Z.-X., Bogdanova, S., Collins, A.S., Davidson, A., De Waele, B., Ernst, R.E., Fitzsimons, I.C.W., Fuck, R.A., Gladkochub, D.P., Jacobs, J. & Karlstrom, K.E. (2008). Assembly, configuration, and break-up history of Rodinia: a synthesis. Precambrian Research 160(1-2): 179-210. https://doi.org/10.1016/j.precamres.2007.04.021

Ling, H.-F., Chen, X., Li, D. A., Wang, D., Shields-Zhou, G. A. & Zhu, M. (2013). Cerium anomaly variations in Ediacaran–earliest Cambrian carbonates from the Yangtze Gorges area, South China: implications for oxygenation of coeval shallow seawater. Precambrian Research 225: 110-127. https://doi.org/10.1016/j.precamres.2011.10.011

Liu, C., Wang, Z., Raub, T. D., Macdonald, F. A. & Evans, D. A. (2014). Neoproterozoic cap-dolostone deposition in stratified glacial meltwater plume. Earth and Planetary Science Letters, 404, 22-32.

Liu, X.-M., Hardisty, D. S., Lyons, T. W. & Swart, P. K. (2019). Evaluating the fidelity of the cerium paleoredox tracer during variable carbonate diagenesis on the Great Bahamas Bank. Geochimica et Cosmochimica Acta, 248, 25-42. https://doi.org/10.1016/j.gca.2018.12.028

Lloyd, J. C., Blades, M. L., Counts, J. W., Collins, A.S ., Amos, K. J., Wade, B. P., Hall, J. W., Hore, S., Ball, A. L., Shahin, S. & Drabsch, M. (2020). Neoproterozoic geochronology and provenance of the Adelaide Superbasin. Precambrian Research, 350, 105849. https://doi.org/10.1016/j.precamres.2020.105849

Lloyd, J. C., Preiss, W. V., Collins, A. S., Virgo, G. M., Blades, M. L., Gilbert, S. E., Subarkah, D., Krapf, C. B. E. & Amos, K. J. (2022). Geochronology and formal stratigraphy of the Sturtian Glaciation in the Adelaide Superbasin, Geological Magazine. https://doi.org/10.31223/X50G9N

Macdonald, F. A., Schmitz, M.D., Crowley, J.L., Roots, C.F., Jones, D.S., Maloof, A.C., Strauss, J.V., Cohen, P.A., Johnston, D.T. & Schrag, D.P. (2010). Calibrating the cryogenian. Science 327(5970): 1241-1243. 10.1126/science.1183325

MacLennan, S., Park, Y., Swanson-Hysell, N., Maloof, A., Schoene, B., Gebreslassie, M., Antilla, E., Tesema, T., Alene, M. and Haileab, B. (2018). The arc of the Snowball: U-Pb dates constrain the Islay anomaly and the initiation of the Sturtian glaciation. Geology, 46(6), 539-542. https://doi.org/10.1130/G40171.1

Mawson, D. & Sprigg, R. (1950). Subdivision of the Adelaide system. Australian Journal of Science, 13(3), 69-72.

McKirdy, D. M., Burgess, J. M., Lemon, N. M., Yu, X., Cooper, A. M., Gostin, V. A., Jenkins, R. J. & Both, R. A. (2001). A chemostratigraphic overview of the late Cryogenian interglacial sequence in the Adelaide Fold-Thrust Belt, South Australia. Precambrian Research, 106(1-2), 149-186. https://doi.org/10.1016/S0301-9268(00)00130-3

Merdith, A. S., Collins, A. S., Williams, S. E., Pisarevsky, S., Foden, J. D., Archibald, D. B., Blades, M. L., Alessio, B. L., Armistead, S., Plavsa, D. and Clark, C. (2017). A full-plate global reconstruction of the Neoproterozoic. Gondwana Research, 50, 84-134. https://doi.org/10.1016/j.gr.2017.04.001

Merdith, A. S., Williams, S. E., Brune, S., Collins, A. S. & Müller, R. D. (2019). Rift and plate boundary evolution across two supercontinent cycles. Global and planetary change, 173, 1-14. https://doi.org/10.1016/j.gloplacha.2018.11.006

Merdith, A.S., Williams, S.E., Collins, A.S., Tetley, M.G., Mulder, J.A., Blades, M.L., Young, A., Armistead, S.E., Cannon, J., Zahirovic, S., Müller, R.D. (2021). A continuous, kinematic full-plate motion model from 1 Ga to present. Earth Science Reviews. https://doi.org/10.1016/j.earscirev.2020.103477

Miller, N. R., Stern, R. J., Avigad, D., Beyth, M. & Schilman, B. (2009). Cryogenian slate-carbonate sequences of the Tambien Group, Northern Ethiopia (I): Pre-"Sturtian" chemostratigraphy and regional correlations. Precambrian Research, 170(3-4), 129-156. https://doi.org/10.1016/j.precamres.2008.12.004

Moretti, M., Soria, J. M., Alfaro, P. & Walsh, N. (2001). Asymmetrical soft-sediment deformation structures triggered by rapid sedimentation in turbiditic deposits (Late Miocene, Guadix Basin, Southern Spain). Facies 44(1): 283-294. https://doi.org/10.1007/BF02668179

O'Connell, B., Wallace, M. W., Hood, A. v.S, Lechte, M. A. & Planavsky, N. J. (2020). Iron-rich carbonate tidal deposits, Angepena Formation, South Australia: a redox-stratified Cryogenian basin. Precambrian Research 342: 105668. https://doi.org/10.1016/j.precamres.2020.105668

Olivarez, A. M. & Owen, R. M. (1991). The europium anomaly of seawater: implications for fluvial versus hydrothermal REE inputs to the oceans. Chemical Geology, 92(4), 317-328. https://doi.org/10.1016/0009-2541(91)90076-4

Park, Y., Swanson-Hysell, N. L., MacLennan, S. A., Maloof, A. C., Gebreslassie, M., Tremblay, M. M., Schoene, B., Alene, M., Anttila, E. S., Tesema, T. & Haileab, B. (2020). The lead-up to the Sturtian Snowball Earth: Neoproterozoic chemostratigraphy time-calibrated by the Tambien Group of Ethiopia. Bulletin, 132(5-6), 1119-1149. https://doi.org/10.1130/B35178.1

Peral, L. E. G., Poiré, D. G., Strauss, H. & Zimmermann, U. (2007). Chemostratigraphy and diagenetic constraints on Neoproterozoic carbonate successions from the Sierras Bayas Group, Tandilia System, Argentina. Chemical Geology, 237(1-2), 109-128. https://doi.org/10.1016/j.chemgeo.2006.06.022

Postma, G. (1983). Water escape structures in the context of a depositional model of a mass flow dominated conglomeratic fan-delta (Abrioja Formation, Pliocene, Almeria Basin, SE Spain). Sedimentology 30(1): 91-103. https://doi.org/10.1111/j.1365-3091.1983.tb00652.x

Preiss, W. (2000). The Adelaide Geosyncline of South Australia and its significance in Neoproterozoic continental reconstruction. Precambrian Research 100(1-3): 21-63. https://doi.org/10.1016/S0301-9268(99)00068-6

Preiss, W. & Cowley, W. (1999). Genetic stratigraphy and revised lithostratigraphic classification of the Burra Group in the Adelaide Geosyncline. MESA Journal 14: 30-40.

Preiss, W., Dyson, I., Reid, P. & Cowley, W. (1998). Revision of lithostratigraphic classification of the Umberatana Group. MESA Journal, 9, 36-42.

Preiss, W. V., Drexel, J. F. & Parker, A. J. (1993). The Geology of South Australia: The Precambrian (Vol. 1): Mines and Energy, South Australia, Geological Survey of South Australia.

Preiss, W. V., Gostin, V. A., McKirdy, D. M., Ashley, P. M., Williams, G. E. & Schmidt, P. W. (2011). Chapter 69 The glacial succession of Sturtian age in South Australia: the Yudnamutana Subgroup. Geological Society, London, Memoirs, 36(1), 701-712. https://doi.org/10.1144/M36.69

Rieger, P., Magnall, J. M., Gleeson, S. A., Oelze, M., Wilke, F. D. & Lilly, R. (2022). Differentiating between hydrothermal and diagenetic carbonate using rare earth element and yttrium (REE+ Y) geochemistry: a case study from the Paleoproterozoic George Fisher massive sulfide Zn deposit, Mount Isa, Australia. Mineralium Deposita, 57(2), 187-206. https://doi.org/10.1007/s00126-021-01056-1

Rooney, A. D., Macdonald, F. A., Strauss, J. V., Dudás, F. Ö., Hallmann, C. & Selby, D. (2014). Re-Os geochronology and coupled Os-Sr isotope constraints on the Sturtian snowball Earth. Proceedings of the National Academy of Sciences, 111(1), 51-56. https://doi.org/10.1073/pnas.1317266110

Sarmiento, J. L. (2013). Ocean biogeochemical dynamics. Ocean Biogeochemical Dynamics, Princeton University Press. https://doi.org/10.1515/9781400849079

Sawaki, Y., Kawai, T., Shibuya, T., Tahata, M., Omori, S., Komiya, T., Yoshida, N., Hirata, T., Ohno, T., Windley, B.F. & Maruyama, S. (2010). 87Sr/86Sr chemostratigraphy of Neoproterozoic Dalradian carbonates below the Port Askaig glaciogenic Formation, Scotland. Precambrian Research, 179(1-4), 150-164. https://doi.org/10.1016/j.precamres.2010.02.021

Schidlowski, M. (1988). A 3,800-million-year isotopic record of life from carbon in sedimentary rocks. Nature, 333(6171), 313-318. https://doi.org/10.1038/333313a0

Shields-Zhou, G. & Och, L. (2011). The case for a Neoproterozoic oxygenation event: geochemical evidence and biological consequences. GSA Today 21(3): 4-11. http://dx.doi.org/10.1130/GSATG102A.1

Shuster, A. M., Wallace, M. W., Hood, A. v.S. & Jiang, G. (2018). The Tonian Beck Spring Dolomite: Marine dolomitization in a shallow, anoxic sea. Sedimentary Geology 368: 83-104. https://doi.org/10.1016/j.sedgeo.2018.03.003

Spötl, C. & T. W. Vennemann (2003). Continuous-flow isotope ratio mass spectrometric analysis of carbonate minerals. Rapid communications in mass spectrometry 17(9): 1004-1006. https://doi.org/10.1002/rcm.1010

Stromberg, S. G. & Bluck, B. (1998). Turbidite facies, fluid-escape structures and mechanisms of emplacement of the Oligo-Miocene Aljibe Flysch, Gibraltar Arc, Betics, southern Spain. Sedimentary Geology, 115(1-4), 267-288. https://doi.org/10.1016/S0037-0738(97)00096-1

Sumartojo, J. & Gostin, V. (1976). Geochemistry of the late Precambrian Sturt Tillite, Flinders Ranges, South Australia. Precambrian Research, 3(3), 243-252. https://doi.org/10.1016/0301-9268(76)90011-5

Swanson-Hysell, N. L., Maloof, A. C., Condon, D. J., Jenkin, G. R., Alene, M., Tremblay, M. M., Tesema, T., Rooney, A. D. & Haileab, B. (2015). Stratigraphy and geochronology of the Tambien Group, Ethiopia: Evidence for globally synchronous carbon isotope change in the Neoproterozoic. Geology 43(4): 323-326. https://doi.org/10.1130/G36347.1

Swanson-Hysell, N. L., Rose, C. V., Calmet, C. C., Halverson, G. P., Hurtgen, M. T. & Maloof, A. C. (2010). Cryogenian glaciation and the onset of carbon-isotope decoupling. Science 328(5978): 608-611. 10.1126/science.1184508

Them, T. R., Gill, B. C., Selby, D., Gröcke, D. R., Friedman, R. M. & Owens, J. D. (2017). Evidence for rapid weathering response to climatic warming during the Toarcian Oceanic Anoxic Event. Scientific reports, 7(1), 5003. https://doi.org/10.1038/s41598-017-05307-y

Thomson, B., Coats, R. P., Mirams, R. C., Forbes, B. G., Dalgarno, C. R. & Johnson, J. E. (1964). Precambrian rock groups in the Adelaide Geosyncline: a new subdivision. Quarterly Journal of the Geological Survey of South Australia 9: 1-19.

Tostevin, R., Shields, G. A., Tarbuck, G. M., He, T., Clarkson, M. O. & Wood, R. A. (2016). Effective use of cerium anomalies as a redox proxy in carbonate-dominated marine settings. Chemical Geology, 438, 146-162. https://doi.org/10.1016/j.chemgeo.2016.06.027

Tucker, M. E. & Wright, V. P. (2009). Carbonate sedimentology. John Wiley & Sons.

Tziperman, E., Halevy, I., Johnston, D. T., Knoll, A. H. & Schrag, D. P. (2011). Biologically induced initiation of Neoproterozoic snowball-Earth events. Proceedings of the National academy of Sciences, 108(37), 15091-15096. https://doi.org/10.1073/pnas.1016361108

Vakarelov, B. K. & Ainsworth, R. B. (2013). A hierarchical approach to architectural classification in marginal-marine systems: Bridging the gap between sedimentology and sequence stratigraphyHierarchical Marginal-Marine Architectural Classification. AAPG bulletin 97(7): 1121-1161. https://doi.org/10.1306/11011212024

Verdel, C., Phelps, B. & Welsh, K. (2018). Rare earth element and 87Sr/86Sr step-leaching geochemistry of central Australian Neoproterozoic carbonate. Precambrian Research, 310, 229-242. https://doi.org/10.1016/j.precamres.2018.02.014

Virgo, G. M., Collins, A. S., Amos, K. J., Farkaš, J., Blades, M. L. & Subarkah, D. (2021). Descending into the "snowball": High resolution sedimentological and geochemical analysis across the Tonian to Cryogenian boundary in South Australia. Precambrian Research 367: 106449. https://doi.org/10.1016/j.precamres.2021.106449

Wallace, M. W., Shuster, A., Greig, A., Planavsky, N. J. & Reed, C. P. (2017). Oxygenation history of the Neoproterozoic to early Phanerozoic and the rise of land plants. Earth and Planetary Science Letters 466: 12-19. https://doi.org/10.1016/j.epsl.2017.02.046

Wallace, M. W., Hood, A. v.S, Fayle, J., Hordern, E. S. & O'Hare, T. F. (2019). Neoproterozoic marine dolomite hardgrounds and their relationship to cap dolomites. Precambrian Research 328: 269-286. https://doi.org/10.1016/j.precamres.2019.04.026

Walter, M., Veevers, J. J., Calver, C. R., Gorjan, P. & Hill, A. C. (2000). Dating the 840–544 Ma Neoproterozoic interval by isotopes of strontium, carbon, and sulfur in seawater, and some interpretative models. Precambrian Research 100(1-3): 371-433. https://doi.org/10.1016/S0301-9268(99)00082-0

Wanless, H. R., Tedesco, L. P. & Tyrrell, K. M. (1988). Production of subtidal tubular and surficial tempestites by hurricane Kate, Caicos Platform, British West Indies. Journal of Sedimentary Research 58(4): 739-750. https://doi.org/10.1306/212F8E31-2B24-11D7-8648000102C1865D

Ward, J. F., Verdel, C., Campbell, M. J., Leonard, N. & Nguyen, A. D. (2019). Rare earth element geochemistry of Australian Neoproterozoic carbonate: Constraints on the Neoproterozoic oxygenation events. Precambrian Research, 335, 105471. https://doi.org/10.1016/j.precamres.2019.105471

Wei, G.Y., Hood, A. c.S, Chen, X., Li, D., Wei, W., Wen, B., Gong, Z., Yang, T., Zhang, Z.F. & Ling, H.F. (2019). Ca and Sr isotope constraints on the formation of the Marinoan

cap dolostones. Earth and Planetary Science Letters, 511, 202-212. https://doi.org/10.1016/j.epsl.2019.01.024

Chapter 6: Summary and recommendations

6.1 Research Findings

6.1.1 Lithostratigraphic Analysis

Facies and sequence stratigraphic analyses in this thesis provide high-resolution palaeoenvironmental interpretations for Tonian and Cryogenian stratigraphy in the northern Flinders Ranges of the Adelaide Superbasin, South Australia. This built upon previous sedimentological analyses from broad studies through the basin (Von der Borch, 1980; Preiss & Forbes, 1981; Preiss, 1987; Preiss et al., 1993; Preiss, 2000; Counts, 2017) and detailed interpretations from specific formations throughout the Tonian-Cryogenian succession (Link & Gostin, 1981; Young & Gostin, 1988; 1991; Uppill, 1990; McKirdy et al., 2001; Frank & Fielding, 2003; Giddings et al., 2009; Giddings & Wallace, 2009, 2009a; Preiss et al., 2009, 2011; Fromhold & Wallace, 2011, 2012; Le Heron et al., 2011, 2011a, 2014; Busfield & Le Heron, 2014; Lechte & Wallace, 2015, 2016; Wallace et al., 2015; Counts et al., 2016; Cox et al., 2018; Corkeron & Slezak, 2020; O'Connell et al., 2020; 2022). However, these studies have drawbacks, including the lack of resolution for the broad studies and lack of temporal and spatial context for the specific studies.

Findings from this thesis reveal multiple regressive-transgressive cycles through this interval, associated with fluctuations in tectonics (uplift/subsidence), sediment supply and climatically driven eustatic shifts. The pre-glacial (Tonian) succession is defined by deltaic rippled and cross-stratified sandstones, through inner platform intraclastic magnesite and stromatolitic carbonates, to subtidal laminated siltstone and platform carbonates. These are unconformably overlain by Cryogenian subglacial to grounded ice-margin pebbly diamictites with immature, massive sand interbeds that reflect glacial grounding-line advance and retreat in a glaciomarine setting. These grade into turbiditic laminated sandstone and mudstone with dropstones, which were deposited during deglaciation in a proglacial environment. The post-glacial succession consists of subtidal laminated shales and carbonates that coincide with widespread transgression and relative sea level rise following the Sturtian glaciation.

6.1.2 Chemostratigraphic Analysis

Isotopic and elemental geochemistry were analysed to better constrain the basin water chemistries, and hence the depositional conditions, through the Tonian and Cryogenian in the northern Flinders Ranges. Similar to the lithostratigraphic analyses, this research added to previous geochemical studies that provided a foundation for the broad trends in isotopic and elemental variation through the Tonian–Cryogenian in South Australia (Sumartojo & Gostin, 1976; Belperio, 1990; Barovich & Foden, 2000; Hill & Walter, 2000; Walter et al., 2000; McKirdy et al., 2001; Frank & Fielding, 2003; Halverson et al., 2005; Giddings & Wallace, 2009; 2009a; Swanson-Hysell et al., 2010; Grey et al., 2011; Hood et al., 2011; 2016; 2018; Hood & Wallace, 2012; 2014; 2015; Cox et al., 2016; Lechte & Wallace, 2016; Wallace et al., 2017; 2019; Ward et al., 2019; O'Connell et al., 2020).

Elemental analysis from the pre-glacial succession records low Y/Ho, slight light rare earth element (LREE) depletion, weak negative Ce/Ce* and high Eu/Eu*. This suggests a nearshore, dysoxic setting fed by anoxic deep waters and more oxic shallow waters. Further, C- and Sr-isotope signatures reveal overall positive $\delta^{13}C$ values, two $^{87}Sr/^{86}Sr$ clusters, and two $\delta^{88/86}Sr$ clusters in the base of the measured pre-glacial sections. Here, the most radiogenic values and lightest $\delta^{13}C$ values are recorded from maximum regressive surfaces (MRS), representing a low in relative water level. This likely resulted from increased riverine input of more evolved Sr and delivery of isotopically light C waters to the inner platform setting. Up-section, positive trends in $\delta^{13}C$ and $^{87}Sr/^{86}Sr$, paired with light $\delta^{88/86}Sr$ values represent a trend from an anoxic, deep-water subtidal setting to a dysoxic, shallow-water supratidal environment. In the syn-glacial succession, REE tracers record increased Y/Ho, moderate LREE depletion, slight negative Ce/Ce* and low Eu/Eu*. This characterises a shift to a more open, oxic to suboxic subtidal setting and reiterates the basinwide transgression following the glacial period.

6.1.3 Regional Correlation

Once the key temporal trends in depositional setting through the Tonian–Cryogenian had been established in the first half of this thesis, chapters 4 and 5 investigated the spatial variation of these environments across the northern Flinders Ranges.

Seven sites were measured across a 150 km east–west transect, which provided broad coverage across most of the northern area of the Adelaide Rift Complex. A lithostratigraphic framework was constructed from facies and sequence stratigraphic analyses, and chemostratigraphic correlations were interpreted from isotopic and elemental data sets. The facies architecture reveals a carbonate platform setting for the pre-glacial succession, with varying degrees of carbonate and clastic deposition. This was largely controlled by basin geometry and proximity to uplifted source areas, where topographic variability resulted from active faulting and salt diapirism. Climatically driven regression into the syn-glacial succession was marked by two glacial advance-retreat phases. Glacial succession thickness varied greatly across the basin and was likely the result of ongoing faulting and glacial erosion. Recent geochronological work has dated shales from a period of glacial retreat using in-situ laser Rb–Sr dating at 684 ± 37 Ma (Lloyd et al., 2023), supporting an intriguing contention that these advance and retreat phases may be separated by significant amounts of time (Hood et al. pers. comms., 2023, presentation at the Geological Society of Australia, SA Division). Following the Sturtian glaciation, basin subsidence and widespread transgression into a more distal subaqueous environment deposited varying proportions of clastic and carbonate deposition across the measured sections.

Six of the seven locations that were measured for their lithostratigraphy were chosen for Tonian chemostratigraphic analysis. Isotopic systems, REE tracers and the previously identified sequence stratigraphic trends were analysed to interpret fluctuations in productivity, redox and relative water level, and sediment input into the basin. The interaction between these systems reveal four depositional conditions that exist during deposition of Tonian stratigraphy in the northern Flinders Ranges: (1) a bioproductive, dysoxic inner platform setting that developed during slow transgression; (2) a bioproductive, suboxic outer platform setting that formed during a highstand systems tract; (3) a biologically inactive inner platform setting, associated

with continental progradation during a highstand systems tract; (4) and a biologically inactive, anoxic deep subtidal setting that formed during a transgressive systems tract.

6.1.4 Global Correlation

Finally, the depositional trends in this basin were compared to sites in North America, Africa, China, United Kingdom and Baltica to investigate globally synchronous fluctuations in tectonics, eustacy and climate.

Lithostratigraphically, pre-glacial successions at these sites are represented by similar mixed carbonate and clastic pre-glacial sequences that represent marginal marine deposition. The deposition of these sediments were largely controlled by local rifting related to the breakup of Rodinia. The bipartite division of the syn-glacial succession in South Australia was common in other global sections. However, some sections recorded numerous glacial cycles (Scotland) and others have been argued to record a singular glacial event (South China and Namibia—although in both these cases there are multiple diamictite horizons separated by a major argillaceous/arenaceous unit devoid of dropstones, similar to that seen in South Australia). The most lithostratigraphically consistent interval is the post-glacial succession, which records the deposition of fine-grained carbonates and clastics during a transgression. This is interpreted as a climatically controlled sea level rise driven by melting of major continental ice sheets.

One of the most significant negative $\delta^{13}C$ excursions (-0.2‰ to -7.75‰) in the Tonian geochemical record in South Australia corresponds to a widely accepted global excursion referred to as the Islay anomaly of ca. 735 Ma (Park et al., 2020). This major shift in the global $\delta^{13}C$ record has been preserved within a number of basins, including those in Ethiopia, Canada, Scotland and Svalbard. Conversely, other negative $\delta^{13}C$ excursions present in this study do not appear to correlate with global shifts. Further, the Tonian geochemical record in South Australia is represented by more overall negative values than those globally. The disparity between basin geochemistry may be a result of relative restriction of the northern Flinders Ranges from the global oceans during the Neoproterozoic. In this scenario, variations in the geochemical record may be related to local variations in tectonics, sediment input and climate. The northern Flinders carbon isotope record is interpreted to record major global marine anomalies at times of highstand and transgression when waters are interpreted to be well mixed with the global ocean. However, in times of lower relative sea-level other isotopic excursions are imposed on this global record due to local hydrographic effects.

6.2 Research Questions

(1)How does the lithostratigraphic framework in the northern Flinders Ranges fit with existing models for the Snowball Earth climate state?

Some of the largest discussions around the "Snowball Earth" event involve establishing exactly what environmental conditions facilitated the global icehouse, and constraining how extreme the event was. The lithostratigraphic framework constructed in this thesis provides a detailed palaeoenvironmental record that aligns with existing models for the overall climate conditions before, during and after the Sturtian glaciation. One of the more polarising debates is the

magnitude of the icehouse, represented by two end member hypotheses: "snowball" or "hard-snowball" and "slushball", also referred to as "soft-snowball" and more recently "waterbelt" (Pierrehumbert et al., 2011; Hoffman et al., 2017). The "snowball" hypothesis postulates a completely frozen world, where the ocean was entirely covered by sea ice for the duration of the icehouse (Kirschvink, 1992; Hoffman et al., 1998; Hoffman & Schrag, 2002); while the "slushball" hypothesis argues for finite open waters throughout the glaciation, where there was an active hydrological cycle and oases of bioproductivity (Christie-Blick et al., 1999; Runnegar, 2000; Leather et al., 2002; Olcott et al., 2005; Corsetti et al., 2003, 2006; Peltier et al., 2007; Moczydłowska, 2008). In this study, flow-generated bedforms deposited between diamictite units in glacial successions was used as evidence for glacial advance-retreat. This indicates that icehouse conditions were likely severe but cyclical, where hydrological processes were periodically active during sea ice free conditions. This interpretation shares aspects of both the "hard-snowball" and "soft-snowball" hypotheses but provides a more conservative alternative to the end-member theories. Interpretations for glacial conditions presented in this thesis also align with more recent literature that suggests "Snowball Earth" was a fully dynamic planet, and there was significant interaction between the atmosphere and oceans (Micheels & Montenari, 2008; Hoffman et al., 2017). Although the scientific community is yet to come to a consensus on this topic, new research, like the one presented in this study, improves our understanding of these important and enigmatic global climatic shifts.

(2)Was the northern part of the Adelaide Superbasin restricted from the global ocean during the Tonian and if so, how did this influence the chemostratigraphy and viability for global correlation?

Analysis of elemental geochemistry and isotopic systems provides a useful insight into palaeo-water chemistries and their subsequent depositional settings. The record of overall low Y/Ho, weak negative Ce/Ce*, slight LREE depletion and high Eu/Eu* in Tonian carbonate samples from this study is consistent with deposition in a dysoxic, shallow water setting that likely had significant input from weathered continental material. Further, $^{87}Sr/^{86}Sr$ values are very radiogenic (0.7084–0.7182) and $\delta^{88/86}Sr$ values are extremely light (ca. 0.21‰), indicating substantial riverine input and carbonate dissolution. These combined datasets indicate that the depositional setting in the northern part of the Adelaide Superbasin was very proximal, and possibly restricted from the global ocean. To address this global correlation, preservation of comparable geochemical excursions recorded from successions in palaeo-geographically separated locations can be examined (i.e., chemostratigraphy) (Halverson et al., 2010). This is especially useful when there is limited chronostratigraphic constraints, which is common in Neoproterozoic stratigraphy. Strontium isotope systems $^{87}Sr/^{86}Sr$ and $\delta^{88/86}Sr$ recorded in this study vary considerably from the global average (0.7061–0.7073) (Park et al., 2020), recording significantly more radiogenic $^{87}Sr/^{86}Sr$ values and lighter $\delta^{88/86}Sr$ values than for known Tonian marine carbonates (ca. 0.386‰) (Sarvian et al., 2019). Although shifts in $\delta^{13}C$ from this study may appear to correlate with some of the global $\delta^{13}C$ excursions (e.g., Islay anomaly), re-evaluation of geochemical data at other global locations has interpreted these excursions as the result of possible secondary alteration, rather than primary signatures (Park et al., 2020). This calls into question the validity of these geochemical excursions, and whether they represent

primary conditions, let alone global signatures. Overall, this illustrates the challenge with chemostratigraphic correlations between Neoproterozoic basins, due to the opportunity for secondary resetting of primary geochemical signatures and possible restriction between palaeo-water columns.

(3)Do the environmental conditions and geochemical variations recorded for palaeo-water in the northern Flinders Ranges support the evolution of complex multicellular life?

It is well established that the Neoproterozoic was a time of significant environmental and biological change, including global icehouses, carbon cycle variations, oceanic oxygenation, and eukaryotic evolution. Several researchers have attributed this biological evolution to the changing environment (i.e., increased atmospheric oxygen oxygenated the ocean and facilitated the evolution of metazoans) (Nursall, 1959; Raff & Raff, 1970; Towe, 1970; Catling et al., 2005; Canfield et al., 2007; Knoll, 2011; Sahoo et al., 2012). Other studies suggest alternative mechanisms for the oxygenation of the deep ocean that do not require atmospheric oxygenation, and centres more around the co-evolution of the environment and metazoans (i.e., eukaryote evolution increased efficiency of carbon circulation in the ocean and oxygenated greater depths) (Logan et al., 1995; Lenton et al., 2014). Regardless of the exact cause of this metazoan evolution, environmental and biological shifts are widely accepted as being closely coupled. Sequence stratigraphic analysis for relative water depth, along with geochemical signatures for redox, carbonate saturation, and sediment input are useful tools for understanding the overall bioproductivity and thus abundance of organisms in palaeo-water. Tonian data from this study supports overall bioproductive surface waters, where oxic shallow water (due to ocean stratification), stable climatic conditions and abundant platform environments provided ideal conditions for microbial precipitation. Data collected from mid-Cryogenian samples demonstrate deposition under similar environmental conditions, however, increased nutrient input following the Sturtian glaciation may have resulted in more oxygenated waters and precipitation of larger microbial communities. Although the relationship between environmental conditions and prokaryote abundance was demonstrated in this study, identifying the evolvability of eukaryotes is much more challenging, and was beyond the scope of this research. With that said, the detailed litho- and chemo-stratigraphy established in this study provides a framework that could be critical for understanding biological data collected in the future.

6.3 Future Work

While this research has contributed to our understanding of the palaeoenvironments during the Tonian and Cryogenian in South Australia, there are still uncertainties and research gaps that can be explored further. The following suggestions highlight my suggestions for key research areas for future work in this scientific space.

Despite the research into the paleoenvironmental constraints for Tonian rocks in the northern Flinders Ranges, uncertainty still exists regarding the geochemical conditions under which these sediments formed. This is because ancient environments are notoriously challenging to piece together due to the limited availability of modern analogues and opportunity for

geochemical resetting. The Skillogalee Dolomite is characterised by a distinctive suite of carbonate lithologies, including interbedded dolostones and intraclastic magnesite. These also record several geochemical shifts that can be difficult to interpret. The Coorong Lagoon in southern South Australia is a semi-restricted lagoon with ephemeral lakes that precipitate both dolomite and magnesite mineralogies. This has in the past been used as a modern analogue for the facies of the Skillogalee Dolomite (von der Borch and Lock, 1979; Belperio, 1990; Uppill, 1990; Preiss, 2000), but contemporary research into the comparison in isotopic and elemental signatures of these modern and ancient carbonates has not been explored. Future research prospects into the fractionation of Mg-rich carbonates and ephemeral/brackish waters in the Coorong could be used as a tool to better understand the Tonian system.

To date, there is no detailed palaeoenvironmental study across the southern portion of the Adelaide Rift Complex. Like the northern Flinders Ranges, research has been isolated to regional studies or highly detailed accounts from formations. High resolution lithostratigraphy and chemostratigraphic correlation through this southern region would provide much needed temporal and spatial constraints on the depositional setting. Correlation of this research to the work completed throughout the north would provide a basin-wide framework for palaeoenvironments during the Tonian and Cryogenian. Further, this could offer context for the relative restriction of the northern Flinders Ranges from the open ocean, which would improve our chemostratigraphic interpretations and subsequent correlation of these geochemical trends to the global system.

6.4 References

Alene, M., Jenkin, G. R., Leng, M. J. & Darbyshire, D. F. (2006). The Tambien Group, Ethiopia: an early Cryogenian (ca. 800–735 Ma) neoproterozoic sequence in the Arabian–Nubian shield. Precambrian Research 147(1-2): 79-99. https://doi.org/10.1016/j.precamres.2006.02.002

Ali, D. O., Spencer, A. M., Fairchild, I. J., Chew, K. J., Anderton, R., Levell, B. K., Hambrey, M. J., Dove, D. & Le Heron, D. P. (2018). Indicators of relative completeness of the glacial record of the Port Askaig Formation, Garvellach Islands, Scotland. Precambrian Research 319: 65-78. https://doi.org/10.1016/j.precamres.2017.12.005

Anderson, R. P., Fairchild, I. J., Tosca, N. J. & Knoll, A. H. (2013). Microstructures in metasedimentary rocks from the Neoproterozoic Bonahaven Formation, Scotland: Microconcretions, impact spherules, or microfossils? Precambrian Research 233: 59-72. https://doi.org/10.1016/j.precamres.2013.04.016

Armistead, S. E., Collins, A. S., Buckman, S. & Atkins, R. (2020). Age and geochemistry of the Boucaut Volcanics in the Neoproterozoic Adelaide Rift Complex, South Australia. Australian Journal of Earth Sciences: 1-10. https://doi.org/10.1080/08120099.2021.1840435

Asmerom, Y., Jacobsen, S. B., Knoll, A. H., Butterfield, N. J. & Swett, K. (1991). Strontium isotopic variations of Neoproterozoic seawater: implications for crustal evolution. Geochimica et Cosmochimica Acta, 55(10), 2883-2894. https://doi.org/10.1016/0016-7037(91)90453-C

Avigad, D., et al. (2007). "Detrital zircon U–Pb geochronology of Cryogenian diamictites and Lower Paleozoic sandstone in Ethiopia (Tigrai): age constraints on Neoproterozoic glaciation and crustal evolution of the southern Arabian–Nubian Shield." Precambrian Research 154(1-2): 88-106.

Balgord, E. A., Yonkee, W. A., Link, P. K. & Fanning, C. M. (2013). Stratigraphic, geochronologic, and geochemical record of the Cryogenian Perry Canyon Formation, northern Utah: Implications for Rodinia rifting and snowball Earth glaciation. Bulletin 125(9-10): 1442-1467. https://doi.org/10.1130/B30860.1

Barovich, K. & Foden, J. (2000). A Neoproterozoic flood basalt province in southern-central Australia: geochemical and Nd isotope evidence from basin fill. Precambrian Research, 100(1-3), 213-234. https://doi.org/10.1016/S0301-9268(99)00075-3

Bartley, J. K., Semikhatov, M. A., Kaufman, A. J., Knoll, A. H., Pope, M. C. & Jacobsen, S. B. (2001). Global events across the Mesoproterozoic–Neoproterozoic boundary: C and Sr isotopic evidence from Siberia. Precambrian Research, 111(1-4), 165-202. https://doi.org/10.1016/S0301-9268(01)00160-7

Batten, K. L., Narbonne, G. M. & James, N. P. (2004). Paleoenvironments and growth of early Neoproterozoic calcimicrobial reefs: platformal Little Dal Group, northwestern Canada. Precambrian Research 133(3-4): 249-269. https://doi.org/10.1016/j.precamres.2004.05.003

Belperio, A. (1990). Palaeoenvironmental interpretations of the Late Proterozoic Skillogalee Dolomite in the Willouran Ranges, South Australia. The Evolution of a Late Precambrian–Early Palaeozoic Rift Complex: The Adelaide Geosyncline. Geol. Soc. Aust. Spec. Publ 16: 85-104.

Boger, S. D. (2011). Antarctica—before and after Gondwana. Gondwana Research, 19(2), 335-371. https://doi.org/10.1016/j.gr.2010.09.003

Bold, U., Smith, E. F., Rooney, A. D., Bowring, S. A., Buchwaldt, R., Dudás, F. Ő., Ramezani, J., Crowley, J. L., Schrag, D. P. & Macdonald, F. A. (2016). Neoproterozoic stratigraphy of the Zavkhan terrane of Mongolia: The backbone for Cryogenian and early Ediacaran chemostratigraphic records. American Journal of Science 316(1): 1-63. https://doi.org/10.2475/01.2016.01

Brasier, M. D., Shields, G., Kuleshov, V. N. & Zhegallo, E. A. (1996). Integrated chemo-and biostratigraphic calibration of early animal evolution: Neoproterozoic–early Cambrian of southwest Mongolia. Geological Magazine, 133(4), 445-485. Bridge, J. S. (2009). Rivers and floodplains: forms, processes, and sedimentary record, John Wiley & Sons. doi:10.1017/S0016756800007603

Brocks, J. J., Jarrett, A. J., Sirantoine, E., Hallmann, C., Hoshino, Y. & Liyanage, T. (2017). The rise of algae in Cryogenian oceans and the emergence of animals. Nature, 548(7669), 578-581. https://doi.org/10.1038/nature23457

Busfield, M. E. & Le Heron, D. P. (2013). Glacitectonic deformation in the Chuos Formation of northern Namibia: implications for Neoproterozoic ice dynamics. Proceedings of the Geologists' Association, 124(5), 778-789. https://doi.org/10.1016/j.pgeola.2012.10.005

Busfield, M. & Le Heron, D. (2014). Sequencing the Sturtian icehouse: dynamic ice behaviour in South Australia. Journal of the Geological Society 171(3): 443-456. https://doi.org/10.1144/jgs2013-067

Busfield, M. E. and Le Heron, D. P. (2016). "A Neoproterozoic ice advance sequence, Sperry Wash, California." Sedimentology 63(2): 307-330.

Busfield, M. E. & Le Heron, D. P. (2016). A Neoproterozoic ice advance sequence, Sperry Wash, California. Sedimentology 63(2): 307-330. https://doi.org/10.1111/sed.12210

Busigny, V., Planavsky, N. J., Goldbaum, E., Lechte, M. A., Feng, L. & Lyons, T. W. (2018). Origin of the Neoproterozoic Fulu iron formation, South China: Insights from iron isotopes and rare earth element patterns. Geochimica et Cosmochimica Acta 242: 123-142. https://doi.org/10.1016/j.gca.2018.09.006

Butterfield, N. J. (2011). Animals and the invention of the Phanerozoic Earth system. Trends in ecology & evolution 26(2): 81-87. https://doi.org/10.1016/j.tree.2010.11.012Cawood, P. A. (2005). "Terra Australis Orogen: Rodinia breakup and development of the Pacific and Iapetus margins of Gondwana during the Neoproterozoic and Paleozoic." Earth-Science Reviews 69(3-4): 249-279.

Canfield, D. E., Poulton, S. W. & Narbonne, G. M. (2007). Late-Neoproterozoic deep-ocean oxygenation and the rise of animal life. Science 315(5808): 92-95. 10.1126/science.1135013Catling, D. C., Glein, C. R., Zahnle, K. J. & McKay, C. P. (2005). Why O2 is required by complex life on habitable planets and the concept of planetary "oxygenation time". Astrobiology 5(3): 415-438. http://doi.org/10.1089/ast.2005.5.415

Cawood, P. A. & Korsch, R. J. (2008). Assembling Australia: Proterozoic building of a continent. Precambrian Research, 166(1-4), 1-35. https://doi.org/10.1016/j.precamres.2008.08.006

Chartrand, F. & Brown, A. (1985). The diagenetic origin of stratiform copper mineralization, Coates Lake, Redstone copper belt, NWT, Canada. Economic Geology 80(2): 325-343. https://doi.org/10.2113/gsecongeo.80.2.325

Christie-Blick, N., Sohl, L. E. & Kennedy, M. J. (1999). Considering a Neoproterozoic snowball earth. Science 284(5417): 1087-1087.

Corkeron, M. L. & Slezak, P. R. (2020). Stromatolite framework builders: ecosystems in a Cryogenian interglacial reef. Australian Journal of Earth Sciences, 67(6), 833-856. https://doi.org/10.1080/08120099.2020.1732464

Corsetti, F. A., Awramik, S. M. & Pierce, D. (2003). A complex microbiota from snowball Earth times: microfossils from the Neoproterozoic Kingston Peak Formation, Death Valley, USA. Proceedings of the National Academy of Sciences 100(8): 4399-4404. https://doi.org/10.1073/pnas.0730560100

Corsetti, F. A., Olcott, A. N. & Bakermans, C. (2006). The biotic response to Neoproterozoic snowball Earth. Palaeogeography, Palaeoclimatology, Palaeoecology 232(2-4): 114-130. https://doi.org/10.1016/j.palaeo.2005.10.030

Counts, J. W., Rarity, F., Ainsworth, R. B., Amos, K. J., Lane, T., Moron, S., Trainor, J., Valenti, C. & Nanson, R. (2016). Sedimentological interpretation of an Ediacaran delta: Bonney Sandstone, South Australia. Australian Journal of Earth Sciences, 63(3), 257-273. https://doi.org/10.1080/08120099.2016.1180322

Counts, J. W. (2017). The Adelaide Rift Complex in the Flinders Ranges: Geologic history, past investigations and relevant analogues. Department of the Premier and Cabinet, South Australia, Adelaide, Report Book 16: 42.

Cox, G. M., Halverson, G. P., Stevenson, R. K., Vokaty, M., Poirier, A., Kunzmann, M., Li, Z. X., Denyszyn, S. W., Strauss, J. V. & Macdonald, F. A. (2016). Continental flood basalt weathering as a trigger for Neoproterozoic Snowball Earth. Earth and Planetary Science Letters 446: 89-99. https://doi.org/10.1016/j.epsl.2016.04.016

Cox, G. M., Isakson, V., Hoffman, P. F., Gernon, T. M., Schmitz, M. D., Shahin, S., Collins, A. S., Preiss, W., Blades, M. L., Mitchell, R. N. & Nordsvan, A. (2018). South Australian U-Pb zircon (CA-ID-TIMS) age supports globally synchronous Sturtian deglaciation. Precambrian Research 315: 257-263. https://doi.org/10.1016/j.precamres.2018.07.007

Crittenden Jr, M. D., Christie-Blick, N. & Karl Link, P. (1983). Evidence for two pulses of glaciation during the late Proterozoic in northern Utah and southeastern Idaho. Geological Society of America Bulletin 94(4): 437-450. https://doi.org/10.1130/0016-7606(1983)94<437:EFTPOG>2.0.CO;2

Direen, N. G. & Crawford, A. J. (2003). The Tasman Line: where is it, what is it, and is it Australia's Rodinian breakup boundary?. Australian Journal of Earth Sciences, 50(4), 491-502. https://doi.org/10.1046/j.1440-0952.2003.01005.x

Eisbacher, G. (1985). Late Proterozoic rifting, glacial sedimentation, and sedimentary cycles in the light of Windermere deposition, western Canada. Palaeogeography, Palaeoclimatology, Palaeoecology 51(1-4): 231-254. https://doi.org/10.1016/0031-0182(85)90087-2

Fairchild, I. J., Bonnand, P., Davies, T., Fleming, E. J., Grassineau, N., Halverson, G. P., Hambrey, M. J., McMillan, E. M., McKay, E., Parkinson, I. J. & Stevenson, C. T. (2016). The Late Cryogenian warm interval, NE Svalbard: chemostratigraphy and genesis. Precambrian Research 281: 128-154. https://doi.org/10.1016/j.precamres.2016.05.013

Fairchild, I. J., Fleming, E. J., Bao, H., Benn, D. I., Boomer, I., Dublyansky, Y. V., Halverson, G. P., Hambrey, M. J., Hendy, C., McMillan, E. A. & Spötl, C. (2016a). Continental carbonate facies of a Neoproterozoic panglaciation, north-east Svalbard. Sedimentology 63(2): 443-497. https://doi.org/10.1111/sed.12252

Fairchild, I. J. & Kennedy, M. J. (2007). Neoproterozoic glaciation in the Earth System. Journal of the Geological Society 164(5): 895-921. https://doi.org/10.1144/0016-76492006-191

Fairchild, I. J., Spencer, A. M., Ali, D. O., Anderson, R. P., Anderton, R., Boomer, I., Dove, D., Evans, J. D., Hambrey, M. J., Howe, J. & Sawaki, Y. (2017). Tonian-Cryogenian boundary sections of Argyll, Scotland. Precambrian Research. https://doi.org/10.1016/j.precamres.2017.09.020

Fanning, C. M., Ludwig, K. R., Forbes, B. G. & Preiss, W. V. (1986). Single and multiple grain U–Pb zircon analyses for the early Adelaidean Rook Tuff, Willouran Ranges, South Australia. Geological Society of Australia Abstracts.

Fanning, C. M. & Link, P. K. (2004). U-Pb SHRIMP ages of Neoproterozoic (Sturtian) glaciogenic Pocatello Formation, southeastern Idaho. Geology, 32(10), 881-884. https://doi.org/10.1130/G20609.1

Foden, J., Elburg, M., Turner, S., Clark, C., Blades, M.L., Cox, G., Collins, A.S., Wolff, K. & George, C. (2020). Cambro-Ordovician magmatism in the Delamerian orogeny: Implications for tectonic development of the southern Gondwanan margin. Gondwana Research 81: 490-521. https://doi.org/10.1016/j.gr.2019.12.006

Foden, J., Elburg, M. A., Dougherty-Page, J. & Burtt, A. (2006). The timing and duration of the Delamerian Orogeny: correlation with the Ross Orogen and implications for Gondwana assembly. The Journal of Geology 114(2): 189-210. https://doi.org/10.1086/499570

Frank, T. D. & Fielding, C. R. (2003). Marine origin for Precambrian, carbonate-hosted magnesite? Geology 31(12): 1101-1104. https://doi.org/10.1130/G20101.1

Frimmel, H. E., Klötzli, U. S. & Siegfried, P. R. (1996). New Pb-Pb single zircon age constraints on the timing of Neoproterozoic glaciation and continental break-up in Namibia. The Journal of Geology 104(4): 459-469. https://doi.org/10.1086/629839

Fromhold, T. & Wallace, M. (2011). Nature and significance of the Neoproterozoic Sturtian–Marinoan Boundary, Northern Adelaide Geosyncline, South Australia. Australian Journal of Earth Sciences 58(6): 599-613. https://doi.org/10.1080/08120099.2011.579624

Fromhold, T. & Wallace, M. (2012). Regional recognition of the Neoproterozoic Sturtian–Marinoan boundary, northern and central Adelaide Geosyncline, South Australia. Australian Journal of Earth Sciences 59(4): 527-546. https://doi.org/10.1080/08120099.2012.673507

Giddings, J. A., Wallace, M. W. & Woon, E. M. (2009). Interglacial carbonates of the Cryogenian Umberatana Group, northern Flinders Ranges, South Australia. Australian Journal of Earth Sciences 56(7): 907-925. https://doi.org/10.1080/08120090903005378

Giddings, J. A. & Wallace, M. W. (2009a). Facies-dependent δ13C variation from a Cryogenian platform margin, South Australia: Evidence for stratified Neoproterozoic oceans? Palaeogeography, Palaeoclimatology, Palaeoecology 271(3-4): 196-214. https://doi.org/10.1016/j.palaeo.2008.10.011

Giddings, J. A. & Wallace, M. W. (2009). Sedimentology and C-isotope geochemistry of the 'Sturtian'cap carbonate, South Australia. Sedimentary Geology 216(1-2): 1-14. https://doi.org/10.1016/j.sedgeo.2009.01.007

Glover, B. & Winchester, J. (1989). The Grampian group: a major Late Proterozoic clastic sequence in the Central Highlands of Scotland. Journal of the Geological Society 146(1): 85-96. https://doi.org/10.1144/gsjgs.146.1.0085

Grey, K., Hill, A. C. & Calver, C. (2011). Biostratigraphy and stratigraphic subdivision of Cryogenian successions of Australia in a global context. Geological Society, London, Memoirs 36(1): 113-134. https://doi.org/10.1144/M36.8

Halverson, G. P., Shen, C., Davies, J. H. & Wu, L. (2022). A Bayesian Approach to Inferring Depositional Ages Applied to a Late Tonian Reference Section in Svalbard. Front. Earth Sci 10: 798739. https://doi.org/10.3389/feart.2022.798739

Halverson, G. P. (2011). Glacial sediments and associated strata of the Polarisbreen Group, northeastern Svalbard. Geological Society, London, Memoirs 36(1): 571-579. http://hdl.handle.net/10214/9436

Halverson, G. P., Hoffman, P. F., Schrag, D. P., Maloof, A. C. & Rice, A. H. N. (2005). Toward a Neoproterozoic composite carbon-isotope record. GSA bulletin, 117(9-10), 1181-1207. https://doi.org/10.1130/B25630.1

Halverson, G. P., Kunzmann, M., Strauss, J. V. & Maloof, A. C. (2017). The Tonian-Cryogenian transition in Northeastern Svalbard. Precambrian Research. https://doi.org/10.1016/j.precamres.2017.12.010

Halverson, G. P., Maloof, A. C. & Hoffman, P. F. (2004). The Marinoan glaciation (Neoproterozoic) in northeast Svalbard. Basin Research 16(3): 297-324. https://doi.org/10.1111/j.1365-2117.2004.00234.x

Halverson, G. P., Maloof, A. C., Schrag, D. P., Dudás, F. Ö. & Hurtgen, M. (2007). Stratigraphy and geochemistry of a ca 800 Ma negative carbon isotope interval in northeastern Svalbard. Chemical Geology, 237(1-2), 5-27. https://doi.org/10.1016/j.chemgeo.2006.06.013

Halverson, G. P., Wade, B. P., Hurtgen, M. T. & Barovich, K. M. (2010). Neoproterozoic chemostratigraphy. Precambrian Research, 182(4), 337-350. https://doi.org/10.1016/j.precamres.2010.04.007

Hill, A. C. & Walter, M. R. (2000). Mid-Neoproterozoic (~ 830–750 Ma) isotope stratigraphy of Australia and global correlation. Precambrian Research, 100(1-3), 181-211. https://doi.org/10.1016/S0301-9268(99)00074-1

Hoffman, P. and G. Halverson (2008). "Otvi Group of the Western Northern Platform, the Eastern Kaoko Zone and the Western Northern Margin Zone."

Hoffman, P. F., Abbot, D.S., Ashkenazy, Y., Benn, D.I., Brocks, J.J., Cohen, P.A., Cox, G.M., Creveling, J.R., Donnadieu, Y., Erwin, D.H. & Fairchild, I.J. (2017). Snowball Earth climate dynamics and Cryogenian geology-geobiology. Science Advances 3(11): e1600983. 10.1126/sciadv.1600983

Hoffman, P. F., Halverson, G. P., Domack, E. W., Maloof, A. C., Swanson-Hysell, N. L. & Cox, G. M. (2012). Cryogenian glaciations on the southern tropical paleomargin of Laurentia (NE Svalbard and East Greenland), and a primary origin for the upper

Russøya (Islay) carbon isotope excursion. Precambrian Research 206: 137-158. https://doi.org/10.1016/j.precamres.2012.02.018

Hoffman, P. F., Halverson, G. P., Schrag, D. P., Higgins, J. A., Domack, E. W., Macdonald, F. A., Pruss, S. B., Blättler, C. L., Crockford, P. W., Hodgin, E. B. & Bellefroid, E. J. (2021). Snowballs in Africa: sectioning a long-lived Neoproterozoic carbonate platform and its bathyal foreslope (NW Namibia). Earth-Science Reviews 219: 103616. https://doi.org/10.1016/j.earscirev.2021.103616

Hoffman, P. F., Kaufman, A. J., Halverson, G. P. & Schrag, D. P. (1998). A Neoproterozoic snowball earth. Science 281(5381): 1342-1346. 10.1126/science.281.5381.1342

Hoffman, P. F., Lamothe, K. G., LoBianco, S. J., Hodgskiss, M. S., Bellefroid, E. J., Johnson, B. W., Hodgin, E. B. & Halverson, G. P. (2017a). Sedimentary depocenters on snowball Earth: Case studies from the Sturtian Chuos Formation in northern Namibia. Geosphere 13(3): 811-837. https://doi.org/10.1130/GES01457.1

Hoffman, P. F. & Schrag, D. P. (2002). The snowball Earth hypothesis: testing the limits of global change. Terra nova, 14(3), 129-155. https://doi.org/10.1046/j.1365-3121.2002.00408.x

Hood, A. v.S, Wallace, M. W., Reed, C. P., Hoffmann, K. H. & Freyer, E. E. (2015). Enigmatic carbonates of the Ombombo Subgroup, Otavi Fold Belt, Namibia: a prelude to extreme Cryogenian anoxia? Sedimentary Geology 324: 12-31. https://doi.org/10.1016/j.sedgeo.2015.04.007

Hood, A. v.S. & Wallace, M. W. (2012). Synsedimentary diagenesis in a Cryogenian reef complex: Ubiquitous marine dolomite precipitation. Sedimentary Geology, 255, 56-71. https://doi.org/10.1016/j.sedgeo.2012.02.004

Hood, A. v.S. & Wallace, M. W. (2015). Extreme ocean anoxia during the Late Cryogenian recorded in reefal carbonates of Southern Australia. Precambrian Research 261: 96-111.

Hood, A. v.S, Planavsky, N. J., Wallace, M. W., Wang, X., Bellefroid, E. J., Gueguen, B. & Cole, D. B. (2016). Integrated geochemical-petrographic insights from component-selective δ238U of Cryogenian marine carbonates. Geology 44(11): 935-938. https://doi.org/10.1130/G38533.1

Hood, A. v.S. & Wallace, M. W. (2014). Marine cements reveal the structure of an anoxic, ferruginous Neoproterozoic ocean. Journal of the Geological Society 171(6): 741-744. https://doi.org/10.1144/jgs2013-099

Hood, A. v.S, Wallace, M. W. & Drysdale, R. N. (2011). Neoproterozoic aragonite-dolomite seas? Widespread marine dolomite precipitation in Cryogenian reef complexes. Geology 39(9): 871-874. https://doi.org/10.1130/G32119.1

Howchin, W. (1929). Geology of South Australia, Govt. Printer, Adelaide.

Jones, D. S., Maloof, A. C., Hurtgen, M. T., Rainbird, R. H. & Schrag, D. P. (2010). Regional and global chemostratigraphic correlation of the early Neoproterozoic Shaler Supergroup, Victoria Island, northwestern Canada. Precambrian Research, 181(1-4), 43-63. https://doi.org/10.1016/j.precamres.2010.05.012

Keeley, J. A., Link, P. K., Fanning, C. M. & Schmitz, M. D. (2013). Pre-to synglacial rift-related volcanism in the Neoproterozoic (Cryogenian) Pocatello Formation, SE Idaho: New SHRIMP and CA-ID-TIMS constraints. Lithosphere 5(1): 128-150. https://doi.org/10.1130/L226.1

Keeman, J., Turner, S., Haines, P.W., Belousova, E., Ireland, T., Brouwer, P., Foden, J. & Wörner, G. (2020). New U-Pb, Hf and O isotope constraints on the provenance of sediments from the Adelaide Rift Complex–documenting the key Neoproterozoic to early Cambrian succession. Gondwana Research. https://doi.org/10.1016/j.gr.2020.02.005

Kirschvink, J. L. (1992)."Late Proterozoic low-latitude global glaciation: the snowball Earth. https://resolver.caltech.edu/CaltechAUTHORS:20130117-100718783

Knoll, A. H. (2011). The multiple origins of complex multicellularity. Annual Review of Earth and Planetary Sciences 39: 217-239. https://doi.org/10.1146/annurev.earth.031208.100209

Kunzmann, M., Halverson, G. P., Scott, C., Minarik, W. G. & Wing, B. A. (2015). Geochemistry of Neoproterozoic black shales from Svalbard: Implications for oceanic redox conditions spanning Cryogenian glaciations. Chemical Geology 417: 383-393. https://doi.org/10.1016/j.chemgeo.2015.10.022

Kuznetsov, A. B., Semikhatov, M. A., Maslov, A. V., Gorokhov, I. M., Prasolov, E. M., Krupenin, M. T. & Kislova, I. V. (2006). New data on Sr-and C-isotopic chemostratigraphy of the Upper Riphean type section (Southern Urals). Stratigraphy and Geological Correlation, 14, 602-628. https://doi.org/10.1134/S0869593806060025

Lamothe, K. G., Hoffman, P. F., Greenman, J. W. & Halverson, G. P. (2019). Stratigraphy and isotope geochemistry of the pre-Sturtian Ugab Subgroup, Otavi/Swakop Group, northwestern Namibia. Precambrian Research 332: 105387. https://doi.org/10.1016/j.precamres.2019.105387

Lan, Z., Li, X. H., Zhang, Q. & Li, Q. L. (2015). Global synchronous initiation of the 2nd episode of Sturtian glaciation: SIMS zircon U–Pb and O isotope evidence from the Jiangkou Group, South China. Precambrian Research 267: 28-38. https://doi.org/10.1016/j.precamres.2015.06.002Le Heron, D. P. & Busfield, M. E. (2016). Pulsed iceberg delivery driven by Sturtian ice sheet dynamics: An example from Death Valley, California. Sedimentology 63(2): 331-349. https://doi.org/10.1111/sed.12225

Le Heron, D. P., Busfield, M. E. & Collins, A. S. (2014). Bolla Bollana boulder beds: A Neoproterozoic trough mouth fan in South Australia? Sedimentology 61(4): 978-995. https://doi.org/10.1111/sed.12082

Le Heron, D. P., Busfield, M. E. & Kamona, F. (2013). An interglacial on snowball Earth? Dynamic ice behaviour revealed in the Chuos Formation, Namibia. Sedimentology 60(2): 411-427. https://doi.org/10.1111/j.1365-3091.2012.01346.x

Le Heron, D. P., Cox, G., Trundley, A. & Collins, A. (2011). Sea ice− free conditions during the Sturtian glaciation (early Cryogenian), South Australia. Geology 39(1): 31-34. https://doi.org/10.1130/G31547.1

Le Heron, D. P., Cox, G., Trundley, A. & Collins, A. S. (2011a). Two Cryogenian glacial successions compared: Aspects of the Sturt and Elatina sediment records of South Australia. Precambrian Research 186(1-4): 147-168. https://doi.org/10.1016/j.precamres.2011.01.014

Le Heron, D. P., Eyles, N. & Busfield, M. E. (2020). The Laurentian Neoproterozoic Glacial Interval: reappraising the extent and timing of glaciation. Austrian Journal of Earth Sciences 113(1): 59-70. https://doi.org/10.17738/ajes.2020.0004

Leather, J., Allen, P. A., Brasier, M. D. & Cozzi, A. (2002). Neoproterozoic snowball Earth under scrutiny: Evidence from the Fiq glaciation of Oman. Geology 30(10): 891-894. https://doi.org/10.1130/0091-7613(2002)030<0891:NSEUSE>2.0.CO;2

Lechte, M. & Wallace, M. (2016). Sub–ice shelf ironstone deposition during the Neoproterozoic Sturtian glaciation. Geology 44(11): 891-894. https://doi.org/10.1130/G38495.1

Lechte, M. A. & Wallace, M. W. (2015). Sedimentary and tectonic history of the Holowilena Ironstone, a Neoproterozoic iron formation in South Australia. Sedimentary Geology 329: 211-224. https://doi.org/10.1016/j.sedgeo.2015.09.014

Lenton, T. M., Boyle, R. A., Poulton, S. W., Shields-Zhou, G. A. & Butterfield, N. J. (2014). Co-evolution of eukaryotes and ocean oxygenation in the Neoproterozoic era. Nature Geoscience 7(4): 257-265. https://doi.org/10.1038/ngeo2108

Li, Z. X., Bogdanova, S., Collins, A. S., Davidson, A., De Waele, B., Ernst, R. E., Fitzsimons, I. C. W., Fuck, R. A., Gladkochub, D. P., Jacobs, J. & Karlstrom, K. E. (2008). Assembly, configuration, and break-up history of Rodinia: a synthesis. Precambrian Research 160(1-2): 179-210. https://doi.org/10.1016/j.precamres.2007.04.021

Li, Z. X., Li, X., Kinny, P., Wang, J., Zhang, S. & Zhou, H. (2003). Geochronology of Neoproterozoic syn-rift magmatism in the Yangtze Craton, South China and correlations with other continents: evidence for a mantle superplume that broke up Rodinia. Precambrian Research 122(1-4): 85-109. https://doi.org/10.1016/S0301-9268(02)00208-5

Li, Z. X. & Powell, C. M. (2001). An outline of the palaeogeographic evolution of the Australasian region since the beginning of the Neoproterozoic. Earth-Science Reviews, 53(3-4), 237-277. https://doi.org/10.1016/S0012-8252(00)00021-0

Link, P. K. & Christie-Blick, N. (2011). Neoproterozoic strata of southeastern Idaho and Utah: Record of Cryogenian rifting and glaciation. Geological Society, London, Memoirs 36(1): 425-436. https://doi.org/10.1144/M36.38

Link, P. K. & Gostin, V. A. (1981). Facies and paleogeography of Sturtian glacial strata (late Precambrian), South Australia. American Journal of Science 281(4): 353-374. https://doi.org/10.2475/ajs.281.4.353

Link, P. K. (1994). Glacial-marine facies in a continental rift environment: Neoproterozoic rocks of the western United States Cordillera. Earth's Glacial Record, 29-46.

Lloyd, J. C., Blades, M. L., Counts, J. W., Collins, A. S., Amos, K. J., Wade, B. P., Hall, J. W., Hore, S., Ball, A. L., Shahin, S. & Drabsch, M. (2020). Neoproterozoic geochronology and provenance of the Adelaide Superbasin. Precambrian Research 350: 105849. https://doi.org/10.1016/j.precamres.2020.105849

Lloyd, J. C., Collins, A. S., Blades, M. L., Gilbert, S. E. & Amos, K. J. (2022). Early Evolution of the Adelaide Superbasin. Geosciences 12(4): 154. https://doi.org/10.3390/geosciences12040154

Lloyd, J. C., Preiss, W. V., Collins, A. S., Virgo, G. M., Blades, M. L., Gilbert, S. E. & Amos, K. J. (2022a). Geochronology and formal stratigraphy of the Sturtian Glaciation in the Adelaide Superbasin. https://doi.org/10.31223/X50G9N

Logan, G. A., Hayes, J. M., Hieshima, G. B. & Summons, R. E. (1995). Terminal Proterozoic reorganization of biogeochemical cycles. Nature 376(6535): 53-56. https://doi.org/10.1038/376053a0

Long, D. & Turner, E. (2013). Formal definition of the Neoproterozoic Mackenzie Mountains Supergroup (Northwest Territories), and formal stratigraphic nomenclature for terrigenous clastic units of the Katherine Group. Geological Survey of Canada.

Lund, K., Aleinikoff, J. N., Evans, K. V. & Fanning, C. M. (2003). SHRIMP U-Pb geochronology of Neoproterozoic Windermere Supergroup, central Idaho: Implications for rifting of western Laurentia and synchroneity of Sturtian glacial deposits. Geological Society of America Bulletin 115(3): 349-372. https://doi.org/10.1130/0016-7606(2003)115<0349:SUPGON>2.0.CO;2

Macdonald, F. A., Schmitz, M.D., Crowley, J.L., Roots, C.F., Jones, D.S., Maloof, A.C., Strauss, J.V., Cohen, P.A., Johnston, D.T. & Schrag, D.P. (2010). Calibrating the cryogenian. Science 327(5970): 1241-1243. 10.1126/science.1183325

Maloof, A. C., Halverson, G. P., Kirschvink, J. L., Schrag, D. P., Weiss, B. P. & Hoffman, P. F. (2006). Combined paleomagnetic, isotopic, and stratigraphic evidence for true polar wander from the Neoproterozoic Akademikerbreen Group, Svalbard, Norway.

Geological Society of America Bulletin 118(9-10): 1099-1124. https://doi.org/10.1130/B25892.1
Mawson, D. & Sprigg, R. (1950). Subdivision of the Adelaide system. Australian Journal of Science 13(3): 69-72.
McKirdy, D. M., Burgess, J. M., Lemon, N. M., Yu, X., Cooper, A. M., Gostin, V. A., Jenkins, R. J. & Both, R. A. (2001). A chemostratigraphic overview of the late Cryogenian interglacial sequence in the Adelaide Fold-Thrust Belt, South Australia. Precambrian Research 106(1-2): 149-186. https://doi.org/10.1016/S0301-9268(00)00130-3
Meffre, S., Direen, N. G., Crawford, A. J. & Kamenetsky, V. (2004). Mafic volcanic rocks on King Island, Tasmania: evidence for 579 Ma break-up in east Gondwana. Precambrian research, 135(3), 177-191. https://doi.org/10.1016/j.precamres.2004.08.004
Merdith, A. S., Collins, A. S., Williams, S. E., Pisarevsky, S., Foden, J. D., Archibald, D. B., Blades, M. L., Alessio, B. L., Armistead, S., Plavsa, D. and Clark, C. (2017). A full-plate global reconstruction of the Neoproterozoic. Gondwana Research, 50, 84-134. https://doi.org/10.1016/j.gr.2017.04.001
Merdith, A. S., Williams, S. E., Brune, S., Collins, A. S. & Müller, R. D. (2019). Rift and plate boundary evolution across two supercontinent cycles. Global and planetary change, 173, 1-14. https://doi.org/10.1016/j.gloplacha.2018.11.006
Merdith, A.S., Williams, S.E., Collins, A.S., Tetley, M.G., Mulder, J.A., Blades, M.L., Young, A., Armistead, S.E., Cannon, J., Zahirovic, S., Müller, R.D. (2021). A continuous, kinematic full-plate motion model from 1 Ga to present. Earth Science Reviews. https://doi.org/10.1016/j.earscirev.2020.103477
Micheels, A. & Montenari, M. (2008). A snowball Earth versus a slushball Earth: Results from Neoproterozoic climate modeling sensitivity experiments. Geosphere 4(2): 401-410. https://doi.org/10.1130/GES00098.1
Miller, N. R., Avigad, D., Stern, R. J. & Beyth, M. (2011). The Tambien Group, Northern Ethiopia (Tigre). Geological Society, London, Memoirs 36(1): 263-276. https://doi.org/10.1144/M36.21
Miller, N. R., Stern, R. J., Avigad, D., Beyth, M. & Schilman, B. (2009). Cryogenian slate-carbonate sequences of the Tambien Group, Northern Ethiopia (I): Pre-"Sturtian" chemostratigraphy and regional correlations. Precambrian Research 170(3-4): 129-156. https://doi.org/10.1016/j.precamres.2008.12.004
Miller, R. M. (2013). Comparative stratigraphic and geochronological evolution of the Northern Damara Supergroup in Namibia and the Katanga Supergroup in the Lufilian Arc of Central Africa. Geoscience Canada 40(2): 118-140. http://dx.doi.org/10.12789/geocanj.2013.40.007
Millikin, A. E., Strauss, J. V., Halverson, G. P., Bergmann, K. D., Tosca, N. J. & Rooney, A. D. (2022). Calibrating the Russøya excursion in Svalbard, Norway, and implications for Neoproterozoic chronology. Geology. https://doi.org/10.1130/G49593.1
Milton, J. E., Hickey, K. A., Gleeson, S. A. & Friedman, R. M. (2017). New U-Pb constraints on the age of the Little Dal Basalts and Gunbarrel-related volcanism in Rodinia. Precambrian Research 296: 168-180. https://doi.org/10.1016/j.precamres.2017.04.030
Moczydłowska, M. (2008). The Ediacaran microbiota and the survival of Snowball Earth conditions. Precambrian Research 167(1-2): 1-15. https://doi.org/10.1016/j.precamres.2008.06.008
Myers, J. S., Shaw, R. D. & Tyler, I. M. (1996). Tectonic evolution of proterozoic Australia. Tectonics, 15(6), 1431-1446. https://doi.org/10.1029/96TC02356
Narbonne, G. M. & Aitken, J. D. (1995). Neoproterozoic of the mackenzie mountains, Northwestern Canada. Precambrian Research 73(1-4): 101-121. https://doi.org/10.1016/0301-9268(94)00073-Z

Narbonne, G. M., Kaufman, A. J. & Knoll, A. H. (1994). Integrated chemostratigraphy and biostratigraphy of the Windermere Supergroup, northwestern Canada: Implications for Neoproterozoic correlations and the early evolution of animals. Geological Society of America Bulletin 106(10): 1281-1292. https://doi.org/10.1130/0016-7606(1994)106<1281:ICABOT>2.3.CO;2

Nelson, L. L., Ahm, A. S. C., Macdonald, F. A., Higgins, J. A. & Smith, E. F. (2021). Fingerprinting local controls on the Neoproterozoic carbon cycle with the isotopic record of Cryogenian carbonates in the Panamint Range, California. Earth and Planetary Science Letters 566: 116956. https://doi.org/10.1016/j.epsl.2021.116956

Nelson, L. L., Smith, E. F., Hodgin, E. B., Crowley, J. L., Schmitz, M. D. & Macdonald, F. A. (2020). Geochronological constraints on Neoproterozoic rifting and onset of the Marinoan glaciation from the Kingston Peak Formation in Death Valley, California (USA). Geology 48(11): 1083-1087. https://doi.org/10.1130/G47668.1

Nursall, J. R. (1959). Oxygen as a prerequisite to the origin of the Metazoa. Nature 183(4669): 1170-1172. https://doi.org/10.1038/1831170b0

O'Connell, B., Wallace, M. W., Hood, A. v.S, Lechte, M. A. & Mahon, E. M. (2022). Nearshore environments before the evolution of land plants. Precambrian Research 382: 106883. https://doi.org/10.1016/j.precamres.2022.106883

O'Connell, B., Wallace, M. W., Hood, A. v.S, Lechte, M. A. & Planavsky, N. J. (2020). Iron-rich carbonate tidal deposits, Angepena Formation, South Australia: a redox-stratified Cryogenian basin. Precambrian Research 342: 105668. https://doi.org/10.1016/j.precamres.2020.105668

Olcott, A. N., Sessions, A. L., Corsetti, F. A., Kaufman, A. J. & De Oliviera, T. F. (2005). Biomarker evidence for photosynthesis during Neoproterozoic glaciation. Science 310(5747): 471-474. 10.1126/science.1115769

Park, J. K. & Jefferson, C. W. (1991). Magnetic and tectonic history of the Late Proterozoic Upper Little Dal and Coates Lake groups of northwestern Canada. Precambrian Research 52(1-2): 1-35. https://doi.org/10.1016/0301-9268(91)90011-X

Park, Y., Swanson-Hysell, N. L., MacLennan, S. A., Maloof, A. C., Gebreslassie, M., Tremblay, M. M., Schoene, B., Alene, M., Anttila, E. S., Tesema, T. & Haileab, B. (2020). The lead-up to the Sturtian Snowball Earth: Neoproterozoic chemostratigraphy time-calibrated by the Tambien Group of Ethiopia. Bulletin 132(5-6): 1119-1149. https://doi.org/10.1130/B35178.1

Peltier, W. R., Liu, Y. & Crowley, J. W. (2007). Snowball Earth prevention by dissolved organic carbon remineralization. Nature 450(7171): 813-818. https://doi.org/10.1038/nature06354

Pierrehumbert, R. T., Abbot, D. S., Voigt, A. & Koll, D. (2011). Climate of the Neoproterozoic. Annual Review of Earth and Planetary Sciences 39: 417-460. https://doi.org/10.1146/annurev-earth-040809-152447

Powell, C. M., Preiss, W. V., Gatehouse, C. G., Krapez, B. & Li, Z. X. (1994). South Australian record of a Rodinian epicontinental basin and its mid-Neoproterozoic breakup (~ 700 Ma) to form the Palaeo-Pacific Ocean. Tectonophysics, 237(3-4), 113-140. https://doi.org/10.1016/0040-1951(94)90250-X

Preiss, W., Dyson, I., Reid, P. & Cowley, W. (1998). Revision of lithostratigraphic classification of the Umberatana Group. MESA Journal, 9, 36-42.

Preiss, W. (2000). The Adelaide Geosyncline of South Australia and its significance in Neoproterozoic continental reconstruction. Precambrian Research, 100(1-3), 21-63. https://doi.org/10.1016/S0301-9268(99)00068-6

Preiss, W. & Cowley, W. (1999). Genetic stratigraphy and revised lithostratigraphic classification of the Burra Group in the Adelaide Geosyncline. MESA Journal, 14, 30-40.
Preiss, W., Dyson, I., Reid, P. & Cowley, W. (1998). Revision of lithostratigraphic classification of the Umberatana Group. MESA Journal, 9, 36-42.
Preiss, W. & Forbes, B. (1981). Stratigraphy, correlation and sedimentary history of Adelaidean (Late Proterozoic) basins in Australia. Precambrian Research, 15(3-4), 255-304. https://doi.org/10.1016/0301-9268(81)90054-1
Preiss, W. V. (1987). The Adelaide Geosyncline: Late Proterozoic stratigraphy, sedimentation, palaeontology and tectonics: Department of Mines and Energy.
Preiss, W. V., Drexel, J. F. & Parker, A. J. (1993). The Geology of South Australia: The Precambrian (Vol. 1): Mines and Energy, South Australia, Geological Survey of South Australia.
Preiss, W. V., Drexel, J. F. & Reid, A. J. (2009). Definition and age of the Kooringa Member of the Skillogalee Dolomite: host for Neoproterozoic (c. 790 Ma) porphyry related copper mineralisation at Burra. MESA Journal, 55, 19-33.
Preiss, W. V., Gostin, V. A., McKirdy, D. M., Ashley, P., Williams, G. & Schmidt, P. (2011). Geological Society, London, Memoirs. Geological Society, London, Memoirs, 36(1), 701-712. https://doi.org/10.1144/M36.69
Raff, R. A. & Raff, E. C. (1970). Respiratory mechanisms and the metazoan fossil record. Nature 228(5275): 1003-1005. https://doi.org/10.1038/2281003a0
Rooney, A. D., Macdonald, F. A., Strauss, J. V., Dudás, F. Ö., Hallmann, C. & Selby, D. (2014). Re-Os geochronology and coupled Os-Sr isotope constraints on the Sturtian snowball Earth. Proceedings of the National Academy of Sciences, 111(1), 51-56. https://doi.org/10.1073/pnas.1317266110
Runnegar, B. (2000). Loophole for snowball Earth. Nature 405(6785): 403-404. https://doi.org/10.1038/35013168
Sahoo, S. K., Planavsky, N. J., Kendall, B., Wang, X., Shi, X., Scott, C., Anbar, A. D., Lyons, T. W. & Jiang, G. (2012). Ocean oxygenation in the wake of the Marinoan glaciation. Nature 489(7417): 546-549. https://doi.org/10.1038/nature11445
Sarvian, N. L., Hurtgen, M.T., Jacobsen, A.D. & Maloof, A.C. (2019). Stable Strontium Isotope (δ88/86Sr) Record of pre-Sturtian Carbonate Rocks Spanning a Large δ13C Anomaly. Goldschmidt2021. Virtual.
Sawaki, Y., Kawai, T., Shibuya, T., Tahata, M., Omori, S., Komiya, T., Yoshida, N., Hirata, T., Ohno, T., Windley, B.F. & Maruyama, S. (2010). 87Sr/86Sr chemostratigraphy of Neoproterozoic Dalradian carbonates below the Port Askaig glaciogenic Formation, Scotland. Precambrian Research, 179(1-4), 150-164. https://doi.org/10.1016/j.precamres.2010.02.021
Segnit, R. W. (1939). The Pre-Cambrian-Cambrian Succession: The General and Economic Geology of These Systems, in Portions of South Australia. Frank Trigg, government printer. 10.1086/624923
Shields-Zhou, G. & Och, L. (2011). The case for a Neoproterozoic oxygenation event: geochemical evidence and biological consequences. GSA Today 21(3): 4-11. http://dx.doi.org/10.1130/GSATG102A.1
Smith, M., Robertson, S. & Rollin, K. E. (1999). Rift basin architecture and stratigraphical implications for basement-cover relationships in the Neoproterozoic Grampian Group of the Scottish Caledonides. Journal of the Geological Society, 156(6), 1163-1173. https://doi.org/10.1144/gsjgs.156.6.1163

Spencer, A. M. & Spencer, M. O. (1972). The Late Precambrian/Lower Cambrian Bonahaven Dolomite of Islay and its stromatolites. Scottish Journal of Geology 8(3): 269-282. https://doi.org/10.1144/sjg08030269

Stephenson, D., Mendum, J. R., Fettes, D. J. & Leslie, A. G. (2013). The Dalradian rocks of Scotland: an introduction. Proceedings of the Geologists' Association 124(1-2): 3-82. https://doi.org/10.1016/j.pgeola.2012.06.002

Sumartojo, J. & Gostin, V. (1976). Geochemistry of the late Precambrian Sturt Tillite, Flinders Ranges, South Australia. Precambrian Research 3(3): 243-252. https://doi.org/10.1016/0301-9268(76)90011-5

Swanson-Hysell, N. L., Maloof, A. C., Condon, D. J., Jenkin, G. R., Alene, M., Tremblay, M. M., Tesema, T., Rooney, A. D. & Haileab, B. (2015). Stratigraphy and geochronology of the Tambien Group, Ethiopia: Evidence for globally synchronous carbon isotope change in the Neoproterozoic. Geology 43(4): 323-326. https://doi.org/10.1130/G36347.1

Swanson-Hysell, N. L., Rose, C. V., Calmet, C. C., Halverson, G. P., Hurtgen, M. T. & Maloof, A. C. (2010). Cryogenian glaciation and the onset of carbon-isotope decoupling. Science 328(5978): 608-611. 10.1126/science.1184508

Thomson, B., Coats, R. P., Mirams, R. C., Forbes, B. G., Dalgarno, C. R. & Johnson, J. E. (1964). Precambrian rock groups in the Adelaide Geosyncline: a new subdivision. Quarterly Journal of the Geological Survey of South Australia 9: 1-19.

Towe, K. M. (1970). Oxygen-collagen priority and the early metazoan fossil record. Proceedings of the National Academy of Sciences 65(4): 781-788. https://doi.org/10.1073/pnas.65.4.781

Uppill, R. K. (1980). Sedimentology of the late Precambrian Mundallio Subgroup: a clastic-carbonate (Dolomite, Magnesite) sequence in the Mt. Lofty and Flinders Ranges, South Australia. Doctoral dissertation. https://hdl.handle.net/2440/37784

Von der Borch, C. (1980). Evolution of late proterozoic to early paleozoic Adelaide foldbelt, Australia: Comparisons with postpermian rifts and passive margins. Tectonophysics, 70(1-2), 115-134. https://doi.org/10.1016/0040-1951(80)90023-2

Von der Borch, C. & Lock, D. (1979). Geological significance of Coorong dolomites. Sedimentology, 26, 813-824. https://doi.org/10.1111/j.1365-3091.1979.tb00974.x

Wallace, M. W., Shuster, A., Greig, A., Planavsky, N. J. & Reed, C. P. (2017). Oxygenation history of the Neoproterozoic to early Phanerozoic and the rise of land plants. Earth and Planetary Science Letters 466: 12-19. https://doi.org/10.1016/j.epsl.2017.02.046

Wallace, M. W., Hood, A. v.S, Fayle, J., Hordern, E. S. & O'Hare, T. F. (2019). Neoproterozoic marine dolomite hardgrounds and their relationship to cap dolomites. Precambrian Research 328: 269-286. https://doi.org/10.1016/j.precamres.2019.04.026

Wallace, M. W., Hood, A. v.S., Woon, E. M., Giddings, J. A. & Fromhold, T. A. (2015). The Cryogenian Balcanoona reef complexes of the Northern Flinders Ranges: implications for Neoproterozoic ocean chemistry. Palaeogeography, Palaeoclimatology, Palaeoecology, 417, 320-336. https://doi.org/10.1016/j.palaeo.2014.09.028

Walter, M. R. & Veevers, J. (1997). Australian Neoproterozoic palaeogeography, tectonics, and supercontinental connections. AGSO Journal of Australian Geology and Geophysics, 17(1), 73-92. http://www.ga.gov.au/metadata-gateway/metadata/record/81480/

Walter, M., Veevers, J. J., Calver, C. R., Gorjan, P. & Hill, A. C. (2000). Dating the 840–544 Ma Neoproterozoic interval by isotopes of strontium, carbon, and sulfur in seawater, and some interpretative models. Precambrian Research 100(1-3): 371-433. https://doi.org/10.1016/S0301-9268(99)00082-0

Wang, J. & Li, Z. X. (2001). Sequence stratigraphy and evolution of the Neoproterozoic marginal basins along southeastern Yangtze Craton, South China. Gondwana Research 4(1): 17-26. https://doi.org/10.1016/S1342-937X(05)70651-1

Ward, J. F., Verdel, C., Campbell, M. J., Leonard, N. & Nguyen, A. D. (2019). Rare earth element geochemistry of Australian Neoproterozoic carbonate: Constraints on the Neoproterozoic oxygenation events. Precambrian Research, 335, 105471. https://doi.org/10.1016/j.precamres.2019.105471

Young, G. & Gostin, V. (1988). Stratigraphy and sedimentology of Sturtian glacigenic deposits in the western part of the North Flinders Basin, South Australia. Precambrian Research 39(3): 151-170. https://doi.org/10.1016/0301-9268(88)90040-X

Young, G. & Gostin, V. (1991). Late Proterozoic (Sturtian) succession of the North Flinders Basin, South Australia: an example of temperate glaciation in an active rift setting. Glacial Marine Sedimentation: Paleoclimatic Significance 261: 207-222.

Zhang, Q. R., Chu, X. L. & Feng, L. J. (2011). Neoproterozoic glacial records in the Yangtze Region, China. Geological Society, London, Memoirs 36(1): 357-366.

Zhang, S., Jiang, G. & Han, Y. (2008). The age of the Nantuo Formation and Nantuo glaciation in South China. Terra Nova 20(4): 289-294. https://doi.org/10.1111/j.1365-3121.2008.00819.x